PERFORMANCE OF TWIN-PONTOON FLOATING BREAKWATERS

by

SHANKAR S. BHAT
B.E., Karnataka University, 1984
M.Tech., Mangalore University, 1986
M.A.Sc., University of British Columbia, 1994

A THESIS SUBMITTED IN PARTIAL FULFILMENT OF
THE REQUIREMENTS FOR THE DEGREE OF
DOCTOR OF PHILOSOPHY
in

THE FACULTY OF GRADUATE STUDIES
Department of Civil Engineering

We accept this thesis as conforming
to the required standard

THE UNIVERSITY OF BRITISH COLUMBIA
January, 1998

© Shankar Bhat, 1998

In presenting this thesis in partial fulfillment of the requirements for an advanced degree at the University of British Columbia, I agree that the Library shall make it freely available for reference and study. I further agree that permission for extensive copying of this thesis for scholarly purposes may be granted by the Head of the Department or by his or her representatives. It is understood that copying or publication of this thesis for financial gain shall not be allowed without my written permission.

Department of Civil Engineering
The University of British Columbia
2324 Main Mall
Vancouver, B.C., V6T 1Z4
Canada

Date: January 7TH, 1998

Abstract

A numerical and experimental assessment of the hydrodynamic performance of a moored twin-pontoon floating breakwater made up of either rectangular or circular section pontoons is presented. The performance is described in terms of transmission and reflection coefficients, breakwater motions, and mooring line tensions. The numerical model includes both hydrodynamic and mooring analyses. The hydrodynamic analysis is based on linear potential theory which utilizes Green's theorem. An available hydrodynamic model for single pontoon sections is extended so as to apply to a structure with two distinct portions below the water surface and so as to incorporate a mooring analysis. An iterative procedure involving consistency in the wave drift force is used to link the hydrodynamic and mooring analyses. A comparison of numerical results with and without the iterative procedure indicates its importance for situations with highly nonlinear moorings.

A corresponding experimental study involving two-dimensional laboratory tests of a twin-pontoon moored floating is described. The experiments have been conducted in the wave flume of the Hydraulics Laboratory of the Department of Civil Engineering at the University of British Columbia. In the experiments, the breakwater performance is assessed using measured wave records at selected upwave and downwave locations in the flume, measured time histories of mooring line forces, and a video recording of breakwater motions. Tests with model breakwaters have been conducted for various pontoon spacings, pontoon drafts and mooring conditions, and for various wave conditions. A comparison of these results with the corresponding theoretical predictions is given.

Numerical results of reflection coefficients K_R, for the case of a fixed breakwater indicate a minimum at relative wave frequency parameter ka, ranging from 0.6 to 1.0, which is attributed to the interference effect between the two pontoons. For a moored breakwater, the numerical results indicate the occurrence of negative added mass in heave and an associated

sharp peak in the damping coefficient which may also be attributed to the spacing between two pontoons.

Experimental results confirmed that the size of the pontoon in relation to the incident wave length, (i.e. ka) is a primary parameter governing the wave transmission past the breakwater. It is found that the twin-pontoon breakwater's overall beam should be at least three-quarter the span of an incident wave length (i.e. $B > 3L/4$), and the spacing equal to the width of individual pontoon in order for the breakwater to be effective. A comparison of results for a rectangular section with that of circular section shows that the performance of the two sections is very similar.

The numerical model is found to provide reasonably good estimates of transmission coefficients, except in the vicinity of resonance. For conditions close to resonance, the experimental results of transmission and reflection coefficients, response amplitude operators and mooring line tensions at the anchor all show considerable scatter.

Table of Contents

	Page
Abstract	ii
Table of Contents	iv
List of Tables	viii
List of Figures	ix
List of Symbols	xiv
Acknowledgments	xvii
Dedication	xviii
1. Introduction	1
1.1 General	1
1.2 Literature Review	3
1.2.1 Hydrodynamic Analysis	4
1.2.2 Mooring Analysis	6
1.2.3 Experimental Studies	7
1.3 Objectives of the Present Investigation	8
2. Theoretical Approach	9
2.1 Breakwater Configuration	9
2.2 Design Variables and Dimensional Analysis	10
2.2.1 Freely Floating Breakwater	10
2.2.2 Moored Breakwater	13

2.3 Hydrodynamic Analysis 14

2.3.1 Wave Diffraction Problem 16

2.3.2 Wave Radiation Problem 18

2.3.3 Body Response Problem 19

2.3.4 Equations of Motion 21

2.3.5 Boundary Element Method 23

2.3.6 Transmission and Reflection Coefficients 27

2.3.7 Wave Drift Force 28

2.4 Mooring Analysis 29

2.4.1 Equilibrium Configuration 29

2.4.2 Static Analysis 32

2.4.3 Dynamic Analysis 34

2.5 Moored Breakwater Motions 35

2.6 Effect of Finite Length 35

3. Experimental Investigation 37

3.1 Experimental Facilities 37

3.2 Breakwater Models 38

3.3 Test Procedure 39

3.4 Analysis Technique 40

3.4.1 Reflection and Transmission Coefficients 40

3.4.2 Wave Measurement 42

3.4.3 Mooring Force Measurement 42

3.4.4 Dynamic Characteristics 43

3.4.5 Breakwater Motions 43

3.5 Assessment of Experimental Errors 44

4. Results and Discussion 47

4.1 Numerical Results 47

4.1.1 Accuracy and Efficiency 47

4.1.2 Fixed body 49

4.1.3 Unrestrained Body 50

4.1.4 Mooring Analysis 53

4.1.5 Moored Breakwater Response 54

4.2 Experimental Results 55

4.3 Experimental and Numerical Results 58

4.3.1 Rectangular Section with Chain Moorings 60

4.3.2 Rectangular Section with Nylon Moorings 64

4.3.3 Circular Section 65

4.3.4 Influence of Wave Direction 65

4.3.5 Influence of Pontoon Section and Configuration 66

4.4 Example Problem 68

5. Conclusions and Recommendations 70

5.1 Summary 70

5.2 Conclusions 71

5.2.1 Numerical Model 71

5.2.2 Experimental Results and Comparison with Numerical Model 74

5.3 Recommendations 75

References 77

Tables 84a

Appendix A - Reflection Analysis 169

Appendix B - Motion Analysis 172

List of Tables

Table 1.1	Summary of floating breakwater installations in British Columbia.	85
Table 3.1	Summary of regular wave test conditions.	86
Table 3.2	Summary of ranges of design parameters relating to regular wave tests.	87
Table 3.3	Experimental conditions adopted for rectangular and circular section breakwater models.	88
Table 3.4	Principal dimensions and parameters for the base case of both rectangular and circular twin-pontoon models.	90
Table 4.1	Linearized mooring stiffness matrix for no wave load condition for example application.	91
Table 4.2	Influence of number of iterations on sway drift force and drift for example application.	91
Table 4.3	Comparison of results obtained with and without the iteration procedure.	91
Table 4.4	Summary of experimental results for the rectangular section breakwater.	92
Table 4.5	Summary of experimental results for the circular section breakwater.	94

List of Figures

Fig. 1.1 Various types of floating breakwaters (McCartney (1985)).

Fig. 1.2 Location map relating to floating breakwater facilities in British Columbia.

Fig. 1.3 Comparison of transmission coefficient of various pontoon breakwater types (Blumberg and Cox (1988)).

Fig. 2.1 View of prototype twin-pontoon breakwater at Comox Harbour, B.C.

Fig. 2.2 Variation of buoyancy force and waterline beam as functions of relative draft for a circular pontoon section.

Fig. 2.3 Definition sketch of a moored twin-pontoon floating breakwater. (a) elevation; (b) plan view.

Fig. 2.4 Computational domain relating to the boundary element method. (a) alternative boundary geometry indicating the use of symmetry about the seabed; (b) discretization of twin-pontoon breakwater section; (c) sketch indicating the relationship between $\mathbf{x}$, ξ, and ξ'.

Fig. 2.5 Component steps in the mooring analysis. (a) initial equilibrium configuration for no wave load; (b) static analysis to obtain response to steady loads; (c) quasi-static analysis to obtain response to wave loads.

Fig. 2.6 Mooring line definition sketch. (a) fully suspended cable; (b) partly suspended cable.

Fig. 2.7 Response of a mooring cable due to environmental loads.

Fig. 2.8 Plan view of multiple cable mooring system.

Fig. 2.9 Component steps in breakwater analysis.

Fig. 3.1 Experimental set-up relating to wave flume tests.

Fig. 3.2 Flowchart indicating various components of the experimental scheme.

Fig. 3.3 Photograph of twin-pontoon breakwater models used in wave flume tests. (a) rectangular section; (b) circular section.

Fig. 3.4 Ranges of Keulegan-Carpenter number, K relating to chosen wave conditions for the case of (a) rectangular section, (b) circular section model.

Fig. 3.5 A typical image captured for motion analysis to track the markers.

Fig. 3.6 Experimental values of RAO's for a moored rectangular twin-pontoon breakwater indicating the estimated errors for the video-based motion tracking system, (d/a = 1.67, h/a = 0.45, b/a = 1.0, S/S_o = 1.08).

Fig. 4.1 Comparison of reflection coefficient, K_R, with results reported by Williams and Abul-Azm (1996), for a fixed rectangular twin-pontoon breakwater. (a) influence of draft, h, (d/a = 2.5, b/a = 1.0, β = 0°); (b) influence of pontoon spacing, b, (d/a = 2.5, h/a = 0.5, β = 0°).

Fig. 4.2 Reflection coefficient for a fixed circular twin-pontoon breakwater indicating the influence of spacing, b, (d/a = 2.5, h/a = 0.5, β = 0°).

Fig. 4.3 Variation of hydrodynamic coefficients as a function of normalized wave number, ka, for a single-pontoon rectangular section (d/a = 5.0, h/a = 0.5 and β = 0°), and for a twin-pontoon rectangular section (d/a = 5.0, h/a = 0.5, b/a = 1.0 and β = 0°). (a) added mass in sway, heave, and roll; (b) damping coefficient, in sway, heave, and roll; (c) exciting force coefficient, in sway, heave, and roll; (d) RAO's in sway, heave, and roll; (e) reflection and transmission coefficients, and drift force coefficient.

Fig. 4.4 Variation of hydrodynamic coefficients, as a function of normalized wave number, ka, for a single-pontoon circular section (d/a = 5.0, h/a = 0.5 and β = 0°), and for a twin-pontoon circular section (d/a = 5.0, h/a = 0.5, b/a = 0.5 and β = 0°). (a) added mass in sway, heave, and roll; (b) damping coefficient, in sway, heave, and roll; (c) exciting force coefficient, in sway, heave, and roll; (d) RAO's in sway, heave, and roll; (e) reflection and transmission coefficients, and drift force coefficient.

Fig. 4.5 Variation of added mass and damping coefficients indicating the influence of pontoon spacing. (a) rectangular twin-pontoon section; (d/a = 2.5, h/a = 0.5, β = 0°); (b) circular twin-pontoon section; (d/a = 2.5, h/a = 0.5, β = 0°).

Fig. 4.6 Comparison of stiffness characteristics for a six-point mooring system made up of chain or nylon lines.

Fig. 4.7 Comparison between chain and nylon moorings for a twin-pontoon rectangular section breakwater. (a) transmission coefficient; (b) upwave and downwave mooring line tensions at anchor.

Fig. 4.8 Measured time traces of water surface elevation and mooring line anchor forces for base case of moored rectangular twin-pontoon model, (d/a = 1.67, h/a = 0.45, b/a = 1.0). (a) H = 0.12 m, T = 1.00 sec, with chain mooring, S/S_o = 1.08; (b) H = 0.12 m, and T = 1.00 sec, with nylon mooring, S/S_o = 1.00; (c) H = 0.09 m, T = 1.70 sec, with chain mooring, S/S_o = 1.08.

Fig. 4.9 Measured time traces of breakwater responses and water surface elevation for base case of moored rectangular twin-pontoon model, (d/a = 1.67, h/a = 0.45, b/a = 1.0, H = 0.09 m, T = 1.70 sec, with chain mooring, S/S_o = 1.08).

Fig. 4.10 Comparison of measured wave profiles with computed wave profiles based on the reflection analysis for base cases of moored rectangular twin-pontoon breakwater, (d/a = 1.67, h/a = 0.45, b/a = 1.0, H = 0.12 m, T = 1.0 sec).

Fig. 4.11 Numerical results indicating the influence of different values of viscous damping coefficient for base case of a rectangular twin-pontoon breakwater, (d/a = 1.67, h/a = 0.45, b/a = 1.0, S/S_o = 1.08, $\beta = 0°$). (a) RAO's in sway, heave and roll; (b) reflection, transmission and energy dissipation coefficients.

Fig. 4.12 Comparison of experimental values and numerical results for base case of rectangular twin-pontoon breakwater with chain mooring, (d/a = 1.67, h/a = 0.45, b/a = 1.0, S/S_o = 1.0, $\beta = 0°$). (a) transmission coefficient; (b) RAO's in sway, heave and roll; (c) RAO phases.

Fig. 4.13 Comparison of experimental values with that of numerical results to indicate the influence of draft for a rectangular twin-pontoon breakwater with chain mooring, (d/a = 1.67, b/a = 1.0, S/S_o = 1.08, $\beta = 0°$). (a) RAO's in sway, heave, and roll; (b) phase angles of RAO's for sway, heave and roll.

Fig. 4.14 Comparison of experimental values and numerical results of reflection and transmission coefficients to indicate the influence of draft for a rectangular twin-pontoon breakwater with chain mooring, (d/a = 1.67, b/a = 1.0, S/S_o = 1.08, $\beta = 0°$).

Fig. 4.15 Comparison of experimental values and numerical results to indicate the influence of spacing for a rectangular twin-pontoon breakwater with chain mooring, (d/a = 1.67, h/a = 0.45, S/S_o = 1.08, $\beta = 0°$). (a) RAO's in sway, heave, and roll; (b) phase angles of RAO's for sway, heave and roll.

Fig. 4.16 Comparison of experimental values and numerical results of reflection and transmission coefficients to indicate the influence of spacing for a rectangular twin-pontoon breakwater with chain mooring, (d/a = 1.67, h/a = 0.45, S/S_o = 1.08, $\beta = 0°$).

Fig. 4.17 Comparison of experimental and numerical results to indicate the influence of slackness for a rectangular twin-pontoon breakwater with chain mooring, (d/a = 1.67, h/a = 0.45, b/a = 1.0, $\beta = 0°$). (a) RAO's in sway, heave, and roll; (b) phase angles of RAO's for sway, heave and roll.

Fig. 4.18 Comparison of experimental values and numerical results of reflection and transmission coefficients to indicate the influence of slackness for a rectangular

twin-pontoon breakwater with chain mooring, (d/a = 1.67, h/a = 0.45, b/a = 1.0, $\beta = 0°$).

Fig. 4.19 Comparison of experimental values and numerical results of maximum mooring line tensions at anchor to indicate the influence of slackness for a rectangular twin-pontoon breakwater with chain mooring, (d/a = 1.67, h/a = 0.45, b/a = 1.0, $\beta = 0°$).

Fig. 4.20 Comparison of experimental values and numerical results to indicate the influence of draft for a rectangular twin-pontoon breakwater with nylon mooring, (d/a = 1.67, b/a = 1.0, $S/S_o = 1.0$, $\beta = 0°$). (a) transmission coefficients; (b) RAO's in sway, heave, and roll; (c) maximum mooring line tensions at anchor.

Fig. 4.21 Comparison of experimental values of transmission coefficient and maximum mooring line tensions at anchor with that of numerical results for a rectangular twin-pontoon breakwater with nylon mooring, (d/a = 1.67, h/a = 0.65, $S/S_o = 1.0$, $\beta = 0°$). (a) influence of draft; (b) influence of spacing.

Fig. 4.22 Comparison of experimental values with that of numerical results for a circular section twin-pontoon breakwater with chain mooring, (d/a = 2.5, h/a = 0.5, b/a = 2.0, $S/S_o = 1.08$, $\beta = 0°$). (a) transmission coefficient; (b) RAO's in sway, heave and roll; (c) maximum mooring line tensions at anchor.

Fig. 4.23 Comparison of experimental values with that of numerical results for a circular section twin-pontoon breakwater with nylon mooring, (d/a = 2.5, h/a = 0.5, b/a = 2.0, $S/S_o = 1.0$, $\beta = 0°$). (a) transmission coefficient; (b) RAO's in sway, heave and roll; (c) maximum mooring line tensions at anchor.

Fig. 4.24 Experimental results to indicate the influence of draft for a circular twin-pontoon breakwater with chain mooring, (d/a = 2.5, b/a = 2.0, $S/S_o = 1.08$, $\beta = 0°$). (a) RAO's in sway, heave, and roll; (b) reflection and transmission coefficients.

Fig. 4.25 Experimental results to indicate the influence of spacing for a circular twin-pontoon breakwater with chain mooring, (d/a = 2.5, h/a = 0.65, $S/S_o = 1.08$, $\beta = 0°$). (a) RAO's in sway heave, and roll; (b) reflection transmission coefficients.

Fig. 4.26 Experimental results to indicate the influence of draft for a circular twin-pontoon breakwater with nylon mooring, (d/a = 2.5, b/a = 2.0, $S/S_o = 1.0$, $\beta = 0°$). (a) RAO's in sway heave, and roll; (b) reflection and transmission coefficients, and maximum mooring line tension at anchor.

Fig. 4.27 Experimental results of reflection and transmission coefficients, and maximum mooring line tensions at anchor for a circular twin-pontoon breakwater with nylon mooring, (d/a = 2.5, b/a = 2.0, $S/S_o = 1.0$, $\beta = 0°$). (a) influence of draft; (b) influence of spacing.

Fig. 4.28 Numerical results indicating the influence of wave direction for a fixed rectangular twin-pontoon breakwater, (d/a = 2.5, h/a = 0.45, b/a = 1.0). (a) exciting force coefficients; (b) reflection and transmission force coefficients.

Fig. 4.29 Numerical results of transmission coefficient indicating the influence of pontoon section, (d/a = 1.67, h/a = 0.45, b/a = 1.0). (a) fixed; (b) chain mooring, $S/S_o = 1.08$.

Fig. 4.30 Numerical results of transmission coefficient indicating the influence of different configurations of rectangular section breakwaters, (d/a = 2.5, h/a = 0.45). (a) fixed; (b) chain mooring, $S/S_o = 1.08$.

Fig. 4.31 Comparison of numerical results of transmission coefficient for the twin-pontoon and single-pontoon section breakwaters with the experimental values of an A-frame breakwater (Byres, 1988).

Fig. 4.32 Sketch indicating the related dimensions of a moored twin-pontoon floating breakwater. (a) elevation; (b) plan view.

Fig. 4.33 Tension at anchor for a most heavily and the least loaded mooring line, and the associated restoring force in sway for a ten-point chain mooring system.

Fig. 4.34 Numerical results as functions of wave frequency, f, for a rectangular twin-pontoon section breakwater, (a = 2.0 m, d = 3.4 m, b = 2.0, h = 0.9 m), with chain mooring, $S/S_o = 1.08$. (a) exciting forces; (b) drift, and sway motion, wave drift force, and transmission coefficient; (c) maximum mooring line tension at anchor.

Fig. A.1 Definition sketch related to reflection analysis.

Fig. B.1 Measurement of breakwater motions.

List of Symbols

Hydrodynamic Analysis

a	characteristic breakwater dimension
A	submerged volume of section per unit length
B	overall breakwater beam
b	gap between pontoons
c_{ij}	hydrostatic stiffness matrix
c'_{ij}	mooring stiffness matrix
d	still water depth
F'_d	wave drift force coefficient
F'_k	exciting force coefficient
g	gravitational constant
h	pontoon draft
H	wave height
K	Keulegan-Carpenter number
k	wave number
K_R	reflection coefficient
K_T	transmission coefficient
L	wave length
m	mass per unit length of the breakwater
m_{ij}	mass matrix

N	number of segments on $S_B + S_F + S_R$
n	unit normal vector directed out of fluid region
n_x, n_z	direction cosines of n
r_G	breakwater radius of gyration about centre of gravity
S_B	immersed body surface (see Fig. 2.4(a))
S_F	still water level (see Fig. 2.4(a))
S_R	radiation surface (see Fig. 2.4(a))
T	wave period
x_f	x coordinate of centroid of waterplane area
x, y, z	coordinate system
z_B	z coordinate of centre of buoyancy
z_G	z coordinate of centre of gravity
ς_i	viscous damping coefficient
β	incident wave direction (see Fig. 2.4(a))
η	free surface elevation
λ_{ij}	damping coefficient matrix
λ'_{ij}	viscous damping matrix
μ_{ij}	added mass coefficient matrix
ν	nondimensional frequency parameter, ka sinβ
ρ	fluid density
ω	wave angular frequency
ξ'_i	response amplitude operator

ζ_i complex radiated wave amplitude

Mooring Analysis

EA axial stiffness of mooring line

H horizontal component of mooring line tension

N number of mooring lines

q buoyant weight per unit length of mooring line

S unstretched length of mooring line

S_l unstretched length of suspended portion of mooring line

T mooring line tension

V vertical component of mooring line tension

X horizontal distance from the anchor to attachment point

x, y, z coordinate system

$\bar{x}, \bar{y}, \bar{z}$ location for the upper end of mooring line

X_l horizontal span of suspended portion of mooring line

Z anchor depth

ΔX displacement of the structure due to the steady drag and drift forces

ϕ direction of mooring line, measured counter-clockwise from the positive x axis (see Fig. 2.8)

λ mooring line spacing at attachment points

θ slope of mooring line (see Fig. 2.6)

Acknowledgments

The author would like to express his sincere appreciation and gratitude to his thesis advisor, Professor Michael Isaacson, for his advice, constant support and guidance throughout this research. The author thanks John Baldwin for his assistance in developing the numerical model used in this study, and Kurt Neilson for his help in the construction of the physical models. Thanks are also due to the author's colleagues Premasiri Sundaralingam, Gang Yang, Nathalie Garceau, Brenda Manuel, Sumathy Ganapathy and Hiroshi Shiratani for their contributions in the related experimental investigation. The author also wishes to thank his wife, Jyoti, for her support and encouragement throughout the study.

Financial support in the form of a Canadian Commonwealth Scholarship is gratefully acknowledged.

To my family

1. Introduction

1.1 General

Many coastal activities require protection from waves, and breakwaters are widely used in order to provide such protection. The oldest and most common breakwaters are bottom-founded structures such as rubble-mound breakwaters. These generally provide excellent protection from waves. However, they may become uneconomical for large water depths, and limited water circulation behind such breakwaters may lead to problems associated with sedimentation and increased pollutant concentrations within protected areas. Floating breakwaters have proven to be an attractive and economical alternative at locations where water depths are relatively large and the wave climate is not too severe. They have also been used at locations where temporary or seasonal protection is required.

A wide variety of floating breakwater designs has been adopted in the past, and Fig. 1.1 shows various categories of such designs. These structures can be classified on the basis of their configuration and their wave attenuation mechanism. A classification relating to breakwater configuration includes scrap-tire breakwaters, A-frame breakwaters, concrete caisson breakwaters, and more recently twin-pontoon breakwaters. The choice between these depends primarily on local wave and site conditions, the availability of construction materials, and on functional and operational aspects of the breakwater.

With respect to the latter type of classification, wave attenuation arises from a combination of energy dissipation and wave reflection, and the relative contribution of these two mechanisms depends on the nature of the breakwater and its configuration. The wave reflection mechanism can generally be modelled approximately by linear wave diffraction/radiation theory, whereas the energy dissipation mechanism involves viscous dissipation and nonlinear wave breaking, and as such cannot readily be dealt with using ideal

fluid theory. However, empirical coefficients may be used in the breakwater's equations of motion such that linear wave diffraction/radiation theory may continue to be used.

In order to keep a floating breakwater at a designated location, two types of restraint are generally adopted; either piles or mooring lines. Piles have the advantage of restricting sway and roll motions almost completely, resulting in lower transmission coefficients. However, they have the disadvantage of wear problems at the points of contact with the breakwater, and their use may be limited by large water depths and poor soil conditions at the seabed. On the other hand, mooring lines may be more suitable in deeper water, but may give rise to problems related to connection points to the breakwaters, lifting or dragging anchors and they may not limit sufficiently the breakwater motions, leading to increased transmission coefficients.

The performance of a floating breakwater is primarily characterized by the *transmission coefficient*, which is the ratio of transmitted to incident wave height. Other aspects of a floating breakwater's design include a consideration of the breakwater motions, and the possibilities of structural failure of the breakwater and its restraint or mooring system. Possible difficulties that a satisfactory design should overcome include a breakwater's inability to provide adequate wave protection, excessive breakwater motions, and damage or failure, which is most often associated with connections between individual units of a breakwater or with its moorings or anchors. Typically, floating breakwaters have been used at locations where the wave period ranges up to about 5 sec and wave heights up to about 1 m. A selection of floating breakwater sites in British Columbia is listed in Table 1.1, corresponding to the locations shown in Fig. 1.2.

Current designs of floating breakwaters are reasonably effective at attenuating moderate to high frequency waves. Although most of the energy in a deep-water wave is concentrated near the surface, some of it is contained in the water at depth. Breakwaters of practical dimensions can therefore intercept only a part of the total wave energy. In addition, the motions of the breakwater itself generate waves that propagate outward, contributing to the

transmitted wave height. Under certain wave conditions, the breakwater may undergo resonance and become less effective at attenuating waves. This implies that knowledge not only of expected design wave conditions is required but also an understanding of the response of the floating body under that sea state.

Present practice relating to floating breakwater designs is often based on experience with past designs. The large number of variables involved and the variety of existing breakwaters has made it difficult for empirical relationships to be derived. For most large scale applications, it has therefore been necessary to resort to site-specific physical model tests before a particular breakwater design is adopted. In addition, there have been numerous attempts to develop numerical models, which may be used in place of or in conjunction with physical model studies.

Twin-pontoon breakwaters may be particularly advantageous with respect to breakwater motions and lower transmission coefficients compared to single-pontoon breakwaters (Fig. 1.3), in part because they generally have a relatively high stiffness with respect to roll motions. Each unit may be relatively small and light compared to other single unit breakwaters, and this allows flexibility relating to fabrication and installation procedures. Therefore, the present study is oriented towards addressing the hydrodynamic performance of twin-pontoon floating breakwaters and focuses on various design aspects of circular and rectangular cross-section pontoons with respect to wave loading.

1.2 Literature Review

Surveys of the design of floating breakwaters include those by Jones (1971), McLaren (1981), McCartney (1985), Werner (1988), and Isaacson (1993a). Comprehensive bibliographies relating to analytical formulations and in-situ experiences with particular designs have been compiled by Western Canada Hydraulics Laboratory (1981) and Cammaert *et al.* (1994). General design criteria and related considerations relevant to floating docks

and small craft harbour facilities have been summarized by Cox (1989), Gaythwaite (1990), the ASCE Ports and Harbors Task Committee (1994), and Tsinker (1995).

1.2.1 Hydrodynamic Analysis

Regular Waves

Numerical models of floating breakwater response to waves have originated largely from ship hydrodynamics, and reference may be made to Wehausen (1971) and Newman (1977) for the theoretical approaches generally used. In a linear analysis, the structure is assumed rigid and to oscillate harmonically in six degrees of freedom, corresponding to three translational (surge, sway and heave) and three rotational (roll, pitch and yaw) motions. The fluid is assumed incompressible and inviscid, and the flow irrotational, so that potential theory is used to solve for the fluid flow associated with a specified incident wave motion. The velocity potential relating to the flow is considered to be made up of components due to the incident waves, scattered waves associated with the structure in its equilibrium position, and forced waves associated with each mode of motion of the floating structure. If the floating breakwater is reasonably long, a two-dimensional analysis may be carried out in place of a three-dimensional analysis. General discussions of potential theory and the hydrodynamic analysis of floating breakwaters are presented in the texts by Sarpkaya and Isaacson (1981), Chakrabarti (1987), Faltinsen (1990) and Rahman (1994).

The hydrodynamic analysis is generally carried out numerically by a wave source method. In a linear analysis, the wave diffraction problem (wave interactions with a fixed structure) and the wave radiation problem (waves generated by an oscillating structure) are uncoupled and may be solved separately. The resulting hydrodynamic forces may then be applied to equations of motion of the structure to determine its motion. As examples of this general approach, Adee and Martin (1974) developed a two-dimensional model of a rectangular section breakwater; Hanif (1983) presented an application of the finite element method to analyze hydrodynamic properties of a floating breakwater subject to heaving and swaying

motions; Drimer *et al.* (1992) described an analytical solution for a simplified case of a box-type floating breakwater; and Isaacson (1993b) presented hydrodynamic coefficients including added mass and damping coefficients for a series of rectangular breakwaters.

Oblique Waves and Mach-Stem Effects

The incident wave direction with respect to the breakwater orientation has a significant influence on a breakwater's performance. In this context, the case of oblique wave interaction with a long horizontal cylinder has been investigated numerically by Bai (1975), Garrison (1984), and Isaacson and Nwogu (1987). Isaacson and Nwogu (1987) also presented a reduction factor for wave exciting force, to account for wave direction as well as finite length of the breakwater.

For waves which are so oblique as to have a propagation direction almost parallel to the breakwater axis, the phenomena of Mach-stem reflection may occur. Using an analogy to gas dynamics and on the basis of acoustic principles, Wiegel (1964a and b) has described Mach reflections. Berger and Kohlhase (1976) conducted experiments to study the stem effects due to wave interaction with a fixed vertical wall. Results obtained indicated that the wave height measured very close to the wall was more than double the incident wave height. They pointed out that this effect should be interpreted as a diffraction problem. Melville (1980) experimentally investigated various features relating to Mach reflection of a solitary wave by a vertical wall and reported critical angles of incidence at which Mach reflection is replaced by regular reflection. Yoon and Liu (1989) presented a numerical study relating to the formation of stem waves along a breakwater and discussed the relation between incident and stem wave characteristics.

Wave Interaction with Multiple Cylinders

Studies of wave interactions with multiple horizontal cylinders first originated from the hydrodynamics of catamarans and other multi-hull vessels. These include Wang and Wahab (1971), Ohkusu (1974), and Wang (1981). The hydrodynamic interference arising from multiple two-dimensional horizontal cylinders interacting with obliquely incident linear

monochromatic waves has been studied by Leonard *et al.* (1983). Recently, Valioulis (1990) developed a mathematical model to compute the motion response and wave attenuation of two linked and moored breakwaters. Chen and Mahrenholtz (1992) applied the boundary integral method to calculate the radiated waves generated by twin bodies oscillating in water. Carvalho and Mesquita (1994) studied the hydrodynamic interactions of closely spaced two-dimensional floating bodies by also employing the boundary element method and presented numerical results of body responses and exciting forces.

Short-Crested Waves

In most cases, floating breakwaters are subjected to the actions of local wind-generated waves which are essentially random and short-crested, and this short-crestedness leads to lower wave loads than would otherwise occur. Hartz and Georgiadis (1982) presented a finite element response model of a continuous floating structure subjected to short-crested waves and compared the results with experimental measurements of the dynamic response. Hutchinson (1984) presented a frequency domain technique to determine the responses of a floating breakwater in all six degrees-of-freedom motions as well as the resulting nodal shear and bending moments induced in the body of the breakwater.

1.2.2 Mooring Analysis

Apart from a hydrodynamic analysis, the design of moored floating breakwaters also requires a mooring analysis in order to determine motion responses and mooring system loads. Mooring systems are generally made up of uniform cables with or without concentrated loads at various points along each cable. The behaviour of most cables tends to be planar (two-dimensional) because of the predominance of dead weight loading on flexible cable segments. A mooring analysis is generally comprised of three steps: (a) the calculation of initial line configuration and equilibrium, (b) a static analysis, and (c) a dynamic analysis. Leonard (1988) has presented the elastic catenary equations and describes a procedure to arrive at principal loads in the initial equilibrium configuration due to the self weight of the

line. A static analysis is carried out to obtain the steady offset of the floating breakwater due to wave, current and wind loads. This involves the development of a stiffness model of the mooring system about the initial configuration. Various approximate expressions for stiffness are given in Faltinsen (1990). The dynamic response of the breakwater system about its steady displaced position is computed to provide the extreme displacements of the mooring line attachment points, maximum anchor forces and mooring line tensions. A detailed review of the dynamics of mooring lines with an emphasis on the mechanism of dynamic amplification is given by Triantafyllou (1994).

Several studies have reported on different analysis procedures to obtain the dynamic response of a breakwater. Yamamoto and Takahashi (1974) carried out an experimental study to investigate the influence of various design parameters such as cross-sectional area, moment of inertia and mooring arrangements on the performance of a floating breakwater. Yamamoto *et al.* (1982) developed a two-dimensional model of a floating body with linear elastic springs. Yamamato (1982) then applied this model to study floating breakwater response to regular and irregular waves. Skop (1988) solved for the dynamic response of the system by assuming the mooring lines as inertialess springs. de Kat and Dercksen (1989) and Patel (1989) reported that the effects of wave and current loading on mooring lines may be negligible for situations relating to floating breakwaters, for which dynamic amplification in the mooring line is small.

1.2.3 Experimental Studies

Field data relating to breakwater motions and wave heights in the vicinity of the structure generally compare well with the results of laboratory tests and numerical models (see, for example, Adee (1976), Miller and Christensen (1984), Nece and Skjelbreia (1984), Nelson and Broderick (1984)). Bando and Sonu (1987) reviewed a large number of existing state-of-the-art numerical models for the purpose of selecting an efficient model to be used for routine analysis of wave attenuation and mooring forces associated with a floating breakwater.

Isaacson *et al.* (1994) carried out physical and numerical modelling of a circular cross-section floating breakwater subjected to normal and oblique waves, and reported the variation of transmission coefficient, breakwater motions and mooring line forces as functions of various breakwater parameters. Jamieson *et al.* (1994) conducted wave flume tests of scaled models of two steel pontoon floating breakwaters subjected to regular waves to quantify the efficiency of pontoon configuration.

1.3 Objectives of the Present Investigation

The primary objective of the present thesis is to improve the understanding of the hydrodynamic and response characteristics of twin-pontoon floating breakwaters. Specific goals of the study are:

(a) to develop a numerical model for predicting the performance of a twin-pontoon floating breakwater subject to specified wave conditions,

(b) to validate the numerical model with respect to two-dimensional laboratory tests,

(c) to obtain suitable hydrodynamic coefficients relating to different configurations of twin-pontoon floating breakwaters, and

(d) to assess the influence of various design parameters such as breakwater beam, draft, and pontoon diameter, on the breakwater performance.

For the numerical model, the corresponding linear diffraction/radiation problem assuming small amplitude incident waves is treated in combination with a mooring analysis and a solution of the breakwater's equations of motion. The hydrodynamic interference arising from two-dimensional structures having two-distinct wetted portions interacting with linear monochromatic obliquely incident waves are treated. Laboratory studies of twin-pontoon rectangular and circular section model breakwaters subjected to regular normally incident (two-dimensional) waves are carried out for different combinations of wave characteristics and breakwater configurations to obtain transmission and reflection coefficients, mooring forces and breakwater motions.

2. Theoretical Approach

2.1 Breakwater Configuration

In the present study, a twin-pontoon moored floating breakwater with either rectangular and circular section pontoons is taken to be the prototype structure. A moored breakwater structure located at Comox, B.C., (Rowland (1995)) provides a primary example of such a floating breakwater which is the focus of the present study. A view of the breakwater is shown in Fig. 2.1. The breakwater consists of two circular-section pontoon units rigidly connected to each other. The breakwater structure is typically comprised of two simple fabricated units: a pontoon sub-unit and a dog bone sub-unit. Each unit is relatively small and light as compared to a single-pontoon floating breakwater, and this allows flexibility in the selection of fabrication sites. The prototype conditions relating to the breakwater correspond to a diameter, D (= a) = 1.05 m, an overall beam, B = 8.0 m, a water depth, d = 10.0 m and a wave period range, T = 1.5 - 4.5 sec. Also, the mooring lines are made up of anchor chain spaced 20.0 m apart at attachment points and with a horizontal span of 60.0 m under equilibrium conditions. The overall length of the breakwater is 100.0 m.

The breakwater pontoons are usually water ballasted such that the structure has the required draft and inertial properties. The interior of the pontoons is also fitted with foam billets to provide the necessary buoyancy and to limit sloshing of the ballast water within the pontoon. The choice of a suitable draft for a given location is governed by a balance between excessive overtopping caused by too deep a draft, and the advantages of added inertia at deeper drafts. Figure 2.2 indicates the variation of the normalized buoyancy force $F'_b = F_b/(\rho g \pi D^2/4)$, as a function of relative draft, $h' = h/(D/2)$, where ρ is the density of water, g is the gravitational constant, and D is the diameter, for the case of a circular pontoon section. The variation of normalized waterplane beam $B' = B_w/(D/2)$, as a function of relative draft is superposed on this plot. In the case of rectangular section pontoons of a given aspect

ratio, the waterplane beam remains constant for all drafts and the buoyancy force is a linear function of the draft.

2.2 Design Variables and Dimensional Analysis

Figure 2.3 provides a definition sketch of the problem under consideration. It is convenient to consider the design parameters relating to a moored floating breakwater by considering first a simple freely floating body interacting with a regular wave train approaching at an angle to the longitudinal axis of the body; and subsequently considering the case of restrained structures, for which additional variables relating to mooring cables must be included.

2.2.1 Freely Floating Breakwater

Design criteria for a freely floating breakwater involve dependent parameters which may be broadly taken to include (i) wave characteristics in the vicinity of the breakwater, and (ii) the motions of the breakwater. Thus, for the two-dimensional case of an infinitely long breakwater subjected to a regular oblique wave train, the following dependent variables are of interest:

H_T transmitted wave height;

H_R reflected wave height;

ξ_i breakwater motions: i = 1, sway; i = 2, heave; i = 3, roll.

A list of independent parameters that may influence the breakwater performance for this case is given below:

H incident wave height;

T wave period;

d water depth;

β incident wave direction;

ρ water density;

ν kinematic viscosity;

g gravitational constant;

a characteristic section dimension: diameter of a circular section pontoon, or width of a rectangular section pontoon;

h pontoon draft;

B overall breakwater beam;

z_G centre of gravity of pontoon section;

r_G radius of gyration for roll;

Other variables such as the mass per unit length of the breakwater, or the gap between pontoons, may readily be expressed in terms of the above variables and hence have been excluded.

There are a total of 12 independent variables, in which water density ρ, may be eliminated for the case of a freely floating body. Thus, on the basis of a 2 unit system (L and T), 9 dimensional groups influencing each dependent variable can be formed. A dimensional analysis for the transmission coefficient, K_T, thus provides, for example, the following relationship:

$$K_T = \left(\frac{a}{L}, \frac{B}{a}, \frac{h}{a}, \frac{z_G}{a}, \frac{r_G}{a}, \frac{a}{d}, \frac{H}{L}, \mathrm{Re}, \beta \right) \tag{2.1}$$

The significance of the various dimensionless parameters listed in Eq. 2.1 is as follows: a/L is a ratio of characteristic pontoon size to wave length; B/a is indicative of gap size to pontoon size ratio; h/a represents the relative draft of the breakwater; a/d represents the influence of water depth and may become important in shallower water; H/L is the wave steepness and is indicative of nonlinear effects; and Re is a Reynolds number, which accounts for viscous effects and may be defined as:

$$\mathrm{Re} = \frac{U_m a}{\nu} = \left(\frac{\pi H}{T} \frac{1}{\tanh(kd)} \right) \frac{a}{\nu} \tag{2.2}$$

where, U_m is the horizontal water particle velocity amplitude at the still water level, given by linear wave theory.

When wave diffraction effects are important in modelling the breakwater, appreciable flow separation should not occur and the effect of viscosity should be confined to the boundary layers on the body. It is then appropriate to treat the flow as irrotational and so attempt to solve the problem on the basis of potential theory. In view of this, the characteristic Reynolds number may then generally be omitted from Eq. 2.1. In addition, if the wave steepeness is small, it is then appropriate to adopt a linearizing approximation such that H/L may be also omitted from Eq. 2.1. In fact, the possible significance of flow separation effects is often taken to be indicated by a characteristic Keulegan-Carpenter number K, which may be defined as:

$$K = \frac{U_m T}{a} = \left(\frac{\pi H}{T} \frac{1}{\tanh(kd)} \right) \frac{T}{a} \tag{2.3}$$

Finally, for relatively deep water a/d may be omitted and in the two-dimensional case of normally incident waves, β may be omitted from Eq. 2.1. Thus Eq. 2.1 is approximated as:

$$K_T = \left(\frac{a}{L}, \frac{B}{a}, \frac{h}{a}, \frac{z_G}{a}, \frac{r_G}{a} \right) \tag{2.4}$$

The dependent parameters relating to reflected and transmitted waves, and the three component motions may readily be used to develop dimensionless parameters describing the breakwater performance. Relevant dimensionless groups of the dependent parameters include the following:

$$\begin{aligned} K_R &= \frac{H_R}{H} \\ K_T &= \frac{H_T}{H} \end{aligned} \tag{2.5}$$

$$\xi'_i = \begin{cases} \dfrac{\xi_i}{H/2} & \text{for } i = 1 \text{ (sway)},\ i = 2 \text{ (heave)} \\ \dfrac{\xi_i a}{H/2} & \text{for } i = 3 \text{ (roll)} \end{cases} \tag{2.6}$$

where $\hat{\xi}_i$ is the amplitude of the oscillatory motion of the breakwater in sway, heave and roll modes of motion.

2.2.2 Moored Breakwater

In the case of a moored breakwater, a number of additional parameters must be specified in order to describe the performance of a breakwater restrained by mooring lines. These are (see Fig. 2.3):

- Z anchor depth relative to connection points;
- S unstretched length of mooring line;
- X horizontal span of mooring line;
- q' mooring line submerged weight per unit length and per unit line spacing;
- E' mooring line elasticity per unit length and per unit line spacing;

The mooring line pretension could be used as an alternative independent variable in place of the unstretched cable length, S for the case of braided nylon rope. However, it is observed that initial line pretension may be lost due to permanent elongation of the line and hence is not considered in this study. In addition, the location of mooring attachment points to the breakwater may also have an influence on the breakwater's response. Since twin-pontoon structures have large roll stability, the influence of the location of the mooring cable attachment points is considered to be negligible, and is not included as an independent parameter.

Combining these independent variables with those of an unrestrained body, a dimensional analysis yields the following extension to Eq. 2.4:

$$K_T = \left(\frac{a}{L}, \frac{B}{a}, \frac{h}{a}, \frac{z_G}{a}, \frac{r_G}{a}, \frac{q'}{\rho g a}, \frac{E'}{\rho g a^2}, \frac{Z}{a}, \frac{X}{a}, \frac{S}{a} \right) \tag{2.7}$$

where $q'/\rho ga$ is the relative submerged weight of the mooring lines, $E'/\rho ga^2$ is the relative elasticity of the mooring lines, and Z/X and S/Z are dimensionless parameters relating to

mooring line slope and slackness respectively. The horizontal spacing between the mooring lines, λ, is excluded since q' and E' are used and are defined so as to account for λ.

In the case of a moored breakwater, the upwave and downwave mooring line tensions, denoted by T_1 and T_2 respectively, become additional dependent variables. These may refer to the points of attachment to the breakwater or to the anchors. The relevant additional dimensionless group may be written as:

$$T'_j = \frac{\hat{T}_j}{\rho g a H \lambda} \qquad \text{for } j = 1 \text{ (upwave)}, j = 2 \text{ (downwave)} \tag{2.8}$$

where $\hat{T}_j$ is the maximum mooring line tension.

On the basis of Eq. 2.3 which incorporated Froude's scaling law, the same length scale factors K_l applies to all the relevant length variables and the scale factors of the other variables may be expressed in terms of K_l as follows:

$$\frac{T_m}{T_p} = \sqrt{K_l}$$

$$\frac{q'_m}{q'_p} = \frac{E'_m}{E'_p} = K_l^2 \tag{2.9}$$

The subscripts m and p denote variables corresponding to the model and prototype respectively. Equation 2.7 can be used to develop relationships with respect to other dependent variables.

2.3 Hydrodynamic Analysis

The numerical prediction of the breakwater response to a specified wave train is now considered. The approach described provides a summary of the conventional treatment of linear diffraction theory by the boundary element method (e.g. Sarpkaya and Isaacson (1981), and Isaacson and Nwogu (1987)). Thus, the interaction of a regular oblique wave train with an infinitely long semi-immersed horizontal rigid cylinder is considered. The cylinder is assumed to be large enough so as to diffract the incident flow field.

Flow separation effects are important in certain circumstances, such as for a structure which possesses sharp corners. A fundamental analysis of the forces induced by flow separation and vortex shedding off a sharp edge has been given by Graham (1980) and Downie *et al.* (1993). Similarly, a numerical solution for potential flows including the effects of vortex shedding is given by Wong and Calisal (1993). However, in practice, for large structures, flow separation effects have been assumed not to be significant since the amplitude of water particle motions relative to the characteristic structure dimension is sufficiently small for flow separation not to occur in most cases. Thus, effects of viscosity are assumed confined to a thin boundary layer on the body surface.

The Keulegan-Carpenter number, K, given by Eq. 2.3 provides an indication of the importance of flow separation effects. For the range of frequencies used in this study with $K < 2$, flow separation associated with circular sections should be negligible, whereas for the case of rectangular cylinder sections, vortices are usually formed at the sharp corners, which may lead to localized flow separation effects (Sarpkaya and Isaacson, 1981). However, despite the formation of the vortices, earlier studies indicate good agreement between potential flow theory and experimental results for such cylinders, provided an empirical damping coefficient is then used in the equations of motion of the structure. The fluid flow can thus be considered to be irrotational and the problem is solved using potential flow theory.

A monochromatic linear wave train of height H and angular frequency ω propagates in water of constant depth d, and is obliquely incident upon an infinitely long structure. The direction of wave propagation makes an angle β with the x axis as shown in Fig. 2.3. A right-handed Cartesian coordinate system (x,y,z) is employed in which z is measured upwards from the still water level and the y axis is parallel to the longitudinal axis of the cylinder. The structure is taken to respond at the same frequency ω, with three degrees-of-freedom; sway, heave and roll.

Ideal fluid, irrotational flow boundary value problems may be posed corresponding to (i) the scattering of waves obliquely incident upon the fixed body, and (ii) the wave radiation caused by the forced sway, heave and roll oscillations of the body in otherwise still water. The scattering problem leads to exciting forces proportional to the incident wave height, whereas the radiation problem gives rise to hydrodynamic forces which are proportional to the component breakwater motions, and which may be expressed in terms of added masses and damping coefficients. The wave height and oscillatory motions of the body are taken to be small so that the complete problem of wave interaction with a floating cylinder can be represented by a linear superposition of the diffraction and forced motion problems. The oscillations are assumed to vary sinusoidally in both time and space along the y axis.

In the following sections, the wave diffraction and radiation boundary value problems, and the forced response problem are treated separately.

2.3.1 Wave Diffraction Problem

First, the case of an oblique wave train interacting with a fixed body is considered. An incident wave train which propagates at an oblique angle β with respect to x axis may be represented by a velocity potential given by:

$$\Phi_0(x,y,z;t) = \mathrm{Re}\left[-\frac{igH}{2\omega}\phi_0(x,z)\exp\{i(ky\sin\beta-\omega t)\}\right] \tag{2.10}$$

where Re[ ] denotes the real part of a complex variable, $i = \sqrt{-1}$, g is the gravitational constant, k is the wave number, given by $k = 2\pi/L$, L is the wave length, t is time, and ϕ_0 is a two-dimensional potential function given as:

$$\phi_0(x,z) = \frac{\cosh[k(d+z)]}{\sinh(kd)}\exp\{i(kx\cos\beta)\} \tag{2.11}$$

The wave number, k is related to angular frequency, ω by the linear dispersion relationship:

$$\omega^2 = gk\tanh(kd) \tag{2.12}$$

The linear wave diffraction problem is described by a scattered velocity potential, denoted Φ_4, which varies sinusoidally in time and along the y axis according to:

$$\Phi_4(x,y,z;t) = \mathrm{Re}\left[-\frac{igH}{2\omega}\phi_4(x,z)\exp\{i(ky\sin\beta-\omega t)\}\right] \tag{2.13}$$

where $\phi_4(x,z)$ is an initially unknown scattered velocity potential function. The scattered velocity potential satisfies the Laplace equation given by:

$$\nabla^2\Phi_4 = \left[\frac{\partial^2}{\partial x^2}+\frac{\partial^2}{\partial y^2}+\frac{\partial^2}{\partial z^2}\right]\Phi_4 = 0 \qquad \text{within the fluid} \tag{2.14}$$

In fact, the boundary value problem is considered in terms of dimensionless parameters by normalizing all the variables with respect to ρ, g, and a as necessary. Substituting Eq. 2.13 into Eq. 2.14, the three-dimensional Laplace equation reduces to the two-dimensional modified Helmholtz equation:

$$\frac{\partial^2\phi_4}{\partial x^2}+\frac{\partial^2\phi_4}{\partial z^2}-\nu^2\phi_4 = 0 \qquad \text{in fluid domain } \Omega \tag{2.15}$$

where $\nu = ka\sin\beta$. ϕ_4 must satisfy various boundary conditions on the free surface, seabed, body surface and in the far field. These are given respectively as (Isaacson and Nwogu (1987)):

$$\frac{\partial\phi_4}{\partial z}-\mu\phi_4 = 0 \qquad \text{at } z = 0 \tag{2.16}$$

$$\frac{\partial\phi_4}{\partial z} = 0 \qquad \text{at } z = -d \tag{2.17}$$

$$\frac{\partial\phi_4}{\partial n}+\frac{\partial\phi_0}{\partial n} = 0 \qquad \text{on } S_B \tag{2.18}$$

$$\frac{\partial\phi_4}{\partial x}\mp ik\cos\beta\phi_4 = 0 \qquad \text{at } x = \pm\infty \tag{2.19}$$

where $\mu = \omega^2 a/g$, and n is the unit normal vector on the cylinder surface S_B and directed out of the fluid.

2.3.2 Wave Radiation Problem

The radiation problem corresponding to an infinitely long flexible cylinder oscillating in sway, heave and roll, in turn is now considered. Each mode of motion is taken to be periodic in time as well as along the axis of the cylinder. The displacement or rotation in the k-th mode is given by:

$$\chi_k(x,y,z;t) = \mathrm{Re}[\xi_k(x,z)\exp\{-i(\nu y - \omega t)\}] \tag{2.20}$$

where ξ_k is the complex amplitude of oscillation of the cylinder with k = 1, 2 and 3 corresponding to the sway, heave and roll modes respectively. Each wave radiation problem may now be described by a radiation velocity potential as:

$$\Phi_k(x,y,z;t) = \mathrm{Re}[-i\omega a^2 \xi_k(x,z)\phi_k(x,z)\exp\{i(\nu y - \omega t)\}] \tag{2.21}$$

The linear radiation boundary value problem is defined similar to the diffraction problem by various boundary conditions on the free surface, seabed, body surface and in the far field. These are given respectively as (Isaacson and Nwogu (1987)):

$$\frac{\partial^2\phi_k}{\partial x^2} + \frac{\partial^2\phi_k}{\partial z^2} - \nu^2\phi_k = 0 \qquad \text{within the fluid} \tag{2.22}$$

$$\frac{\partial\phi_k}{\partial z} - \mu\phi_k = 0 \qquad \text{at } z = 0 \tag{2.23}$$

$$\frac{\partial\phi_k}{\partial z} = 0 \qquad \text{at } z = -d \tag{2.24}$$

$$\frac{\partial\phi_k}{\partial n} - n_k = 0 \qquad \text{on } S_B \tag{2.25}$$

$$\frac{\partial\phi_k}{\partial x} \mp ik\cos\beta\phi_k = 0 \qquad \text{at } x = \pm\infty \tag{2.26}$$

where

$$\begin{aligned} n_1 &= n_x \\ n_2 &= n_z \\ n_3 &= (z-e)n_x - xn_z \end{aligned} \tag{2.27}$$

in which n_x and n_z are the direction cosines of the unit normal vector $\bar{n}$ on the wetted body surface and (0,e) denotes the point about which the roll motion is prescribed. In the present study, the motion is prescribed about the origin, and thus e is taken to be zero. The boundary value problem for the radiation problem is similar to that of the scattered problem, except that the body boundary condition in Eq. 2.25 is applied such that the normal velocity of the fluid at the immersed body surface is equal to the normal velocity of the body surface itself. The generalized radiation problem statement in Eqs. 2.22 - 2.26 describes a flexural wave that travels along the surface of the body and generates an oblique wave in the water.

If $\beta = 0^\circ$, corresponding to normally incident waves, the radiation boundary condition reduces to the two-dimensional problem in the vertical x-z plane. For the special case $\beta = 90^\circ$, which corresponds to a head sea, the radiation condition reduces to that of a rigid wall boundary.

2.3.3 Body Response Problem

Since the incident wave amplitude, and hence the resulting responses, are assumed to be small, the velocity potential for the wave field may be expressed by a linear superposition of the incident, scattered and radiation potentials. The total potential is thus expressed as:

$$\Phi(x,y,z;t) = \mathrm{Re}\left[\left\{-\frac{igH}{2\omega}(\phi_0 + \phi_4 + \sum_{k=1}^{3}\xi_k\phi_k)\right\}\exp[i(\nu y - \omega t)]\right] \tag{2.28}$$

The hydrodynamic pressure within the fluid may be expressed in terms of Φ by the linearized Bernoulli equation:

$$p = -\rho\frac{\partial\Phi}{\partial t} = i\omega\rho\Phi \tag{2.29}$$

in which ρ is the fluid density. The hydrodynamic forces on the body can then be obtained by integrating the pressure over the wetted surface of the body S_B. These hydrodynamic forces are usually separated into exciting forces associated with the diffraction problem, and hydrodynamic restoring forces associated with the radiation problem.

Exciting Force

The exiting force per unit length due to the incident and scattered waves is proportional to the wave height and may be expressed by:

$$F_k(y,t) = \frac{1}{2}\rho g H a^m \, \mathrm{Re}\left[\int_{S_B} (\phi_0 + \phi_4) n_k ds\right] \exp\{i(vy - \omega t)\} \tag{2.30}$$

where m = 1 for k = 1, 2 (surge, heave) and m = 2 for k = 3, (roll). Also, F_1 and F_2 denote the sway and heave force components respectively, and F_3 denotes the roll moment about the origin O.

The dimensionless exciting force is thus given by:

$$F_k' = \frac{F_k(y,t)}{\frac{1}{2}\rho g H a^m} = \int_{S_B} (\phi_0 + \phi_4) n_k ds \tag{2.31}$$

Added Mass and Damping Coefficients

Now consider the motion problem where the floating body is forced to oscillate in otherwise still water by a hydrodynamic force obtained as above. These forces are associated with the motions of the cylinder which are proportional to the amplitude of cylinder motion in each direction. The k-th component of force due to the i-th component of motion can be expressed as:

$$F_{ik} = i\omega\rho \, a^m \int_{S_B} \Phi_k n_i \, ds \qquad \text{for i, k = 1,2,3} \tag{2.32}$$

where m = 1 for i = 1, 2 and m = 2 for i = 3. Substituting the expression for Φ_k given in Eq. 2.21 the hydrodynamic force can be rewritten as:

$$F_{ik} = \rho\omega^2 \xi_k a^m \, \mathrm{Re}\left[\int_{S_B} \phi_k n_i ds\right] \exp\{i(vy - \omega t)\} \tag{2.33}$$

in which m = 3 for i = 1, 2 and m = 4 for i = 3. This force can also be expressed in terms of two components; one component in phase with the acceleration $\ddot{\chi}_i$ and the other in phase with the velocity $\dot{\chi}_i$ as:

$$F_{ik} = -\mu_{ik}\ddot{\chi}_i - \lambda_{ik}\dot{\chi}_i \tag{2.34}$$

where μ_{ik} and λ_{ik} are the added mass and damping coefficients respectively. Substituting the time derivatives of the response χ_i, gives

$$F_{ik} = \mathrm{Re}[(\omega^2\mu_{ik} + i\omega\lambda_{ik})\xi_i \exp\{i(vy - \omega t)\}] \tag{2.35}$$

Comparing the expressions for the hydrodynamic forces associated with the motions, the dimensionless added mass and damping coefficients can be given as:

$$\frac{\mu_{ik}}{\rho a^m} = \mathrm{Re}\left[\int_{S_B} \phi_k n_i \, ds\right] \tag{2.36}$$

$$\frac{\lambda_{ik}}{\rho\omega a^m} = \mathrm{Im}\left[\int_{S_B} \phi_k n_i \, ds\right] \tag{2.37}$$

where the constant m = 2 for (i,k) = (1,1) and (2,2), m = 3 for (i,k) = (1,3) and (3,1) and m = 4 for (i,k) = (3,3).

2.3.4 Equations of Motion

The response of the body in waves, which varies sinusoidally with y and t, may now be calculated by solving the equations of motion:

$$\sum_{k=1}^{3}\left[-\omega^2(m_{ik} + \mu_{ik}) - i\omega(\lambda_{ik} + \lambda'_{ii}) + (c_{ik} + c'_{ik})\right]\chi_k = F_i(y,t) \qquad i = 1,2,3 \tag{2.38}$$

in which m_{ik} and c_{ik} are the mass and hydrostatic stiffness coefficients respectively, c'_{ik} are mooring stiffness coefficients, and λ_{ik} are the damping coefficients. Also, λ'_{ii} are viscous damping coefficients. These may be particularly important for resonant roll motions (e.g. Standing (1991)). For the present problem, an empirical relationship is used to calculate the viscous damping coefficients from specified viscous damping ratios ς_i, as $\lambda'_{ii} = 2\varsigma_{ii}\sqrt{c_{ii}(m_{ii}+\mu_{ii})}$. The mooring stiffness coefficients c'_{ik} may be obtained from a separate mooring analysis as outlined in Section 2.4.

The mass matrix is defined as, (Newman, 1977):

$$m_{ik} = \begin{bmatrix} m & 0 & mz_G \\ 0 & m & 0 \\ mz_G & 0 & I_0 \end{bmatrix} \tag{2.39}$$

where m is the mass per unit length of the body, z_G is the z coordinate of the centre of gravity and I_0 is the polar mass moment of inertia about the longitudinal axis per unit length, $I_0 = m(r_G^2+z_G^2)$, in which r_G is the roll radius of gyration of the body.

The hydrostatic stiffness matrix components may be determined by calculating the forces required to restore the body to its equilibrium position for small amplitude displacements; and are given as:

$$c_{ik} = \begin{bmatrix} 0 & 0 & 0 \\ 0 & c_{22} & c_{23} \\ 0 & c_{32} & c_{33} \end{bmatrix} \tag{2.40}$$

For a twin-pontoon breakwater which is symmetrical about the y axis, the stiffness components are defined as:

$$c_{22} = 2\rho g B_w \tag{2.41}$$

$$c_{23} = c_{32} = \rho g B_w x_f \tag{2.42}$$

$$c_{33} = \rho g A[(S_{11}/A) + z_B - z_G) \tag{2.43}$$

in which B_w is the beam of the single pontoon at the waterplane line, x_f is the x coordinate of the centroid of waterplane area, b is the gap between the pontoons, z_B is the z coordinate of the centre of buoyancy, A is the displaced volume per unit length, and S_{11} is the second moment of waterplane area about the y axis per unit length. In fact $S_{11} = B_w^3/12 + Ab^2/4$. Note that static stability in roll requires that c_{33} is positive, which implies that the metacentre $S_{11}/A + z_B$ is higher than the centre of gravity z_G.

Once all the matrix components for any specified wave frequency and direction are known, the equations of motion can readily be solved to obtain the complex motion

amplitudes, ξ_k. These body motions can be nondimensionalized with respect to the incident wave amplitude and hence are given in terms of response amplitude operators (RAO's) defined as:

$$\xi'_k = \begin{cases} \dfrac{|\xi_k|}{H/2} & \text{for } k = 1, 2 \\ \dfrac{a|\xi_k|}{H/2} & \text{for } k = 3 \end{cases} \tag{2.44}$$

2.3.5 Boundary Element Method

A numerical solution of the diffraction/radiation boundary value problem for the case of the twin-pontoon configuration may be obtained by a direct extension of the formulation relating to a single pontoon configuration (Isaacson and Nwogu (1987)). A summary of the method is now given.

Green's Theorem

In the boundary element method, it is convenient to use Green's second identity as the basis for a numerical evaluation of the unknown potentials ϕ_k (k = 1,2,3,4). The Green's second theorem may be applied over the closed surface S containing the fluid region in order to relate the values of the potential $\phi(\mathbf{x})$ at a point $\mathbf{x}$ on the fluid boundary to the remaining boundary values of the potential $\phi(\xi)$ and its normal derivative $\partial\phi(\xi)/\partial n$. This can be expressed as:

$$\phi(\mathbf{x}) = \frac{1}{2\pi}\int_S \left[\phi(\xi)\frac{\partial G}{\partial n}(\mathbf{x};\xi) - \frac{\partial \phi}{\partial n}(\xi)\, G(\mathbf{x};\xi)\right] ds \tag{2.45a}$$

where $G(\mathbf{x},\xi)$ is the Green function satisfying the required boundary conditions, $\mathbf{x}$ is a point located at (x,z) where the potential is to be evaluated, and ξ is the point located at (ξ, ζ) on the closed surface over which the integration is performed. The closed surface S comprises of the immersed body surface S_B, the mean free surface S_F, the radiation surface S_R, and the seabed S_D as shown in Fig. 2.4(a).

When the interior point **x** approaches the boundary from within the fluid, Eq. 2.45a reduces to the following integral equation.

$$\phi(\mathbf{x}) = \frac{1}{\pi}\int_S \left[\phi(\xi)\frac{\partial G}{\partial n}(\mathbf{x};\xi) - \frac{\partial \phi}{\partial n}(\xi)\, G(\mathbf{x};\xi)\right] ds \qquad (2.45b)$$

The Green's theorem which satisfies the modified Helmholz equation (2.15) in an unbounded fluid is singular at the point $\mathbf{x} = \xi$ and is given by, $G(\mathbf{x};\xi) = -K_0(\nu r)$, where K_0 denotes the modified Bessel function of zero order, r is the distance between the points **x** and ξ, which is given by $r = |\xi - \mathbf{x}| = \sqrt{(\xi - x)^2 + (\zeta - z)^2}$. It may be noted that the function $K_0(x) \approx -\ln x$ as $x \to 0$. The Green's function, which satisfies the two-dimensional Laplace equation, obtained as $\beta \to 0°$, is given by:

$$G(\mathbf{x};\xi) = -\ln(r) \qquad (2.46a)$$

In the present solution, the seabed is assumed to be horizontal. It is computationally efficient to exclude the seabed from the closed surface S and thus select a Green's function, which takes into account symmetry about the seabed (Fig. 2.4(a)). This is:

$$G(\mathbf{x};\xi) = -\left[K_0(\nu r) + K_0(\nu r')\right] \qquad (2.46b)$$

and r' is the distance between points **x** and ξ' given respectively by the expression

$$r' = |\xi' - \mathbf{x}| = \sqrt{(\xi - x)^2 + (\zeta + 2d + z)^2} \qquad (2.47)$$

in which $\xi' = (\xi, -(\zeta + 2d))$.

The first term of the modified Green's function is singular at point $\mathbf{x} = \xi$ and therefore special consideration must be given to evaluating the integrand at that point. The integral equation, Eq. 2.45b is now evaluated numerically using the procedure described below.

Numerical Procedure

In order to evaluate the integral equation, Eq. 2.45b, the boundary S is divided into N segments with the values of ϕ or $\partial\phi/\partial n$ considered constant over each segment and equal to

the value at the midpoint of the segment (see Fig. 2.4(b)). The continuous integral equation, Eq. 2.45b, is therefore replaced by a discrete summation as:

$$\phi_k(x_i) = \frac{1}{\pi}\sum_{j=1}^{N}\left[\phi_k(x_j)\int_{\Delta S_j}\frac{\partial G(x_i;x_j)}{\partial n}ds - \frac{\partial \phi_k(x_j)}{\partial n}\int_{\Delta S_j} G(x_i;x_j)ds\right] \qquad k = 1,2,3,4 \qquad (2.48)$$

where the summation is performed in a counter-clockwise manner around the boundary. This corresponds to four sets of equations:

$$\sum_{j=1}^{N}\left[\left(a_{ij}+\delta_{ij}\right)\phi_j^{(k)} + b_{ij}\frac{\partial \phi_j^{(k)}}{\partial n}\right] = 0 \qquad k = 1,2,3,4 \qquad (2.49)$$

where δ_{ij} is the Kronecker delta function given by:

$$\delta_{ij} = \begin{cases} 1 & \text{for } i = j \\ 0 & \text{for } i \neq j \end{cases}$$

The coefficients a_{ij} and b_{ij} are defined respectively as

$$a_{ij} = \frac{1}{\pi}\int_{\Delta S_j}\frac{\partial}{\partial n}\left[K_0(\nu r_{ij}) + K_0(\nu r'_{ij})\right]ds \qquad (2.50)$$

$$b_{ij} = -\frac{1}{\pi}\int_{\Delta S_j}\left[K_0(\nu r_{ij}) + K_0(\nu r'_{ij})\right]ds \qquad (2.51)$$

where r_{ij} and r'_{ij} are given as:

$$r_{ij} = \sqrt{\left(x_j - x_i\right)^2 + \left(z_j - z_i\right)^2}$$

$$r'_{ij} = \sqrt{\left(x_j - x_i\right)^2 + \left(z_j + 2d + z_i\right)^2} \qquad (2.52)$$

and the points (x_i,z_i) and (x_j,z_j) correspond to the midpoint of each segment. The gradient of Green's function $\partial G/\partial n$ may be expressed in terms of known values as:

$$\left.\frac{\partial G}{\partial n}\right|_{(\bar{x}_i,\bar{x}_j)} = \frac{\partial G}{\partial r}\frac{\partial r}{\partial n} + \frac{\partial G}{\partial r'}\frac{\partial r'}{\partial n} \qquad (2.53)$$

in which the derivative of Green's function with respect to r is given by:

$$\frac{\partial}{\partial r}K_0(\nu r) = -\nu K_1(\nu r) \tag{2.54}$$

where K_1 is the modified Bessel function of order one. The derivative of radial distance r with respect to normal n is evaluated by knowing the included angle γ, between the line connecting the points **x** and ξ, and the normal at ξ. Similarly, the derivative of radial distance r' with respect to normal n is evaluated by knowing the included angle γ' between the line connecting the points **x** and ξ', and normal at ξ' (see Fig. 2.4 (c)).

As the values of ΔS_j in Eqs. 2.50 and 2.51 are generally small, the integrals in these equations can be approximated by assuming a constant value for Green's function over each segment, taken to be the value at the midpoint. For $i \neq j$, the expressions for a_{ij} and b_{ij} therefore become:

$$\begin{aligned} a_{ij} &= -\nu\frac{K_1(\nu r_{ij})}{\pi r_{ij}}\left[(x_j - x_i)\Delta z_j - (z_j - z_i)\Delta x_j\right] \\ &\quad -\nu\frac{K_1(\nu r'_{ij})}{\pi r'_{ij}}\left[(x_j - x_i)\Delta z_j - (z_j + 2d + z_i)\Delta x_j\right] \\ b_{ij} &= -\frac{1}{\pi}\left[K_0(\nu r_{ij}) + K_0(\nu r'_{ij})\right]\Delta S \end{aligned} \tag{2.55}$$

where $\Delta z_j = z_{j+1} - z_j$, $\Delta x_j = x_{j+1} - x_j$ and $\Delta S_j = \sqrt{(\Delta z_j)^2 + (\Delta x_j)^2}$.

Singularities

The Green's function approximation used in Eq. 2.45b is singular at the point $\mathbf{x} = \xi$ and thus special care is required at these points. Physically, the singularities occur in the boundary integral process when the point of interest coincides with the point over which the integration is performed. These points occur in the numerical algorithm only when i = j. At a singular point, the numerical difficulty arises from the fact that the Bessel function $K_0(\nu r)$ approaches infinity as argument νr approaches zero. This can be treated by using an approximate small-argument expression for K_0 (e.g. Abramowitz and Stegun (1964)):

$$K_0(\nu r) \approx -\left[\ln\left(\frac{\nu r}{2}\right)+\gamma\right] \qquad \text{as } \nu r \to 0 \qquad (2.56)$$

where γ is Euler's constant. This provides expressions for the diagonal coefficients a_{ii} and b_{ii} as:

$$a_{ii} = \frac{\nu}{\pi}K_1\left[2\nu(d+z_i)\right]\Delta x_i$$

$$b_{ii} = \frac{\Delta S_i}{\pi}\left[\ln\left(\frac{\nu\Delta S_i}{4}\right)+\gamma-1-K_0\left[2\nu(d+z_i)\right]\right] \qquad (2.57)$$

The expressions involving $K_0(\nu r')$ do not present a difficulty since r' is never zero. Once the coefficients a_{ij} and b_{ij} are determined, N equations can be written relating the N values, each of ϕ and $\partial\phi/\partial n$ at the segment centres along the surface $S_B + S_F + S_R$.

Applying the appropriate boundary conditions over the various surfaces thus leads to a total of 2N equations needed to solve for the 2N values of ϕ or $\partial\phi/\partial n$. The resulting equations are solved using a complex matrix inversion technique to determine the values of ϕ or $\partial\phi/\partial n$.

2.3.6 Transmission and Reflection Coefficients

The transmission and reflection coefficients, which are indicative of the performance of the breakwater, are obtained by computing the wave amplitudes at the radiation boundary. In a numerical approximation, the radiation boundary is truncated at a finite distance, X_R from the origin, at which the evanescent modes due to the presence of the body are assumed to have decayed sufficiently so as to be negligible. These wave amplitudes are due to (i) the oscillations of the cylinder in its three modes, and (ii) the reflection and transmission of the incident wave train by a fixed body. Therefore, by knowing the relationship of wave amplitude with scattered and radiated velocity potentials, the reflection and transmission coefficients can be found by the following:

$$K_R = \left|\phi_4(-X_R,0)+\sum_{k=1}^{3}\zeta_k\xi'_k(\omega,\beta)\right| \qquad (2.58)$$

$$K_T = \left| \phi_0(X_R,0) + \phi_4(X_R,0) + \sum_{k=1}^{3} \zeta_k \xi'_k(\omega,\beta) \right| \tag{2.59}$$

where $|\zeta_k|$ is the wave amplitude given as:

$$|\zeta_k| = \frac{|\eta_k|}{|a\xi_k|} = \frac{\omega^2 a}{g} |\phi_k(x,0)| \qquad \text{at } x = \pm X_R \tag{2.60}$$

and ξ_k are the complex amplitudes of body oscillation.

The incident wave energy flux is partly reflected from the body and partly transmitted to the downwave side of the body and part dissipated. The diffraction solution neglects any such energy losses. More generally, therefore, it is necessary to define an energy dissipation coefficient K_D, which corresponds to the portion of incident wave energy flux that is dissipated. Since energy flux is proportional to the square of the wave heights, a consideration of energy balance leads to:

$$K_T^2 + K_R^2 + K_D = 1 \tag{2.61}$$

2.3.7 Wave Drift Force

Apart from the oscillatory wave forces exerted on the body, the body also experiences a second-order wave force, termed wave drift force, which is proportional to square of the wave height. In the case of regular waves, the drift force is obtained by averaging the contributions to the second order force over a complete wave cycle (Longuet-Higgins (1977)). For the case of a long horizontal cylindrical body, the wave drift force F_d per unit length in a dimensionless form can be expressed directly in terms of the transmission coefficient determined in Eq. 2.59 as:

$$F'_d = \frac{F_d}{\frac{1}{4}\rho g H^2} = \frac{1}{2}\left[1 + \frac{2kd}{\sinh(2kd)}\right](1 - K_T^2)\cos\beta \tag{3.62}$$

2.4 Mooring Analysis

A floating breakwater generally requires some form of mooring or restraint system to maintain its position and limit excursions within certain operational constraints. This may generally be provided by piles or by a mooring line system. Only the latter case is considered here. The behaviour of the mooring line influences the response of the breakwater to environmental loads and generally resembles that of a nonlinear spring. Thus, the hydrodynamic analysis should be carried out in conjunction with a mooring analysis in order to determine the motions of the breakwater.

A mooring system consists of a number of cables arrayed around the structure. Either uniform lines or combinations of chain and wire rope or synthetic line are commonly used. In some applications, floats or clumped weights may also be attached to the mooring lines. The rope may be composed of either steel or synthetic fibres. Chain is generally taken to be inextensible, while rope is elastic with nonlinear stiffness characteristics. Elastic properties of mooring lines have been described by Wilson, (1967) and Flory *et al.* (1992).

The analysis of the mooring line system is generally carried out in three component steps as illustrated schematically in Fig. 2.5: (i) the calculation of the initial equilibrium of the mooring system, including mooring line tensions and configurations; (ii) a static analysis to determine the displacement of the structure due to the steady loads associated with current drag and the mean wave drift force; and (iii) a dynamic analysis to include the effects of oscillatory wave forces and a slowly varying wave drift force on the maximum mooring line tensions and anchor loads. These steps are discussed in turn below.

2.4.1 Equilibrium Configuration

The first step in the mooring analysis involves the calculation of the equilibrium configuration of the mooring system. The principal loads are due to the self weight of the mooring lines, and the analysis of one cable is usually based on the equations for an elastic catenary (e.g. Leonard *et al.* (1988), and Wren *et al.* (1989)).

The initial equilibrium configuration may be considered to be either fully or partly suspended as shown in Fig. 2.6 and the analysis for these two cases is discussed separately below. Only the simpler case of a uniform mooring line is considered.

Fully Suspended Mooring Cable

Initially, the case of a fully suspended cable is considered as shown in Fig. 2.6(a). The cable is assumed to be uniform with a cross-sectional area A, buoyant net weight per unit length q, and elastic modulus E. Let the tension at any point along the cable be T, and the vertical and horizontal components of the cable tension be V and H respectively. Also let the origin of the reference frame Oxz be at the top end of the cable, with z directed downwards.

The shape of the stretched cable in the initial configuration can be parametrically expressed in terms of the unstretched arc length s. The mooring line is assumed to have no bending stiffness, and a consideration of the equilibrium of a section of the unstetched length s gives:

$$\begin{aligned} V &= V_0 - qs \\ H &= \text{constant} \end{aligned} \tag{2.63}$$

By assuming that the mooring line is elastic, the stretched arc length ds' may be related to the unstretched arc length ds by:

$$ds' = \left(1 + \frac{T}{AE}\right) ds \tag{2.64}$$

The differential equations for the shape of the elastic catenary can then be expressed in terms of the unstretched arc length as:

$$\frac{dz}{ds} = \frac{V(s)}{T(s)}\left(1 + \frac{T(s)}{AE}\right) \tag{2.65}$$

$$\frac{dx}{ds} = \frac{H}{T(s)}\left(1 + \frac{T(s)}{AE}\right) \tag{2.66}$$

By integrating Eqs. 2.65 and 2.66 along the unstretched length s, the shape of elastic catenary can be obtained:

$$x = \frac{Hs}{AE} + \frac{H}{q}\log\left(\frac{T(s) - V(s)}{T_0 - V_0}\right) \tag{2.67}$$

$$z = \frac{s}{AE}\left(V_0 - \frac{qs}{2}\right) - \left(\frac{T(s) - T_0}{q}\right) \tag{2.68}$$

where $T = \sqrt{H^2 + V^2}$, and the subscript 0 represents the values at the upper end of the cable.

The expression for the stretched length is given as:

$$s' = s\left(1 + \frac{T}{2AE}\right) + \frac{1}{2AE}\left[\frac{V_0}{q}(T_0 - T) + \frac{H^2}{q}\log\left(\frac{T - V}{T_0 - V_0}\right)\right] \tag{2.69}$$

Substituting the boundary conditions at the bottom end of the cable into Eqs. 2.67 and 2.68, expressions for the horizontal cable span X and the rise Z, as shown in Fig. 2.6(a), can be obtained in terms of the total unstretched length of the cable S, and the horizontal component of the cable tension H, for a given buoyant net weight q:

$$X = \frac{HS}{AE} + \frac{H}{q}\log\left(\frac{\sqrt{1 + \left(\frac{V_0 - qS}{H}\right)^2} - \frac{V_0 - qS}{H}}{\sqrt{1 + \left(\frac{V_0}{H}\right)^2} - \frac{V_0}{H}}\right) \tag{2.70}$$

$$Z = \frac{S}{AE}\left(V_0 - \frac{qS}{2}\right) - \frac{H}{q}\left(\sqrt{1 + \left(\frac{V_0 - qS}{H}\right)^2} - \sqrt{1 + \left(\frac{V_0}{H}\right)^2}\right) \tag{2.71}$$

These equations are clearly nonlinear, and thus for specified values of X, Z, and S, the equilibrium profile defined by H and V_0 can be obtained numerically. In other words, two equations involving five variables are available, so that initial equilibrium configuration of the mooring line can be described by a set of any three variables, and the nonlinear Eqs. 2.70 and 2.71 are solved numerically for the other two. Typically either X, Z and S or H are specified.

The total unstretched length of the cable, S is a useful parameter that gives the degree of slackness of the mooring system when expressed as a ratio S/S_o, where S_o is the shortest distance between the anchor point and the top end of the mooring line.

Partly Suspended Mooring Line

In practice, mooring lines are generally quite slack so as to reduce anchor loads, and most commonly partly suspended as shown schematically in Fig. 2.6(b).

This case is similar to the case of a fully suspended cable as discussed in the previous section, except that a portion of the mooring line now rests on the seabed. The vertical component of the line tension is zero at the touchdown point. Thus, an analysis of the suspended portion of the mooring line gives:

$$X_1 = \frac{HS_1}{AE} - \frac{H}{q}\log\left(\sqrt{1+\left(\frac{qS_1}{H}\right)^2} - \frac{qS_1}{H}\right) \tag{2.72}$$

$$Z = \frac{qS_1^2}{2AE} + \frac{H}{q}\left(\sqrt{1+\left(\frac{qS_1}{H}\right)^2} - 1\right) \tag{2.73}$$

$$S = S_1 + (X - X_1)\left(1 - \frac{H}{AE}\right) \tag{2.74}$$

where S_1 is the total unstretched length of the suspended cable and $(X\text{-}X_1)$ is the unstretched length of the portion of the cable lying on the seabed. Typically the location of the anchor X is specified along with the total unstretched cable length S. Thus, a numerical solution of the equations is required to obtain the horizontal component of the cable tension H, and the unstretched length and horizontal span of the suspended portion of the cable, S_1 and X_1 respectively.

2.4.2 Static Analysis

A static analysis of the mooring system is carried out in order to obtain the steady state offset of the floating structure due to the static components of the environmental loads, including current drag and the mean wave drift force (Fig. 2.5(b)). The restoring force of the mooring system in response to the static offset of the structure is determined from the combined effect of the individual mooring lines.

Response of an Individual Line to Environmental Loads

The response of an individual mooring line to a horizontal load is shown schematically in Fig. 2.7. The mooring line absorbs the external load of the structure primarily through changes in sag and to some extent by stretching. The response is nonlinear and the mooring line tensions and hence the restoring force in the displaced position are determined from the catenary equations. (Various approximate expressions are also available to estimate the restoring force, see for example, Ratcliffe (1985) and Faltinsen (1990)).

Using Eqs. 2.72 - 2.74, the geometry of the mooring line in the loaded position is given by:

$$\hat{X}_1 = \frac{(H+\Delta H)\hat{S}_1}{AE} - \frac{(H+\Delta H)}{q}\log\left(\sqrt{1+\left(\frac{q\hat{S}_1}{H+\Delta H}\right)^2} - \frac{q\hat{S}_1}{H+\Delta H}\right) \tag{2.75}$$

$$Z = \frac{q\hat{S}_1^2}{2AE} + \frac{(H+\Delta H)}{q}\left(\sqrt{1+\left(\frac{q\hat{S}_1}{H+\Delta H}\right)^2} - 1\right) \tag{2.76}$$

$$S = \hat{S}_1 + (\hat{X} - \hat{X}_1)\left(1 - \frac{H+\Delta H}{AE}\right) \tag{2.77}$$

where the capped parameters are the lengths relating to the modified cable configuration, and ΔH is the environmental force as indicated in Fig. 2.7. Thus, for a specified value of an applied total horizontal force at the top end of the cable, $(H+\Delta H)$, the modified horizontal span and unstretched suspended length of the cable can be obtained numerically.

The static offset of the structure ΔX corresponding to the applied load ΔH, may be obtained from the total horizontal span of the new and old profiles:

$$S_1 + (X - X_1) = \hat{S}_1 + (X + \Delta X - \hat{X}_1) \tag{2.78}$$

Rearranging, the static offset ΔX is given as:

$$\Delta X = (\hat{X}_1 - X_1) - (\hat{S}_1 - S_1) \tag{2.79}$$

Note that the force-displacement relationship is nonlinear, and so that this solution generally involves an iterative procedure.

Multiple Mooring Cables

Floating breakwaters are usually restrained by a mooring system consisting of a number of mooring lines as shown in Fig. 2.8. The restoring force of the overall mooring system in response to the static offset of the structure is determined from the combined effect of the individual mooring lines. The restoring force or moment is obtained from the vector sum of all the changes in the horizontal component of the line tensions.

Equilibrium of forces with respect to the x and y directions and rotation about z axis gives:

$$\begin{aligned} F_{dx} + \sum_{i=1}^{N} \Delta H_i \cos(\phi_i) &= 0 \\ F_{dy} + \sum_{i=1}^{N} \Delta H_i \sin(\phi_i) &= 0 \\ M_{dz} + \sum_{i=1}^{N} \left(x_i \Delta H_i \sin(\phi_i) - y_i \Delta H_i \cos(\phi_i) \right) &= 0 \end{aligned} \tag{2.80}$$

where N is the total number of the mooring lines, ϕ_i is the angle between the i-th cable and the positive x direction, and (x_i, z_i) are the coordinates of the point of attachment of the i-th cable to the structure.

2.4.3 Dynamic Analysis

The dynamic effects of the breakwater motions on the mooring line tensions are accounted for by a quasi-static analysis, in which the extreme displacements of the mooring line connection points are calculated from the addition of the steady state and the oscillatory motions of the structure (Isaacson and Baldwin (1996)). The quasi-static approach is generally considered to be adequate where the hydrodynamic loading on the individual mooring lines is small when compared with the energy transmitted by the structure (Triantafyllou (1994)).

2.5 Moored Breakwater Motions

The oscillatory motions of the structure due to wave excitation depend in part on the equivalent linear mooring system stiffness (see Eq. 2.40), and these in turn depend on displaced mean position due to wave drift force and current loading. Hence the breakwater motions depend parametrically on the mean position through changes in the mooring system stiffness i.e. the hydrodynamic and mooring analyses are coupled, and the drift force and associated static offset must be solved by an iterative procedure. The overall procedure is indicated in Fig. 2.9.

First, the equations of motion are solved by considering an unrestrained (freely floating) body to obtain the transmission and reflection coefficients without the influence of mooring stiffness. The wave drift force, calculated from the transmission coefficient using Eq. 2.59, is applied to the static equilibrium condition (Eq. 2.80) to obtain the breakwater offset, and the associated equivalent linear mooring stiffnesses at the offset position (Fig. 2.5(b)). The stiffnesses are then applied to the equations of motion (Section 2.3.4) to obtain modified motion amplitudes. Using these modified motion amplitudes, the transmission coefficient and the wave drift force are recalculated. This procedure is repeated until convergence in the wave drift force is achieved. Since the influence of the mooring stiffness on the breakwater's oscillatory motions is generally small, convergence occurs with relatively few iterations. Once convergence is achieved, the dynamic analysis of the breakwater motions is carried out using the quasi-static approach discussed in Section 2.4.3 and the maximum displacements of the breakwater are then determined by adding the amplitude of the oscillatory motion to the steady offset. The associated maximum mooring line forces are then obtained (Fig. 2.5(c)).

2.6 Effect of Finite Length

Since the preceding analysis has been based on a two-dimensional structure of infinite length, consideration is now given to the effect of a finite length of the breakwater. The length L of the structure is assumed to be much greater than the incident wavelength. The total force on

the structure is obtained by integrating the two-dimensional force along its length $F_k(y,t)$, (see Eq. 2.30), ignoring the end effects.

$$F_k(t) = \int_{-L/2}^{L/2} F_k(y,t)dy = F_k' \frac{2\sin((kL/2)\sin\beta)}{k\sin\beta}\exp(-i\omega t) \tag{2.81}$$

where F'_k is the amplitude of the exciting force F_k. Thus, the k th force component, $F_k(t)$ is obtained by combining the corresponding force per unit length, $F_k(y,t)$. This expression can be thought of as the product of the amplitude of the force per unit length F, the length of the structure L, and a reduction factor $C(kL,\beta)$, defined as:

$$C(kL,\beta) = \frac{2\sin((kL/2)\sin\beta)}{kL\sin\beta} \tag{2.82}$$

The factor $C(kL,\beta)$ can be considered to be a reduction of the load per unit length due to the finite length of the structure for a given angle of approach, or due to the obliqueness of the waves for a given structure length. The hydrodynamic coefficients for a finite structure are obtained by multiplying the sectional coefficients for beam seas (β = 0 deg) with the length of the structure.

3. Experimental Investigation

The experimental investigation that has been carried out relates to two-dimensional laboratory tests of a twin-pontoon floating breakwater in order to verify the numerical model and to provide generic performance characteristics which could subsequently be applied to specific design situations.

3.1 Experimental Facilities

Experiments have been carried out in a wave flume located in the Hydraulics Laboratory of the Department of Civil Engineering, University of British Columbia. Figure 3.1 shows a sketch of the experimental set-up. The wave flume is 20 m long, 0.60 m wide, operates with nominal water depth of 0.50 m, and is equipped with a computer-controlled wave generator capable of producing regular and random waves. A 7.0 m long artificial beach consisting of plywood set at a 1:15 slope and covered with artificial hair matting extends from one end of the flume. This beach, together with a holding tank at the end of the flume, effectively absorb incident wave energy preventing significant wave reflection. The location of the model is at about 9.5 m downwave from the wave paddle.

The main components of the experimental scheme include wave probes to record the time variation of wave profiles at selected locations in the flume; load cells to record time histories of mooring line forces; and a camcorder to obtain video records of the breakwater motions. Other components involve amplifiers, and a multi-channel data acquisition system and a digital to analog and analog to digital converters. A flowchart indicating these components is given in Fig. 3.2. The data generation and acquisition system, consisting of a DEC Vaxstation 3200 computer, was used to load the wave actuator with signals related to selected wave conditions, and to store the data acquired from probes and load cells. The GEDAP library of software, developed by the Hydraulics Laboratory of the National Research Council, Canada was used to generate signals relating to selected wave conditions

and to record the measured wave data (Miles, 1989). This system allows for the simultaneous generation of waves as well as sampling of the wave probe and load cell signals.

3.2 Breakwater Models

Breakwater models with both rectangular and circular cross-section pontoons have been considered. The two-dimensional twin-pontoon model with rectangular section pontoons was fabricated by constructing two perspex boxes, each 0.30 m wide, 0.20 m high and 0.53 m long, and connecting these to each other by an aluminum C section with an arrangement for adjusting the pontoon spacing. A photograph of the model is shown Fig. 3.3(a). This arrangement resembles a deck rigidly connected to the two pontoons in prototype situations. Roller bearings attached to the ends of each pontoon act as frictionless restrainers against the flume wall permitting surge, yaw and pitch motions only. Lead ballast was used to achieve the required breakwater draft, centre of gravity location, and roll radius of gyration. Mooring lines, made from 1/8 inch flat link stud chain and 1/8 inch braided nylon rope, were attached at the bottom outer corners of each pontoon. These were fixed to the flume bottom so as to simulate anchors with the ratio of rise to horizontal span of the mooring line Z/X chosen to be equal to 0.403.

For the case of the circular section twin-pontoon breakwater model, arrangements were similar to those of the breakwater with rectangular section pontoons, except that two PVC pipes of diameter 0.20 m and length 0.53 m were used in place of the perspex boxes as shown in Fig. 3.3(b). The mooring lines were attached on the underside of the pontoons at angles of 45° to the vertical. Each of the pipe ends was made water tight with a lexicon disk, and roller bearings were attached to each disk to minimize friction between the flume wall and model ends.

3.3 Test Procedure

All tests were conducted in the wave flume with monochromatic regular waves. Table 3.1 lists the wave conditions adopted for both the rectangular and circular section breakwater models. Figure 3.4 shows the ranges of Keulegan-Carpenter number K for these waves in relation to the characteristic dimension of the model.

The selected wave conditions chosen were grouped into two categories; one associated with a constant steepness and the other with a constant wave number (Table 3.1). In all, 18 different wave signals were used.

The attachment point and the mooring line rise to horizontal span ratio Z/X were left unchanged throughout the tests, since the attachment location is assumed to have no significant influence on the motions (Isaacson *et al.* (1994) and Whiteside (1994)). For the case of nylon mooring lines, only a taut case was considered since the line is buoyant and the case of slack lines is not as relevant. Bearing in mind the above discussion, the parameters varied in the experiments include the wave period, the wave height, the breakwater draft, the pontoon spacing, and the mooring line type (and the mooring line slackness for chain only). The parameters held constant were the water depth, pontoon diameter, mooring line attachment points and mooring line horizontal span. Table 3.2 summarizes the ranges of these variables, and Table 3.3 gives a complete set of the test scheme adopted in the experimental investigation.

A total of 80 tests were performed with respect to each of the models, corresponding to various combinations of wave conditions and breakwater configurations. The following parameters were measured in each of the tests:

$\eta_i^{(m)}$ incident wave surface elevation with the wave probe located at the origin, O (without the model in place);

$\eta_{r1}^{(m)}$, $\eta_{r2}^{(m)}$, $\eta_{r3}^{(m)}$ water surface elevations at three probes located at 1.0, 1.25 and 1.45 m upwave from the reflecting face, respectively;

$\eta_{t1}^{(m)}$, $\eta_{t2}^{(m)}$ water surface elevations located at two probes at 1.0 and 1.25 m downwave from the downstream face, respectively;

$\hat{\xi}_i$ breakwater motion amplitudes (sway, heave, and roll);

$\hat{T}_j$ maximum mooring line tensions at the anchor point (j=1, upwave, and j=2, downwave).

3.4 Analysis Technique

3.4.1 Reflection and Transmission Coefficients

In the case of a reflection analysis involving a regular, uni-directional incident wave train, there are three parameters to be determined; (i) the incident wave height, (ii) the reflection coefficient, and (iii) the reflection phase angle. General methods that may be used for such an analysis have been outlined by Isaacson (1991). These include the following:

Method I: two fixed probes - two heights and one phase angle measured;

Method II: three fixed probes - three heights and two phase angles measured; and

Method III: three fixed probes - three heights measured.

In the following, the basis for developing each of the three methods listed above is outlined briefly.

The water surface elevation η in front of the breakwater is assumed to correspond to the superposition of sinusoidal incident and reflected wave trains and may be expressed as:

$$\eta = a_i \cos(kx - \omega t) + a_r \cos(kx + \omega t - \beta) \tag{3.1}$$

where a_i and a_r are the amplitudes of incident and reflected wave trains, and β a phase angle between the incident and reflected wave trains. The reflection coefficient K_R, is the ratio a_r/a_i. Assuming that ω and k are known from measurements, the three unknowns to be determined are a_i, a_r, and β. The incident wave height, H and the reflection coefficient K_R, are given in terms of a_i and a_r as:

$$H = 2a_i \tag{3.2}$$

$$K_R = a_r/a_i \tag{3.3}$$

Equation 3.1 is applied at a series of probe locations x_n, n = 1, 2, ... that may be substituted in Eq. 3.1 as:

$$\eta_n = a_i \cos(kx_n - \omega t) + a_r \cos(kx_n + \omega t - \beta) \tag{3.4}$$

where kx_n is given by $kx_1 + \Delta_n$, in which Δ_n, the dimensionless distance between the n-th probe and the first probe, and is equal to $k\lambda_n$, (please see Appendix I). As an alternative, Eq. 3.4 can be expressed in complex form as:

$$\eta_n = \mathrm{Re}[\{a_i \exp(ikx_n) + a_r \exp(ikx_n - \beta)\}\exp(-i\omega t)] \tag{3.5}$$

where Re[ ] denotes the real part. The actual measurements at the probe locations will provide corresponding amplitudes and relative phases, such that the measured elevation at the n-th probe may be written in complex form as:

$$\eta_n^{(m)} = \mathrm{Re}[A_n \exp(i(\phi_1 + \delta_n))\exp(-i\omega t)] \tag{3.6}$$

where A_n is the measured amplitude of the n th record, ϕ_1 is the phase angle, δ_n is the measured phase of the n th record relative to that of the first record. Once the measured amplitudes and the relative locations of the probes are known, it is now possible to use Eqs. 3.5 and 3.6 to develop expressions for a_i, a_r and β, depending on which of the three methods is used. For completeness, the expressions for the unknown variables a_i, a_r and β derived from all three methods are summarized in Appendix A.

In the above calculation of K_R, rather than using a_i obtained from a reflection analysis, the incident wave height measured at the wave probe placed at the origin O (see Fig. 3.1) in the absence of the breakwater model has been used instead. For the case of transmission coefficient K_T, measurements from two wave probes on the downwave side of the model were taken and only Method I was used. In this case, K_T was obtained as:

$$K_T = a_i'/a_i \tag{3.7}$$

where, a_i' is taken to be the amplitude of the transmitted wave obtained from a reflection analysis, whereas a_i is the amplitude of the measured signal from the probe at the location O, without the model in place. From the measured wave elevations at different locations at the upwave and downwave side of the model, the incident, reflected, and transmitted waves were obtained by following Isaacson (1991).

3.4.2 Wave Measurement

Capacitance-type wave probes were used for measurements of the water surface elevation. The wave probes exhibit a linearity better than 98.5% and a resolution of better than 1 mm. The duration of the recording was selected so as to ensure that measurements of waves upwave of the breakwater were not contaminated by reflected waves which were re-reflected by the wave generator; and that the measurements of waves downwave of the breakwater were not contaminated by the waves reflected by the beach. Also, the time origin of the data recording was selected such that the shorter period waves reach the location of the model and there were sufficient numbers of wave cycles within a chosen record length. Hence, a recording length of 14 sec was chosen and data were recorded at a sampling frequency of 50 Hz.

3.4.3 Mooring Force Measurement

Mooring line tensions were also measured simultaneously with the water surface elevation for all the tests. Two sealed shear beam load cells were placed in series with the mooring lines near the anchor points to measure tensions in the upwave and downwave mooring lines. The load cells have a 50 lb (222 N) capacity with 99.5 % linearity through their working range. Data were recorded at a sampling frequency of 50 Hz to ensure that no sharp peaks in the data were lost.

3.4.4 Dynamic Characteristics

The dynamic characteristics of the two models are required for the purpose of applying the numerical model to simulate the test conditions. These characteristics include the position of the centre of gravity, the roll radius of gyration and the system damping.

When the mass distribution of a floating breakwater model is not known *a priori*, the centre of gravity and roll radius of gyration can be determined from swing tests. First, the location of the centre of gravity was determined by pivoting the whole system about a point far from the vertical axis (line of symmetry) of the breakwater and then dropping a plumb line through the pivot point; the centre of gravity then lies at the intersection of the plumb line and the vertical axis. Next, the model was allowed to oscillate as a pendulum about a point A, which is a known distance from the centre of gravity. The relationship between the roll radius of gyration and the oscillation period can be obtained from the equation governing the motion, and is given by $I_o = mg\ell/\omega^2$. Here, I_o is the moment of inertia about point A, ℓ is the distance between the point A and the centre of gravity G, and ω is the angular frequency of the oscillation. Once the moment of inertia I_o is known, the radius of gyration r_G, can be easily determined. Table 3.4 gives values of the location of centre of gravity z_G, radius of gyration r_G, for the base cases of both the rectangular and circular models.

3.4.5 Breakwater Motions

The two-dimensional motions of the breakwater were video taped using an S-VHS camcorder as indicated in Fig. 3.1. Two distinct marker locations on the model are shown in Fig. 3.5. The camcorder was fixed at an elevation that coincides with the elevation of the origin O of the coordinate system, and oriented such that the markers are always within the camera range. This position and the settings of the camera correspond to a field of view area of approximately 1.7 m x 1.25 m at the face of the wave flume wall. All relevant dimensions are measured such that co-ordinates in the user plane can be evaluated from the video images using a motion tracking package.

The video record of the required duration was then played to a FAST FPS/60 frame-grabber card installed on an IBM compatible PC and saved as a movie file. This was then read by the motion analysis software package Photo4D, and thereby converted to a sequence of single-frame still image files (see Fig. 3.5). These images were then viewed for marking purposes. Once the user identifies the markers on the first frame and inputs values related to the camera position, user coordinates, and the size of the markers, the analysis package automatically tracks the markers in the subsequent frames. Using scale information initially supplied by the user, the positions of markers in pixel coordinates are converted to user coordinates, and finally stored in an ASCII file. Based on these time variations of coordinates of each of the markers, the three-degrees-of-freedom motions (sway, heave and roll) can be obtained as described in Appendix B.

It is important to synchronize the time origin of these motion traces with that of the data recording relating to wave probes and mooring line forces. This was accomplished by sending a trigger voltage such that a small bright light bulb, placed within the range of the view finder of the camcorder, was illuminated at the start and turned off at the end of each data recording. When the video is played back, the illuminated status of the light bulb indicates the duration of data collection on the GEDAP data acquisition system. It is noted, even though the bulb appears to brighten over a finite duration, it is generally possible to select a specific video frame at the onset of the bulb lighting up.

3.5 Assessment of Experimental Errors

Part of the scatter observed in the experimental results is likely due to the limitations of the laboratory facilities and the measurement techniques. As mentioned earlier, in the present study, time histories of water surface profiles and mooring loads, and the video capture of breakwater motions were recorded. The water surface elevations were measured by placing probes at selected locations on the upwave and downwave side of the model. Limitations include an assessment of reflected waves from the combined incident and reflected wave

field measured on the upwave side, and an assessment of beach reflected waves on the downwave side of the model. It was also found that, after a large duration (> 20 sec), the flume showed standing wave and cross-wave patterns on the upwave side of the breakwater and subsequent overtopping. These situations limited the total duration of the recorded data that were analyzed, so as to keep the contamination of the wave field as low as possible at both the upwave and downwave sides of the breakwater. A series of preliminary tests were conducted to evaluate the influence of reflection so as to choose an appropriate recording length as described in the previous section.

The time histories of the mooring line tension at the anchors indicated sharply rising snap loads due to excessive drift of the breakwater model. This may be attributed to the limited scope of the mooring lines.

The use of the video motion tracking system appears suitable for estimating the component motions of the breakwater. The limitation of this technique basically arises from the hardware of the system rather than the tracking software itself. A frame-grabber card installed on an IBM compatible computer was used to convert the analogue video record to digital 'avi' files. The card can capture frames at a maximum rate of 30 frames per sec. This sampling rate is not critical for component motions since the wave periods considered are in the range of 0.6 to 1.7 sec, and the motion tracking technique is thus associated with a possible error of only 1/30 sec. In the present study, the size of a captured image was chosen to be 320 pixels (horizontal) x 280 pixels (vertical). By knowing the dimensions of the physical frame, a resolution of 3 pixels per mm was achieved.

The response measurements are prone to error due to various factors and an assessment of the degree of error in the video-based motion analysis is presented now considered. The possible error sources include:

(a) differences between the mouse location and a marker point (i.e. the actual point to be tracked),

(b) differences between marker locations and the reference points used for scale selection, and

(c) the strength of the video image itself.

The Photo4D (1996) software package was used to identify the marker points and then to track the coordinates of the marker points. The package requires the camera position and user coordinates as inputs. It also requires the locations of two markers as reference points and the distance between the two reference points. Based on these inputs, the Photo4D package estimates the coordinates of the markers and the associated error in estimating the location in user coordinates.

Test runs were conducted with known values of rigid body locations in air and recorded on video in order to calibrate the motion analysis package. The ratio of the responses obtained from the motion analysis to that of known values gave 7 – 9 % error for the sway and heave motions, and 10 – 12 % for the roll motion. In the experimental study, maximum values of responses observed were not greater than 8 cm for translation and 5.0° for the roll. Thus, errors corresponding to translation and roll motions were less than 7 – 8 mm and 0.5 – 0.9°, respectively. Figure 3.6 indicates the estimated percentage error in component motions for the video-based motion tracking system. The figure shows these for the particular case of a moored rectangular twin-pontoon breakwater with d/a = 1.67, h/a = 0.45, b/a = 1.0 and $S/S_o = 1.08$.

4. Results and Discussion

This chapter summarizes results obtained from the numerical model and the experiments, described in Section 2.3 and Chapter 3 respectively, including a comparison with selected results reported in previous studies. First, the numerical model results relating to added masses and damping coefficients, response amplitude operators, reflection and transmission coefficients, and force coefficients are presented. Experimental results consisting of reflection and transmission coefficients, response amplitude operators, and maximum mooring forces in the upwave and downwave lines are then presented, and compared with corresponding numerical values. Finally, as an example application of the moored twin-pontoon breakwater analysis, a prototype situation is considered and related numerical results are presented.

4.1 Numerical Results

In this section, the accuracy and computational efficiency of the numerical model is first assessed, and a parametric study is then carried out to investigate the sensitivity of the breakwater performance to various wave and structural parameters. The performance of the breakwater is expressed in terms of pontoon draft ratio h/a, spacing ratio b/a and mooring slackness ratio S/S_0. In the parametric study, numerical results are presented first for a fixed body, followed by results for a freely floating body. Next, the mooring analysis is considered, and finally results for a moored structure are presented.

4.1.1 Accuracy and Efficiency

An assessment of the accuracy of an earlier version of the numerical model has been carried out by Nwogu (1985), by comparing results for the case of a single-pontoon rectangular section breakwater with those reported by Bai (1975) and based on the finite element method. In the present study, an assessment of the accuracy of the integral equation method for the case of twin-pontoon sections has been made by considering a series of numerical test cases

with different sizes of elements on the free surface and the different numbers of elements on the body. Element sizes ranging from L/50 to L/10 have been considered, where L is the wave length, and the number of elements on a single pontoon, N, ranging from 20 to 40 have been considered. The corresponding results indicated that there is less than 0.1% change in the hydrodynamic coefficient values for element sizes smaller than 1/40 of the wave length and for N greater than 30. However, it has been noted that the hydrodynamic coefficient values are particularly affected by the element size along the free surface lying between the two pontoons. Therefore, the element length here was taken to be one-half of that for the upwave and downwave free surfaces. Overall, an element size of L/40 along upwave and downwave free surfaces and L/80 along the free surface between the two pontoons were chosen, together with 30 elements on each pontoon surface. These values were held constant through out the analysis.

It is also important to consider the computational efficiency of the numerical model. The program was developed in the FORTRAN language and was run on an IBM compatible PC Pentium running at 200 MHz with 64 MB RAM and with a Microsoft FORTRAN Power Station 4.0 compiler. The CPU time log for the algorithm indicates that a large fraction of the time was required for the calculation of the element matrix coefficients. As an example, the CPU time is denoted τ for the case of a freely floating single-pontoon rectangular section breakwater with relative draft h/a = 0.5, in water of finite depth d/a = 1.67, a range of ka from 0.3 to 3.0 with 10 equal intervals. For the case of a twin-pontoon breakwater with the same sectional parameters along with the relative spacing b/a as 1.0, the relative CPU time observed is 2.6τ. For single- and twin-pontoon circular sections the corresponding times are 0.96τ and 2.5τ, respectively.

Recently, the use of higher-order element methods has been extended to water wave problems (see Teng and Eatock Taylor (1995)). In a higher-order boundary element approach, the velocity potential is no longer assumed uniformly distributed along each element and its values at the element nodes become the unknowns. The velocity potential

and its derivatives within an element are expressed in terms of the corresponding nodal values and shape functions. It may be recalled that in the present context of a linearized two-dimensional twin-pontoon wave interaction problem a constant potential approach is reasonably accurate.

4.1.2 Fixed body

Initially, the body is taken as fixed such that only the wave scattering problem is considered. Results are presented for a twin-pontoon rectangular section with a base case corresponding to d/a = 2.5, h/a = 0.5 and b/a = 1.0, where a is the width of a single-pontoon (diameter for a circular section pontoon). Each parameter is varied from the base case value, keeping the other parameters constant. The variation of reflection coefficient as a function of the frequency parameter ka is presented in Fig. 4.1. For comparison, numerical results from Williams and Abul-Azm (1996), are superposed on the plot. Williams and Abul-Azm also used boundary integral method, however, the computational domain was made up three separate regions pertaining to two pontoons and a trapped middle section. A matching boundary condition along the adjacent boundaries was introduced to solve the complete boundary value problem. Good agreement over the whole frequency range is obtained. The differences are in general less than 0.5% except for small ka values, where a more than 1.0 % difference exists.

Figure 4.1(a) indicates the influence of pontoon draft on the reflection coefficient. Three cases of draft ratio h/a (0.25, 0.50 and 1.00) are taken, keeping the other parameters constant. As expected, it is observed that in the high frequency range, the reflection coefficient approaches unity for all three cases and that the deeper draft section is the most efficient barrier. Also, it can be seen that all three curves are similar and have a sharp minimum in the frequency range of interest. It is interesting to note that this minimum does not occur for the fixed single-pontoon section, for which K_R is a monotonic function of ka, and thus it is associated with hydrodynamic interference effects between the two pontoons.

In Fig. 4.1(b) the effect of relative pontoon spacing on the reflection coefficient is examined by considering three different values of b/a (0.5, 1.0 and 2.0), while keeping the other parameters constant. Once again, the reflection coefficient exhibits a minimum in the mid-frequency range and tends to reach unity at higher frequencies. It is noted that at low frequencies ($0.50 < ka < 0.75$) the smallest spacing, $b/a = 0.25$, leads to a maximum reflection coefficient, while at higher frequencies ($ka > 1.00$), the largest pontoon spacing results in higher values of reflection coefficient. This is because in long waves (low frequency) the smaller spacing allows the two pontoons to act as a continuous structure functioning like a single unit spanning a significant part of the wavelength, whereas in short waves pontoons with a larger spacing tend to act independently as two separate single pontoon breakwaters in series.

In a similar way, Fig. 4.2 compares the reflection coefficient for the fixed case of circular twin-pontoon breakwaters ($d/a = 2.5$, $h/a = 0.5$, $b/a = 1.0$) indicating the influence of pontoon spacing. The results are analogous to those of rectangular section breakwaters.

4.1.3 Unrestrained Body

Consider now the case of a freely floating twin-pontoon rectangular section breakwater ($h/a = 0.5$, $b/a = 1.0$) in water of finite depth $d/a = 5.0$ interacting with a monochromatic normally incident wave train. Figure 4.3 shows the variations of added masses, damping coefficients, exciting force coefficients and response amplitude operators (RAO's), as functions of the frequency parameter, ka. Also, results relating to a single-pontoon rectangular section breakwater corresponding to one pontoon of the twin-pontoon breakwater (i.e. $d/a = 5.0$, $h/a = 0.5$) are superposed in the figure, together with corresponding experimental results reported by Vugts (1968). As expected, the added mass in sway for the twin-pontoon breakwater is approximately twice that for the single-pontoon configuration. However, for the case of the heave mode of motion, the added mass variation with ka

exhibits a marked change with a minimum value of -1.25 at ka = 0.73 and remains negative in the range of $0.75 < ka < 1.00$.

The occurrence of negative added mass for the case of twin bodies such as catamarans, as well as bulbous bodies close to the free surface and ships close to a quay, have been reported previously. Also, it has been observed that the negative added mass occurs near the natural frequency for a given mode of motion. In most cases this has been observed in theoretical or numerical computations, but laboratory model test results have also confirmed such a phenomenon. This phenomenon mainly arises because of the out-of-phase motion of the body in relation to the water surface in the vicinity of the body (e.g. Sarpkaya and Isaacson (1981)). Cases giving rise to a negative added mass generally have a configuration that allows a localized resonance to occur in the fluid domain adjacent to the structure. In the present case of a twin-pontoon section, the space between the pontoons forms an oscillating water column, which may respond as a separate oscillator. Vinje (1989) proposed a coupled two-degrees-of-freedom oscillator to model such a system, and thereby showed the basic nature of the added mass for this configuration by varying parametrically the mass and stiffness characteristics of the model.

Figure 4.3(a) also indicates that the variation of roll added mass for the case of a twin-pontoon section is fairly constant over the range of ka considered in the study and is twice the corresponding value for a single-pontoon section.

Although previous studies relating to twin-pontoon sections are generally available, previously reported results of hydrodynamic coefficients for the case of a twin-pontoon rectangular section appear not to be available. Therefore, numerical results only for a single-pontoon rectangular section are compared in the figure with the corresponding experimental values reported by Vugts (1968). These two sets of results compare reasonably well.

Figure 4.3(b) shows the variation of damping coefficients for the sway, heave and roll modes of motion for the same breakwater configuration. While the damping coefficient in sway for both sections follow similar variations, there are more pronounced differences for

the heave and roll modes of motion. In the heave mode, the damping coefficient drops to zero from a peak value, at the same ka value (= 0.73) as that at which the heave added mass reaches a (negative) minimum (see Fig. 4.3(a)). For the roll mode, the damping coefficient reaches a peak value at about ka = 0.55, and is higher than that of a single-pontoon section. Figure 4.3(c) shows the exciting force coefficients for sway, heave and roll as functions of ka, and a comparison of Figs. 4.3(b) and 4.3(c) confirms that the exciting forces and damping coefficients are directly related, in accordance with the Haskind relations (e.g. Sarpkaya and Isaacson (1981)).

Consideration is now given to the sway, heave and roll responses of the same breakwater where the relative radius of gyration, $r_G/a = 1.08$, the relative centre of gravity, $z_G/a = -0.125$, and the relative centre of buoyancy, $z_B/a = -0.25$, where a is taken to be the pontoon width. The uncoupled natural frequency in heave and roll may be estimated from the known values of the overall stiffness and mass in the respective degrees of freedom, and correspond to ka = 0.88 and 0.99, respectively. For the case of a single-pontoon section, the relative radius of gyration, r_G/a, is taken to be 0.20, and the natural frequencies in heave and roll are estimated to correspond to 0.87 and 0.41 respectively. Figure 4.3(d) shows the variation of sway, heave and roll RAO's with ka. It can be seen that the maximum heave RAO's are almost the same, whereas in roll, the maximum RAO is about 20% of that single-pontoon section. This is mainly due to the increased roll stiffness for the case of the twin-pontoon section. As ka increases, the heave RAO drops from an initial value of 1.0 to zero and then reaches a maximum. This is indicative of the interference effect and the associated negative added mass.

Figure 4.3(e) provides a comparison of the reflection and transmission coefficients, and the wave drift force coefficient for the twin- and single-pontoon rectangular sections. Once more, the interference effect is clearly seen in the twin-pontoon results.

In a similar manner to the preceding comparison for rectangular section breakwaters, Fig. 4.4 shows a comparison of the hydrodynamic coefficients, exciting force coefficients,

and RAO's for the case of twin- and single-pontoon circular section breakwaters. Here, the values relating to the twin-pontoon circular section are compared with the results of Leonard *et al.* (1983), who used the finite element method to solve the corresponding boundary value problem. From Fig. 4.4(a) it can be seen that the estimated values of sway added mass compare reasonably well over the whole range of ka shown, except that for the low frequency range ($ka < 0.35$) the present results and Leonard's deviate by about 10%. Figures 4.4(b)-(e) indicate similar features as that for the rectangular twin-pontoon section.

Since the preceding added mass and damping coefficient variations exhibit sharp peaks, it is of interest to compare the effect of pontoon spacing on these coefficients. Figures 4.5(a) and 4.5(b) present such a comparison for rectangular and circular twin-pontoon sections respectively with $d/a = 2.5$, $h/a = 0.5$, $\beta = 0°$. In Fig. 4.5(a), results are shown for relative spacings, $b/a = 0.25$, 1.0 and 4.0, (rectangular section), while in Fig. 4.5(b) they are shown for $b/a = 0.25$, 2.0, and 4.0, (circular section). Consider first the rectangular section breakwater. It can be noticed that for closely spaced pontoons, the hydrodynamic coefficients do not exhibit any peaks, while for the case of widely spaced pontoons, the variations of both the sway and roll added mass coefficients exhibit maxima and minima at $ka \approx 1.25$. In addition, the variations of damping coefficient indicate corresponding peaks at the same ka value. On the other hand, the heave added mass coefficient shows no such variations for both closer and wider spacings. Similar variations can be observed in the variation of hydrodynamic coefficients relating to the circular section pontoon (Fig. 4.5(b)).

4.1.4 Mooring Analysis

As part of the overall analysis of a moored floating breakwater, a mooring analysis is carried out in conjunction with the hydrodynamic analysis. Initially, a separate mooring analysis is carried out here for the case of a six-point mooring system made up of chain or nylon lines in order to investigate the mooring line stiffness properties. The mooring lines are taken to have the configuration shown in the inset to Fig. 4.6, with each of the lines having a rise,

Z = 2.5 m, and a horizontal span, X = 6.6 m. For the case of chain moorings a slackness ratio, S/S_o = 1.08 is assumed and the chain submerged weight per unit length, q, and section modulus per unit length, EA, are taken to be 183.0 N/m and 20.0 MN respectively. For the case of nylon moorings, a taut line (S/S_o = 1.00) without any pre-tension is assumed, and q and EA are taken to be 2.08 N/m and 50.8 kN respectively. The breakwater length, ℓ is taken to be 20.0 m and the mooring lines attachment points are spaced equally at λ = 10.0 m. The water depth d is taken to be equal to 3.4 m.

The net horizontal force as a function of displacement in the sway direction is presented in Fig. 4.6 for both types of mooring. As can be seen in the figure, the force-displacement curve for the chain mooring (slackness S/S_o = 1.03), is linear up to a displacement δ = 0.19 m, and for δ > 0.30 m the form of the curve becomes more nonlinear. For the case of nylon moorings, the curve is approximately linear over the displacement range shown. A comparison of chain moorings of nearly taut case (S/S_o = 1.03) with that of nylon moorings (taut case, S/S_o = 1.00) indicates that the restoring force for the former is consistently higher and becomes greater than two times the restoring force associated with the nylon moorings for δ > 0.19 m. This would not only reduce the required design strength of the anchor system, but also the breaking strength requirement of the mooring line itself when compared with the case of nylon lines.

4.1.5 Moored Breakwater Response

It is of interest to investigate the use of the iterative procedure in evaluating the wave drift force of a moored breakwater described in section 2.5. Consider therefore a twin-pontoon breakwater with a depth d = 3.4 m, a draft, h = 0.9 m, and a spacing, b = 2.0 m. In addition, the radius of gyration, r_G is taken to be 2.16 m, the centre of gravity, z_G = -0.25 m, and the centre of buoyancy, z_B = -0.5 m. The six-point mooring system described above is once again considered, now with a slackness ratio S/S_o = 1.03, which indicates a stronger nonlinear force-displacement relationship (see Fig. 4.6). Table 4.1 shows the corresponding

linearized stiffness matrix without any environmental loads applied on the structure, whereas Table 4.2 indicates the influence of iteration on the convergence of the wave drift force for constant values of ka = 0.675 and H/L = 0.1. The iteration procedure adopted here is given in section 2.5. The wave drift force at the end of the iteration is consistent with both the hydrodynamic and the mooring analyses. This in turn implies that the motions in sway, heave and roll modes are also consistent with the corresponding values of total stiffness of the system.

Table 4.3 compares the results from the present analysis involving the iteration procedure for wave drift force with an analysis that does not consider the iteration procedure. The table also indicates the percentage difference in the results between the two analyses. The values suggest that the iteration procedure for the wave drift force is essential for cases where the relationship between the net horizontal force and the displacement is strongly nonlinear and the wave steepness is notably large. In other words, for conditions where breakwaters are taut moored, and are exposed to steep waves, the force-displacement relationship is strongly nonlinear and thus requires an iteration procedure to arrive at a consistent drift force and the linearized mooring stiffness matrix at this drifted position.

Figures 4.7(a) and (b) compare the results of chain and nylon moorings for the base cases of rectangular and circular section twin-pontoon breakwaters. Although, the estimated transmission coefficients do not show marked differences, the maximum tension at the anchor for the upwave line indicates significant differences between chain and nylon moorings.

4.2 Experimental Results

The experiments were carried out for both the rectangular and circular section twin-pontoon breakwaters. As described in Chapter 3, for the base case of a rectangular section model, the pontoon width a = 0.30 m, and the height h = 0.20 m, and the gap b = 0.30 m. Similarly, for the base case of a circular section model, the pontoon diameter a = 0.20 m, and the gap

b = 0.40 m. For the two base cases, the draft was chosen to be 65% of the pontoon height, and the mooring lines were taken to have a rise to span ratio Z/X = 0.403, with a slackness ratio S/S_o = 1.08 and 1.00 for chain and nylon respectively.

The entire program of test wave conditions was generated in the flume before placement of the breakwaters in order to allow the incident wave trains to be examined in the absence of any reflected waves from the breakwater. The resulting incident waves were measured to ensure that the desired wave height was attained in the flume for a given wave period.

For the rectangular section model base case, Figs. 4.8 and 4.9 show measured time histories of the five probe signals, and the mooring line forces at the anchors. Figures 4.8(a) and 4.8(b) correspond to a shorter wave period, T = 1.0 sec, and a larger wave height, H = 0.12 m, for both chain and nylon moorings, whereas Fig. 4.8(c) corresponds to a longer wave period, T = 1.70 sec and a smaller wave height, H = 0.09 m, for chain moorings only. As can be seen from the component figures, the transmitted waves are slightly bigger than one third the incident waves, indicating clearly the effectiveness of the breakwater to provide adequate wave protection. Comparing Figs. 4.8(a) and 4.8(b), it can be inferred that the type of mooring system mainly influences the line tensions rather than the transmitted or reflected wave profiles. The mooring line forces are markedly different for the two systems; the time variation is cyclic for the case of nylon moorings whereas it contains sharp peaks for the case of chain moorings.

All the data collection has been carried out for a length of 10.0 sec. The analysis has been carried out for a duration of 6 sec, between the time periodic conditions are established at the wave probes, and the time at which the wave record begins to exhibit some modulation. Also, it may be recalled that the experiments were carried out with wave periods ranging from 0.5 sec to 1.7 sec (see Table 3.2), ensuring 4 to 12 cycles of recorded data. The reflected and radiated waves in front of the breakwater seem to contaminate the incident wave field after 7 sec. Thus, the initial duration of 6 sec shown in Fig. 4.8(a) corresponds to the duration of the data analyzed.

Figure 4.9 shows time histories of measured sway, heave and roll motions of the breakwater model, as well as the incident wave profile, for the same condition as in Fig. 4.8(c). As expected, the sway motion seems to have a mean as well as an oscillatory component. Also, the sway and heave motions are closely in phase and heave motions lag the sway by about 0.3 sec. The figure also indicates the heave motion to be of the same order as the wave amplitude.

At a wave period of 1.7 sec (not shown here), which is close to the heave and roll natural periods, the motions were quite large with a large amount of water getting on the deck. Also, the water contained between the two pontoons showed a very noticeable out-of-phase motion with respect to the heave mode. In fact, the wave generator has to be stopped immediately after completing the required 6.0 sec length of data recording.

Measured time traces of wave probe signals were analyzed to provide the incident, reflected and transmitted waves based on the three different methods explained in Section 3.4. It may be recalled that the water surface profiles were recorded at three different locations on the upwave side of the model, and two locations on the downwave side. Thus, it was possible to apply all the three methods of reflection analysis to the upwave side, whereas only Method-I was used for the downwave side. A comparison of the measured wave profile $\eta_{r1}^{(m)}$ at an upwave location with the computed profile $\eta_{r1}^{(c)}$ based on Eq. 3.4 is presented in Fig. 4.10. For the upwave side of the model, the results from three different methods did not compare well mutually, however the method of least squares (Method II) seems to compare reasonably well with the measured wave profiles.

When analyzing the data it was assumed that the response of the breakwater is periodic and of the same frequency as the incident waves. However, the nonlinearities in the problem largely due to line snapping in the case of chain moorings resulted in notable cycle to cycle variations. The partially non-periodic mooring tensions, combined with the limited length of the tests for the reasons explained above, may be responsible for some scatter in the data.

The importance of the breakwater motions is mainly due to their role in the transmission of waves past the breakwater. Therefore, it is useful to discuss the type of results that may be expected. The heave degree of freedom is uncoupled from the other two degrees of freedom, whereas the sway and roll degrees of freedom are coupled, largely because mooring line attachment points do not coincide with the centre of gravity of the breakwater. However, this coupling is very weak, and even though both the modes are present, one can expect that either the roll or sway mode predominates. Furthermore, for slack lines, mooring forces are smaller than the hydrodynamic forces.

4.3 Experimental and Numerical Results

Numerical results were obtained by carrying out the hydrodynamic analysis in conjunction with the mooring analysis. Viscous damping, due in part to flow separation around the breakwater, plays an important role in the characteristics of the breakwater's response. Damping is associated with the waves that radiate out from the body due to its motion; but for situations in which the radiated waves are relatively small, that is when the system is lightly damped, the main contribution of the surface waves is to provide a forcing function. This effect is obvious in the case of roll, particularly near resonance, and the response is greatly over predicted by the linear potential theory (Standing (1991)). Therefore, a set of different viscous damping coefficients was used in the numerical model in order to obtain reflection, transmission and energy dissipation coefficients, and RAO's for comparison with the experimental results. This comparison is presented in Figs. 4.11 and 4.12 for rectangular and circular models respectively. The experimental values correspond to Table 4.4 for the rectangular section and to Table 4.5 for the circular section.

Consider Fig. 4.11(a) indicating the RAO's for the case of the rectangular section. Numerical results for sway and heave responses compare reasonably well with those obtained from the experimental study. Also, these plots indicate that the sway and heave responses are closely in phase. However, for the roll response the agreement between the numerical result

with observed experimental values is poor. The location of peak roll responses from numerical predictions with different damping coefficients are in the range of $0.9 < ka < 1.1$, where as the location of peak response obtained from the experiments lie at $ka = 1.4$ approximately. This discrepancy may be attributed to the fact that the mooring line tends to become fully suspended imparting sharp snap loads on the mooring lines, thereby limiting the roll amplitude in the vicinity of resonance ($0.9 < ka < 1.5$).

Consider Fig. 4.11(b), which indicates the numerical values of reflection, transmission and energy dissipation coefficients including the associated experimental results. The numerical values of these coefficients do not show good agreement with the experimental results. This may be largely attributed to the interference effect of the two pontoons that imparts sharp variations in the plots of these coefficients as functions of ka. Similarly, the experimental study indicates significant sloshing and related energy dissipation. However, it may be noted that the transmission coefficient compares reasonably well except in the vicinity of resonance. Based on these comparisons viscous damping coefficients of 2.5% was assumed for numerical predictions of response for rectangular section breakwater.

Similar analysis was carried out for the case of a circular section breakwater where the energy dissipation seemed less compared to that of a rectangular section. Thus, viscous damping coefficient of 1.0% was adopted in the numerical model for the circular section breakwater.

Figures 4.12 through 4.21 relate to rectangular twin-pontoon section and Figs. 4.22 through 4.27 correspond to circular twin-pontoon section. These figures present the influence of draft, pontoon spacing and mooring line material, and slackness parameters on the RAO's, the RAO phases, reflection and transmission coefficients, and the maximum mooring line tension coefficients at the anchors. These cases are now considered in turn by first considering the base case of a moored rectangular twin-pontoon section breakwater.

4.3.1 Rectangular Section with Chain Moorings

Figure 4.12 relates to the base case of twin-pontoon rectangular breakwater with relative water depth, d/a = 1.67, relative draft, h/a = 0.45 and relative pontoon spacing, b/a = 1.0, and moored with a chain of relative slackness, S/S_o = 1.08. The figure compares the experimental values with those of numerical results for transmission coefficient, K_T, response amplitude amplitudes, RAO's, and RAO phases.

The numerical values of K_T are greater than 0.6 for ka < 1.25. The variation of K_T exhibits a dip at ka ≈ 1.5, and is less than 0.5 for ka > 1.5 (Fig. 4.12(a)). For larger ka values, the corresponding experimental results compare reasonably well. For a twin-pontoon breakwater to be effective, it is noted that the minimum width of an individual pontoon must not be less than a quarter of the wavelength.

Consider now Fig. 4.12(b) relating to the RAO's. The sway and heave RAO's exhibit an initial dip near ka = 1.0 with an associated phase shift, while the roll RAO exhibits a peak corresponding to a roll resonance. The heave RAO peaks near ka = 1.4 indicating a higher frequency for heave resonance. The numerical values of RAO phases are compared with the corresponding experimental results in Fig. 4.12(c). It is recalled that the RAO phases indicated here are defined with respect to a wave crest. The comparison between the theoretical and experimental results seems to be reasonably good. In the subsequent plots of RAO phases, the experimental results are not included.

Influence of Draft

A base case of a rectangular section with a relative water depth ratio d/a = 1.67, spacing ratio b/a = 1.0, and chain moorings with slackness ratio S/S_o = 1.08 was considered. Three different relative drafts considered in the study correspond to h/a = 0.33, 0.45 and 0.55, and associated results are tabulated in Table 4.4.

Figure 4.13(a) indicates the influence of draft on the sway, heave and roll RAO's. Experimental values have been superposed on these plots, which indicate reasonable agreement with the numerical results with some discrepancies at resonance.

The numerical results indicate that the effect of draft on sway is relatively insignificant. The influence of draft on the heave RAO is limited to a change in the heave natural frequency only: the heave natural frequency reduces as the draft increases, since the submerged volume and thus the effective mass increases, while the stiffness does not change. In the high frequency range, experimental results indicate some degree of rise in the magnitude of heave RAO when compared with the numerical values. This may be due to the fact that the heave response is in phase with the oscillation of the enclosed water column, leading to a discrepancy in heave RAO. For both sway and heave, the RAO's tend to zero near ka = 1.0 indicative of the pontoon interference effects. In the case of roll response, an increase in draft results in a lower roll natural frequency and the associated response becomes sharper.

Figure 4.13(b) presents the phase relating to the sway, heave and roll RAO's. The phase angle is defined here as a lag in the maximum value relative to a wave crest crossing the origin. For the case of sway, as ka increases the phase changes from 90° to 0° and then eventually becomes -90°. In heave, the motion is in phase with the wave at low ka values and changes to -90° near the heave natural frequency. For the case of roll in the low frequency range, the response is in-phase with sway, but as ka increases the roll phase increases gradually from -90° to zero and then to 90° approximately. The form of the phase-frequency parameter curves generally remains the same for all three relative drafts considered.

Figure 4.14 shows a plot of the variation of reflection and transmission coefficients with ka for the three relative drafts, obtained from both the numerical analysis and experiments. As expected, the numerical results indicate that the deeper draft sections give rise to higher reflection coefficients and lower transmission coefficients, (see also Fig. 4.1). However, the experimental values for the deeper draft show higher K_T values than for the shallower drafts, which may be attributed to wave overtopping due to a reduced freeboard.

Influence of Spacing

Three different pontoon spacings, b/a = 0.5, 1.0 and 1.5 have been considered. Corresponding experimental results are tabulated in Table 4.4 and a comparison is given in Figs. 4.15 and 4.16.

For the case of sway, Fig. 4.15(a) indicates that in low and moderate ranges of ka, a bigger spacing reduces sway amplitude by a reasonable amount. For larger values of ka (> 2.5) the system behaves like an individual pontoon, and indicates a higher sway amplitude. The variation of sway motion for the freely floating case of the single-pontoon section given in Fig 4.3(d) shows similar results. In the heave mode, the pontoon spacing only influences the natural frequency of the system. However, for the roll mode, the larger spacing reduces the roll amplitude significantly, because of the associated increase in the roll radius of gyration leading to a stiffer model. The experimental values compare reasonably well, but deviate near the natural frequencies of the corresponding modes.

Figure 4.15(b) indicates the influence of spacing on the phases of the RAO's. The variations are similar to those given in Fig. 4.13(b), but for the case of small period waves, the phase changes from negative to positive and then returns to negative.

Figure 4.16 shows the reflection and transmission coefficients. As the spacing increases, the reflection coefficient increases and the transmission coefficient decreases, but in the higher range of ka, these coefficients include maxima and minima respectively. Once again, the transmission coefficient indicates that at higher ranges of ka, the twin-pontoon configuration practically acts as an individual unit. Earlier the influence of spacing on the reflection coefficient was presented in Fig. 4.1 for the case of fixed breakwater which included only scattered potentials. Fig. 4.1 for the variation of K_R indicated that a twin-pontoon breakwater with larger spacings performed similar to a single-pontoon breakwater. For a twin-pontoon breakwater to be effective, it can be noted that the spacing is taken to be approximately equal to the width of a single-pontoon. Thus, with ka $\approx$ 1.5 and b/a = 1.0, the

overall beam B (=2a+b), for a twin-pontoon breakwater can be estimated to be, approximately 3L/4, such that $K_T < 0.4$, where L is the wave length.

Experimental values superposed on Fig. 4.16 show reasonable agreement for the case of transmission coefficient. However, there exists considerable disagreement in the variation of the reflection coefficient.

Influence of Mooring Line Slackness

Three slackness values of chain moorings have been considered here: S/S_0 = 1.03, 1.08 and 1.16. The mooring configuration and the associated stiffness characteristics adopted here are those considered in arriving at Fig. 4.6. Corresponding results are tabulated in Table 4.4 and plotted in Figs. 4.17 - 4.19.

Since the hydrostatic stiffnesses in heave and roll are much larger than the corresponding mooring line stiffnesses, it is expected that the moorings would have no significant influence on the RAO's and RAO phases, except for the sway mode; and indeed Fig. 4.17(a) bears this out. Here, the plots of RAO's and corresponding phases, and the reflection and transmission coefficients indicate that there is no significant influence of mooring slackness (see Figs. 4.17, and 4.18). On the other hand, the mooring line forces are the only parameters of interest that are influenced by the slackness. Reduced slackness introduces increased nonlinearities as can be seen in Fig. 4.6. Figure 4.19 shows a plot of numerical results of maximum line tension at the anchor for the case of mooring line 5 (upwave side) in Fig. 4.6. The tension coefficient for mooring 5 is denoted as T'_1 (upwave) and corresponding experimental values are superposed in the figure. The upwave chain tensions only are presented, since the downwave moorings become relatively slack. The comparison with experimental values is not satisfactory because the measured tensions include impulsive loads (see Figs. 4.8(a) and 4.8(c)), which are not predicted in the numerical model.

4.3.2 Rectangular Section with Nylon Moorings

Attention is now given to the case of the rectangular section breakwater with nylon moorings. Figure 4.20 shows plots of the transmission coefficient K_T, the RAO's and the tension coefficients T_i's for the base case. As already indicated, only the taut case of $S/S_o = 1.0$ is considered. Figure 4.20(a), which shows the transmission coefficient, indicates reasonably good agreement between numerical predictions and experimental results. The RAO's compare fairly well overall, although the experimental values exhibit some scatter for ka values close to resonance (see Fig. 4.20(b)). Figure 4.20(c) shows a comparison of the maximum tension at the anchor for the upwave mooring line. Since the time variation of the mooring line tension is reasonably sinusoidal (see Fig. 4.8(b)), the estimates from the numerical analysis give a better agreement than that with the chain mooring system.

Figure 4.21 indicates the influence of draft and spacing on the transmission coefficient and the maximum mooring line tensions at the anchors. The variation of transmission coefficient is similar to that for the chain system (see Fig. 4.14), and as expected the transmission is smaller for deeper drafts. The maximum tensions, however, do not show significant change for the different drafts. The experimental results reasonably agree with the numerical predictions in the higher ranges of frequency, ka > 1.75. However, in the moderate to lower frequency ranges, the numerical values are as low as 60% of the experimental results. This discrepancy may be attributed to the mooring line stretch, which causes peak loads at resonance. It is also noted that because of line stretching, the peak loads observed in the nylon mooring system are not snap loads. Therefore, the experimental values of maximum mooring tensions are closer to numerical results than those observed for the case of chain mooring system (see Fig. 4.19). Similar results are also observed in Fig. 4.21(b) for different spacings. Again, for ka > 2.5 the transmission coefficient reaches a maximum and drop to 0.60 as observed in Fig. 4.16 for the case of chain moorings. Although, the comparison between numerical results and experimental values indicate a reasonable

agreement for most part of the ka ranges, the experimental values deviated from the numerical estimation considerably, for larger spacings with ka > 2.5.

4.3.3 Circular Section

Similar to the rectangular twin-pontoon breakwater, results relating to the circular section breakwater are presented in Figs. 4.22 - 4.27 and experimental values are tabulated in Table 4.5.

Figure 4.22 relates the case of a circular twin-pontoon breakwater with a 50% draft, a water depth ratio h/a = 2.5 and a spacing ratio b/a = 2.0. Once again, a six-point mooring system similar to the case of the rectangular section breakwater was considered, with a slackness ratio, S/S_0 = 1.08, in the case of chain moorings. Figures 4.23 and 4.24 relate to chain and nylon moorings respectively. In both figures, the results from the corresponding experimental study are superposed. It is clear that the numerical estimates compare reasonably well with experimental observations for the case of nylon moorings as seen in Fig. 4.23(c).

Figures 4.24 - 4.27 indicate the influence of draft and spacing on the RAO's, and the reflection and transmission coefficients, for both chain (see Figs. 4.24 and 4.25) and nylon moorings (see Figs. 4.26 and 4.27). Numerical results for drafts greater than 50% have not been estimated. These results follow a similar trend to those for the case of a rectangular section.

4.3.4 Influence of Wave Direction

The influence of incident wave direction on the hydrodynamic coefficients and the reflection and transmission coefficients has been reported in a number of studies for the case of a single pontoon section (see e.g., Bai 1975, Isaacson and Nwogu 1987, Garrison 1984). Here, numerical results have been obtained for the case of a fixed rectangular twin-pontoon breakwater with waves approaching the structure at angles β = 0°, 15° and 30°, and the resulting exciting force coefficients, and reflection and transmission coefficients are

presented as functions of ka in Fig. 4.28. These results are similar to those for a single pontoon section. As can be seen from the figure, the exciting force coefficient, and the reflection coefficients generally decrease with increasing angle of incidence.

4.3.5 Influence of Pontoon Section and Configuration

Pontoon Section

Figures 4.29(a) and 4.29(b) show a comparison of the transmission coefficient for rectangular and circular section twin-pontoon breakwaters for the fixed and moored cases respectively. Both the sections considered here have a water depth ratio d/a = 1.67, draft ratio h/a = 0.45, and spacing ratio b/a = 1.0, and for the moored case the slackness ratio S/So = 1.08. The comparison for the moored case indicates that the K_T value is higher for most part of ka for the circular section and is considerably higher over a reasonable midrange of ka. For ka > 1.75, both sections indicate small values of K_T. Overall, the rectangular section breakwater appears to perform better than the circular section breakwater.

Pontoon Configuration

Finally, it is of interest to compare the transmission coefficient relating to a rectangular twin-pontoon breakwater with that of a rectangular single-pontoon breakwater of various possible dimensions. Consider a twin-pontoon rectangular section breakwater with a relative water depth d/a = 2.5, a draft ratio h/a = 0.45 and a spacing ratio b/a = 1.0 as indicated in Fig. 4.30. The comparison is carried out for three different cases of a single pontoon section. These include a single-pontoon with a waterline beam equal to (i) the overall beam of the twin-pontoon section, B/a = 3, (ii) two times the width of an individual pontoon, B/a = 2, and (iii) the width of an individual pontoon, B/a = 1. Here, B is taken to be the overall beam, and a is the width of an individual pontoon as defined earlier in Fig. 2.3. Figures 4.30(a) and 4.30(b) relate to the fixed case and the case with chain moorings respectively. In Fig. 4.30(a), the transmission coefficient, K_T for B/a = 3 stays consistently low, and that for B/a = 1 stays consistently high as expected, while results for B/a = 2 lie in between. These results compare

reasonably well with that of the twin-pontoon breakwater. However, near ka ≈1.0, the transmission coefficient rises to approximately 1.0, deviating from the results corresponding to single pontoon case of B/a = 2. At higher ka values, K_T remains more or less the same for all cases.

Figure 4.30(b) presents corresponding results with the breakwaters now taken to be moored by chains with a slackness ratio, $S/S_o = 1.08$, and a rise to span ratio, $Z/X = 0.403$. In this case, the twin-pontoon section provides lower transmission coefficients than those for the case of a single-pontoon section with B/a = 3. This indicates the advantage of using a twin-pontoon configuration over a single-pontoon configuration. This reduction is mainly due to the increased hydrostatic roll stiffness related to the twin-pontoon section.

It is interesting to compare the transmission coefficient for the fixed case of a twin-pontoon section with that of a moored breakwater. The variation of K_T for the fixed case indicates a peak in the low ka range (Fig. 4.30(a)), whereas for the case of moored breakwater this peak is no longer present (Fig. 4.30(b)). This confirms the presence of interference effects for the fixed case as there are dynamics associated with body motions present. Now consider the moored case as in Fig. 4.30(b), for the twin- and single-pontoon sections. The variation of K_T exhibits a dip for all of the configurations shown except for the single-pontoon section with B/a = 3. This indicates that the dip in K_T is essentially a feature of the dynamics of the system and is associated with a phase shift in RAO; it is not associated with any particular section configuration such as the twin-pontoon considered here.

It is also interesting to note the performance of the twin-pontoon section in relation to that of an A-frame floating breakwater (see Fig. 1.1). An A-frame section is similar to a twin-pontoon section, except that it includes a rigid vertical centre-board with a draft larger than that of the pontoon itself, and also each pontoon is much smaller in size. Experimental and field studies have been reported by a few investigators (e.g. Byres, 1988). Consider Fig. 4.31, which compares the transmission coefficient of a twin-pontoon section with that of an A-frame section breakwater. The twin-pontoon section considered here has sectional ratios

d/a = 6.0, b/a = 6.0, and h/a = 0.5, while the A-frame section has a similar section, including a draft ratio for the centre-board to pontoon width equals to 3.5. (In practice relatively small pontoons would be used for the A-frame breakwater.) For ka values smaller than 1.0, the transmission coefficient for the A-frame section is smaller than that for the twin-pontoon section, as expected. In addition, for a spacing ratio b/a > 1.5 and with ka > 1.5, it is observed that the twin-pontoon section essentially behaved like a single-pontoon section. In Fig. 4.31, the K_T values for a single-pontoon section with d/a = 6.0 and h/a = 0.5 are also superposed and a comparison indicates that the A-frame section also exhibits a similar trend for ka > 1.5. However, the presence of the centre-board essentially reduces the K_T for values of ka close to 1.0.

The numerical approach based on a boundary integral method appears not to predict reasonable values of the transmission coefficient for the A-frame breakwater. This may be attributed to inconsistencies associated with the distribution of singular potentials on the centre-board, and also the wave-structure interaction may not be in the diffraction regime because the size of each pontoon is generally smaller.

4.4 Example Problem

The suitability of a floating breakwater design depends on several factors such as the water depth, soil conditions, incident wave climate, tidal range and currents, and the degree of wave protection required. In order to illustrate the present approach in the context of a typical application, consideration is given to a twin-pontoon breakwater similar to the one deployed at Comox, British Columbia. Figure 4.32 shows plan and sectional views of the breakwater. Two rectangular section pontoons each 2.0 m wide and 0.9 m in draft are rigidly connected to one another. The gap between the pontoons is taken to be equal to 2.0 m and the water depth at the site is considered to be 3.4 m. The breakwater is 40.0 m long and is moored with a ten-point chain mooring system. The mooring lines are equally spaced at 10.0 m apart, as indicated in Fig. 4.32. The chain has a submerged weight per unit length, q = 183.0 N/m, an

elastic rigidity per unit length, EA = 20.0 MN, a slackness ratio S/S_o = 1.08 and a rise to span ratio Z/X = 0.403. Waves at the site are taken to correspond to a wave period range of 1.8 to 6.0 sec and a constant wave steepness of 0.04. The incident wave direction is taken to be normal to the longitudinal axis of the breakwater.

Figure 4.33 provides a plot of mooring line tensions at the anchors as functions of breakwater displacement in sway, for the two chains at the centre of the breakwater. In addition, the restoring force as a function of breakwater displacement is shown superposed on the plot. The plot is useful in arriving at the mooring stiffnesses, operational line tensions associated with the maximum allowable line load capacity, and corresponding breakwater excursions. Figure 4.34 shows the exciting forces, the wave drift force, the breakwater drift, the amplitudes of sway motion, the transmission coefficient, and the maximum mooring line tensions at anchor, all as functions of incident wave frequency. In the figures, the exciting forces, the wave drift force, the drift and sway motions are presented with dimensions.

Generally, moderate condition with wave frequency ranging from 0.25 to 0.4 Hz (i.e. wave periods from 2.5 to 4.0 sec), is assumed to be a desirable for floating breakwater to be effective. Thus, for example, consider a wave period of 3.3 sec interacting with the breakwater. From Fig. 4.34 values extracted include, the exciting forces in sway and heave noted to be equal to 3000 and 7000 N per m length respectively, and the exciting moment in roll as 5000 Nm per m length approximately. The corresponding wave drift force is about 50 N per m length, and the maximum mooring line tension at the anchors is approximately 3,000 N for the most heavily loaded line. The breakwater excursion (drift and oscillatory) for this frequency range is approximately 0.22 m. The transmission coefficient, K_T, for this case is about 0.80. In the computation, the proposed iterative procedure for the wave drift force has been adopted.

5. Conclusions and Recommendations

5.1 Summary

The hydrodynamic performance of moored twin-pontoon breakwaters of rectangular and circular sections has been studied in the thesis. The hydrodynamic analysis of the breakwater was treated using an available numerical method based on Green's theorem, and extended so as to include two distinct bodies below the water surface corresponding to a twin-pontoon breakwater. A mooring analysis was carried out in conjunction with the hydrodynamic analysis in order to calculate the static and dynamic responses of the breakwater, and the associated tensions and displacements in the mooring system. An iterative procedure was adopted such that the wave drift force is consistent for both the hydrodynamic and mooring analyses. Experiments have been carried out to investigate the influence of design variables on engineering parameters and to compare the results with those of the numerical analysis.

Thus, the original aspects of this study include:

(a) the extension of a numerical model to a twin-pontoon breakwater;

(b) the integration of hydrodynamic and mooring analyses into a single comprehensive breakwater design computer model;

(c) a detailed experimental investigation for moored twin-pontoon breakwaters with rectangular and circular sections;

(d) the implementation of a simple but reasonably accurate method of motion analysis to obtain breakwater model responses, and

(e) a comparison of experimental results and numerical predictions, which highlights the feasibility and limitations associated with the numerical model for design purposes.

5.2 Conclusions

Bearing in mind the discrepancies between experimental results and numerical prediction that have been observed, the important conclusions of the study are summarized below.

5.2.1 Numerical Model

- In contrast to the case a fixed single-pontoon section, the variations of reflection and transmission coefficients with respect to frequency parameter, ka, for a fixed twin-pontoon section exhibit minima and maxima respectively, this being attributed to interference effects between the two pontoons. Here k is the wave number and a is the pontoon width (diameter in the case of a circular section).
- Flow separation effects are significant in certain situations, such as for a structure which possesses sharp corners. The numerical model based on linear potential theory neglects the flow separation effects and thus, the responses are over predicted, especially for the case of roll motion. This deficiency of the linear potential theory is overcome by incorporating empirical viscous damping coefficients. In the present study, by comparing the numerical results of transmission, reflection and energy dissipation coefficients, and RAO's with those of experiments, viscous damping coefficients of 2.5% and 1.0% were estimated for both the rectangular and circular section breakwaters. It is noted that the scale ratio for a rectangular section is taken to be 5.0 and that for a circular section 6.67. Also, it is important to bear in mind that the experiments were carried out by considering Froude's scaling effects and assuming Reynold's scaling effects (viscous effects) are less significant. Therefore, the values of viscous damping estimated from experimental studies need to be reduced for prototype situations and this in general, leads to larger responses.
- The frequency parameter, ka is a dominant parameter in determining the efficiency of the breakwater. As ka increases, the degree of wave transmission generally decreases. To be effective, a floating breakwater should have a pontoon width or diameter of at least one

quarter of the design wave length (i.e. ka > 1.5). In addition, the overall beam of the twin-pontoon section must be about three quarter of the design wave length such that the transmission coefficient is less than 0.4.

- The dynamic analysis of the moored rectangular breakwater indicated that the maximum heave RAO is also about 1.25 and is located at ka = 1.2, and the maximum roll RAO is about 1.25 and is located at ka = 1.0. However, the heave and sway modes indicate a minimum RAO (≈ zero) at ka = 1.0. Similarly, for the case of a moored circular section breakwater, the heave RAO is indicated to be about 1.1 and is located at ka = 1.6, and the maximum roll RAO is about 0.6 and is located at ka = 0.95. However, the heave and sway modes indicate a minimum RAO (≈ zero) at ka = 0.9, which is attributed to the interference effect between two pontoons.
- The relative spacing b/a between the pontoons of a twin-pontoon breakwater is an important parameter that brings in additional waterline beam for a given individual pontoon width. As b/a increases, the wave transmission decreases for moderate ka values, but at large b/a values, a twin-pontoon section performs as a single-pontoon section. Thus, for twin-pontoon section to be effective, the spacing should be approximately equal to the pontoon width.
- The occurrence of negative added mass and an associated sharp peak in the damping coefficient may be attributed to the effect of the spacing between the pontoons. This is largely because of the out-of-phase motion of the body in relation with the water surface in the vicinity of the body. In the case of a twin-pontoon section, the space between the pontoons effectively forms an oscillating water column, responding as a separate oscillator.
- The relative draft h/a, directly influences the heave natural frequency decreasing its value as h/a increases. It may be recalled that as b/a increases, added mass coefficients in both sway and roll sharply rise and then drop to negative values. Consequently, an associated sharp rise is also expected in the damping coefficient variation. However, as b/a

increases, the heave added mass and damping coefficient show a sharp rise only in the moderate ranges of the frequency parameter ($0.6 < ka < 1.0$). A local minimum in the transmission curve is observed when ka is close to the heave natural frequency.

- As h/a increases, the breakwater motions decrease due to increased inertia, but overtopping may also occur resulting in higher transmission coefficients. An optimum value of the relative draft h/a also depends on the frequency parameter, ka, and the wave steepness, H/L.
- In the present study, for moored structures, the hydrodynamic analysis is carried out in conjunction with a mooring analysis. The two separate problems are coupled through the wave drift force and the effective linearized stiffness of the mooring system. An iterative procedure is required to provide a solution to this problem, particularly when the mooring system force-displacement characteristics are noticeably nonlinear.
- An increase in the mooring slackness does not noticeably influence the breakwater motions and wave transmission, but greatly reduces mooring line forces. The choice of mooring line does not appear to significantly affect the overall performance of the breakwater.
- The exciting force coefficient generally decreases with increasing angle of incidence, except for differences to this trend associated with a resonance peak in the heave exciting force. The reflection and transmission coefficients also show similar features.
- Transmission coefficients for rectangular and circular section twin-pontoon breakwaters of equivalent size are generally comparable. The amplitudes of the sway, heave and roll motions are also very similar.
- The wave transmission past a twin-pontoon breakwater is compared with that past a single-pontoon breakwater with three different beams. The transmission coefficient for the fixed case of a twin-pontoon breakwater compares more closely with that of a single-pontoon breakwater of beam equal to the sum of the widths of the two individual pontoons. For the moored case, the transmission coefficient compares reasonably well

with that of a single-pontoon breakwater with beam equal to the overall width of the twin-pontoon breakwater.

5.2.2 Experimental Results and Comparison with Numerical Model

- In general, the numerical results relating to reflection and transmission coefficients compare reasonably well with those of the experiments, except at frequencies near resonance. Numerical results for pontoon behaviour compare reasonably well with those of experiments for the case of nylon moorings. However, they do not agree for the case of chain moorings because the measured tensions include impulsive loads that are not predicted in the numerical model. In the case of experiments, the chain moorings tend to become fully suspended and impart sharply rising snap loads.
- The experimental results relating to reflection coefficients were obtained by three different methods as outlined in Appendix A. The estimates based on all three methods do not mutually agree, however, the least-square method appears to estimate the reflected wave profile reasonably well for the wave conditions considered in the present study.
- In the experiments, response time histories have been obtained by using a video motion tracking system as described in Appendix B. This method of motion measurement has the advantage of not requiring special tracking cameras, but a rather simple camcorder and an IBM compatible PC with a frame grabber card are sufficient for the motion tracking purposes. It is quite simple to track the marked points on the model, and the results are sufficiently accurate to about 7 – 8% in translation and 10 – 12% in rotation.
- The numerical model provides a parametric measure that can be related to a design application and the results are in reasonably good agreement with the experimental values, except in the vicinity of resonance. Thus, the numerical model can be used as a preliminary tool to obtain related engineering design parameters.

5.3 Recommendations

The present study considers the case of a twin-pontoon floating breakwater interacting with monochromatic, regular wave train. A linearized boundary value problem is solved assuming the fluid as ideal, the flow irrotational, and considering the waves as non-breaking. The work carried out and the study performed of the related literature indicates that there are several extensions of the present research which may improve the overall understanding of the performance of floating breakwaters. Prospective extensions of the present study include the following:

- In the present study the case of a twin-pontoon breakwater interacting with a regular wave train is considered, whereas it is of interest to consider the response of a twin-pontoon floating breakwater to random waves. Such a study would be useful to assess the extent to which the regular wave results can be applied to random waves. For example, by first estimating the spectral density functions for the incident and reflected wave fields and then, calculating the reflection coefficient can be estimated as a function of frequency. This reflection coefficient function can be directly compared to the reflection coefficients for each wave period measured in the regular wave tests.
- The present study largely considers the two-dimensional case of a breakwater interacting with normally incident regular waves, although a limited number of numerical results indicating the effects of wave direction on the hydrodynamic coefficients have also been presented. Examination of the influence of oblique regular waves on a rigid floating breakwater of finite length would provide phase difference information relating to RAO's and exciting forces. In particular, the influence of the hydrodynamic loads and moorings associated with oblique waves on the bending moments and torsion at a breakwater section needs to be assessed in this effective design.

- In practice, the incident waves are both random and short crested (i.e. made up of multi-directional components) with an oblique mean direction. Therefore, the influence of short crested random waves on a floating breakwater needs to be assessed. This may be carried out on the basis of both experiments using a segmented wave generator, and a numerical model based on a superposition technique.
- Finally, the present study has indicated the influence of impulsive loads in the mooring lines, unless these are relatively slack. It may be possible to simulate these numerically using a time-domain method. This would be helpful in the evaluation of extreme motions and forces.

References

Abramowitz, M., and I. A. Stegun. (1964). "Handbook of mathematical functions", Dover Publications, New York.

Adee, B. H., and W. Martin. (1974). "Analysis of floating breakwater performance", Proceedings of the Floating Breakwater Conference, University of Rhode Island, RI, pp. 21 - 40.

Adee, B. H. (1976). "Floating breakwater performance", Proceedings of the 15th Coastal Engineering Conference, ASCE, Honolulu, HI, Vol. 3, pp. 2777 - 2791.

ASCE Ports and Harbors Task Committee. (1994). "Planning and design guidelines for small craft harbours", Manuals and Reports on Engineering Practice No. 50, ASCE, New York, NY.

Bai, K. J. (1975). "Diffraction of oblique waves by an infinite cylinder", Journal of Fluid Mechanics, Vol. 68, pp. 513 - 535.

Bando, K., and C. J. Sonu. (1987). "Evaluation of numerical models for a floating breakwater", Tekmarine Inc., Technical Report No. CERC-MP-87-6, Sierra, CA.

Berger, U., and S. Kohlhase. (1976). "Mach reflection as diffraction problem", Proceedings of the 15th Coastal Engineering Conference, ASCE, Honolulu, HI, Vol. I, pp. 796 - 814.

Blumberg, G. P., and R. J. Cox. (1988). "Floating breakwater physical model testing for marina applications", Bulletin of the Permanent International Association of Navigational Congress, No. 63, pp. 5 - 13.

Byres, R. (1988). 'The application of floating breakwaters in British Columbia', M.A.Sc. Thesis, Department of Civil Engineering, University of British Columbia, Vancouver.

Cammaert, A. B., B. Morey, L. Lesley, and T. Warren. (1994), "The development of a design manual for floating breakwaters in the Atlantic environment", including appendices,

Technical Report, TR-FIS-94002, Ocean Engineering Research Centre, Memorial University of Newfoundland, St. John's, NF.

Carvalho, E. R., and E. Mesquita. (1994). "Numerical evaluation of hydrodynamic forces and stationary response of floating bodies using the boundary element method", Proceedings of the 4th International Offshore and Polar Engineering Conference, ISOPE, Osaka, Japan, Vol. 3, pp. 237 - 243.

Chakrabarti, S. K. (1987). "Hydrodynamics of offshore structures", Elsevier Science Publishing Company, Inc., New York, NY.

Chen, S., and O. Mahrenholtz. (1992). "Interaction of water waves and floating twin cylinders in beam waves", Applied Ocean Research, Vol. 14, pp. 371 - 379.

Cox, J. C. (1989). "Design of a floating breakwater for Charleston Harbour, South Carolina", Proceedings of Ports' 89, ASCE, Boston, MA, pp. 411 - 420.

de Kat, J. O., and A. Dercksen. (1994). "The influence of wave spectrum on the dynamics of a turret-moored tanker", Journal of Offshore Mechanics and Arctic Engineering, ASME, Vol. 116, No. 1, pp. 7 - 13.

Downie, M. J., J. M. R. Graham, and X. Zheng. (1993). "The influence of viscous effects on the motion of a body floating in waves", Journal of Offshore Mechanics and Arctic Engineering, ASME, Vol. 115, No. 2, pp. 41 - 45.

Drimer, N., Y. Agnon, and M. Stiassne. (1992). "A simplified analytical model for a floating breakwater in water of finite depth", Applied Ocean Research, Vol. 14, pp. 33 - 41.

Faltinsen, O. M. (1990). "Sea loads on ships and offshore structures", Cambridge University Press, Cambridge, UK.

Flory, J. F., H. A. Mckenna, and M. R. Parsey. (1992). "Fiber ropes for ocean engineering in the 21st century", Proceedings of the International Conference on Civil Engineering in the Oceans V, ASCE, College Station, Texas, pp. 934 - 947.

Garrison, C. J. (1984). "Interaction of oblique waves with an infinite cylinder", Applied Ocean Research, Vol. 6, No. 1, pp. 4 - 15.

Gaythwaite, J. W. (1990). "Design of marine facilities for berthing, mooring, and repair of vessels", Van Nostrand Reinhold, New York, NY.

Graham, J. M. R. (1980). "The forces on sharp-edged cylinders in oscillatory flows at low Keulegan-Carpenter numbers", Journal of Fluid Mechanics, Vol. 97, pp. 331 - 346.

Hanif, M. (1983). "Analysis of heaving and swaying motion of a floating breakwater by finite element method", Ocean Engineering, Vol. 10, No. 3, pp. 181 - 190.

Hartz, B. J., and C. Georgiadis. (1982). "A finite element program for dynamic response of continuous floating structures in short crested waves", Proceedings of the International Conference on Finite Element Methods, Shanghai, China, pp. 1 - 6.

Hutchinson, B. L. (1984). "Impulse response technique for floating bridges and breakwaters subject to short-crested seas", Marine Technology, Vol. 21, No. 3, pp. 270 - 276.

Isaacson, M. (1991). "Measurement of regular wave reflection", Journal of Waterway, Port, Coastal and Ocean Engineering, ASCE, Vol. 117, No. 6, pp. 553 - 569.

Isaacson, M. (1993a). "Wave effects on floating breakwaters", Proceedings of the 1993 Canadian Coastal Conference, Vancouver, BC, Vol. 1, pp. 53 - 65.

Isaacson, M. (1993b). "Hydrodynamic coefficients of floating breakwaters", Proceedings of the 11th Canadian Hydrotechnical Conference, CSCE, Fredericton, NB, Vol. 1, pp. 485 - 494.

Isaacson, M., and J. Baldwin. (1996). "Moored structures in waves and currents", Canadian Journal of Civil Engineering, CSCE, Vol. 23, pp. 418 - 430.

Isaacson, M., and O. Nwogu. (1987). "Directional wave effects on long structures", Journal of Offshore Mechanics and Arctic Engineering, ASME, Vol. 109, No. 2, pp. 126 - 132.

Isaacson, M., N. Whiteside, R. Gardiner, and D. Hay. (1994). "Modelling of a circular-section floating breakwater", Proceedings of the International Symposium: Waves - Physical and Numerical Modelling, IAHR, Vancouver, BC, Vol. III, pp. 1344 - 1353.

Jamieson, W., G. Mogridge, and D. Williams. (1994). "Model tests of a floating breakwater dock", Proceedings of the International Symposium: Waves - Physical and Numerical Modelling, IAHR, Vancouver, BC, Vol. III, pp. 1334 - 1343.

Jones, D. B. (1971). "Transportable breakwaters - a survey of concepts", Technical Report R-727, Naval Civil Engineering Laboratory, U.S. Navy, Port Huneme, CA.

Leonard, J. W. (1988). "Tension structures - behaviour and analysis", McGraw Hill Book Company, New York, NY.

Leonard, J. W., M-C. Huang, and R. T. Hudspeth. (1983). "Hydrodynamic interference between floating cylinders in oblique seas", Applied Ocean Research, Vol. 5, No. 3, pp. 158 - 166.

Longuet-Higgins, M. S. (1977). "The mean forces exerted by waves on floating or submerged bodies with applications to sand bars and wave power machines", Proceedings of the Royal Society, London, Series A, Vol. 352, pp. 463 - 480.

McCartney, B. L. (1985). "Floating breakwater design", Journal of Waterway, Port, Coastal, and Ocean Engineering, ASCE, Vol. 111, No. 2, pp. 304 - 317.

McLaren, R. W. (1981). "Preparation of floating breakwater manual", Proceedings of the 2nd Conference on Floating Breakwaters, University of Washington, Seattle, WA, pp. 22 - 47.

Melville, W. K. (1980). "On the Mach reflexion of a solitary wave", Journal of Fluid Mechanics, Vol. 98, No. 2, pp. 285 - 297.

Miles, M. D. (1989). "Guide to using GEDAP", Technical Report, Hydraulics Laboratory, Natural Research Council of Canada, Ottawa.

Miller, R. W., and D. R. Christensen. (1984). "Rigid body motion of a floating breakwater", Proceedings of the 19th Coastal Engineering Conference, ASCE, Houston, TX, Vol. 3, pp. 2663 - 2679.

Nece, R. E., and N. K. Skjelbreia. (1984). "Ship wave attenuation tests of a prototype floating breakwater", Proceedings of the 19th Coastal Engineering Conference, ASCE, Houston, TX, Vol. 3, pp. 2514 - 2529.

Nelson, E. E., and L. L. Broderick. (1984). "Floating breakwater prototype test program", Proceedings of the 41st Meeting of the Coastal Engineering Research Board, U. S. Army Coastal Engineering Research Center, Vicksberg, MS.

Newman, J. N. (1977). "Marine hydrodynamics", M.I.T. Press, Cambridge, MA.

Ohkusu, M. (1974). "Hydrodynamic forces on multiple cylinders in waves", Proceedings of the International Symposium on the Dynamics of Marine Vehicles, University College London, London, UK, pp. 107 - 112.

Patel, M. H. (1989). "Dynamics of offshore structures", Butterworths, London, UK.

Photo4D. (1996). "Motion analysis package - user's guide", CompInt, Inc., Nepean, ON.

Rahman, M. (1994). "Water waves: relating modern theory to advanced engineering applications", The Institute of Mathematics and Its Applications Monogram Series, Clarendon Press, Oxford, UK.

Ratcliffe, A. T. (1985). "The validity of quasi-static and approximate formulae in the context of the cable and riser dynamics", Proceedings of the 4th International Conference of the Behaviour of Offshore Structures, Delft, The Netherlands, Vol. 2, pp. 337 - 346.

Rowland, A. (1995). "Floating breakwater performance monitoring and evaluation, Comox, BC", Technical Report, Small Craft Harbours Branch, Department of Fisheries and Oceans, Vancouver, BC.

Sarpkaya, T., and M. Isaacson. (1981). "Mechanics of wave forces on offshore structures", Van Nostrand Reinhold, New York, NY.

Skop, R. A. (1988). "Mooring systems: A state-of-the-art review", Journal of Offshore Mechanics and Arctic Engineering, ASME, Vol. 110, No. 1, pp. 365 - 372.

Standing, R. G. (1991). "Prediction of viscous roll damping and response of transportation barges in waves", Proceedings of the 1st International Offshore and Polar Engineering Conference, Edinburg, UK, Vol. 3, pp. 409 - 419.

Teng , B. and R. Eatock Taylor. (1995). "New higher-oder boundary element methods for wave diffraction/radiation", Applied Ocean Research, Vol. 17, pp. 71 – 77.

Triantafyllou, M. S. (1994). "Cable mechanics for moored floating systems", Proceedings of the 7th International Conference on Behaviour of Offshore Structures, Cambridge, MA, Vol. 2, pp. 57 - 78.

Tsinker, G. P. (1995). "Marine structures engineering, specialized applications", Chapman and Hall, New York, NY.

Valioulis, I. A. (1990). "Motion response and wave attenuation of linked floating breakwaters", Journal of Waterway, Port, Coastal, and Ocean Engineering, ASCE, Vol. 116, No. 5, pp. 558 - 574.

Vinje, T. (1989). "On the significance of the negative added mass", Proceedings of the Eighth International Conference on Offshore Mechanics and Arctic Engineering, ASME, The Hague, Vol. III, pp. 53 - 61.

Vugts, J. H. (1968). "The hydrodynamic coefficients for swaying, heaving, and rolling cylinders in a free surface", International Shipbuilding Progress, Vol. 15, pp. 251 - 276.

Wang, S., and R. Wahab. (1971). "Heaving oscillations of twin cylinders in a free surface", Journal of Ship Research, Vol. 15, pp. 33 - 48.

Wang, S. (1981). "Wave radiation due to oscillations of two parallel spaced cylinders", Ocean Engineering, Vol. 8, No. 6, pp. 599 - 621.

Wehausen, J. V. (1971). "The motion of floating bodies", Annual Review of Fluid Mechanics, Vol. 3, pp. 237 - 268.

Werner, G. (1988). "Experiences with floating breakwaters, a literature review", Bulletin of the Permanent International Association of Navigational Congress, No. 63, pp. 23 - 30.

Western Canada Hydraulics Laboratory. (1981). "Development of a manual for the design of floating breakwaters", Canadian Manuscript Report of Fisheries and Aquatic Sciences, No. 1629, Small Craft Harbours Branch, Department of Fisheries and Oceans, Ottawa, ON.

Whiteside, N. (1994). "Performance of a circular cross-section moored floating breakwater", M.A.Sc. Thesis, Department of Civil Engineering, University of British Columbia, Vancouver, BC.

Wiegel, R. L. (1964a). "Oceanographical engineering", Prentice Hall, New York, NY.

Wiegel, R. L. (1964b). "Water wave equivalent of Mach-reflection", Proceedings of the 9th Coastal Engineering Conference, Lisbon, Portugal, Vol. I, pp. 82 - 102.

Williams, A. N., and A. G. Abul-Azm. (1996). "Hydrodynamic analysis of dual pontoon floating breakwater", Proceedings of the 6th International Offshore and Polar Engineering Conference, ISOPE, Los Angeles, CA, Vol. III, pp. 560 - 565.

Wilson, B. W. (1967). "Elastic characteristics of moorings", Journal of Waterway, Port, Coastal and Ocean Engineering, ASCE, Vol. 93, No. 4, pp.27 - 56.

Wren, T., J. N. Fawcett, and J. S. Burdess. (1989). "Application of extensible cable theory to determine the displacement of a moored ship", Mechanism and Machine Theory, Vol. 2, No. 3, pp. 207 - 212.

Yamamoto, T. (1982). "Moored floating breakwater response to regular and irregular waves", in Dynamic Analysis of Offshore Structures, Ed. C. L. Kirk, Gulf Publishing Company, Vol. I, pp. 114 - 123.

Yamamoto, T., and S. Takahashi. (1974). "Effects of cross-sectional shape and mooring on performance of floating breakwater", Proceedings of the Floating Breakwater Conference, University of Rhode Island, RI, pp. 149 - 162.

Yamamoto, T., A. Yoshida, and T. Ijima. (1982). "Dynamics of elastically moored floating objects", in Dynamics Analysis of Offshore Structures, Ed. C. L. Kirk, Gulf Publishing Company, Vol. I, pp. 106 - 113.

Yoon, S. B., and P. L. -F. Liu. (1989). "Stem waves along breakwater", Journal of Waterway, Port, Coastal, and Ocean Engineering, ASCE, Vol. 115, No. 5, pp. 635 - 648.

Wong, L. H. and S. M. Calisal. (1993). "The influence of viscous effects on the motion of a body floating in waves", Journal of Offshore Mechanics and Arctic Engineering, ASME, Vol. 115, No. 5, pp. 41 - 45.

Tables

Table 1.1 Summary of floating breakwater installations in British Columbia (see Fig. 1.2).

No.	Location	Type	Years of
1	Lund	A-frame	1963-1987
2	Powell River	Ship hull	1930-
3	Howe Sound	Barge	-
4	Eagle Harbour	Pontoon	1977-
5	Burrard YC	Caisson/Barge	1977-
6	Deep Cove YC	Caisson	1976-
7	Port Moody	Log Bundle	1976
8	Richmond	Caisson	1976-
9	Cowichan	A-frame	?
10	Maple Bay	Caisson	1977-
11	Nanaimo	Caisson	1974
12	Northwest Bay	Log/Styrofoam	1975-1983
13	Ford Cove	Log Raft	?
14	Deep Bay	Log Bundle	?
15	Comox	Log Bundle	?-1992

Table 3.1 Summary of regular wave test conditions.

Test No.	T	H	H/L	ka*		K	
	(s)	(m)		Rectangular	Circular	Rectangular	Circular
1	1.032	0.120	0.075	1.178	0.785	1.31	1.96
2	0.930	0.100	0.075	1.414	0.942	1.07	1.60
3	0.858	0.086	0.075	1.649	1.100	0.91	1.36
4	0.802	0.075	0.075	1.885	1.257	0.79	1.18
5	0.716	0.060	0.075	2.356	1.571	0.63	0.94
6	0.683	0.055	0.075	2.592	1.728	0.57	0.86
7	0.654	0.050	0.075	2.827	1.885	0.52	0.79
8	1.032	0.104	0.065	1.178	0.785	1.13	1.70
9	1.032	0.080	0.050	1.178	0.785	0.87	1.31
10	1.032	0.056	0.035	1.178	0.785	0.61	0.92
11	1.032	0.044	0.028	1.178	0.785	0.48	0.72
12	0.716	0.080	0.100	2.356	1.571	0.84	1.26
13	0.716	0.068	0.085	2.356	1.571	0.71	1.07
14	0.716	0.052	0.065	2.356	1.571	0.63	0.82
15	0.716	0.040	0.050	2.356	1.571	0.55	0.63
16	1.704	0.092	0.028	0.565	0.377	0.42	1.96
17	1.439	0.073	0.028	0.707	0.471	0.93	1.39
18	1.182	0.055	0.028	0.942	0.628	0.63	0.94

* a = pontoon width for rectangular section, diameter for circular section.

Table 3.2 Summary of ranges of design parameters relating to regular wave tests.

Parameter	Base Case		Ranges	
	Rectangular	Circular	Rectangular	Circular
Water depth, d	0.50 m	0.50 m	constant	constant
Pontoon size, a*	0.30 m	0.20 m	constant	constant
Cable horizontal span, Z/X	0.403	0.403	constant	constant
Wave frequency parameter, ka	see Table 3.1	see Table 3.1	1.18 – 2.83	0.79 – 1.89
Wave steepness, H/L	0.08	0.08	0.03 - 0.10	0.03 - 0.10
Pontoon spacing, b/a	1.00	2.00	0.50 1.00 1.50	0.50 2.00 3.50
Relative draft, h/a	0.45	0.65	0.33 0.45 0.55	0.50 0.65 0.80
Mooring	Chain Nylon	Chain Nylon	Chain Nylon	Chain Nylon
Cable slackness, S/S_o	1.08 for Chain 1.00 for Nylon	1.08 for Chain 1.00 for Nylon	1.03 1.08 1.16	1.03 1.08 1.16

a = pontoon width for rectangular section, diameter for circular section.

Table 3.3 Experimental conditions adopted for the rectangular and circular section breakwater models.

Test No.	Mooring, Slackness, S/S_o	T (s)	H (m)	Rectangular			Circular		
				h/a	b/a	ka	h/a	b/a	ka
1.1	Chain, 1.080	1.032	0.120	0.450	1.000	1.178	0.650	2.000	0.785
1.2		0.930	0.100			1.414			0.942
1.3		0.858	0.086			1.649			1.100
1.4		0.802	0.075			1.885			1.257
1.5		0.716	0.060			2.356			1.571
1.6		0.683	0.055			2.592			1.728
1.7		0.654	0.050			2.827			1.885
1.8		1.032	0.104			1.178			0.785
1.9		1.032	0.080			1.178			0.785
1.10		1.032	0.056			1.178			0.785
1.11		1.032	0.044			1.178			0.785
1.12		0.716	0.080			2.356			1.571
1.13		0.716	0.068			2.356			1.571
1.14		0.716	0.052			2.356			1.571
1.15		0.716	0.040			2.356			1.571
1.16		1.704	0.092			0.565			0.377
1.17		1.439	0.073			0.707			0.471
1.18		1.182	0.055			0.942			0.628
2.1.1	Chain, 1.030	1.032	0.120	0.450	1.000	1.178	0.650	2.000	0.785
2.1.2		0.858	0.086			1.649			1.100
2.1.3		0.716	0.060			2.356			1.571
2.1.4		0.654	0.050			2.827			1.885
2.2.1	Chain, 1.160	1.032	0.120	0.450	1.000	1.178	0.650	2.000	0.785
2.2.2		0.858	0.086			1.649			1.100
2.2.3		0.716	0.060			2.356			1.571
2.2.4		0.654	0.050			2.827			1.885
3.1.1	Chain, 1.080	1.032	0.120	0.550	1.000	1.178	0.800	2.000	0.785
3.1.2		0.858	0.086			1.649			1.100
3.1.3		0.716	0.060			2.356			1.571
3.1.4		0.654	0.050			2.827			1.885
3.2.1	Chain, 1.080	1.032	0.120	0.330	1.000	1.178	0.500	2.000	0.785
3.2.2		0.858	0.086			1.649			1.100
3.2.3		0.716	0.060			2.356			1.571
3.2.4		0.654	0.050			2.827			1.885
4.1.1	Chain, 1.080	1.032	0.120	0.450	0.500	1.178	0.650	0.500	0.785
4.1.2		0.858	0.086			1.649			1.100
4.1.3		0.716	0.060			2.356			1.571
4.1.4		0.654	0.050			2.827			1.885
4.2.1	Chain, 1.080	1.032	0.120	0.450	1.500	1.178	0.650	3.500	0.785
4.2.2		0.858	0.086			1.649			1.100
4.2.3		0.716	0.060			2.356			1.571
4.2.4		0.654	0.050			2.827			1.885

Table 3.3 Experimental conditions adopted for the rectangular and circular section breakwater models (contd.).

Test No.	Mooring, Slackness, S/S_o	T (s)	H (m)	Rectangular			Circular		
				h/a	b/a	ka	h/a	b/a	ka
5.1	Nylon, 1.000	1.032	0.120	0.450	1.000	1.178	0.650	2.000	0.785
5.2		0.930	0.100			1.414			0.942
5.3		0.858	0.086			1.649			1.100
5.4		0.802	0.075			1.885			1.257
5.5		0.716	0.060			2.356			1.571
5.6		0.683	0.055			2.592			1.728
5.7		0.654	0.050			2.827			1.885
5.8		1.032	0.104			1.178			0.785
5.9		1.032	0.080			1.178			0.785
5.10		1.032	0.056			1.178			0.785
5.11		1.032	0.044			1.178			0.785
5.12		0.716	0.080			2.356			1.571
5.13		0.716	0.068			2.356			1.571
5.14		0.716	0.052			2.356			1.571
5.15		0.716	0.040			2.356			1.571
5.16		1.704	0.092			0.565			0.377
5.17		1.439	0.073			0.707			0.471
5.18		1.182	0.055			0.942			0.628
6.1.1	Nylon, 1.000	1.032	0.120	0.550	1.000	1.178	0.800	2.000	0.785
6.1.2		0.858	0.086			1.649			1.100
6.1.3		0.716	0.060			2.356			1.571
6.1.4		0.654	0.050			2.827			1.885
6.2.1	Nylon, 1.000	1.032	0.120	0.330	1.000	1.178	0.500	2.000	0.785
6.2.2		0.858	0.086			1.649			1.100
6.2.3		0.716	0.060			2.356			1.571
6.2.4		0.654	0.050			2.827			1.885
7.1.1	Nylon, 1.000	1.032	0.120	0.450	0.500	1.178	0.650	0.500	0.785
7.1.2		0.858	0.086			1.649			1.100
7.1.3		0.716	0.060			2.356			1.571
7.1.4		0.654	0.050			2.827			1.885
7.2.1	Nylon, 1.000	1.032	0.120	0.450	1.500	1.178	0.650	3.500	0.785
7.2.2		0.858	0.086			1.649			1.100
7.2.3		0.716	0.060			2.356			1.571
7.2.4		0.654	0.050			2.827			1.885

Table 3.4 Principal dimensions and parameters for the base cases of the rectangular and circular twin-pontoon models.

Parameters	Rectangular	Circular
Length (m)	0.53	0.53
Width or diameter (m)	0.30	0.20
Draft (m)	0.13	0.13
Centre of gravity (m)	(0, -0.08)	(0, -0.06)
Roll radius of gyration (m)	0.45	0.33

Table 4.1 Linearized mooring stiffness matrix for no wave load condition for example application.

	Sway	Heave	Roll
Sway	26.00 kN/m	0.00 kN/m	12.90 kN/rad
Heave	0.04 kN/m	8.30 kN/m	0.39 kN/rad
Roll	12.90 kN/rad	0.00 kN/rad	30.70 kNm/rad

Table 4.2 Influence of number of iterations on sway drift force and drift for example application.

Iteration	Sway stiffness (kN/m)	Wave drift force (kN)	Sway drift (m)
1	32.32	3.11	0.119
2	37.22	3.54	0.136
3	38.82	3.72	0.143
4	39.54	3.80	0.146
5	39.90	3.85	0.147
6	40.10	3.87	0.148
7	40.20	3.88	0.149
8	40.26	3.89	0.150
9	40.29	3.90	0.150

Table 4.3 Comparison of results obtained with and without the iteration procedure.

Methods	Sway stiffness (kN/m)	Drift force (kN)	Sway drift (m)	Max. oscillatory motions sway (m)	heave (m)	roll (rads)	Max. mooring line tensions at anchor (N) T_1	T_2	K_R	K_T
No iteration	32.32	3.11	0.12	0.87	0.78	0.37	2,548	86.5	0.30	0.92
Iteration	40.29	3.90	0.15	1.04	0.79	0.36	2,965	42.5	0.34	0.90
Difference	19.9 %	20.0 %	20.0 %	16.3 %	1.3 %	-2.8 %	14.0 %	-103.0 %	12.6 %	-2.0 %

Table 4.4 Summary of experimental results for the rectangular section breakwater.

Test No.	ka	K_R	K_T	Mooring forces		RAO's		
						sway	heave	roll
				T'_1	T'_2	ξ'_1	ξ'_2	ξ'_3
1.1	1.178	0.327	0.375	1.150	0	0.578	0.327	0.791
1.2	1.414	0.326	0.329	0.911	0	0.121	1.421	0.997
1.3	1.649	0.330	0.235	0.865	0	0.372	0.770	0.682
1.4	1.885	0.570	0.226	0.666	0	0.212	0.514	0.566
1.5	2.356	0.600	0.181	0.082	0	0.282	0.269	0.400
1.6	2.592	0.942	0.152	0.033	0	0.224	0.274	0.390
1.7	2.827	0.960	0.145	0.039	0	0.213	0.351	0.380
1.8	1.178	0.523	0.364	0.954	0	1.146	0.147	0.218
1.9	1.178	0.544	0.318	0.544	0	1.011	0.235	0.619
1.10	1.178	0.413	0.482	0.444	0	1.999	0.476	0.787
1.11	1.178	0.325	0.491	0.060	0	1.142	0.342	0.541
1.12	2.356	0.784	0.194	0.390	0	0.505	0.468	0.513
1.13	2.356	0.745	0.181	0.254	0	0.461	0.325	0.505
1.14	2.356	0.545	0.216	0.089	0	0.401	0.314	0.443
1.15	2.356	0.498	0.146	0	0	0.324	0.214	0.402
1.16	0.565	0.125	0.954	0.375	0.377	0.935	0.891	0.796
1.17	0.707	0.146	0.908	0.337	0.084	0.547	0.791	0.616
1.18	0.942	0.272	0.675	0.442	0	0.353	0.614	0.585
2.1.1	1.178	0.262	0.580	0.769	0	1.000	0.294	0.744
2.1.2	1.649	0.320	0.420	0.749	0	1.269	1.052	0.886
2.1.3	2.356	0.667	0.220	0.200	0	1.134	0.212	0.300
2.1.4	2.827	0.775	0.226	0.342	0	0.851	0.321	0.254
2.2.1	1.178	0.480	0.395	1.250	0.529	0.244	0.151	0.419
2.2.2	1.649	0.659	0.188	1.136	0.514	0.382	0.474	0.136
2.2.3	2.356	0.942	0.138	0.603	0.158	0.231	0.376	0.200
2.2.4	2.827	0.971	0.080	0.602	0.280	0.154	0.301	0.185
3.1.1	1.178	0.220	0.580	0.649	0	0.314	0.239	0.698
3.1.2	1.649	0.294	0.420	0.551	0	0.395	0.851	0.545
3.1.3	2.356	0.500	0.217	0.282	0	0.135	0.418	0.400
3.1.4	2.827	0.700	0.226	0.176	0	0.354	0.351	0.050
3.2.1	1.178	0.374	0.395	0.666	0	0.819	0.176	1.131
3.2.2	1.649	0.416	0.188	0.581	0	0.451	0.476	0.546
3.2.3	2.356	0.907	0.138	0.179	0	0.643	0.471	0.400
3.2.4	2.827	0.980	0.080	0.018	0	0.458	0.675	0.215
4.1.1	1.178	0.400	0.460	0.779	0	0.530	0.645	0.150
4.1.2	1.649	0.350	0.350	0.563	0	0.340	0.473	0.477
4.1.3	2.356	0.873	0.236	0.524	0	0.230	0.318	0.400
4.1.4	2.827	0.872	0.220	0.159	0	0.150	0.312	0.375
4.2.1	1.178	0.168	0.340	0.846	0.632	0.630	0.720	0.990
4.2.2	1.649	0.288	0.173	0.630	0	0.463	0.546	0.341
4.2.3	2.356	0.587	0.120	0.473	0	0.325	0.374	0.300
4.2.4	2.827	-	-	-	-	0.230	0.375	0.430

Table 4.4 Summary of experimental results for the rectangular section breakwater. (contd...)

Test No.	ka	K_R	K_T	Mooring forces		RAO's		
						sway	heave	roll
				T'_1	T'_2	ξ'_1	ξ'_2	ξ'_3
5.1	1.178	0.213	0.476	0.358	0.184	0.517	0.524	0.698
5.2	1.414	0.213	0.394	0.270	0.245	0.415	1.164	0.642
5.3	1.649	0.115	0.306	0.276	0.242	0.383	0.658	0.614
5.4	1.885	0.447	0.368	0.204	0.203	0.341	0.601	0.424
5.5	2.356	0.685	0.242	0.102	0.052	0.292	0.430	0.200
5.6	2.592	0.840	0.330	0.072	0.040	0.281	0.401	0.218
5.7	2.827	0.870	0.407	0.084	0.043	0.252	0.432	0.237
5.8	1.178	0.323	0.516	0.401	0.221	0.173	0.538	1.036
5.9	1.178	0.357	0.488	0.388	0.245	0.684	0.621	0.856
5.10	1.178	0.411	0.564	0.343	0.254	0.750	0.797	0.984
5.11	1.178	0.253	0.585	0.327	0.232	0.516	0.513	0.786
5.12	2.356	0.695	0.256	0.095	0.040	0.432	0.491	0.358
5.13	2.356	0.612	0.242	0.082	0.030	0.374	0.563	0.298
5.14	2.356	0.723	0.235	0.090	0.042	0.261	0.478	0.154
5.15	2.356	0.657	0.156	0.063	0	0.241	0.562	0.185
5.16	0.565	0.178	0.907	0.708	0.272	1.229	1.513	0.367
5.17	0.707	0.194	0.820	0.703	0.305	1.051	1.384	0.413
5.18	0.942	0.200	0.667	0.289	0.230	0.987	1.124	0.786
6.1.1	1.178	0.269	0.435	0.609	0.090	1.110	0.218	0.698
6.1.2	1.649	0.093	0.380	0.240	0	0.857	0.388	0.273
6.1.3	2.356	0.435	0.320	0.120	0	0.730	0.155	0.200
6.1.4	2.827	0.680	0.480	0.096	0	0.514	0.124	0.131
6.2.1	1.178	0.345	0.370	0.188	0.099	0.769	0.481	0.419
6.2.2	1.649	0.250	0.280	0.154	0	1.288	0.531	0.614
6.2.3	2.356	0.806	0.160	0.037	0	0.588	0.362	0.400
6.2.4	2.827	0.935	0.264	0.024	0	0.426	0.216	0.328
7.1.1	1.178	0.292	0.444	0.306	0.177	0.647	0.396	0.837
7.1.2	1.649	0.400	0.483	0.293	0	1.019	0.511	0.682
7.1.3	2.356	0.500	0.380	0.102	0	0.614	0.214	0.300
7.1.4	2.827	0.600	0.480	0.087	0	0.515	0.314	0.256
7.2.1	1.178	0.400	0.434	0.649	0.175	0.602	0.675	0.233
7.2.2	1.649	0.320	0.230	0.283	0.163	0.554	0.624	0.341
7.2.3	2.356	0.800	0.170	0.282	0.256	0.697	0.269	0.200
7.2.4	2.827	0.940	0.179	0.043	0	0.436	0.159	0.121

Table 4.5 Summary of experimental results for the circular section breakwater.

Test No.	ka	K_R	K_T	Mooring forces		RAO's		
						sway	heave	roll
				T'_1	T'_2	ξ'_1	ξ'_2	ξ'_3
1.1	0.785	0.380	0.546	0.208	0.001	1.011	0.700	0.583
1.2	0.942	0.430	0.570	0.328	0	0.650	0.650	0.623
1.3	1.100	0.470	0.465	0.375	0	0.500	0.650	0.651
1.4	1.257	0.571	0.367	0.308	0	0.510	0.660	0.550
1.5	1.571	0.630	0.275	0.103	0	0.600	0.583	0.400
1.6	1.728	0.770	0.155	0.046	0	0.495	1.100	0.405
1.7	1.885	0.960	0.130	0.071	0	0.292	1.650	0.407
1.8	0.785	0.523	0.611	0.452	0	0.848	0.589	0.896
1.9	0.785	0.544	0.781	0.236	0	-	-	-
1.10	0.785	0.413	0.795	0.059	0	0.725	0.348	0.926
1.11	0.785	0.325	0.807	0.037	0	-	-	-
1.12	1.571	0.784	0.156	0.098	0	-	-	-
1.13	1.571	0.745	0.228	0.138	0	-	-	-
1.14	1.571	0.545	0.231	0.174	0	-	-	-
1.15	1.571	0.498	0.225	0.078	0	-	-	-
1.16	0.377	0.070	0.995	0.005	0	2.050	1.866	0.652
1.17	0.471	0.100	0.99	0.019	0	-	-	-
1.18	0.628	0.280	0.600	0.054	0	-	-	-
2.1.1	0.785	0.420	0.670	0.412	0.417	0.604	0.850	0.713
2.1.2	1.100	0.550	0.530	1.052	0.415	0.308	0.387	0.871
2.1.3	1.571	0.680	0.153	0.122	0.060	0.443	0.520	0.455
2.1.4	1.885	0.850	0.200	0.040	0.008	0.368	0.830	0.274
2.2.1	0.785	0.350	0.330	0.215	0	1.150	1.100	0.496
2.2.2	1.100	0.420	0.149	1.071	0	1.270	0.790	0.277
2.2.3	1.571	0.550	0.230	0	0	0.541	1.348	0.227
2.2.4	1.885	0.650	0.110	0.108	0	0.550	1.900	0.050
3.1.1	0.785	0.193	0.490	0.013	0	0.705	0.320	0.496
3.1.2	1.100	0.391	0.310	0.026	0	0.427	0.455	0.326
3.1.3	1.571	0.660	0.200	0.034	0	0.680	0.680	0.333
3.1.4	1.885	0.810	0.320	-	-	0.140	0.880	0.231
3.2.1	0.785	0.351	0.702	0.446	0	0.900	0.580	0.685
3.2.2	1.100	0.437	0.590	0.239	0.019	0.630	0.982	0.915
3.2.3	1.571	0.440	0.250	0.066	0	0.730	1.976	0.732
3.2.4	1.885	0.883	0.190	0.086	0	0.420	1.200	0.542
4.1.1	0.785	0.290	0.840	1.033	0.902	1.027	0.997	0.960
4.1.2	1.100	0.240	0.630	0.105	0	0.948	0.970	0.948
4.1.3	1.571	0.490	0.233	0.083	0	0.735	2.030	0.581
4.1.4	1.885	0.746	0.205	0.033	0	0.550	1.900	0.465
4.2.1	0.785	0.430	0.480	0.123	0	0.560	0.540	0.465
4.2.2	1.100	0.550	0.361	0.041	0	0.426	0.500	0.317
4.2.3	1.571	0.894	0.180	0.192	0	0.457	0.600	0.091
4.2.4	1.885	0.840	0.060	0.047	0	0.368	0.830	0.050

Table 4.5 Summary of experimental results for the circular section breakwater. (contd...)

Test No.	ka	K_R	K_T	Mooring forces		Selected RAO's only		
						sway	heave	roll
				T'_1	T'_2	ξ'_1	ξ'_2	ξ'_3
5.1	0.785	0.340	0.461	0.488	0.015	0.500	0.900	0.589
5.2	0.942	0.280	0.510	0.252	0.017	-	-	-
5.3	1.100	0.386	0.284	0.097	0.040	0.592	0.600	0.409
5.4	1.257	0.480	0.377	0.121	0.104	-	-	-
5.5	1.571	0.540	0.233	0.067	0.110	0.621	0.877	0.400
5.6	1.728	0.470	0.160	0.034	0.175	-	-	-
5.7	1.885	0.870	0.407	0.016	0.226	-	-	-
5.8	0.785	0.323	0.577	0.171	0	0.383	0.149	0.582
5.9	0.785	0.357	0.685	0.139	0	-	-	-
5.10	0.785	0.411	0.680	0.069	0	0.446	0.460	1.787
5.11	0.785	0.253	0.723	0.076	0	-	-	-
5.12	1.571	0.695	0.149	0.059	0	-	-	-
5.13	1.571	0.612	0.199	0.119	0	-	-	-
5.14	1.571	0.723	0.260	0.09	0	-	-	-
5.15	1.571	0.657	0.238	0.117	0	-	-	-
5.16	0.377	0.140	0.800	1.004	0.306	1.870	1.528	0.408
5.17	0.471	0.230	0.817	2.124	0.749	-	-	-
5.18	0.628	0.300	0.721	0.037	0	-	-	-
6.1.1	0.785	0.327	0.357	0.305	0.010	0.831	0.223	0.434
6.1.2	1.100	0.394	0.139	0.040	0.070	0.097	0.097	0.019
6.1.3	1.571	0.800	0.330	0.029	0.067	0.181	0.335	0.273
6.1.4	1.885	0.878	0.178	0.068	0.104	-	-	-
6.2.1	0.785	0.462	0.720	0.449	0.050	0.168	0.154	0.279
6.2.2	1.100	0.802	0.504	0.175	0.125	0.484	0.474	0.396
6.2.3	1.571	0.425	0.282	0.200	0.136	0.556	1.209	0.182
6.2.4	1.885	0.300	0.119	0.150	0.187	0.230	0.950	0.230
7.1.1	0.785	0.230	0.600	1.040	0.610	1.787	0.955	0.465
7.1.2	1.100	0.262	0.371	0.102	0	0.844	1.670	0.575
7.1.3	1.571	0.416	0.341	0.081	0	1.393	0.734	0.136
7.1.4	1.885	0.817	0.274	0.096	0	-	-	-
7.2.1	0.785	0.340	0.400	0.537	0.174	0.871	0.607	0.279
7.2.2	1.100	0.316	0.170	0.469	0.041	0.827	1.213	0.317
7.2.3	1.571	0.650	0.110	0.42	0.078	0.664	0.343	0.136
7.2.4	1.885	0.960	0.185	0.165	0	-	-	-

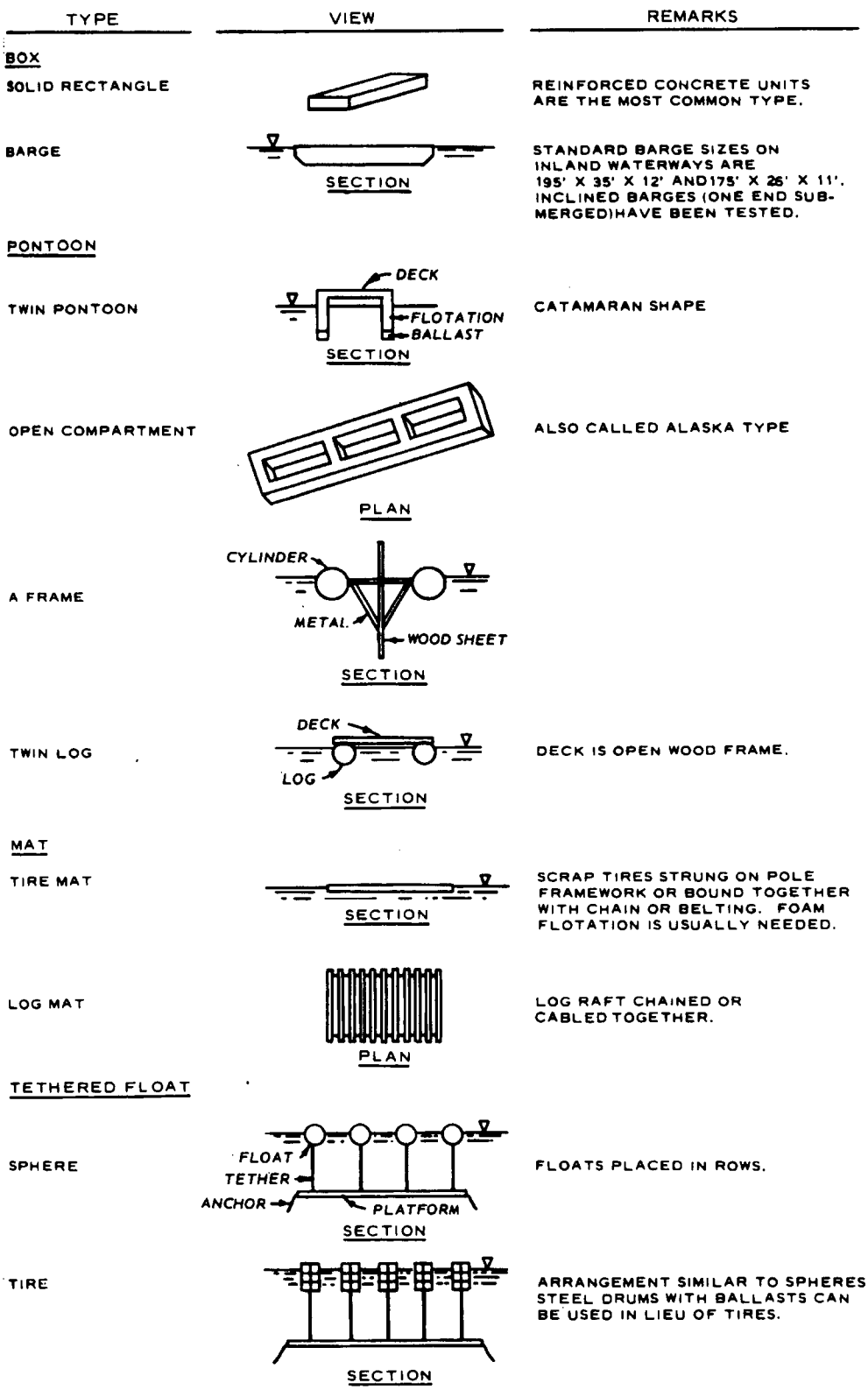

Fig. 1.1 Various types of floating breakwaters (McCartney, 1985).

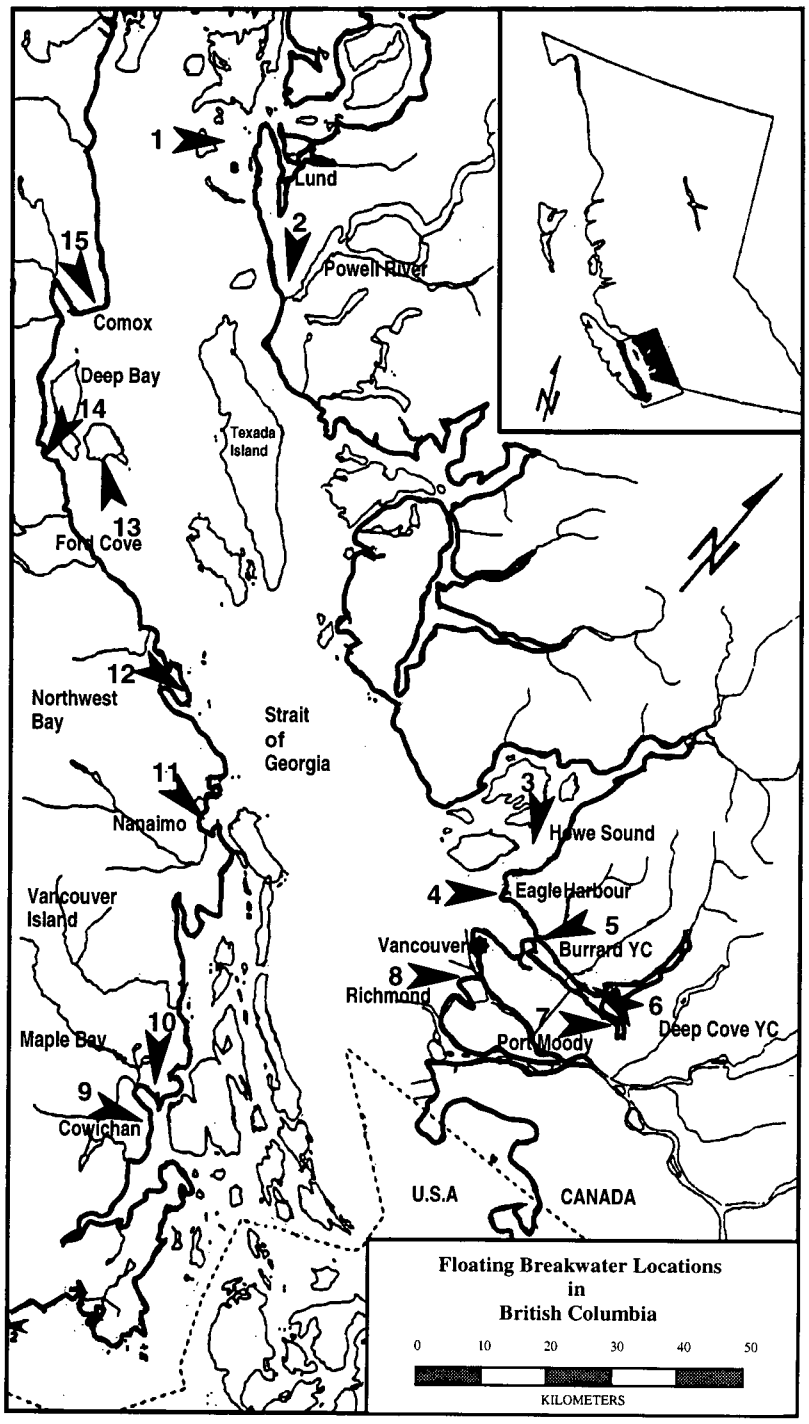

Fig. 1.2 Location map relating to floating breakwater facilities in British Columbia.

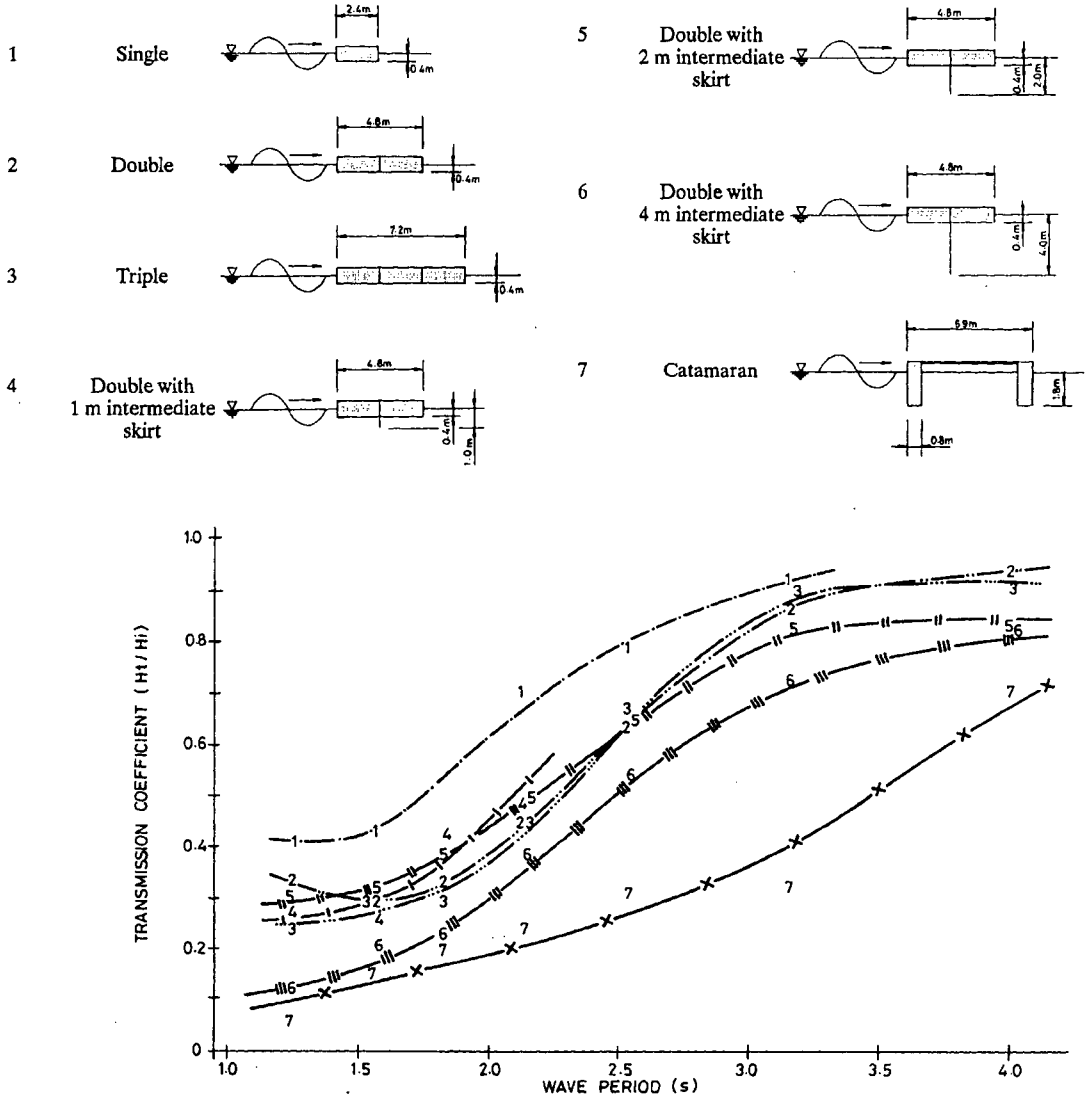

Fig. 1.3 Comparison of transmission coefficient of various pontoon breakwater types (Blumberg and Cox, 1988).

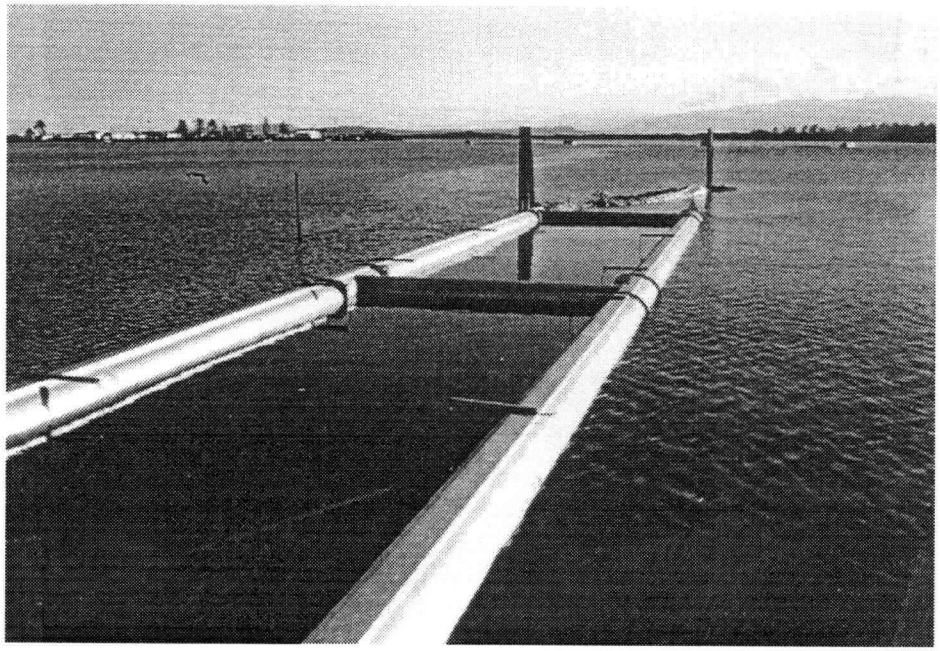

Fig. 2.1 View of prototype twin-pontoon breakwater at Comox Harbour, B.C.

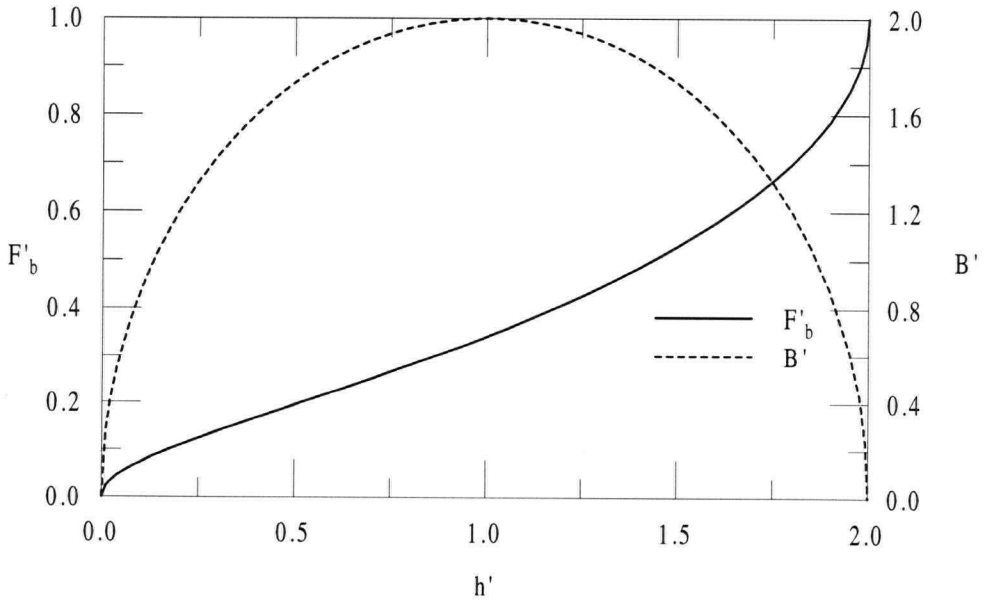

Fig. 2.2 Variation of buoyancy force and waterline beam as functions of relative draft for a circular pontoon section.

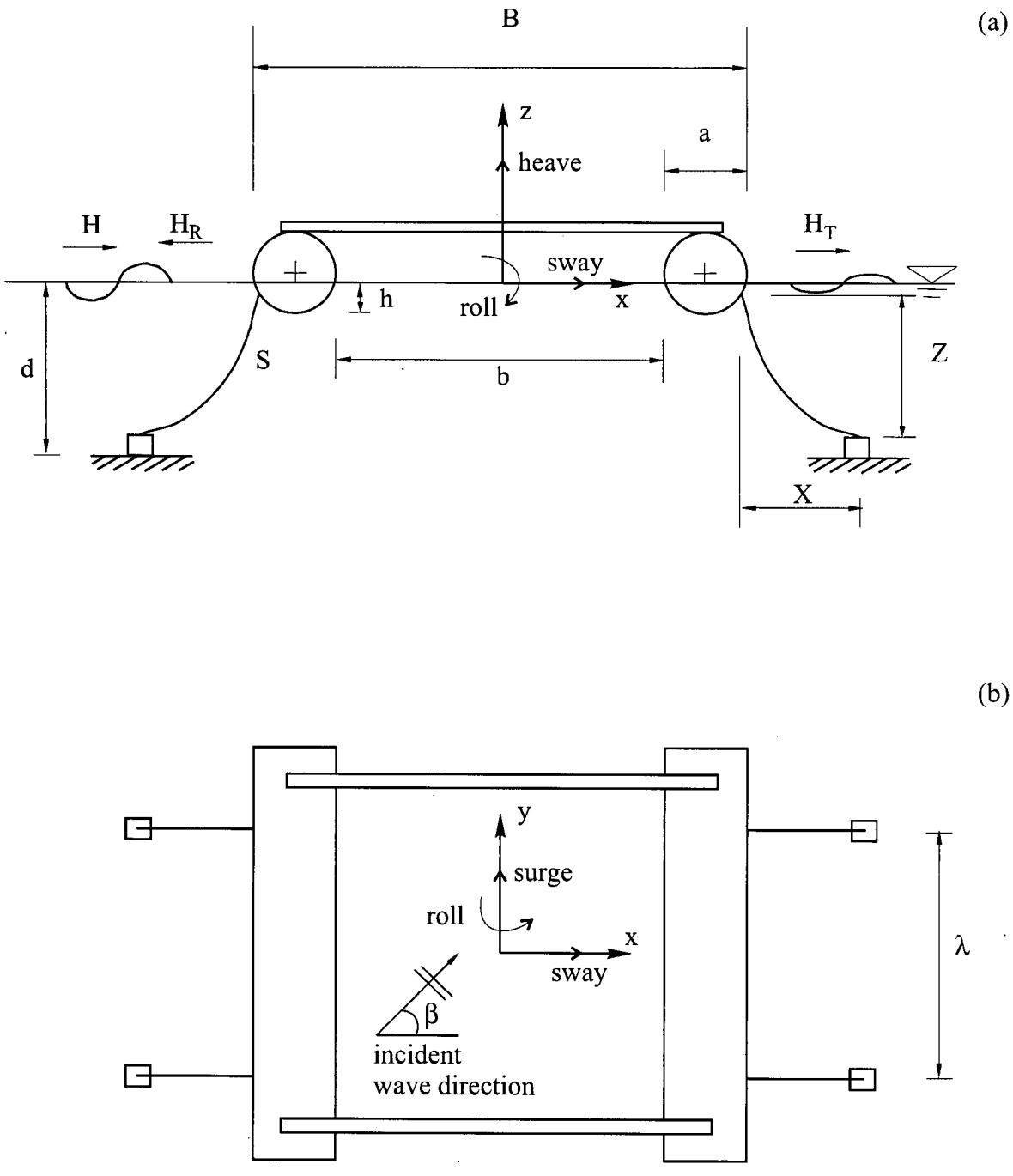

Fig. 2.3 Definition sketch of a moored twin-pontoon breakwater. (a) elevation; (b) plan view.

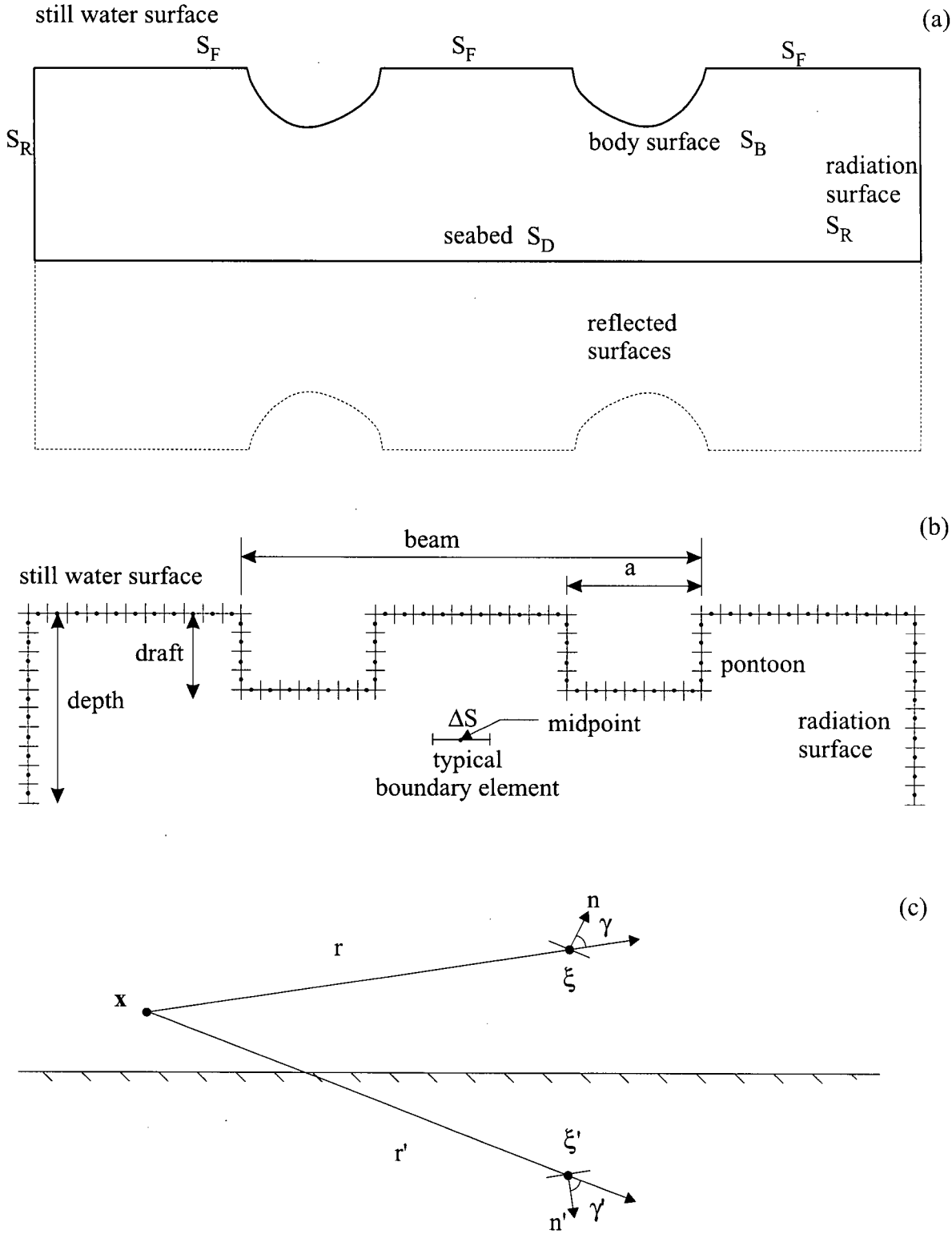

Fig. 2.4 Computational domain relating to the boundary element method.
(a) alternative boundary geometry indication the use of symmetry about the seabed seabed; (b) discretization of twin-pontoon breakwater section; (c) sketch indicating the relationship between **x**, ξ, and ξ'.

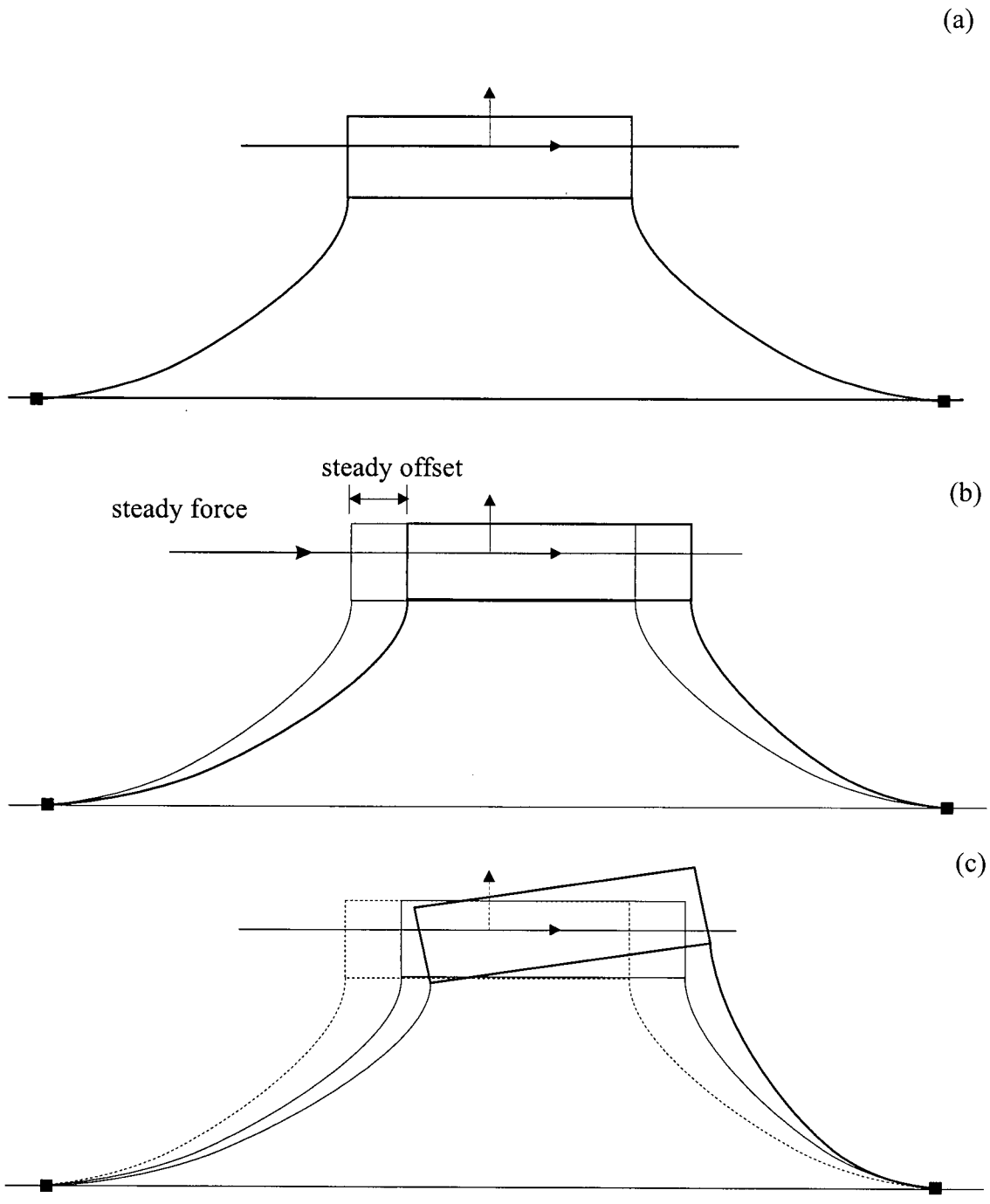

Fig. 2.5 Component steps in the mooring analysis. (a) initial equilibrium configuration for no wave load; (b) static analysis to obtain responses to steady loads; (c) quasi-static analysis to obtain responses to wave loads.

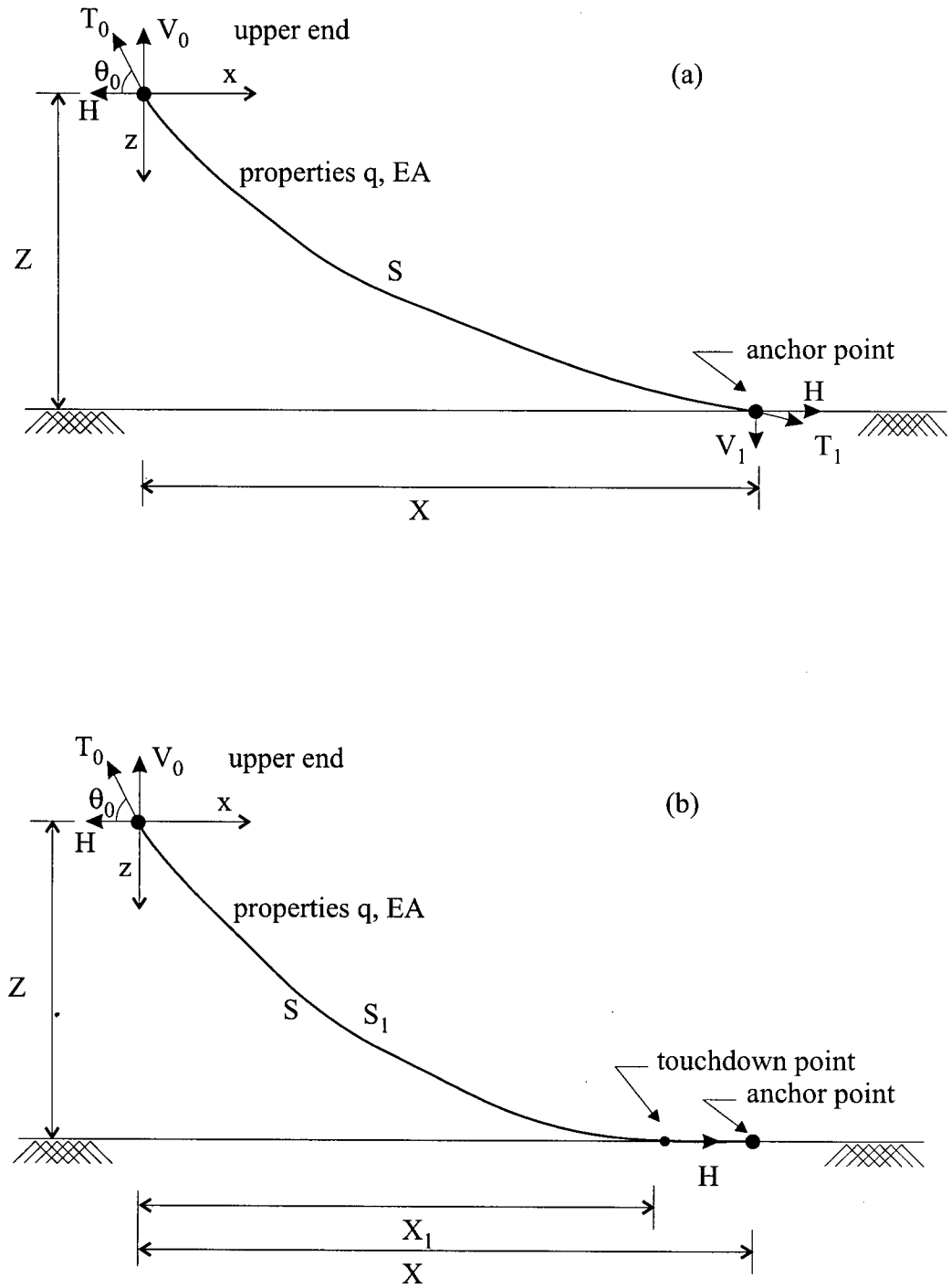

Fig. 2.6 Mooring line definition sketch. (a) fully suspended cable; (b) partly suspended cable.

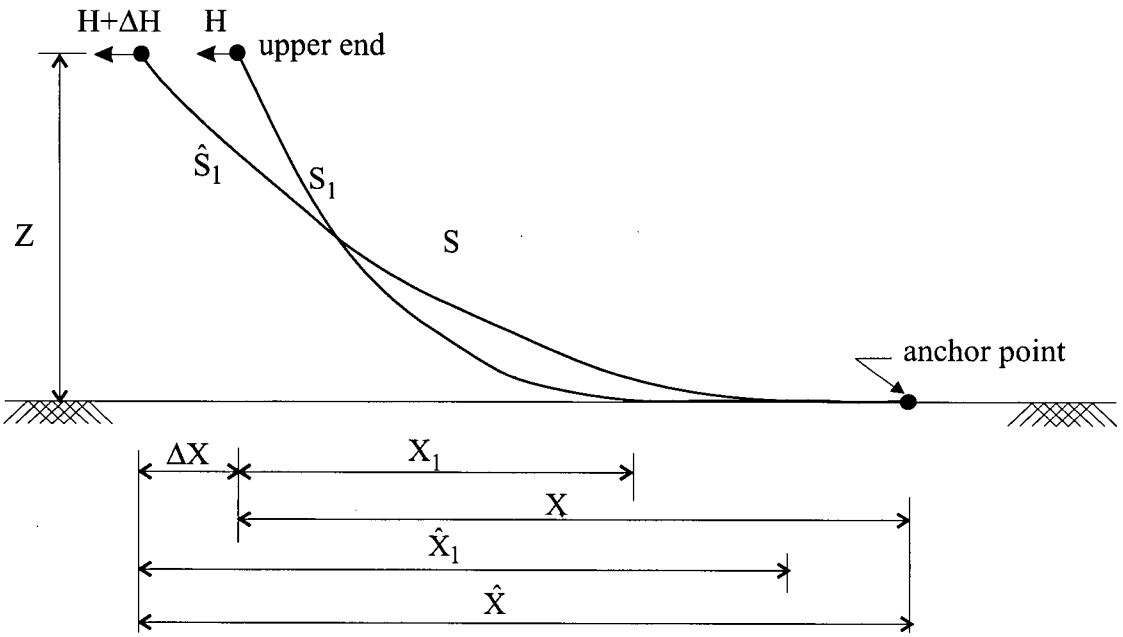

Fig. 2.7 Response of a mooring cable due to environmental loads.

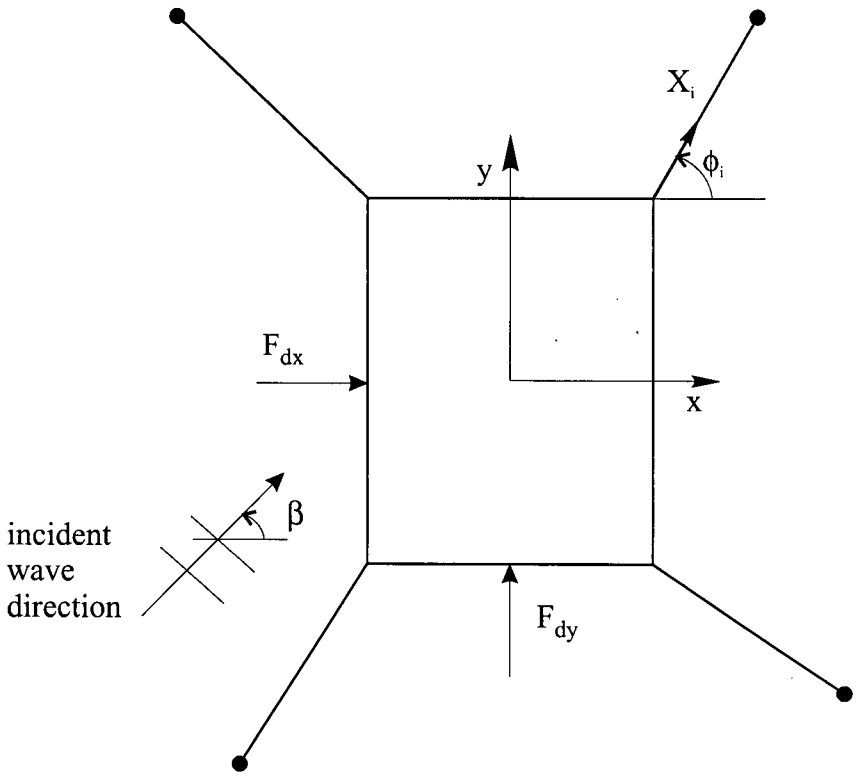

Fig. 2.8 Plan view of multiple cable mooring system.

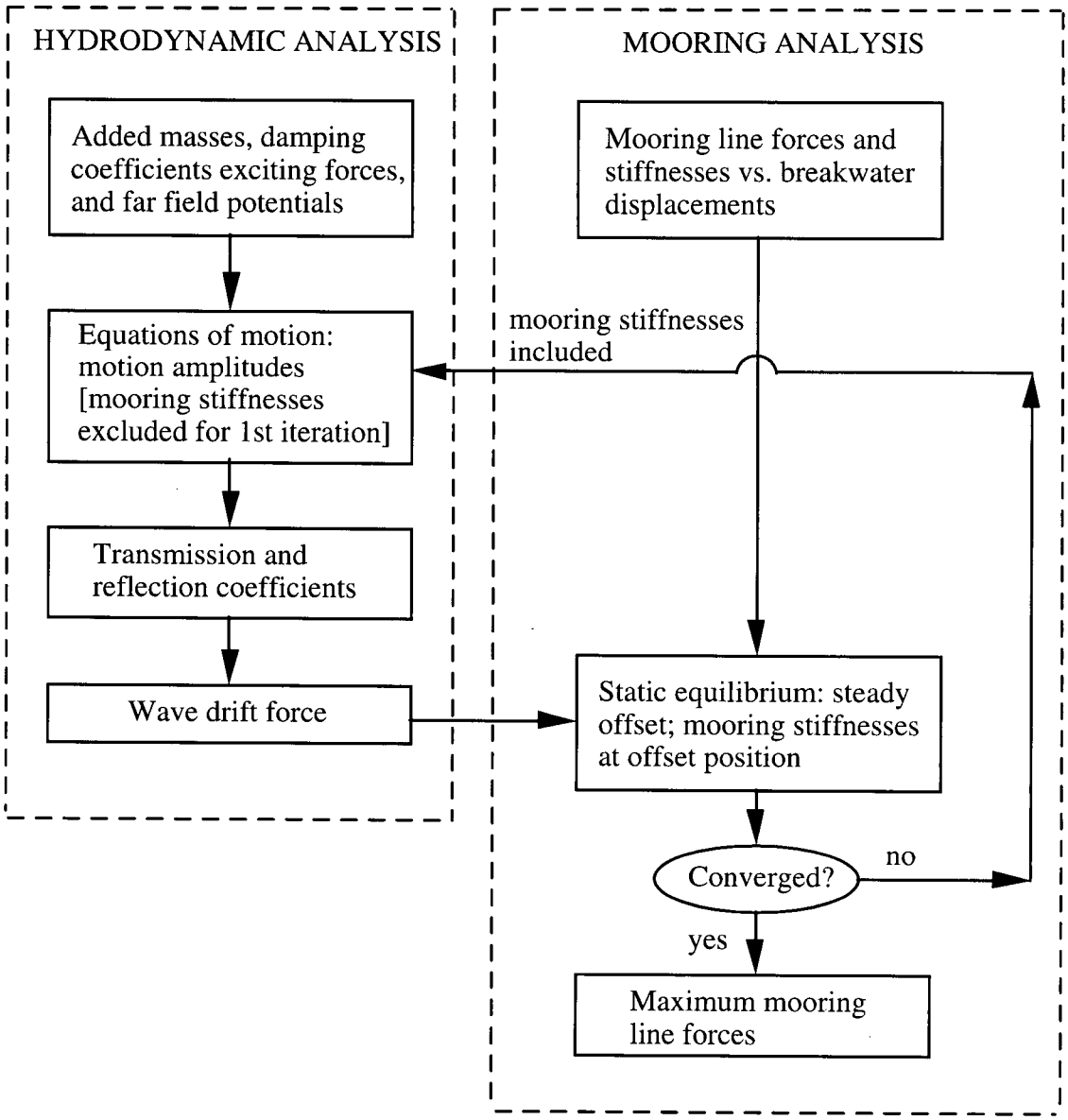

Fig. 2.9 Component steps in breakwater analysis.

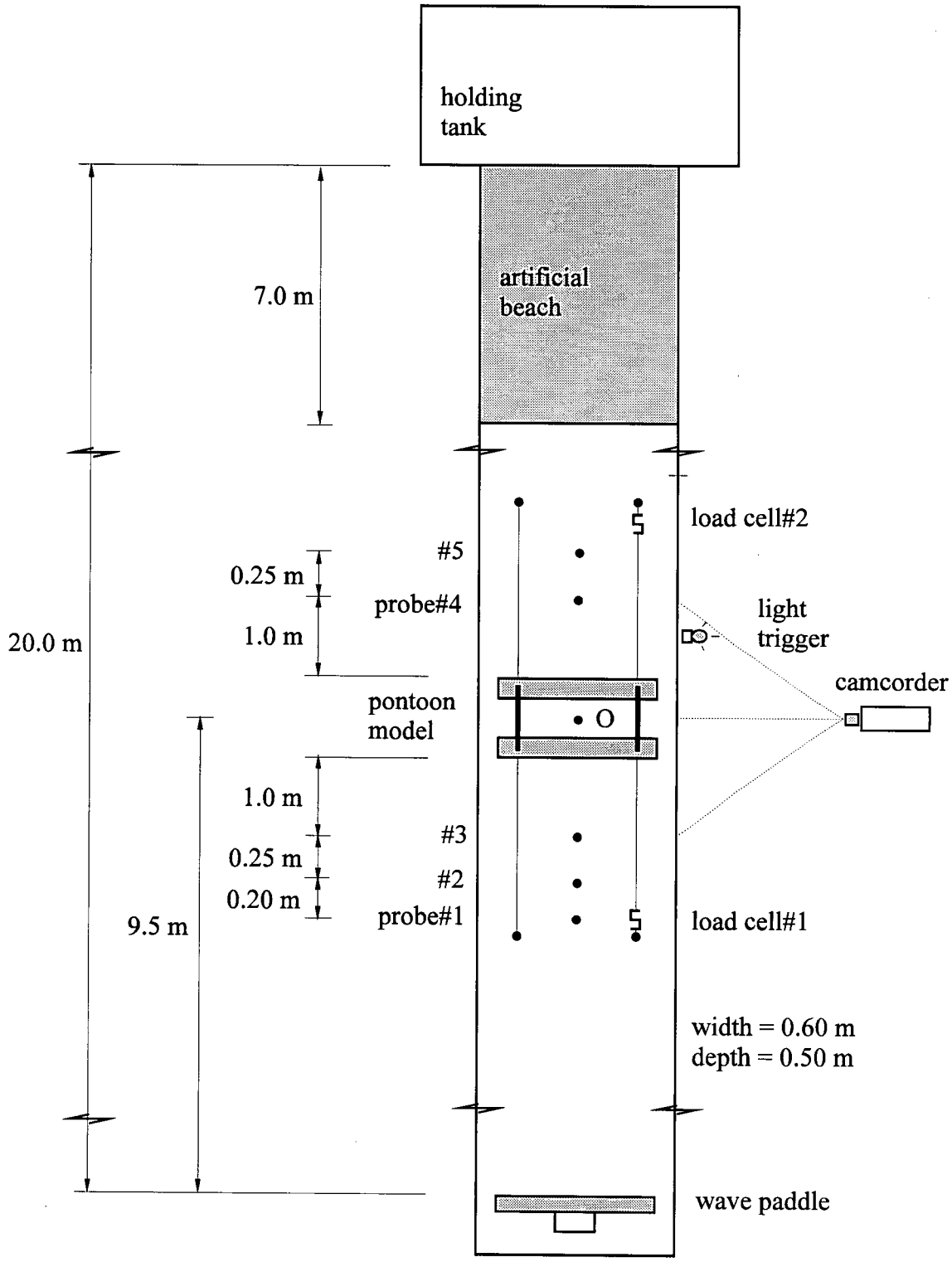

Fig. 3.1 Experimental set-up relating to wave flume tests.

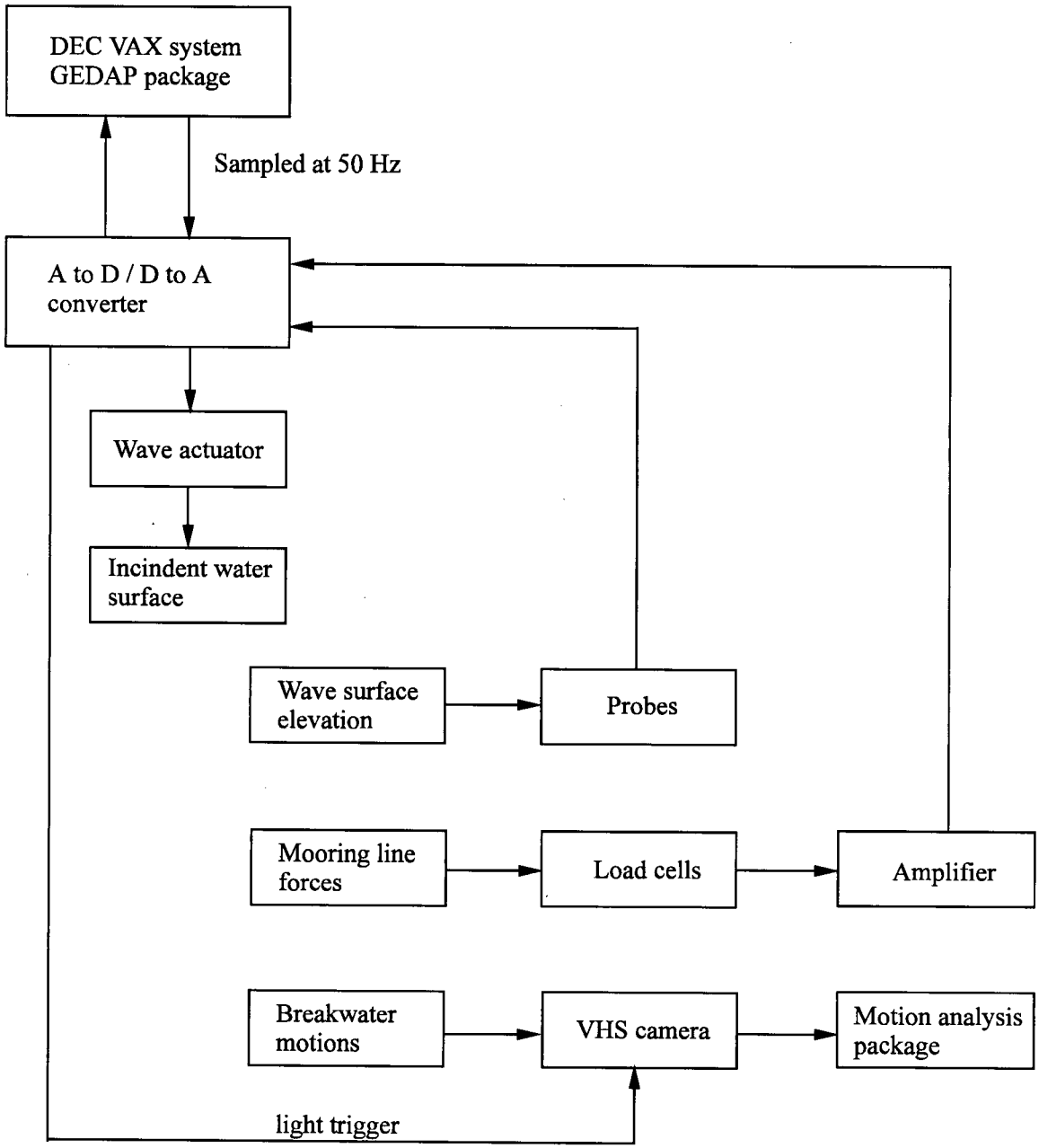

Fig. 3.2 Flowchart indicating various components of the experimental scheme.

(a)

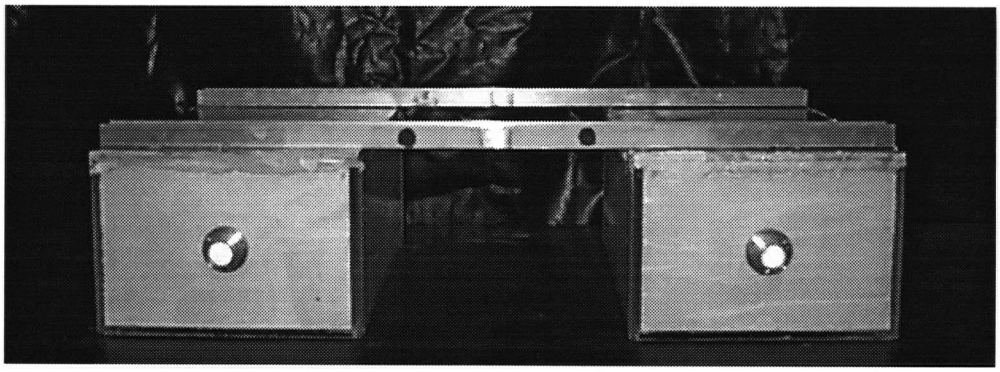

(b)

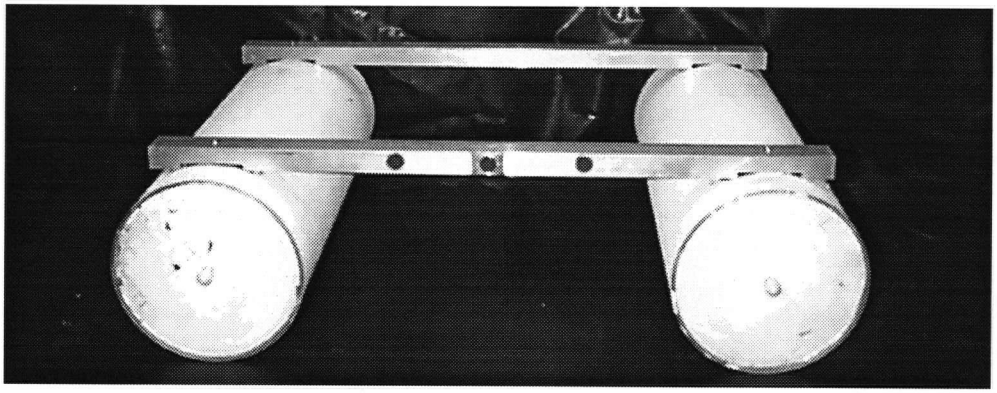

Fig. 3.3 Photograph of twin-pontoon breakwater models used in wave flume tests. (a) rectangular section; (b) circular section.

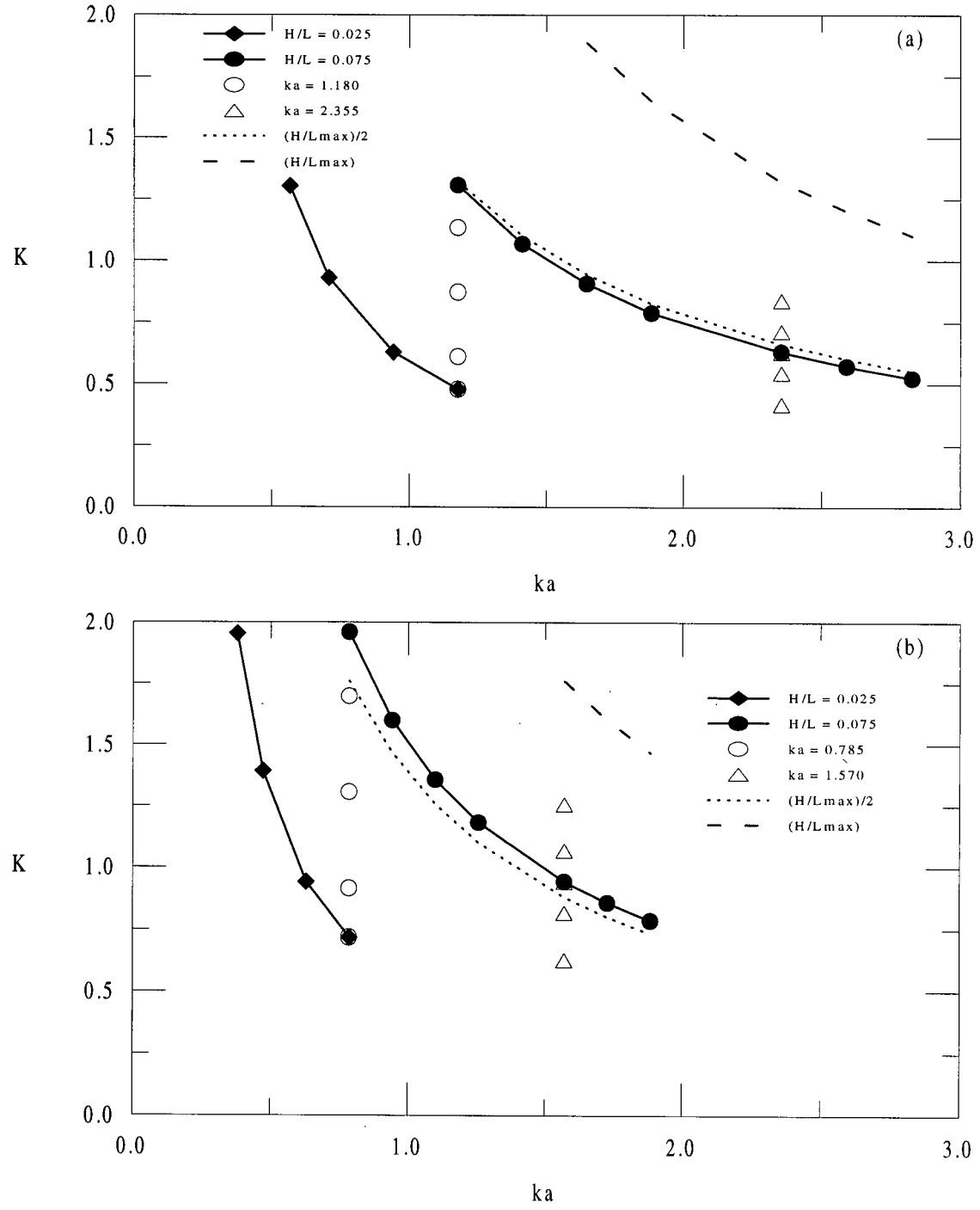

Fig. 3.4 Ranges of Keulegan-Carpenter number, K relating to chosen wave conditions for the case of (a) rectangular section, (b) circular section model.

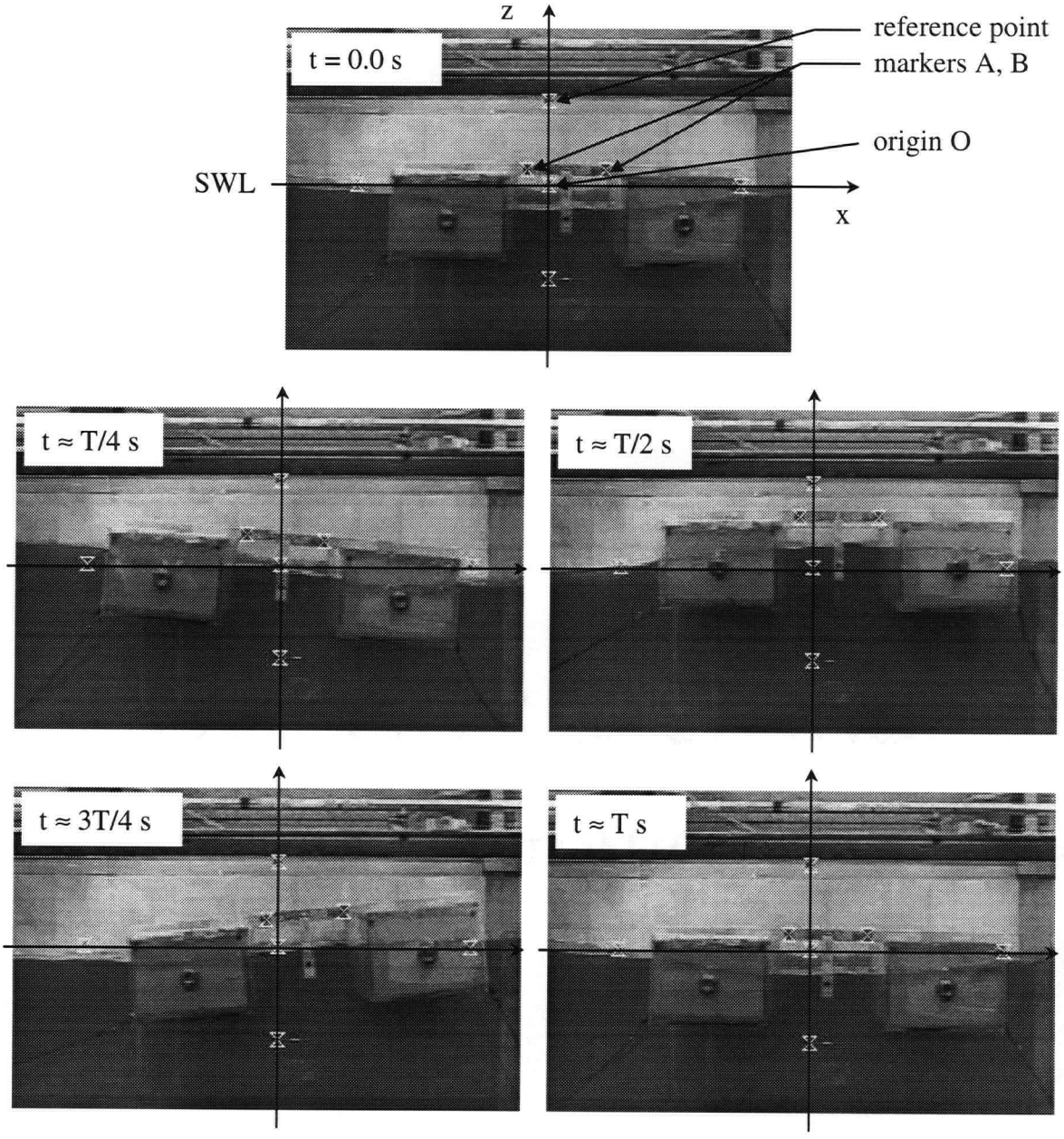

Fig. 3.5 A selection of video captured images used in the motion analysis to track the marker locations. (T = 1.704 s).

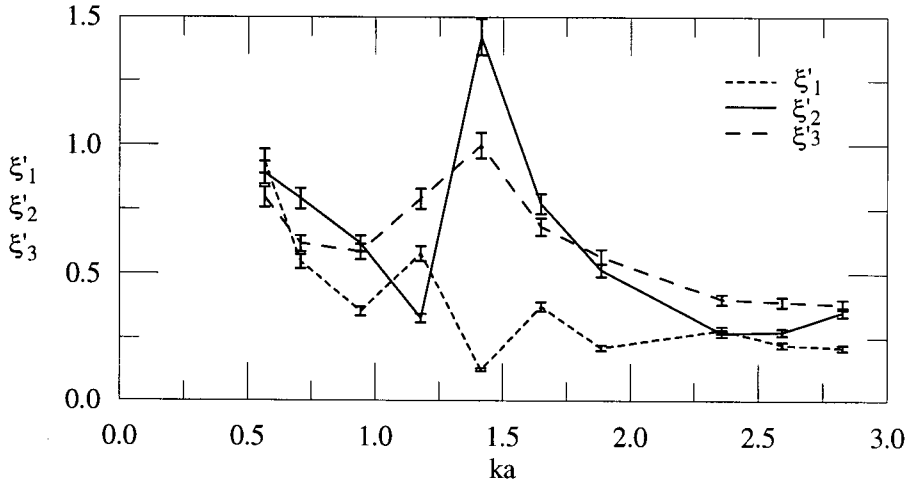

Fig. 3.6 Experimental values of RAO's for a moored rectangular twin-pontoon breakwater indicating the estimated errors for the video-based motion tracking system, (d/a = 1.67, h/a = 0.45, b/a = 1.0, S/S_o = 1.08).

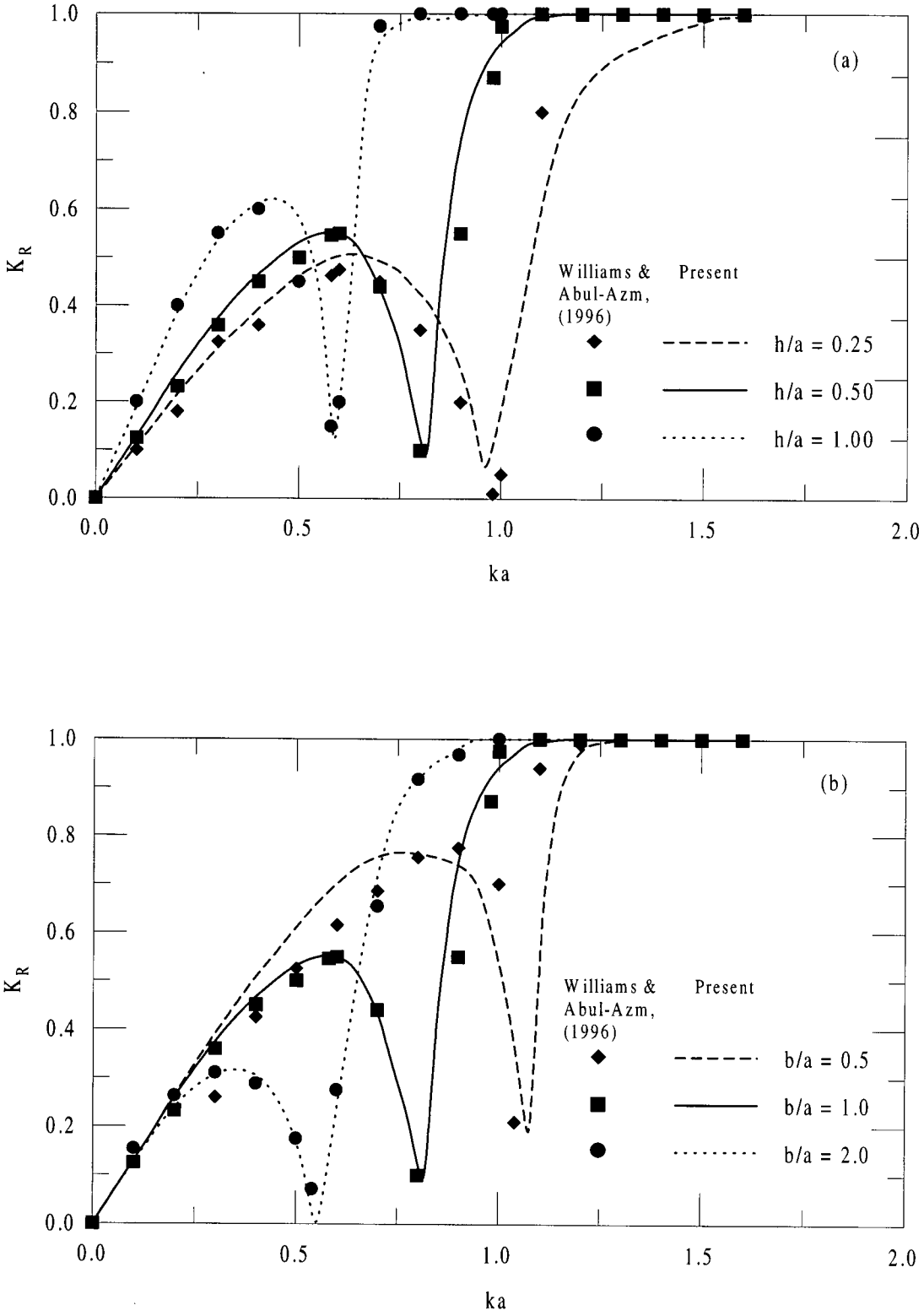

Fig. 4.1 Comparison of reflection coefficient, K_R, with results reported by Williams and Abul-Azm (1996), for a fixed rectangular twin-pontoon breakwater. (a) influence of draft, h, (d/a = 2.5, b/a = 1.0, β = 0°); (b) influence of pontoon spacing, b; (d/a = 2.5, h/a = 0.5, β = 0°).

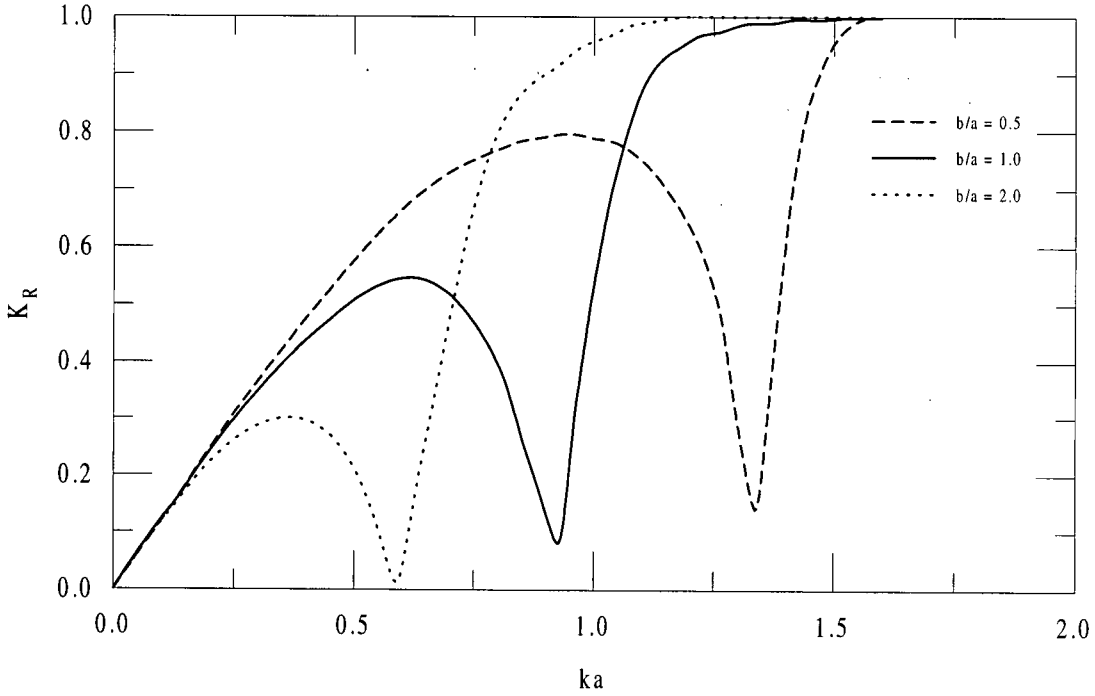

Fig. 4.2 Reflection coefficient for a fixed circular twin-pontoon breakwater indicating the influence of spacing, b, (d/a = 2.5, h/a = 0.5, $\beta = 0°$).

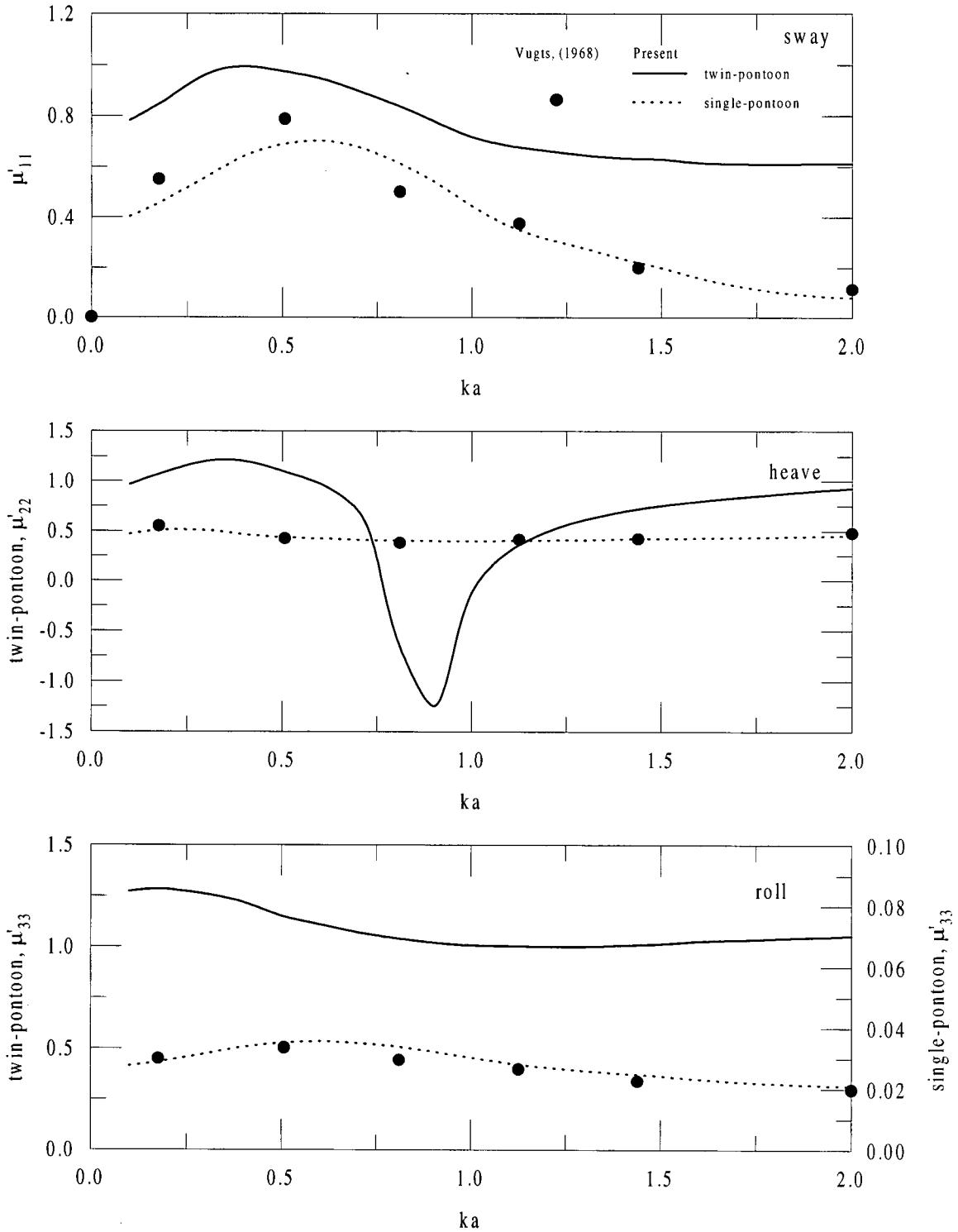

(a) added mass in sway, heave, and roll.

Fig. 4.3 Variation of hydrodynamic coefficients as a function of normalized wave number, ka, for a single-pontoon rectangular section (d/a = 5.0, h/a = 0.5 and β = 0°), and for a twin-pontoon rectangular section (d/a = 5.0, h/a = 0.5, b/a = 1.0 and β = 0°). (contd...)

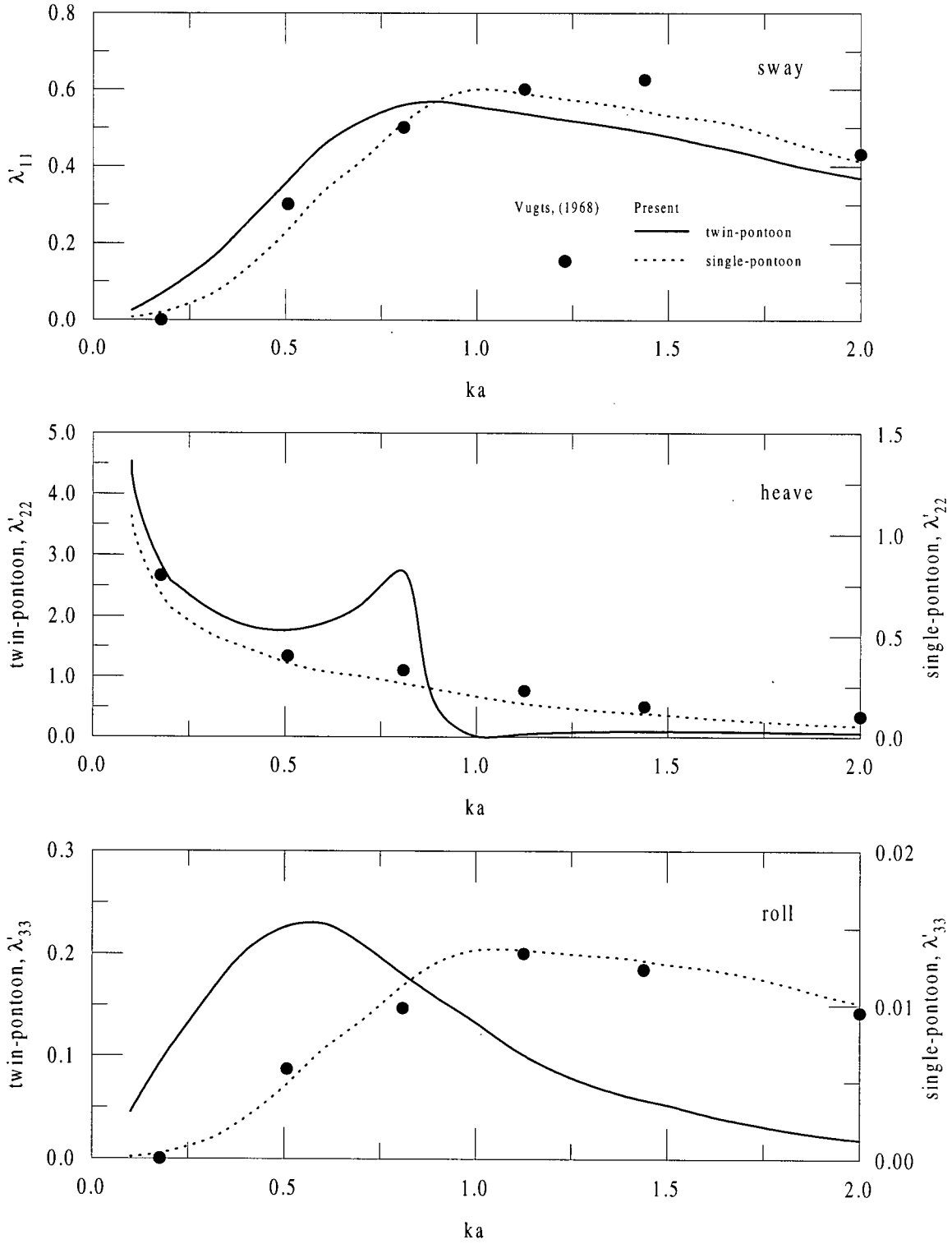

(b) damping coefficient in sway, heave, and roll.

Fig. 4.3 (contd...)

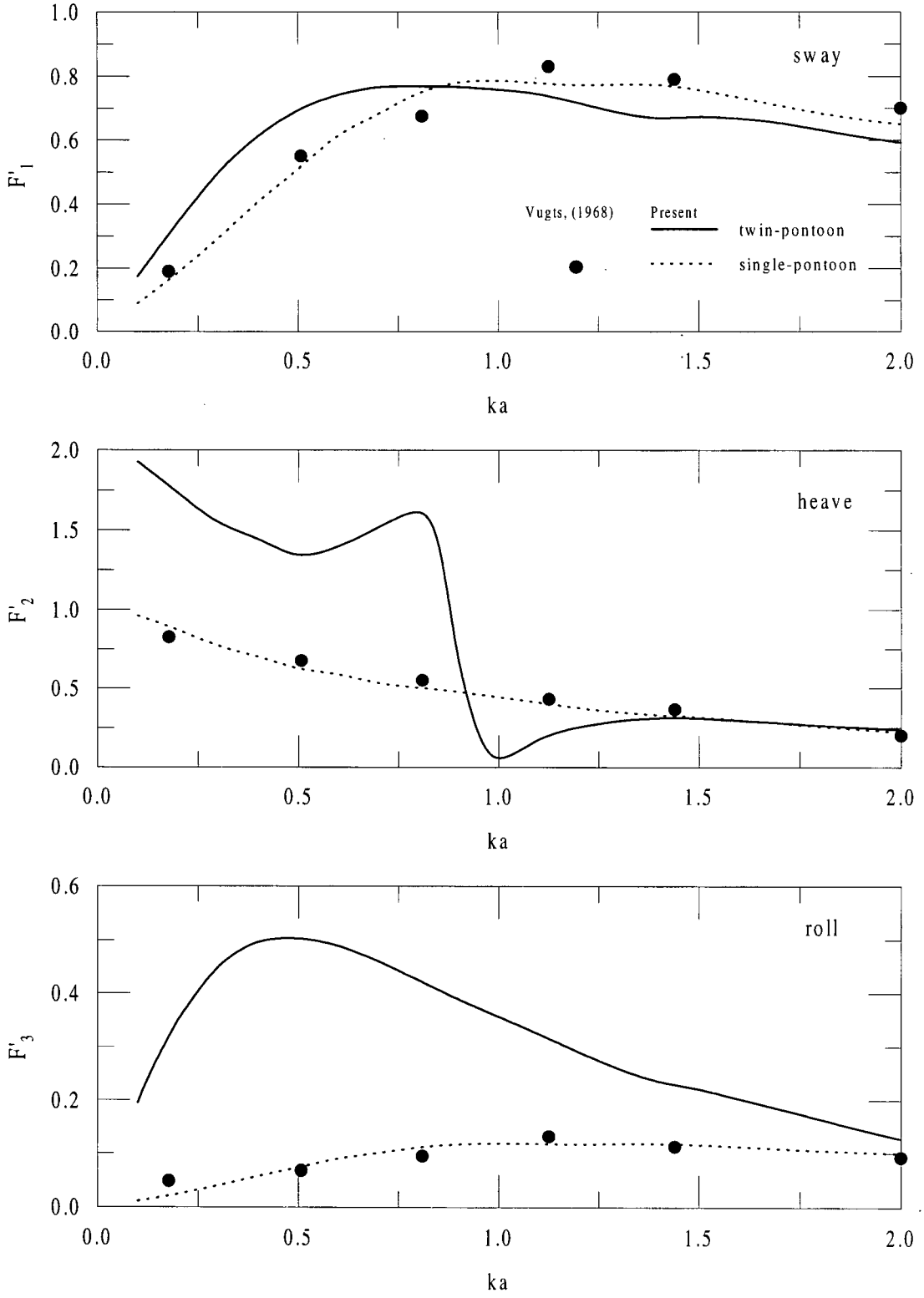

(c) exciting force coefficient in sway, heave, and roll.

Fig. 4.3 (contd...)

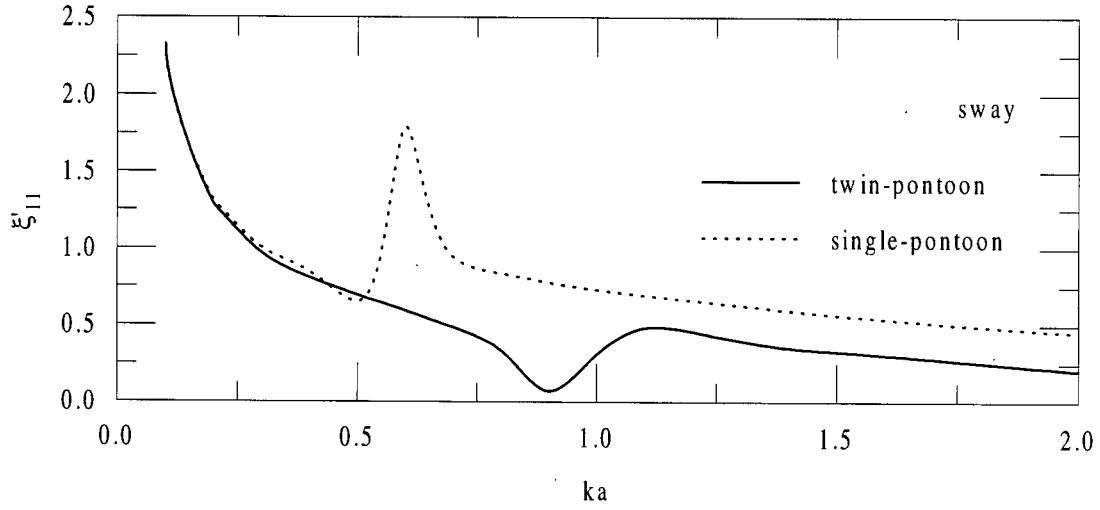

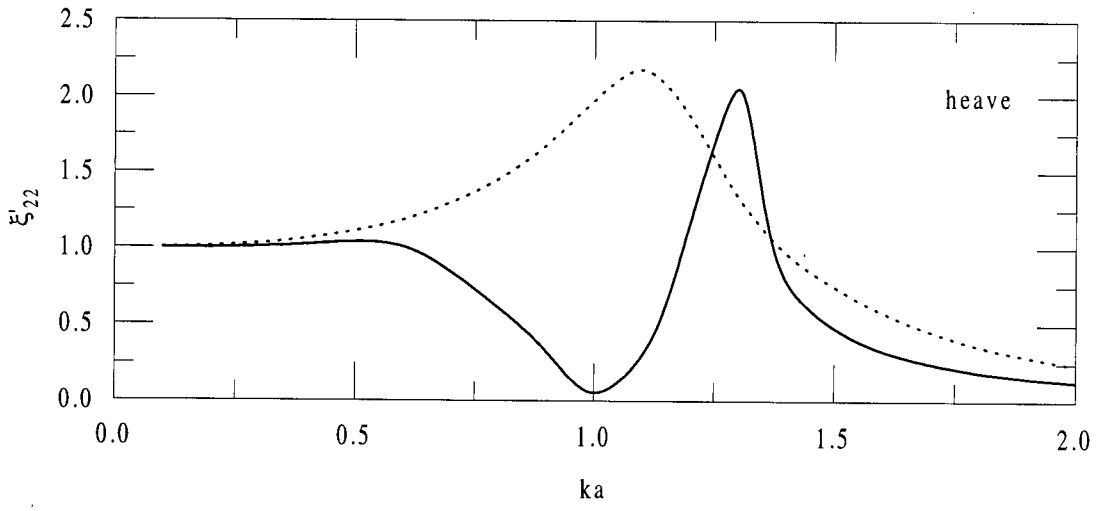

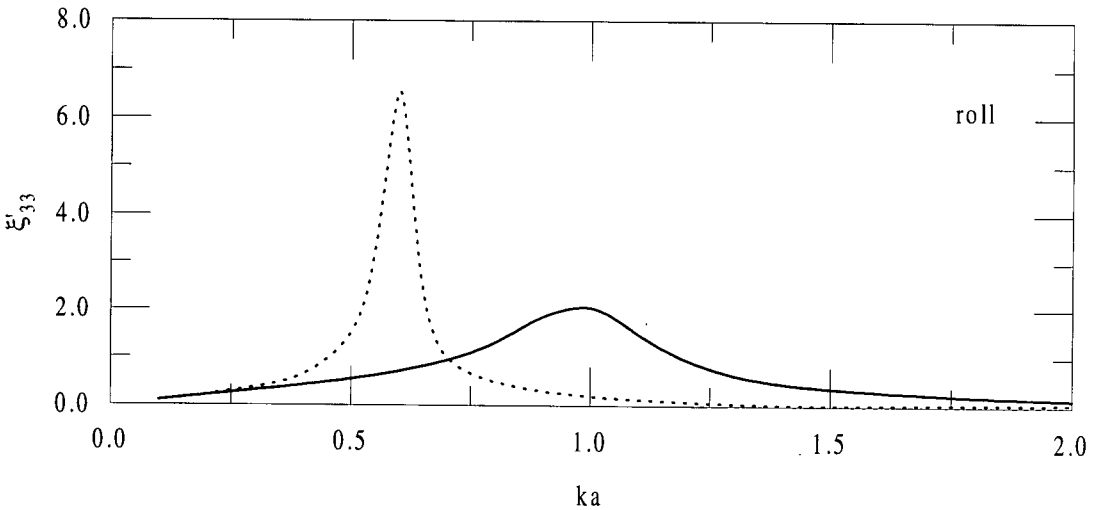

(d) RAO's in sway, heave, and roll.

Fig. 4.3 (contd...)

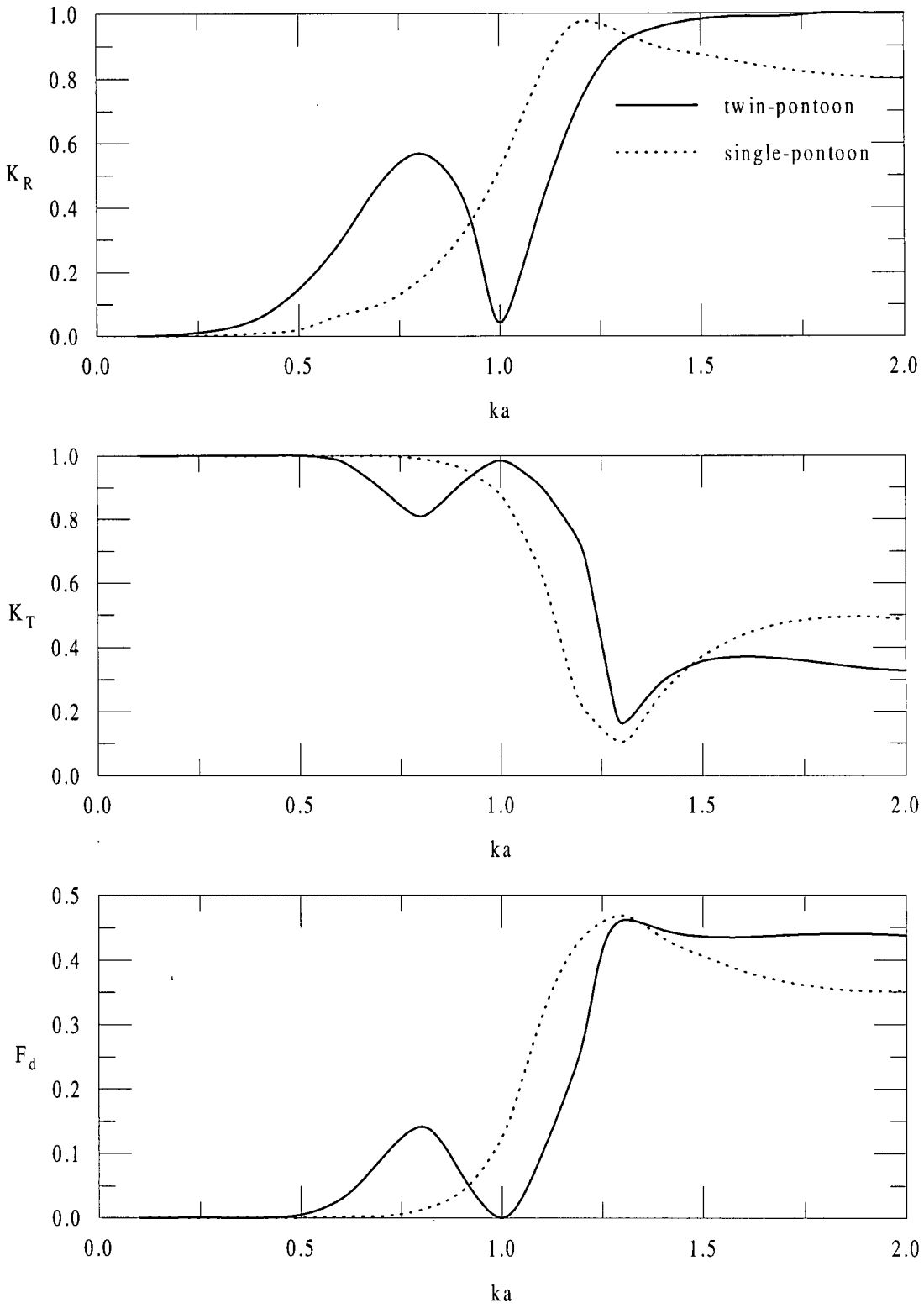

(e) reflection and transmission coefficients, and drift force coefficient.

Fig. 4.3.

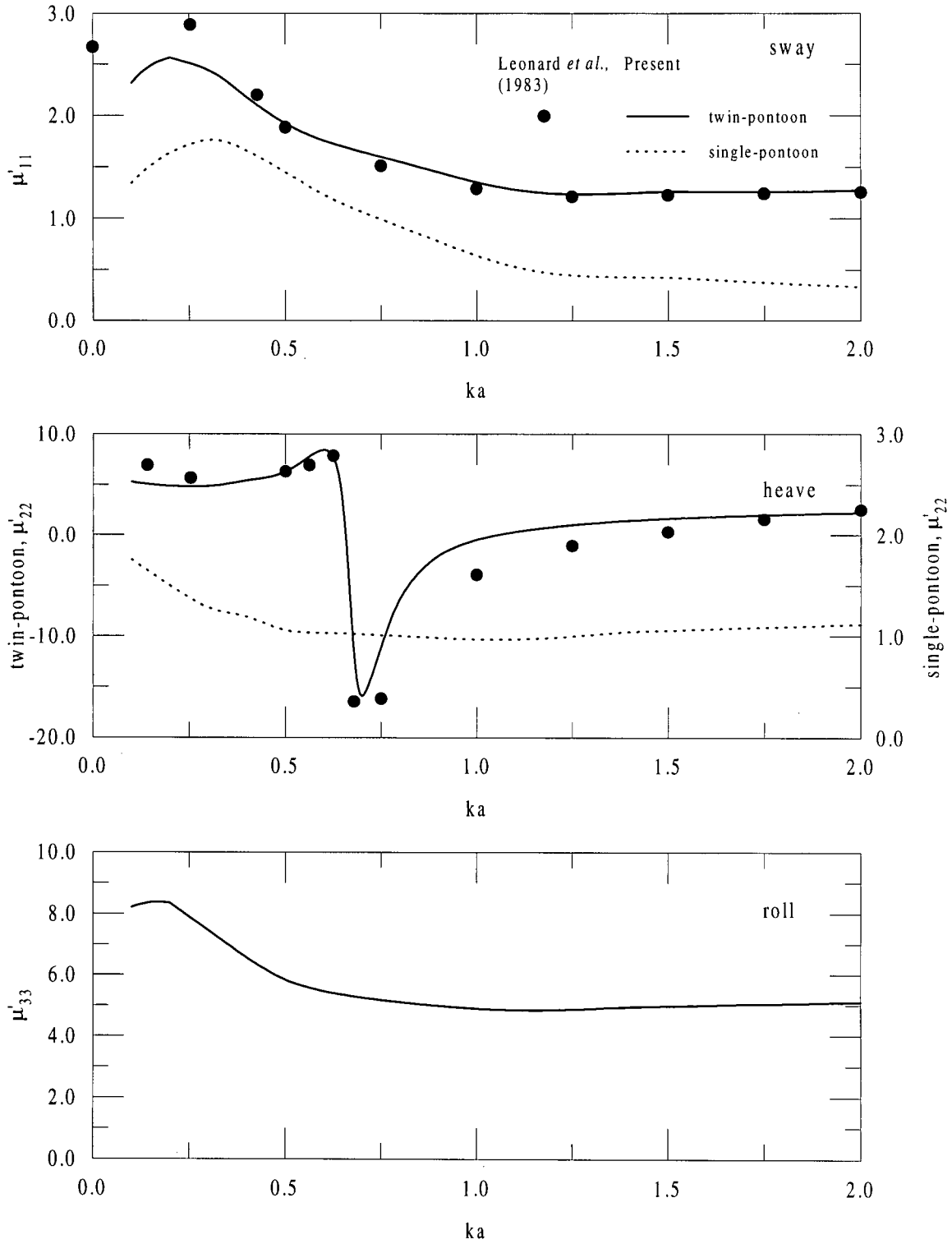

(a) added mass in sway, heave, and roll.

Fig. 4.4 Variation of hydrodynamic coefficients as a function of normalized wave number, ka, for a single-pontoon circular section (d/a = 5.0, h/a = 0.5 and $\beta = 0°$), and for a twin-pontoon circular section; (d/a = 5.0, h/a = 0.5, b/a = 0.5 and $\beta = 0°$). (contd...)

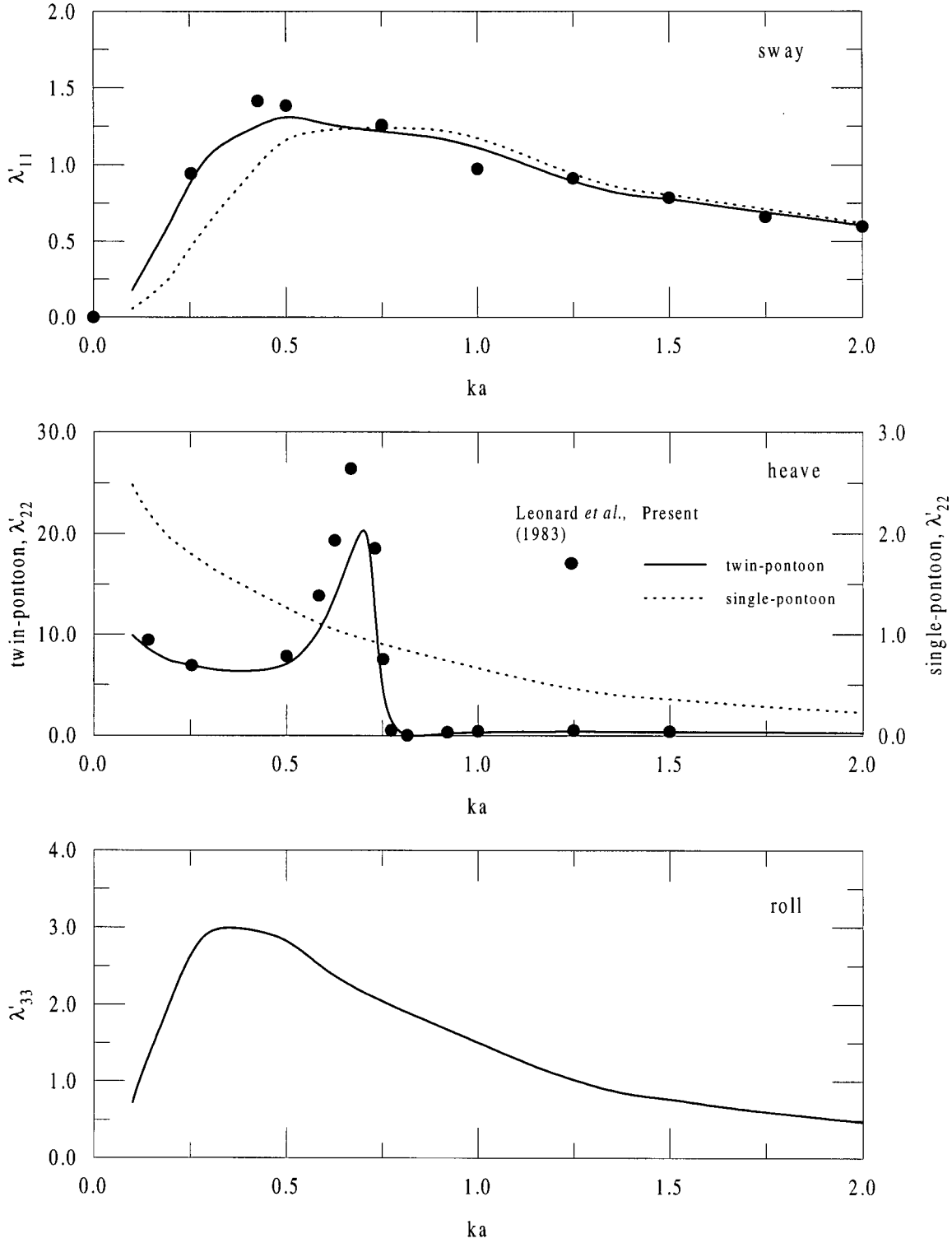

(b) damping coefficient in sway, heave, and roll.

Fig. 4.4 (contd...)

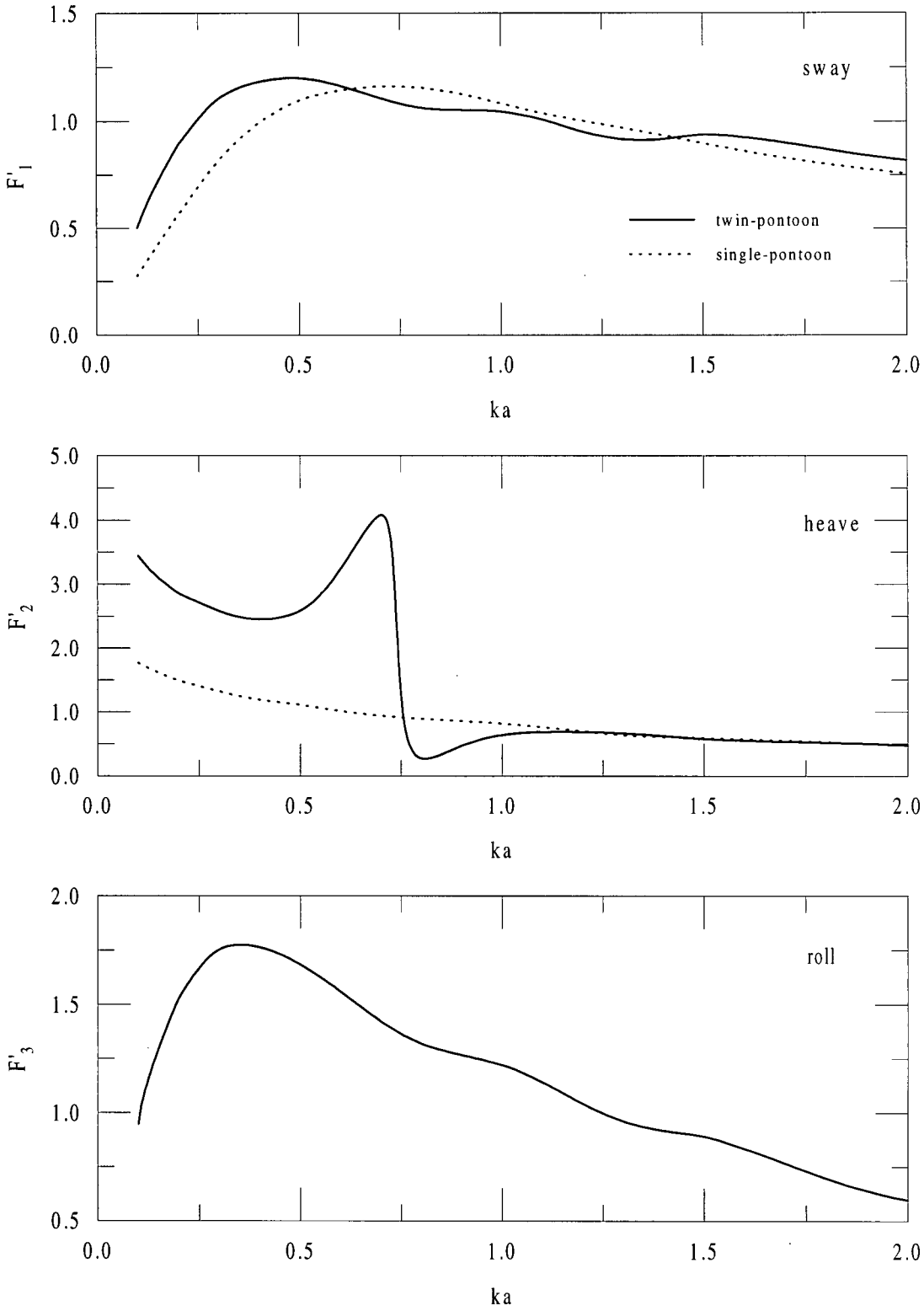

(c) exciting force coefficient in sway, heave, and roll.

Fig. 4.4 (contd...)

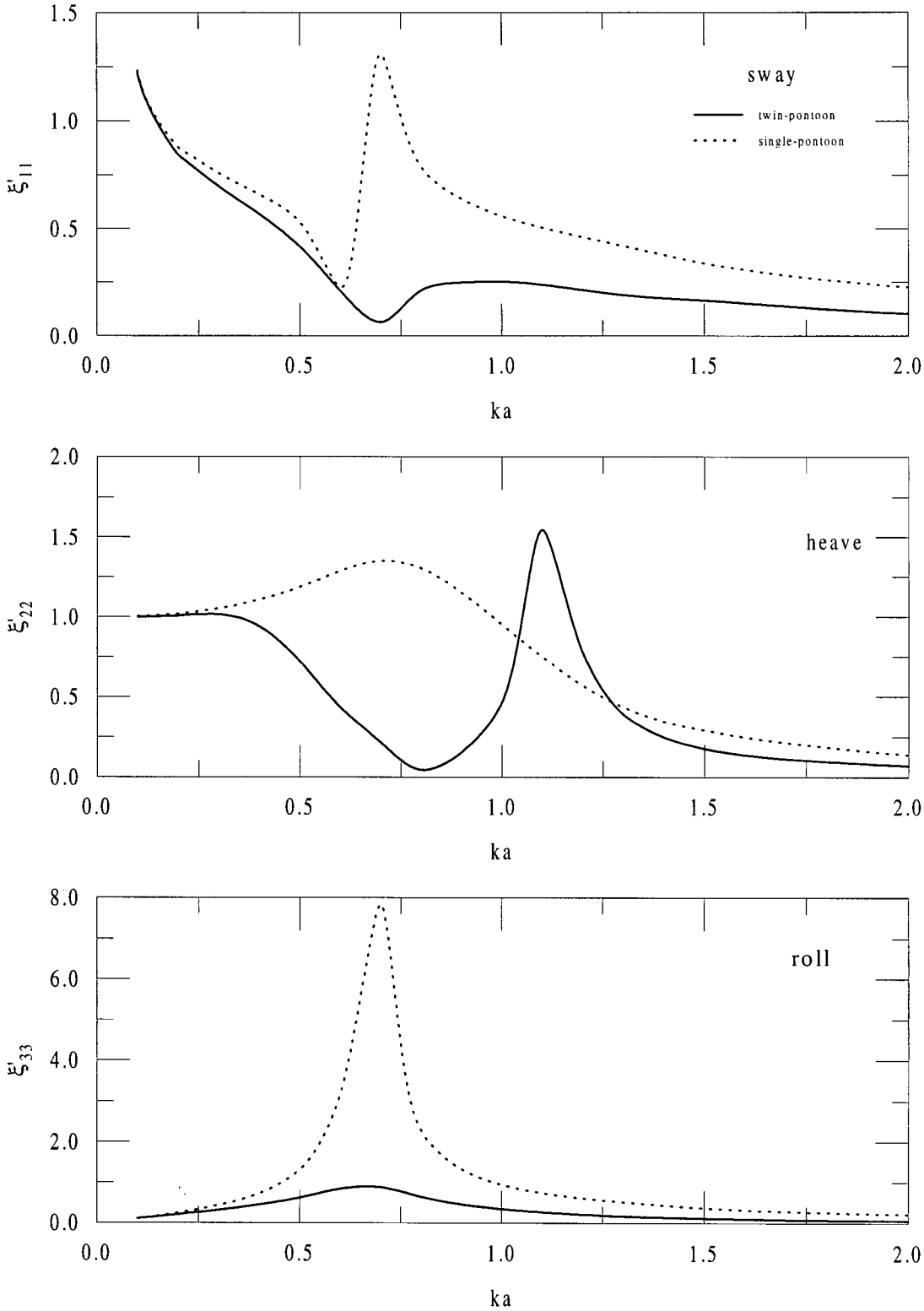

(d) RAO's in sway, heave, and roll

Fig. 4.4 (contd...)

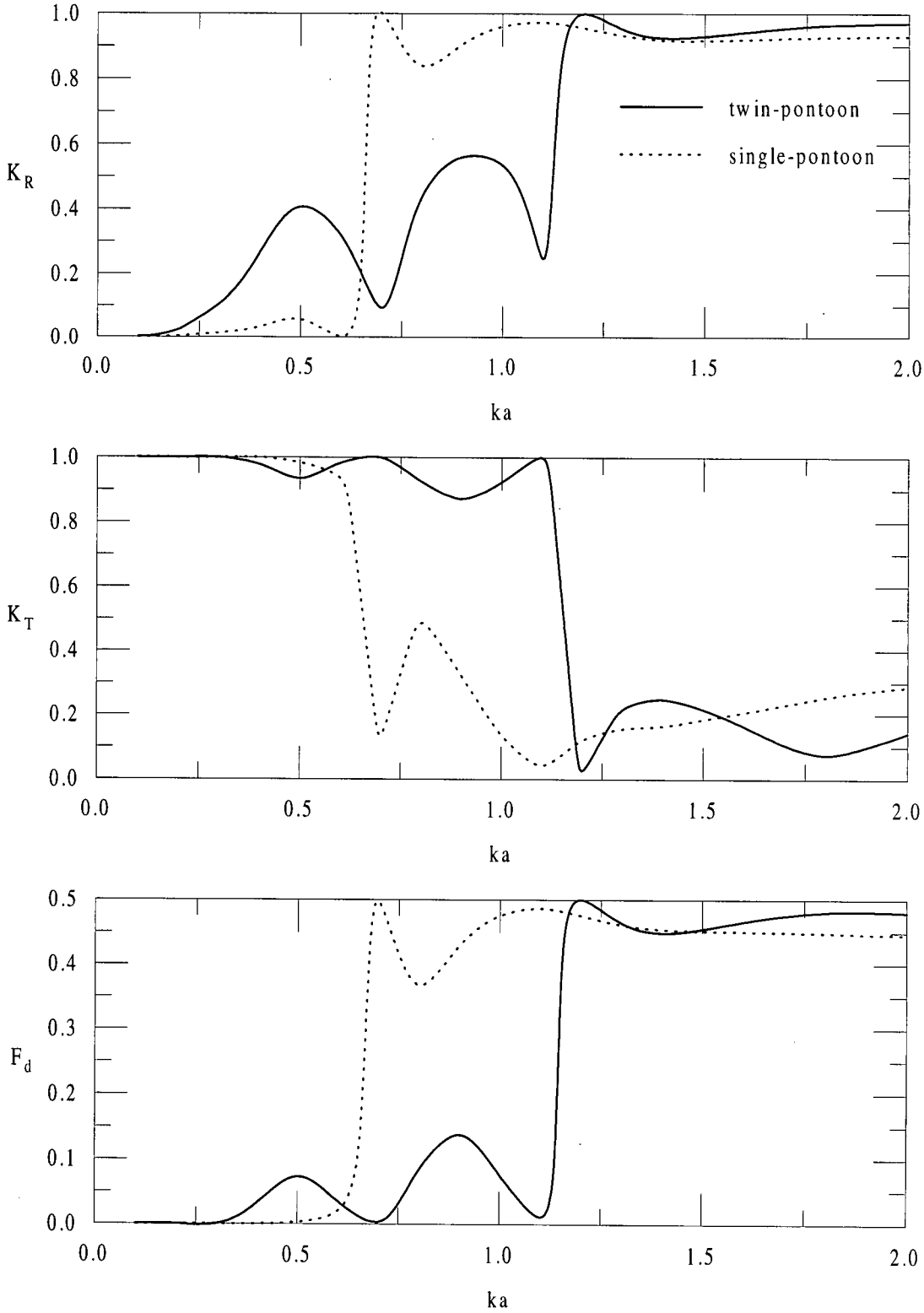

(e) reflection and transmission coefficients, and drift force coefficient

Fig. 4.4.

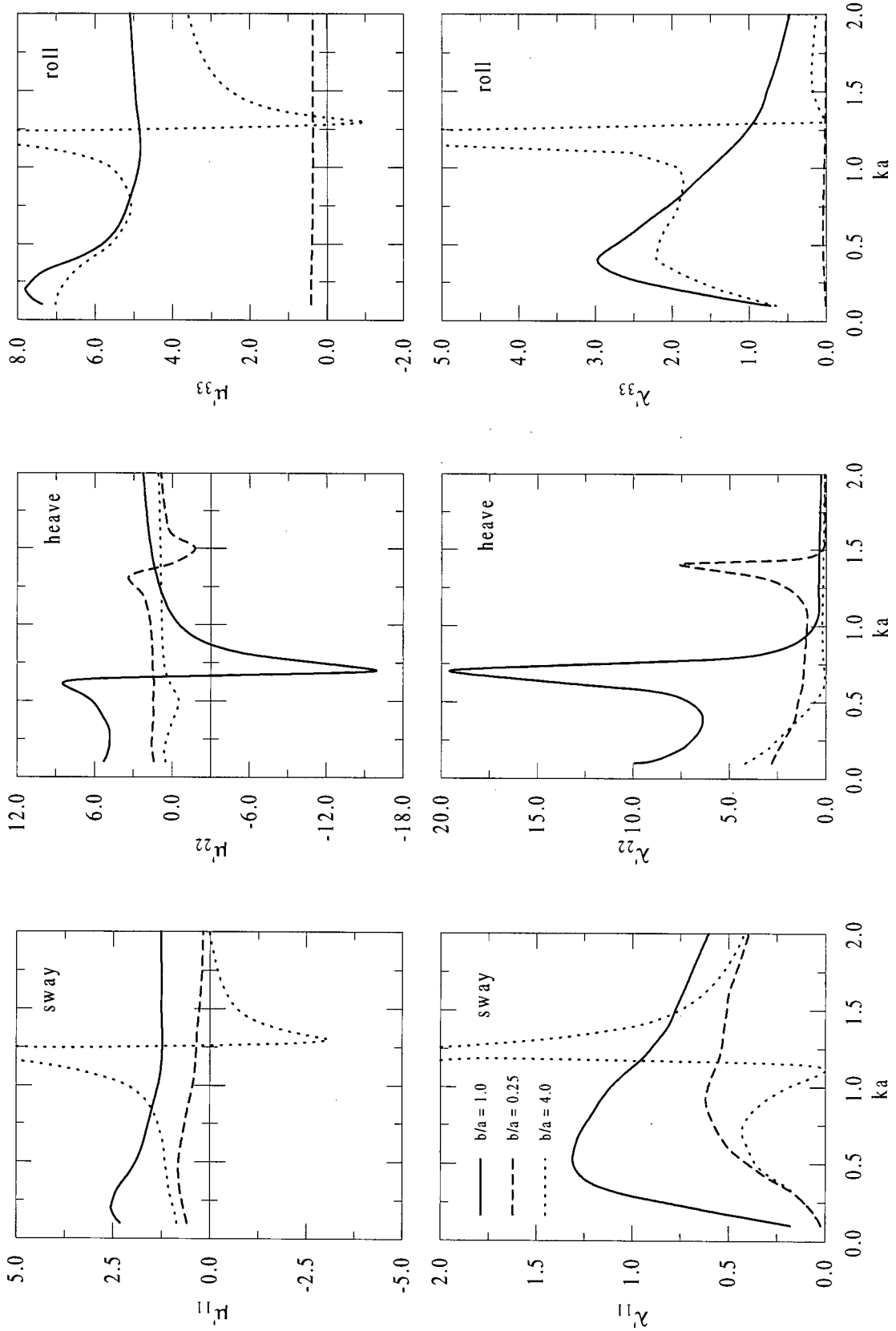

(a) rectangular twin-pontoon section, (d/a = 2.5, h/a = 0.5, β = 0°).

Fig. 4.5 Variation of added mass and damping coefficients indicating the influence of pontoon spacing. (contd...)

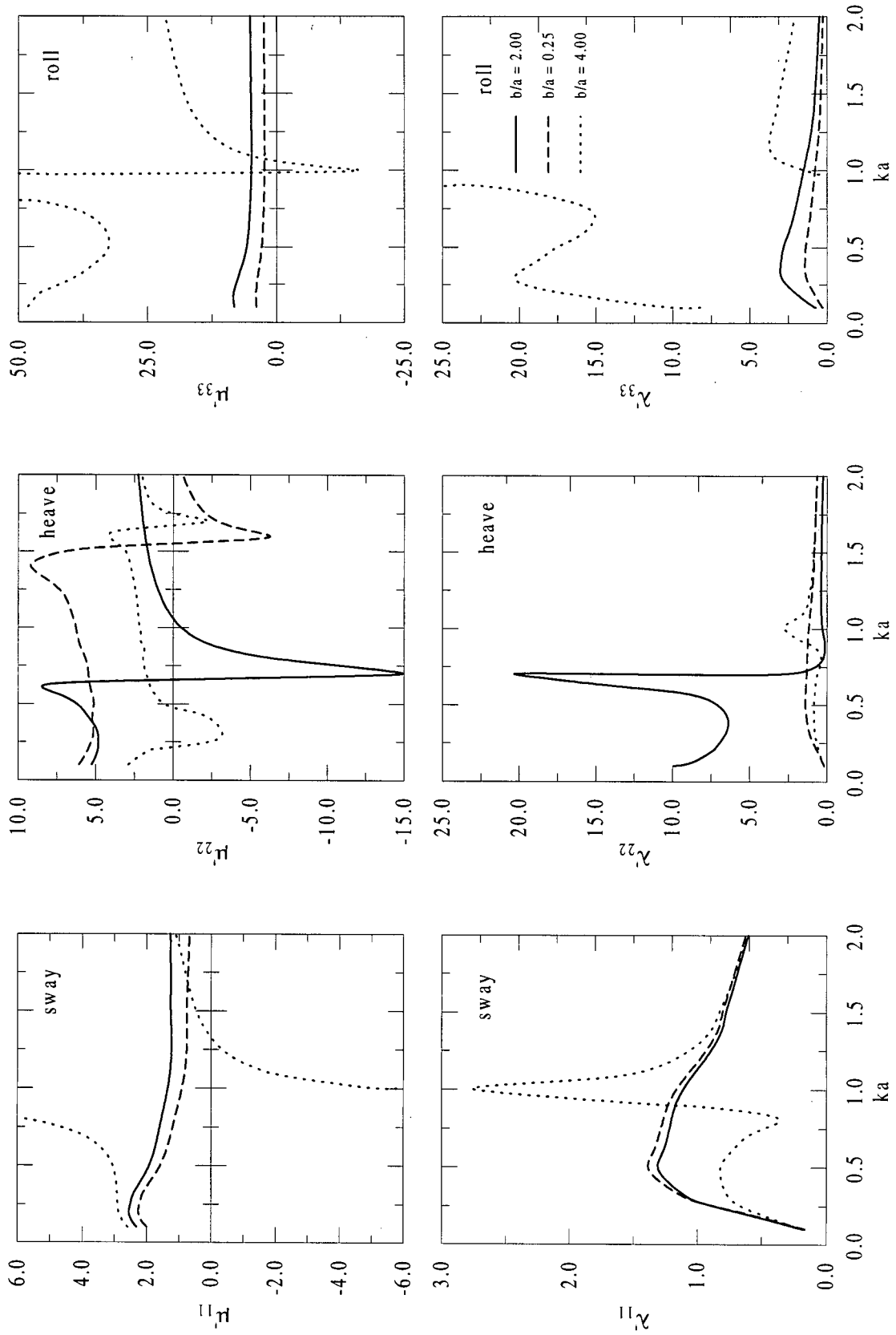

(b) circular twin-pontoon section, (d/a = 2.5, h/a = 0.5, β = 0°).

Fig. 4.5.

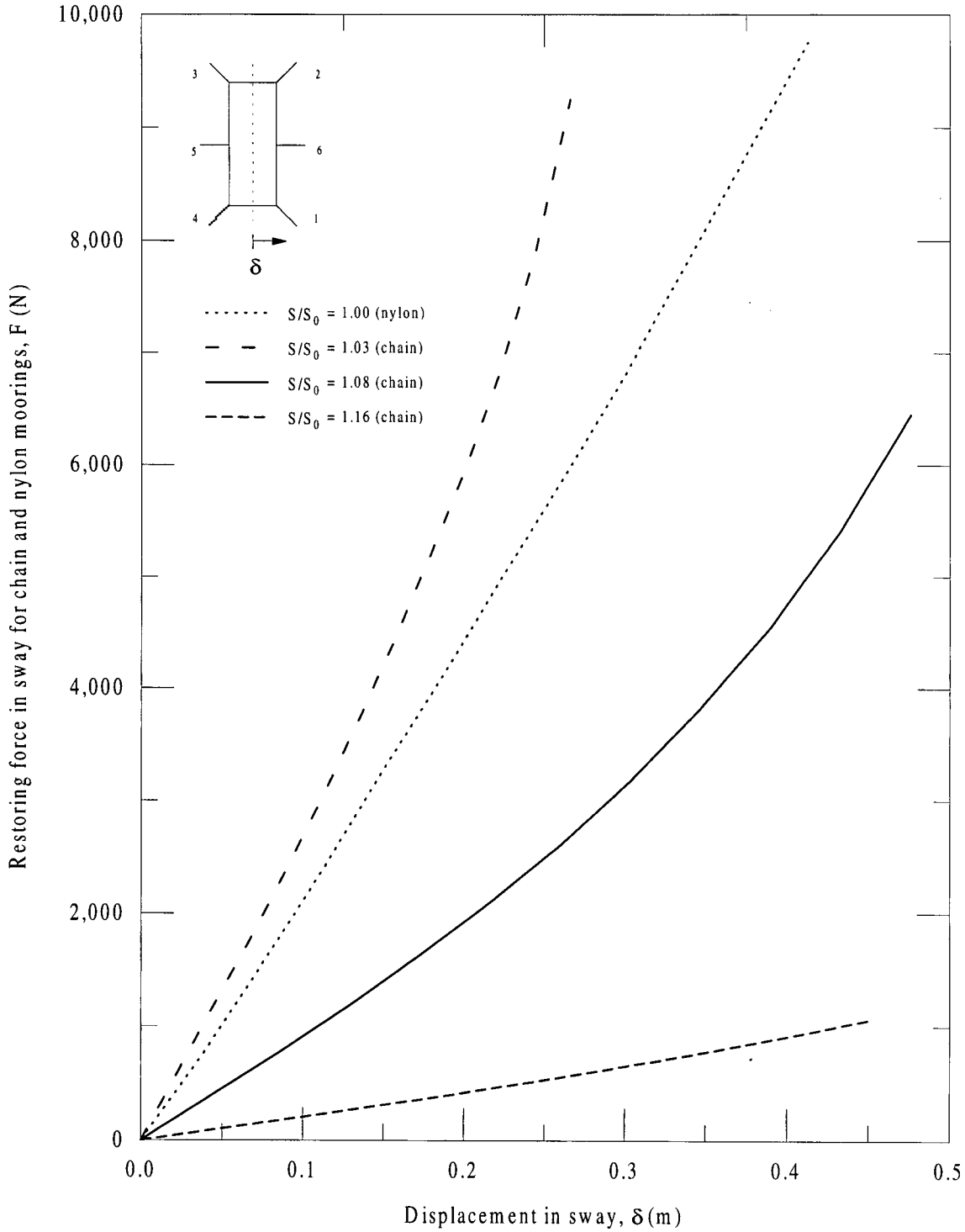

Fig. 4.6 Comparison of stiffness characteristics for a six-point mooring system made up of chain or nylon lines.

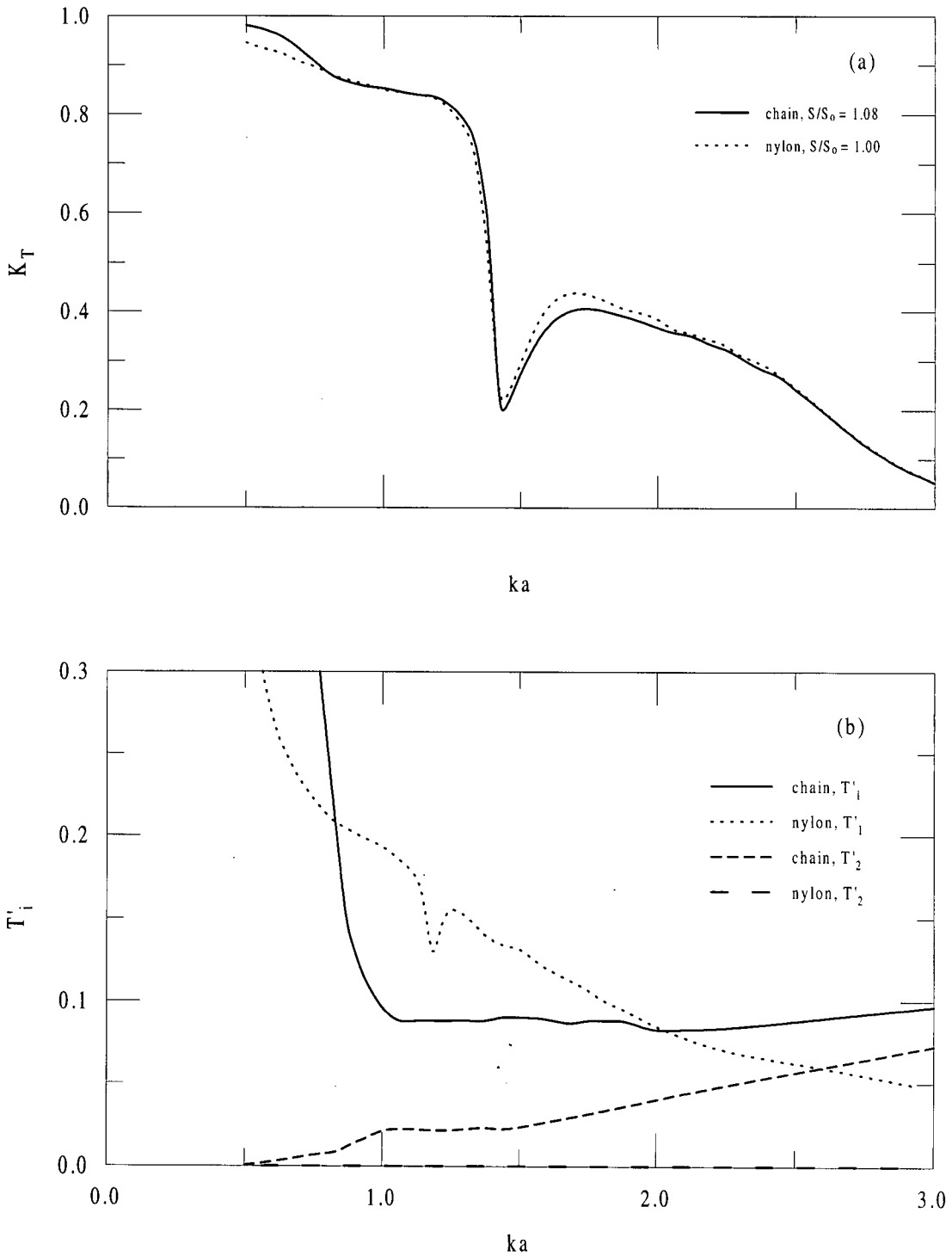

Fig. 4.7 Comparison between chain and nylon moorings for a twin-pontoon rectangular section breakwater. (a) transmission coefficient; (b) upwave and downwave mooring line tensions at anchor.

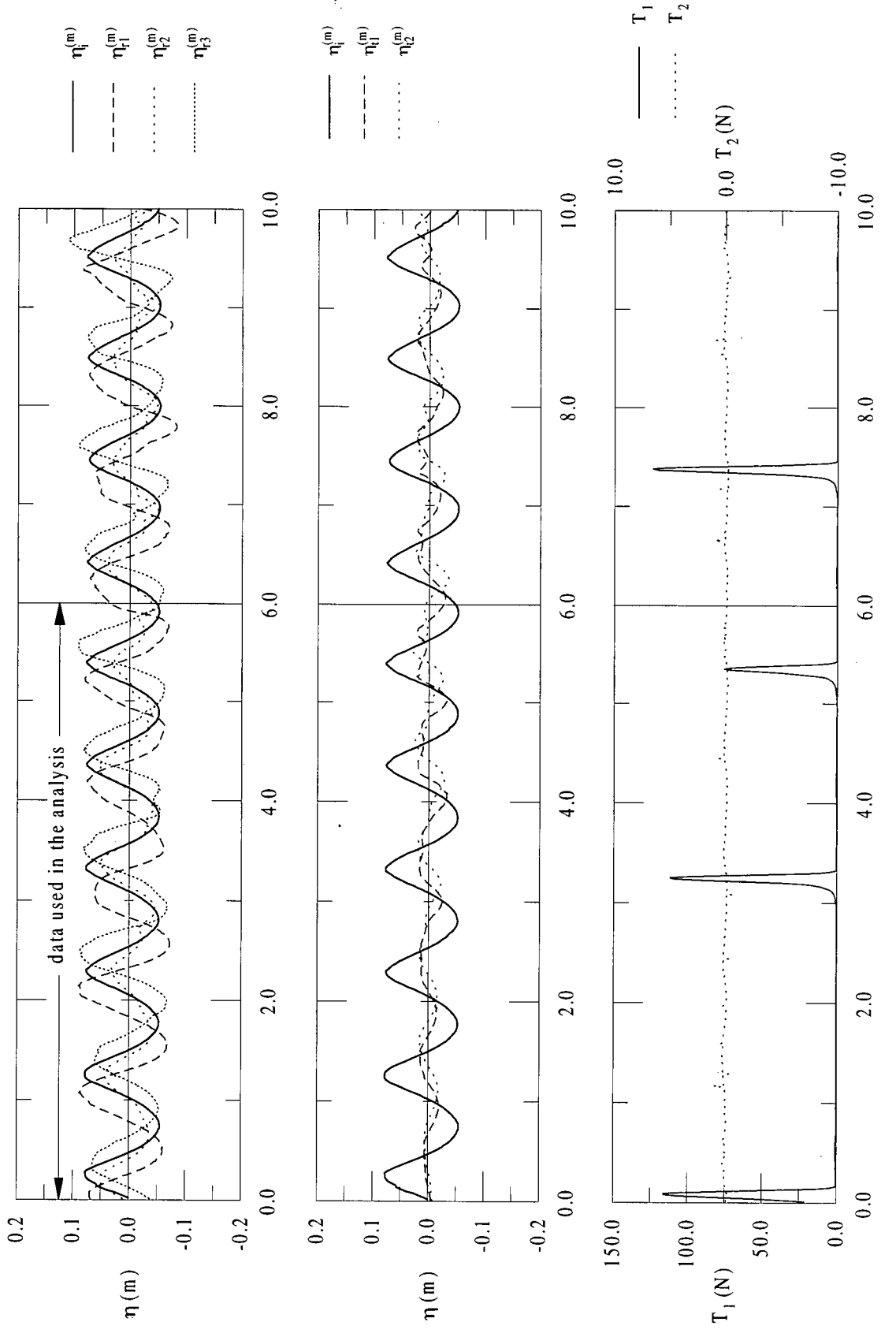

(a) H = 0.12 m, T = 1.00 sec, with chain mooring, $S/S_o = 1.08$.

Fig. 4.8 Measured time traces of water surface elevation and mooring line anchor forces for base case of moored rectangular twin-pontoon model, (d/a = 1.67, h/a = 0.45, b/a =1.0). (contd...)

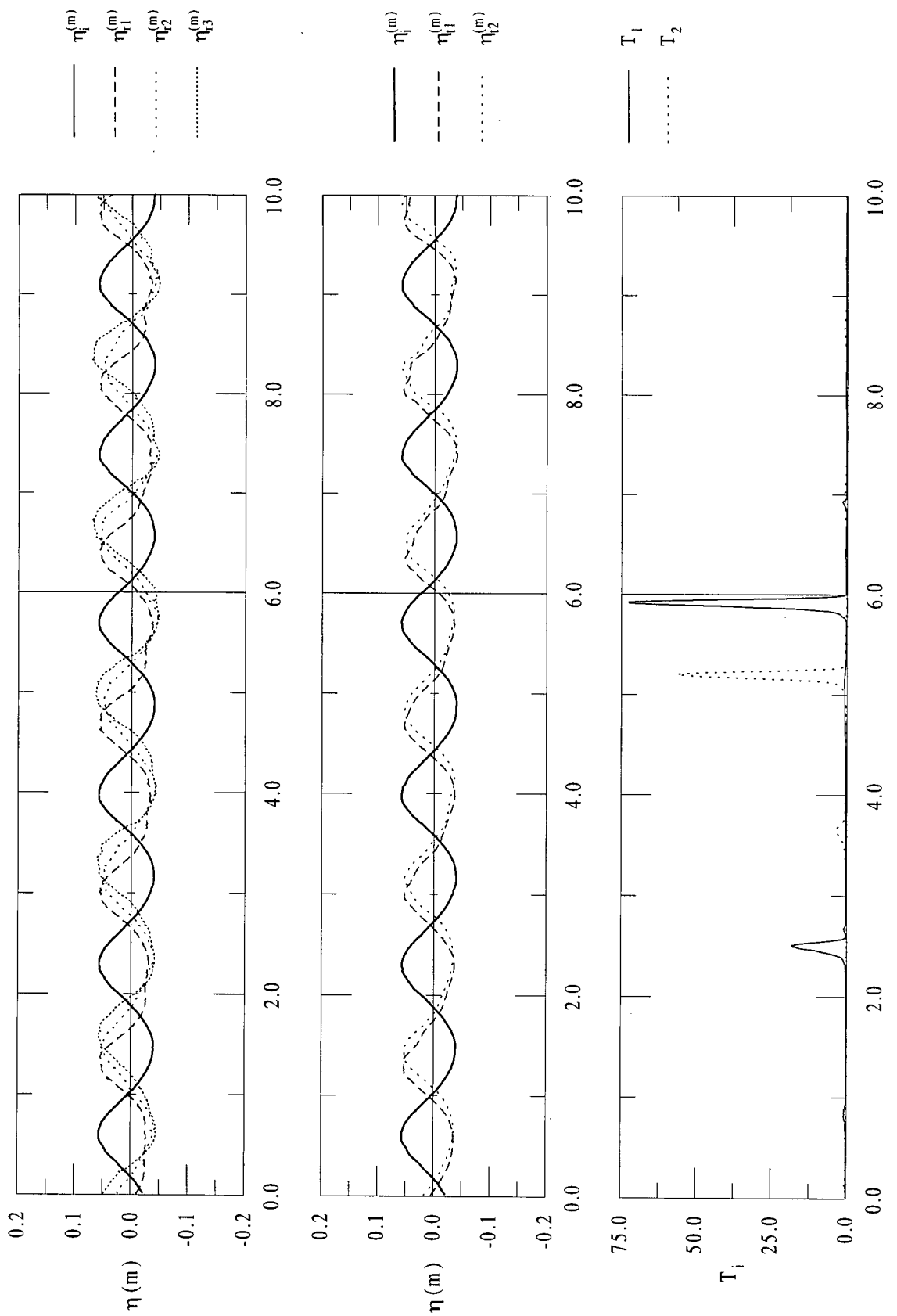

(b) H = 0.12 m, and T = 1.00 sec, with nylon mooring, $S/S_o = 1.00$.

Fig. 4.8 (contd...)

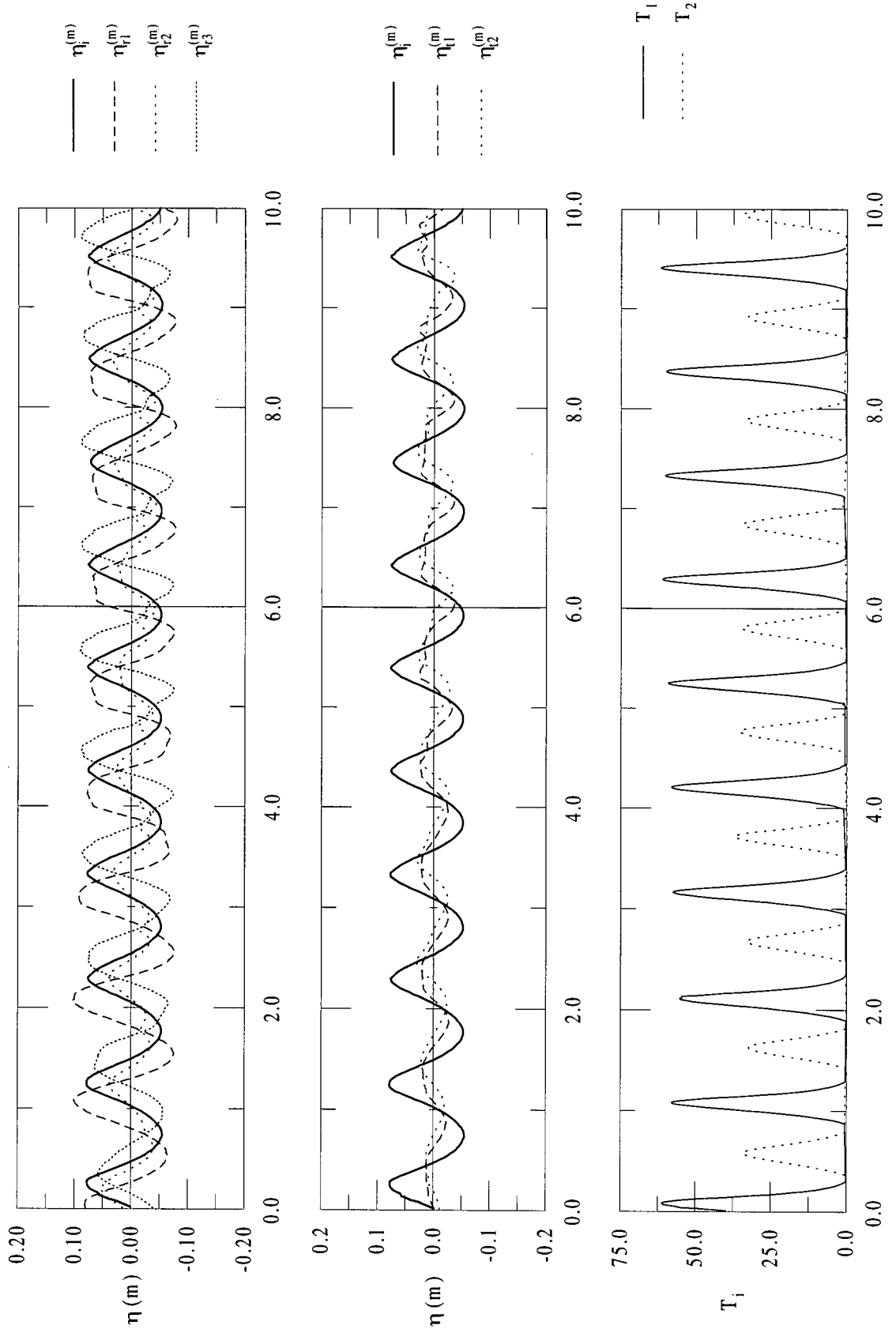

(c) H = 0.09 m, and T = 1.70 sec, with chain mooring, $S/S_o = 1.08$.

Fig. 4.8.

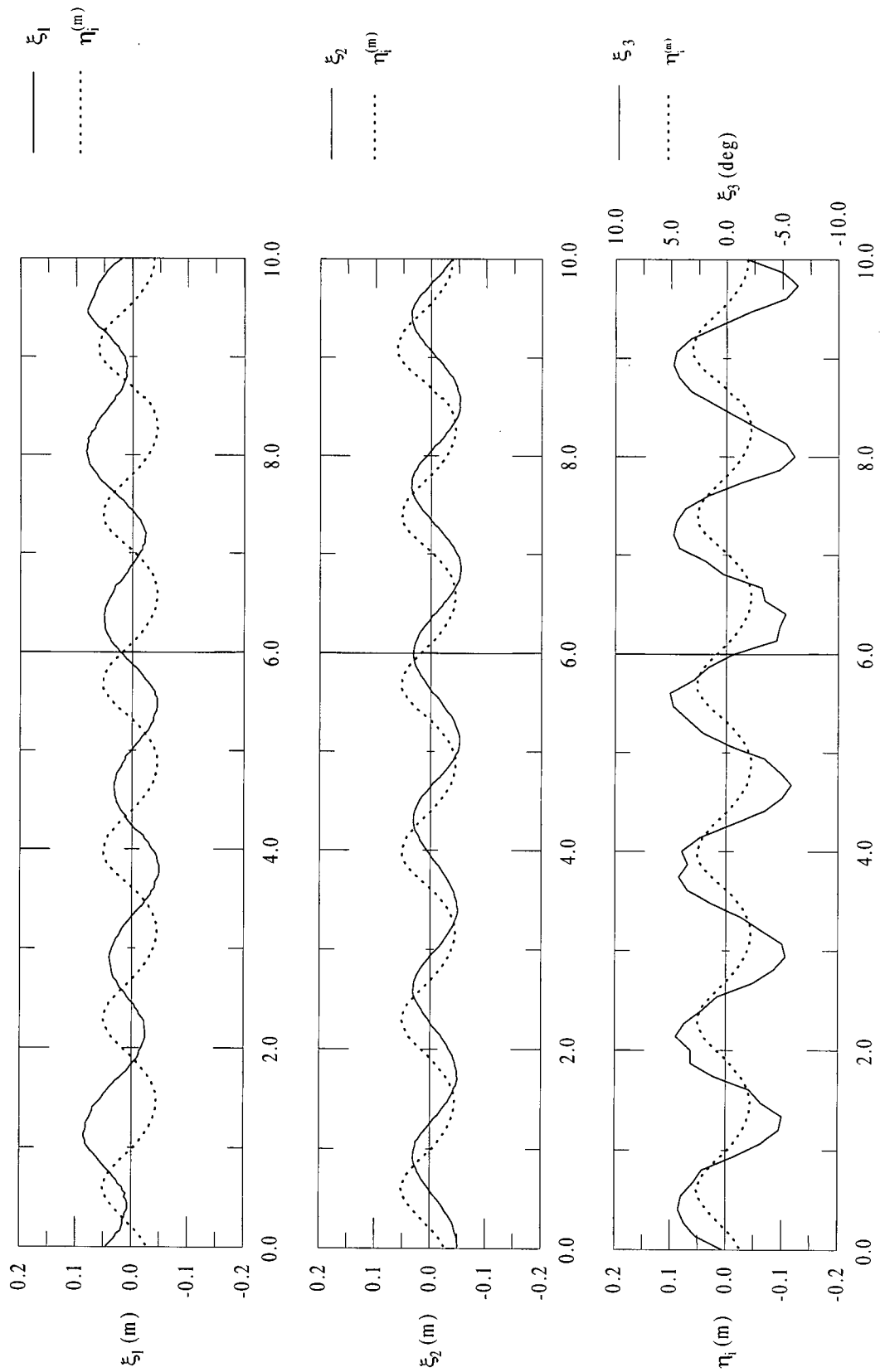

Fig. 4.9 Measured time traces of breakwater responses and water surface elevation for base case of moored rectangular twin-pontoon model, (d/a = 1.67, h/a = 0.45, b/a =1.0, H = 0.09 m, and T = 1.70 sec, with chain mooring, S/S_o = 1.08).

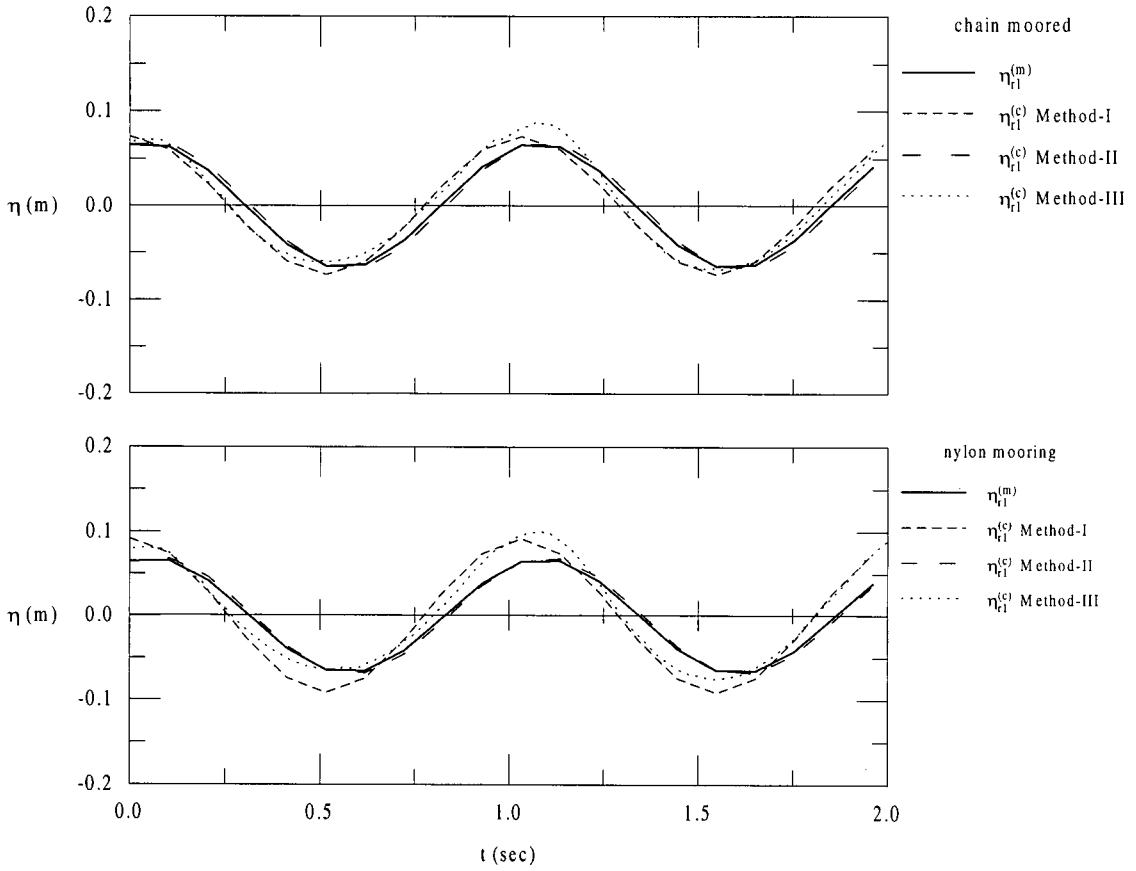

Fig. 4.10 Time traces of both measured and computed wave profiles based on reflection analysis for base cases of moored rectangular twin-pontoon breakwater, (d/a = 1.67, h/a = 0.45, b/a = 1.0, H = 0.12 m, T = 1.0 sec).

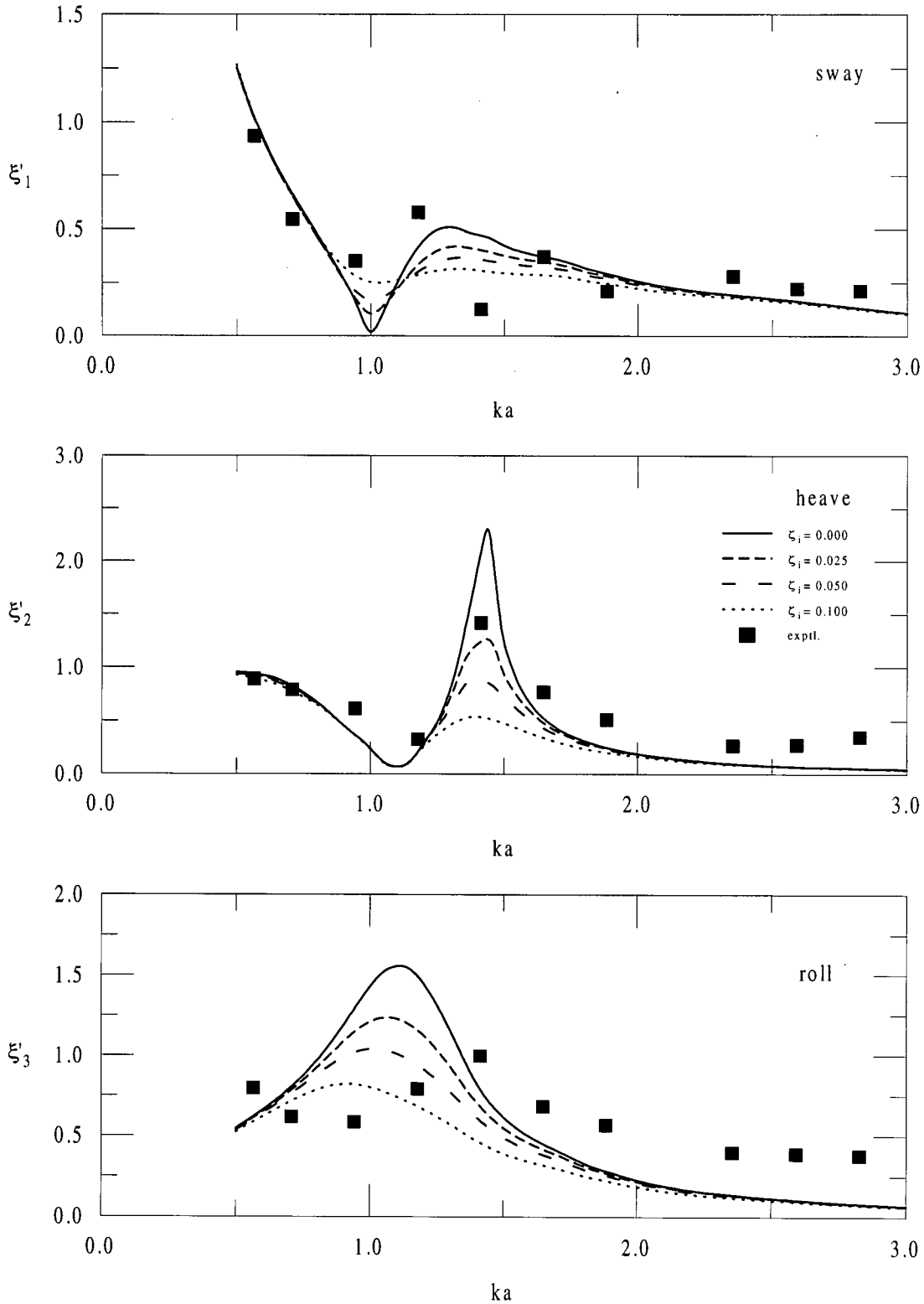

(a) RAO's in sway, heave and roll.

Fig. 4.11 Numerical results indicating the influence of different values of viscous damping coefficient for base case of a rectangular twin-pontoon breakwater, (d/a = 1.67, h/a = 0.45, b/a = 1.0, S/S_o = 1.08, $\beta = 0°$). (contd...)

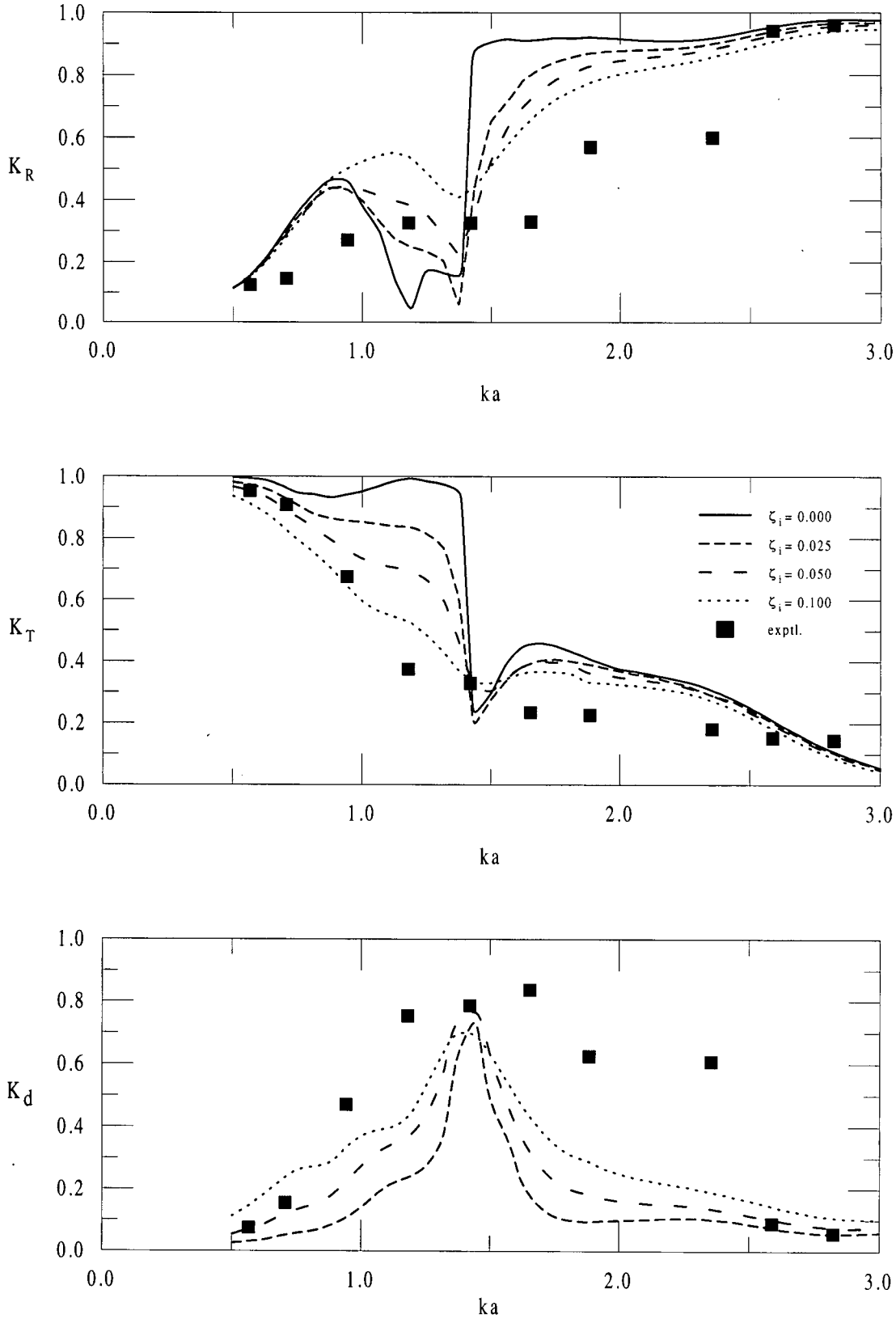

(b) reflection, transmission and energy dissipation coefficients.

Fig. 4.11.

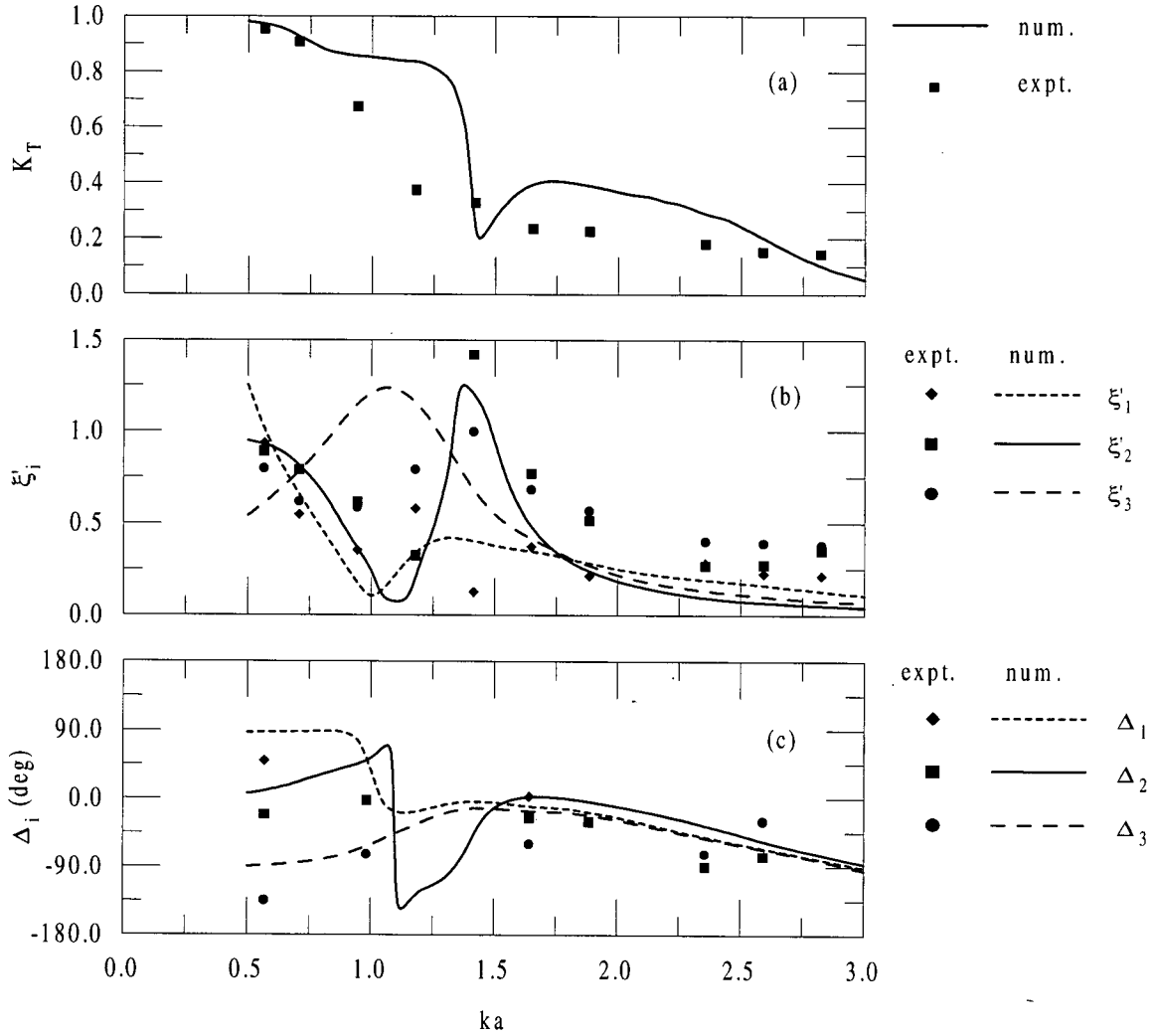

Fig. 4.12 Comparison of experimental values and numerical results for base case of rectangular twin-pontoon breakwater with chain mooring, (d/a = 1.67, h/a = 0.45, b/a = 1.0, S/S_o = 1.0, β = 0°). (a) transmission coefficient; (b) RAO's in sway, heave and roll; (c) RAO phases.

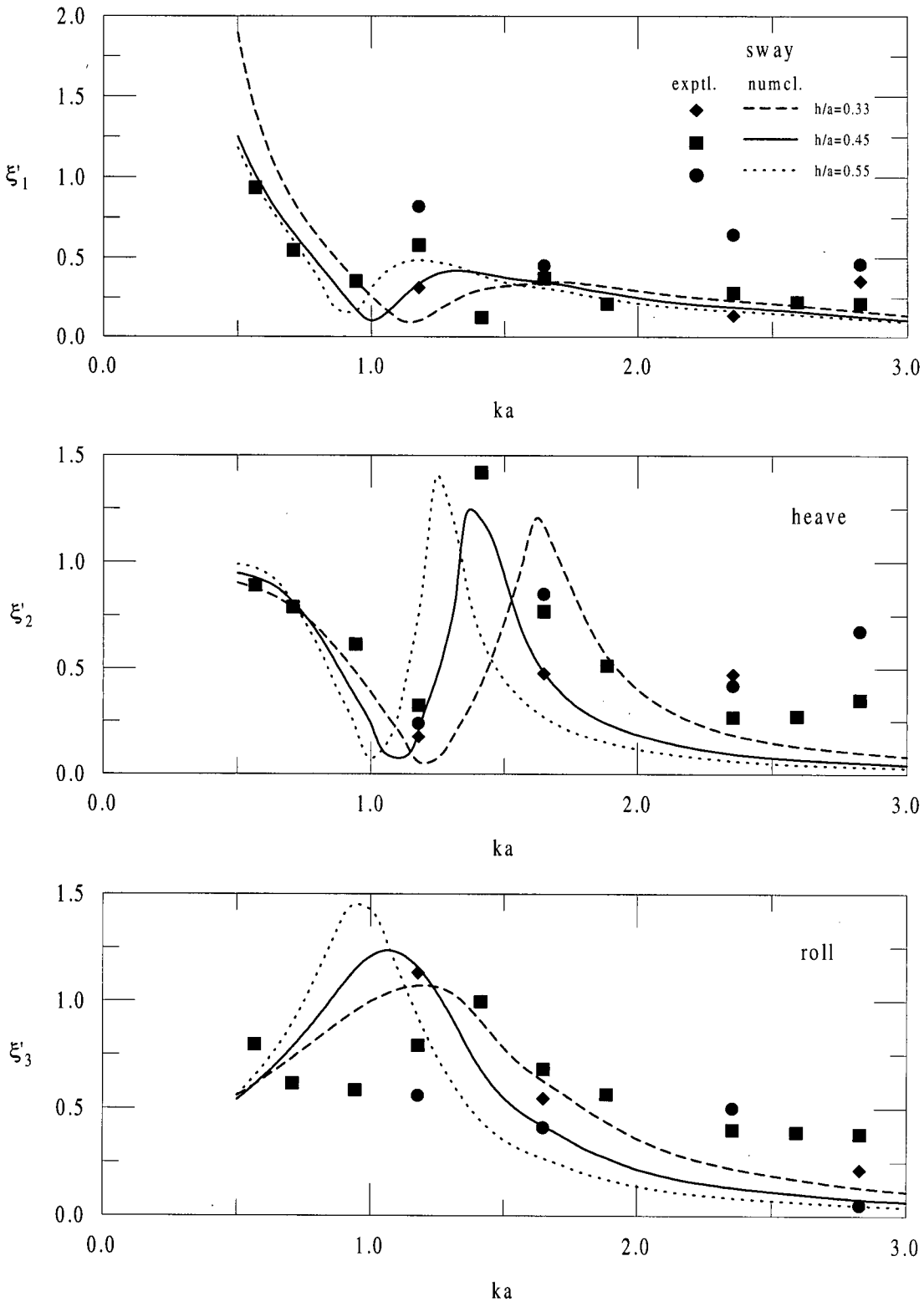

(a) RAO's in sway, heave, and roll.

Fig. 4.13 Comparison of experimental values and numerical results to indicate the influence of draft for a rectangular twin-pontoon breakwater with chain mooring, (d/a = 1.67, b/a = 1.0, S/S_o = 1.08, $\beta = 0°$). (contd....)

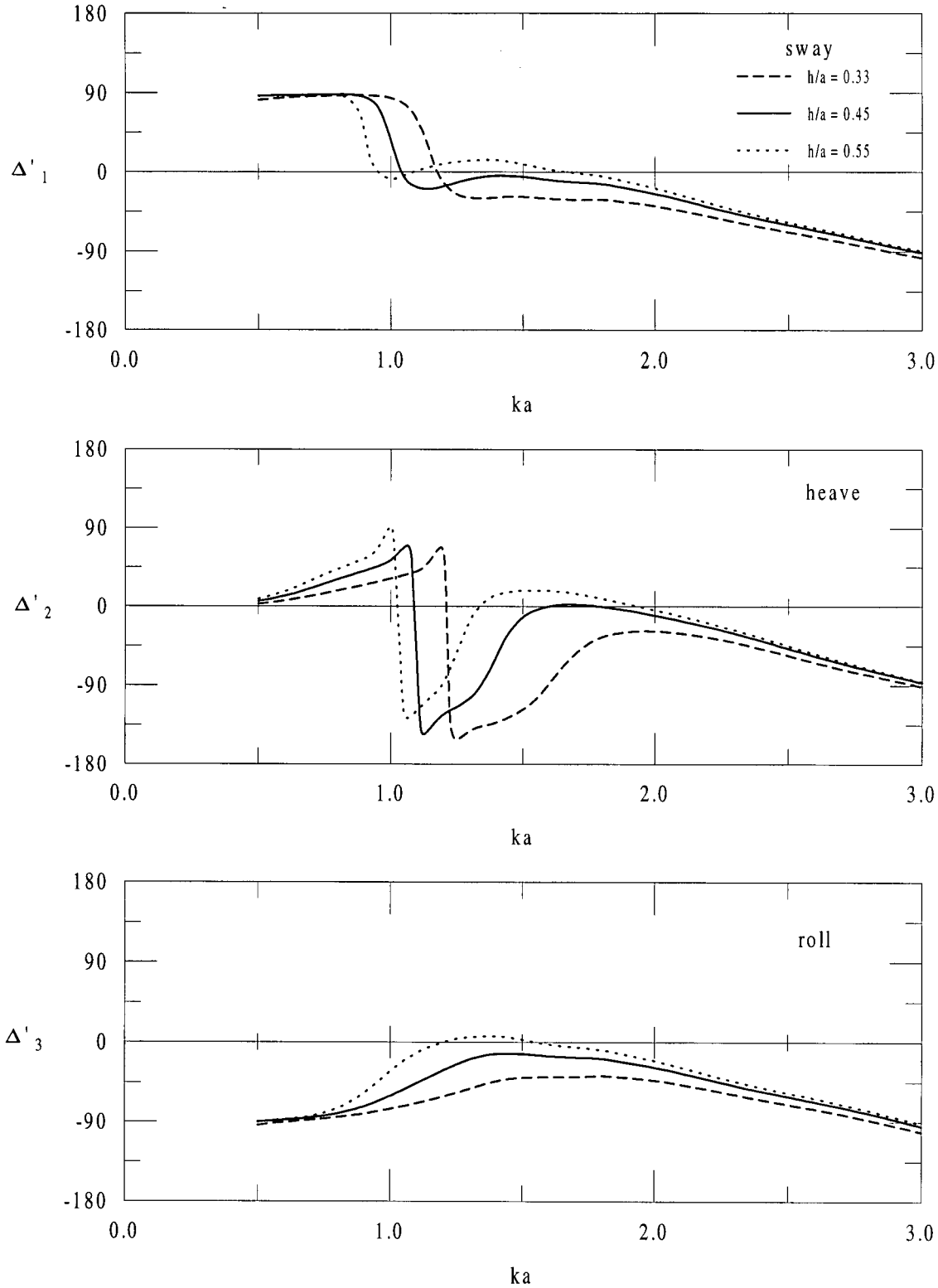

(b) phase of RAO's for sway, heave and roll.

Fig. 4.13 (contd...)

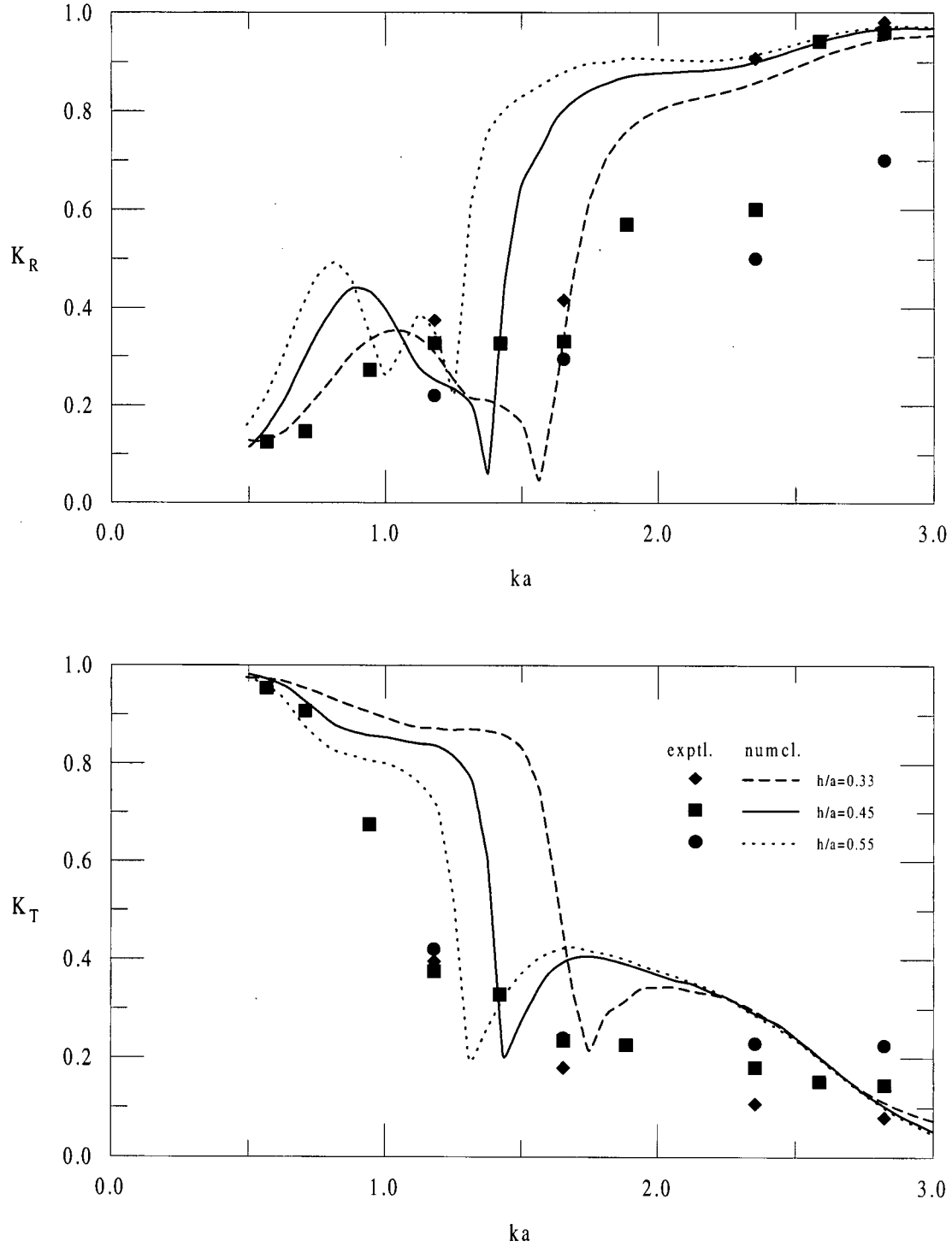

Fig. 4.14 Comparison of experimental values and numerical results of reflection and transmission coefficients to indicate the influence of draft for a rectangular twin-pontoon breakwater with chain mooring, (d/a = 1.67, b/a = 1.0, $S/S_o = 1.08$, $\beta = 0°$).

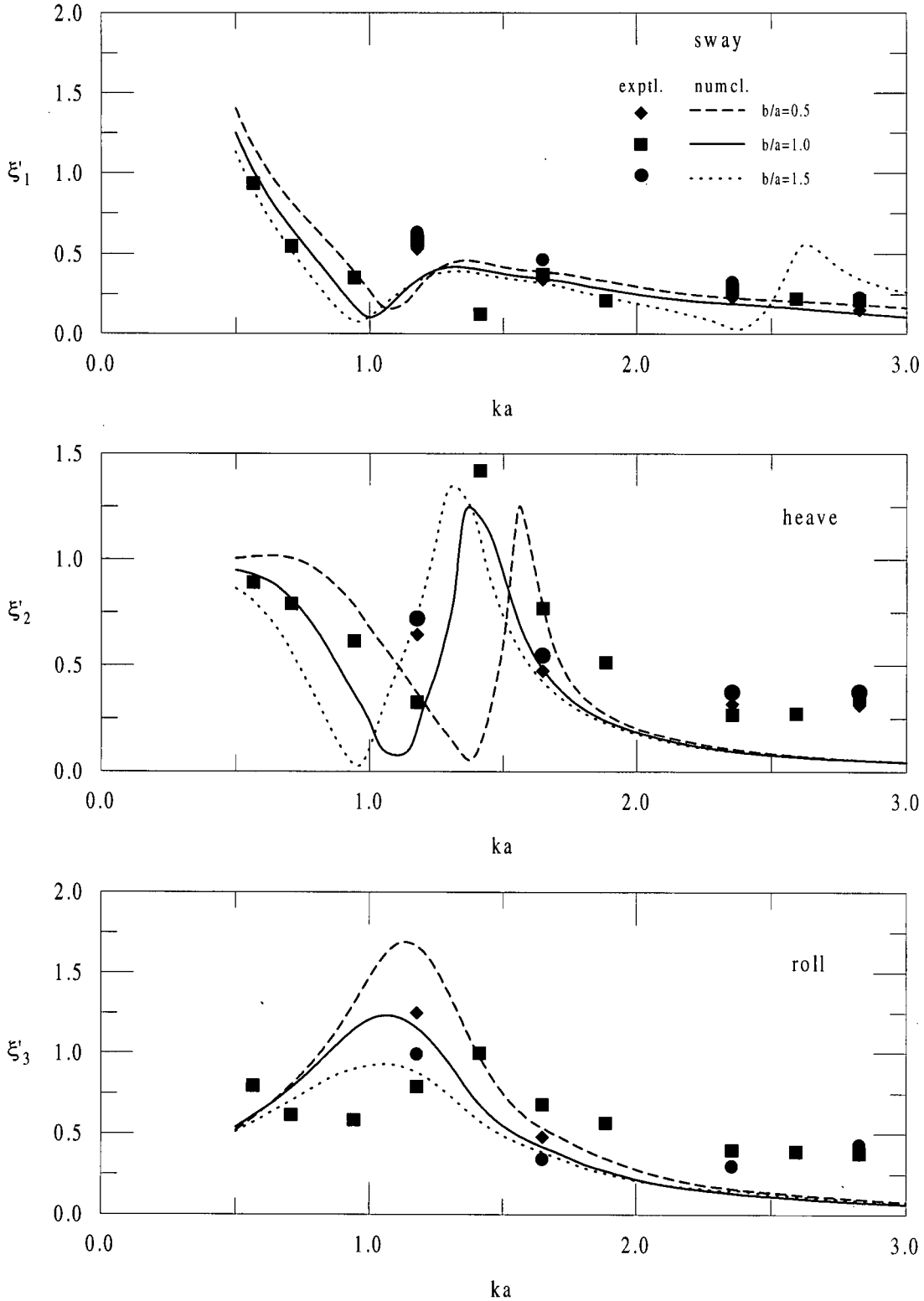

(a) RAO's in sway, heave, and roll.

Fig. 4.15 Comparison of experimental values and numerical results to indicate the influence of spacing for a rectangular twin-pontoon breakwater with chain mooring, (d/a = 1.67, h/a = 0.45, S/S_o = 1.08, $\beta = 0°$). (contd...)

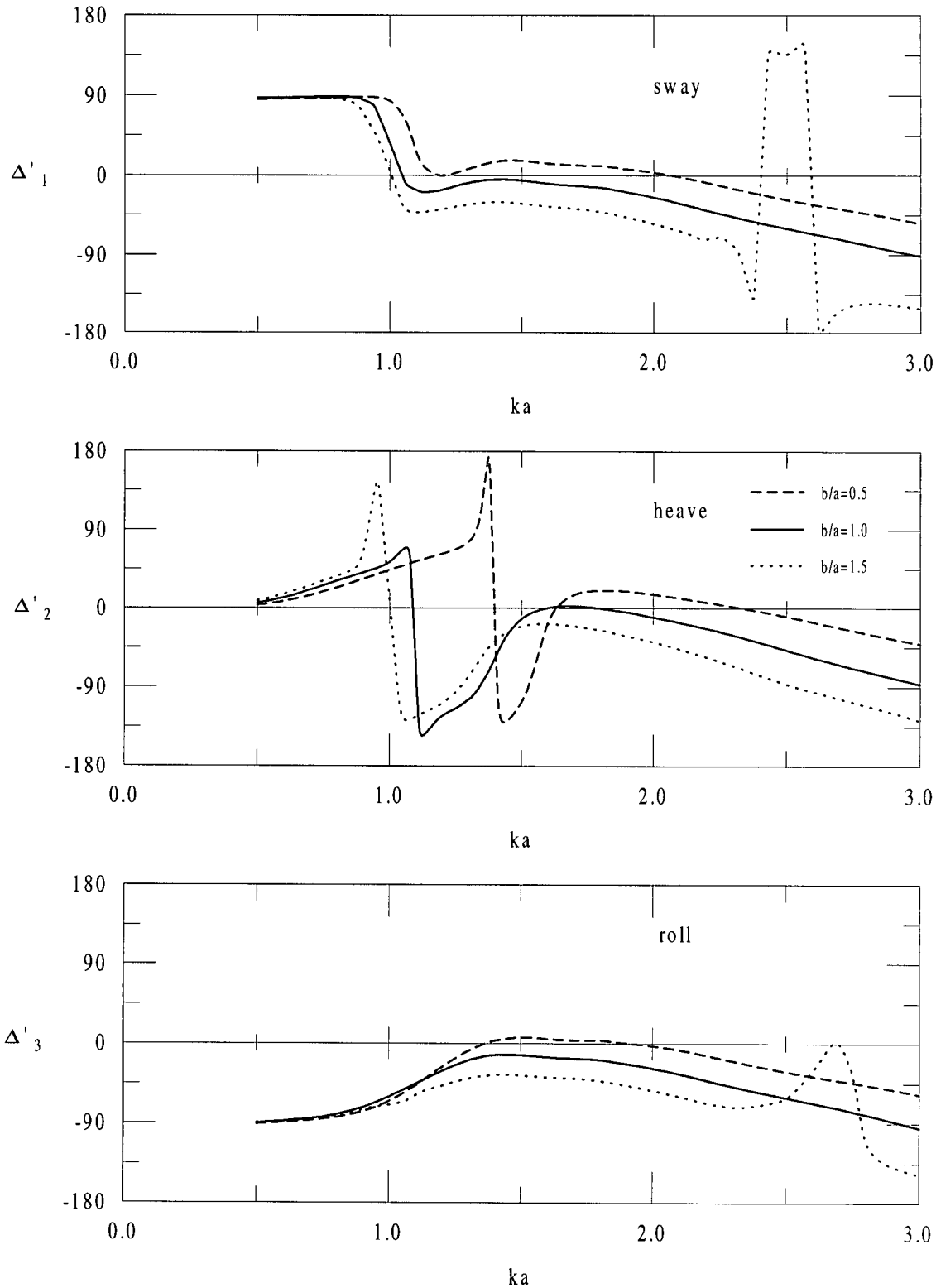

(b) phase of RAO's for sway, heave and roll.

Fig. 4.15 (contd...)

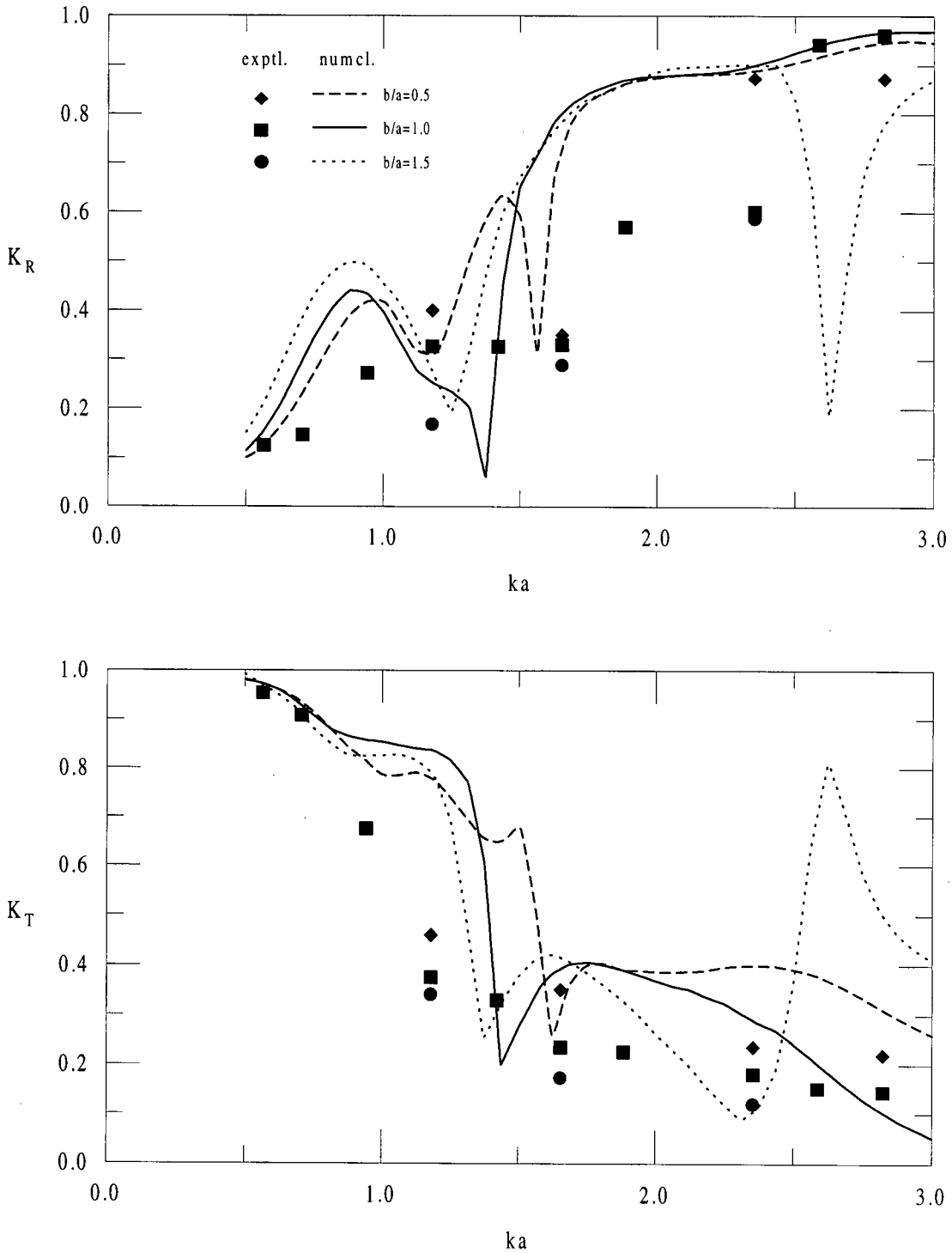

Fig. 4.16 Comparison of experimental values and numerical results of reflection and transmission coefficients to indicate the influence of spacing for a rectangular twin-pontoon breakwater with chain mooring, (d/a = 1.67, h/a = 0.45, $S/S_o = 1.08$, $\beta = 0°$).

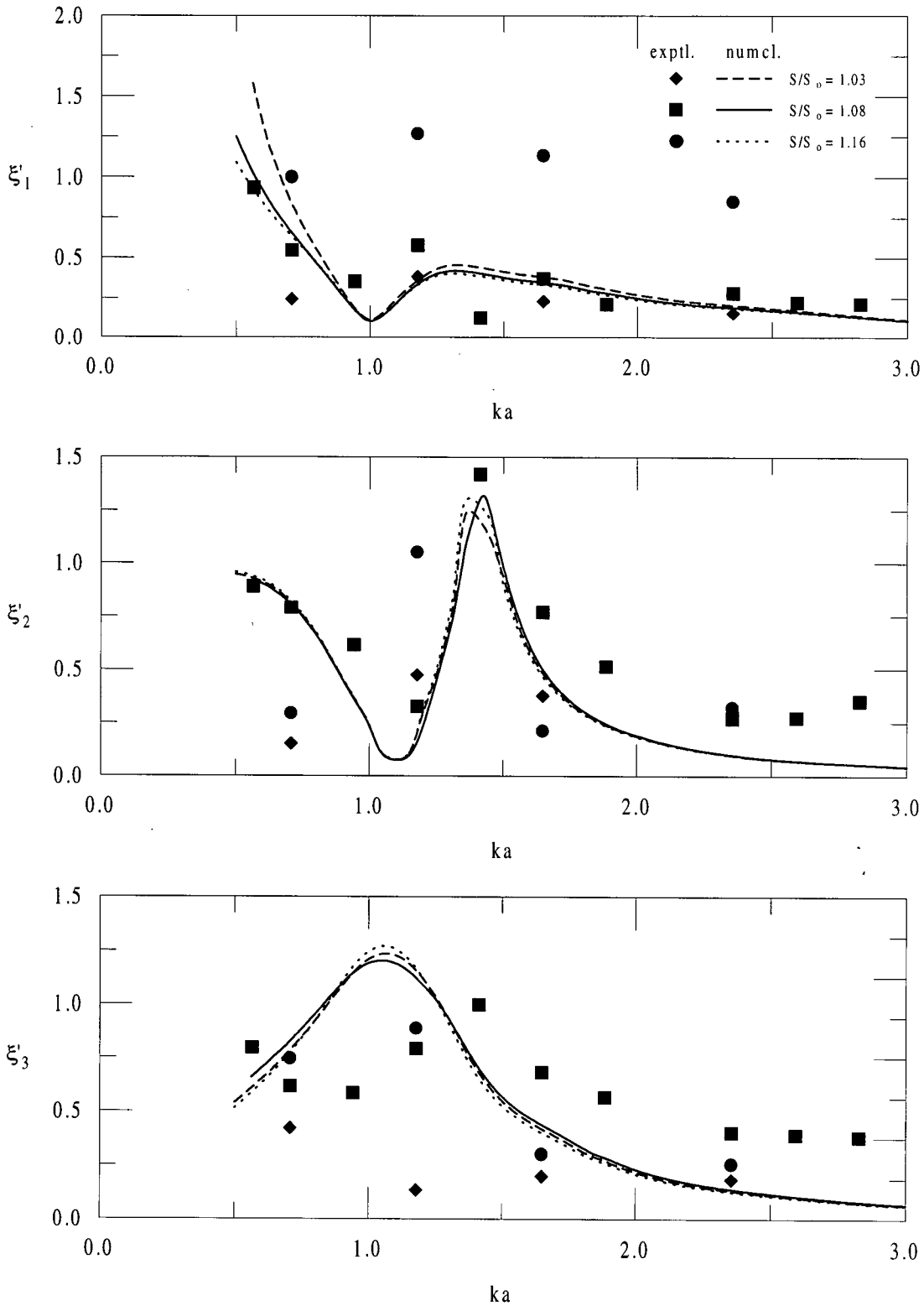

(a) RAO's in sway, heave, and roll.

Fig. 4.17 Comparison of experimental values and numerical results to indicate the influence of slackness for a rectangular twin-pontoon breakwater with chain mooring, (d/a = 1.67, h/a = 0.45, b/a = 1.0, $\beta = 0°$). (contd...)

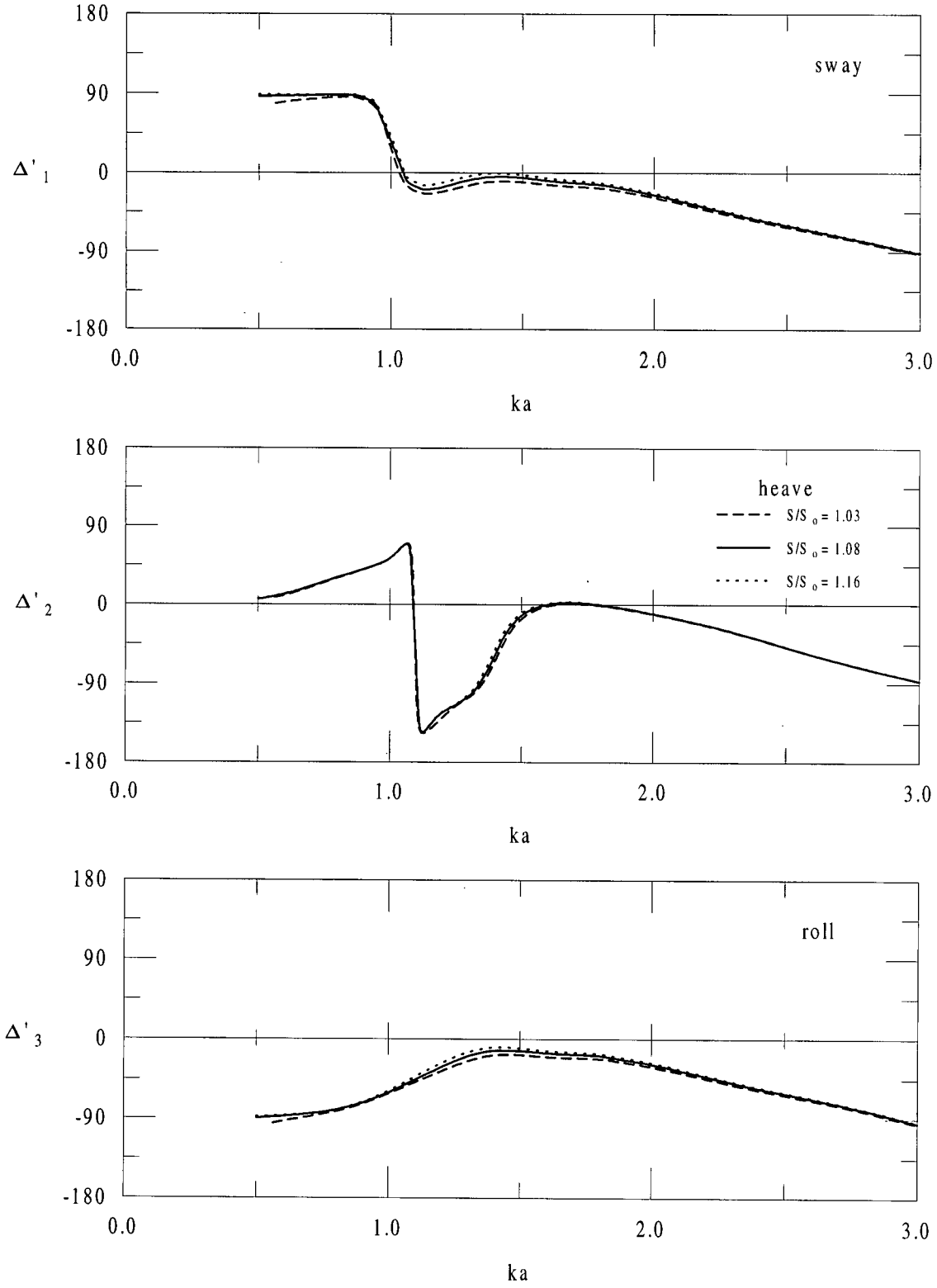

(b) phase of RAO's for sway, heave and roll.

Fig. 4.17 (contd...)

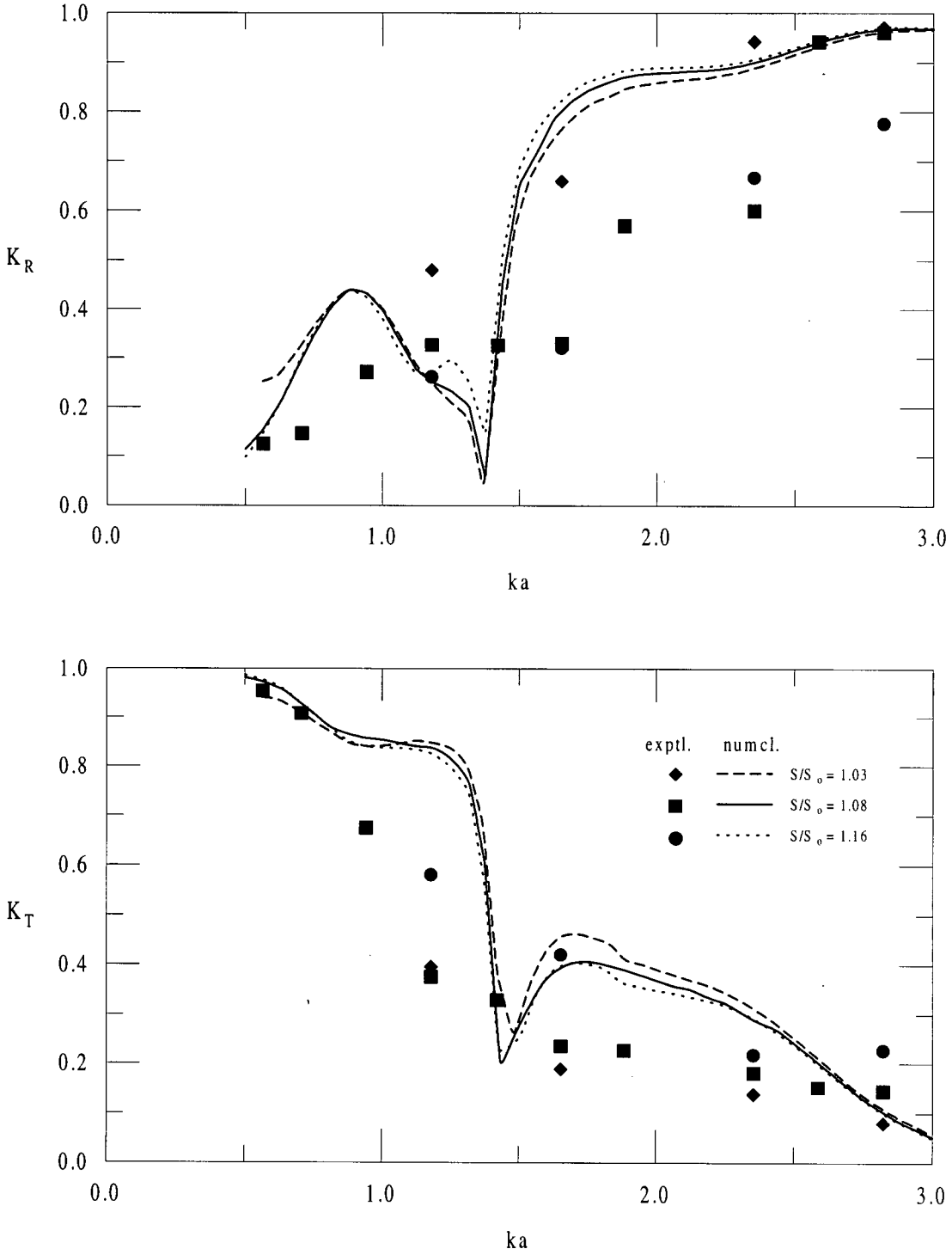

Fig. 4.18 Comparison of experimental values and numerical results of reflection and transmission coefficients indicating the influence of slackness for a rectangular twin-pontoon breakwater with chain mooring, (d/a = 1.67, h/a = 0.45, b/a = 1.0, $\beta = 0°$).

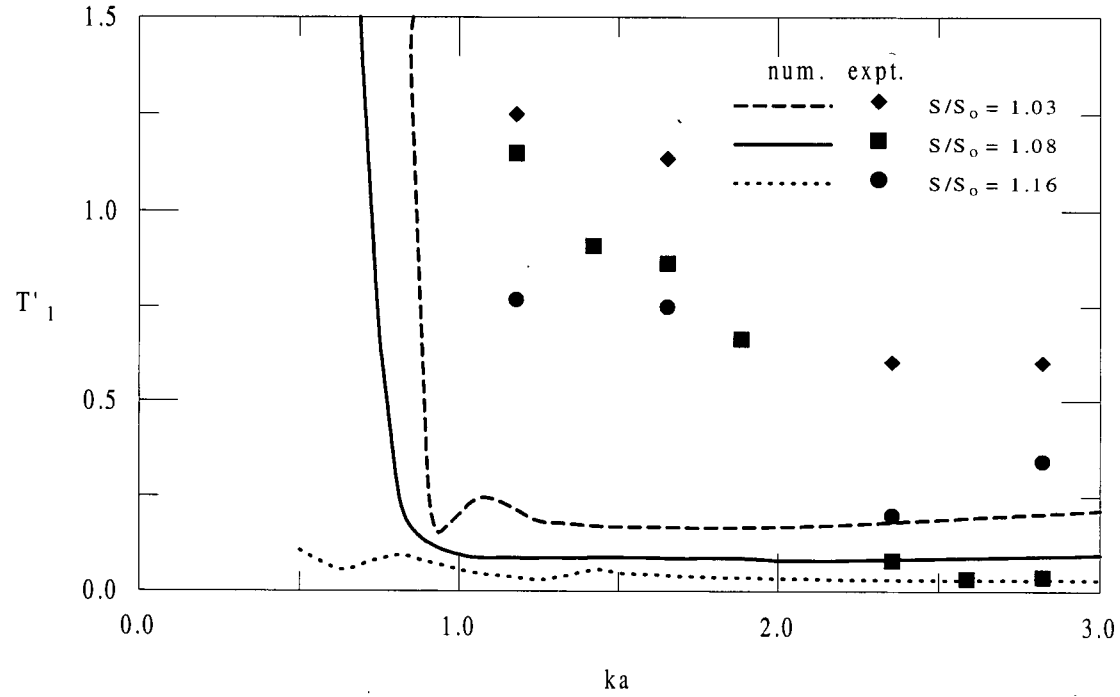

Fig. 4.19 Experimental values and numerical results of maximum mooring line forces at anchor indicating the influence of slackness for a rectangular twin-pontoon breakwater with chain mooring, (d/a = 1.67, h/a = 0.45, b/a = 1.0, $\beta = 0°$).

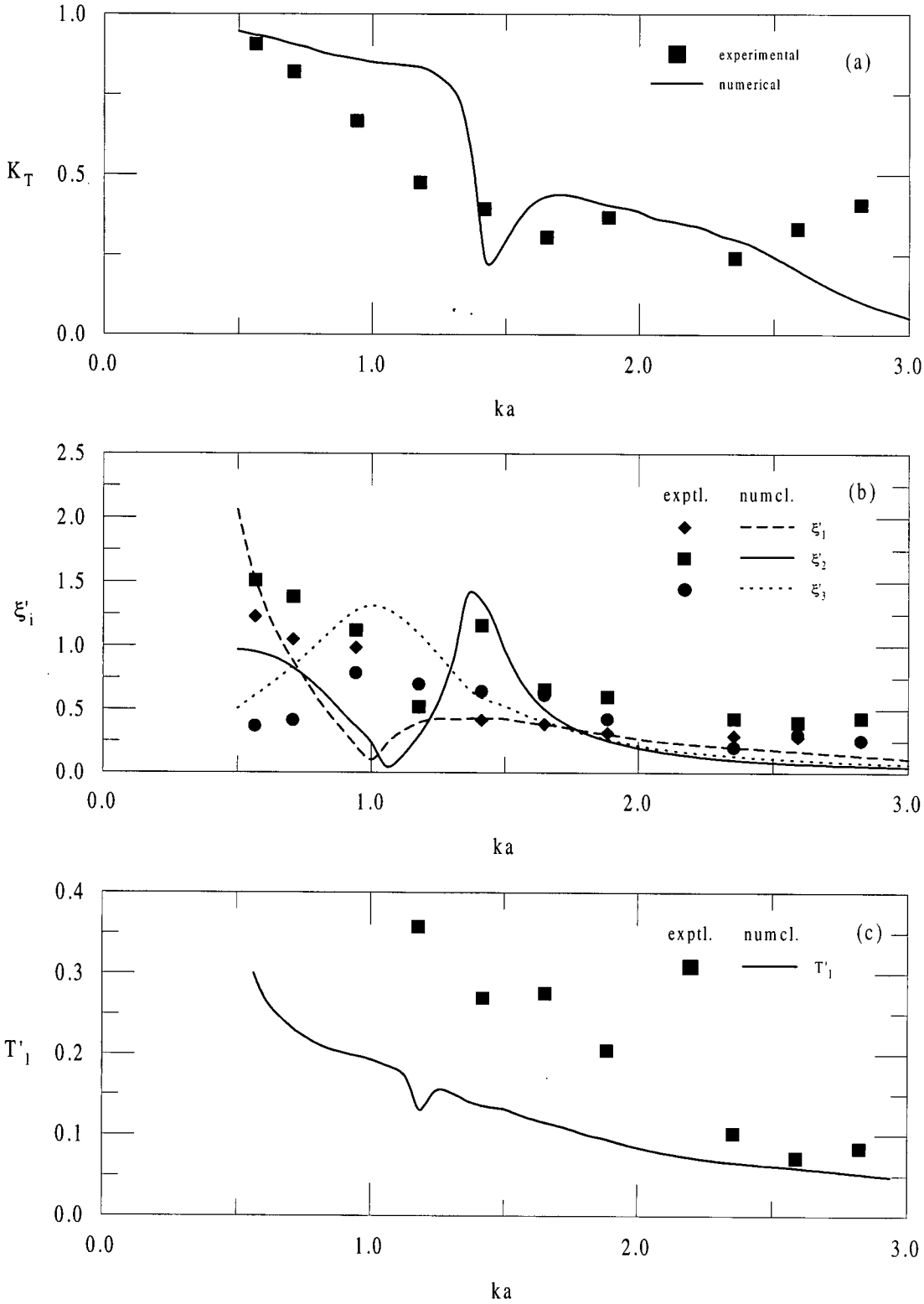

Fig. 4.20 Comparison of experimental values and numerical results for base case of rectangular twin-pontoon breakwater with nylon mooring, (d/a = 1.67, h/a = 0.45, b/a = 1.0, S/S_o = 1.0, β = 0°). (a) transmission coefficient; (b) RAO's in sway, heave and roll; (c) maximum mooring line tensions at anchor.

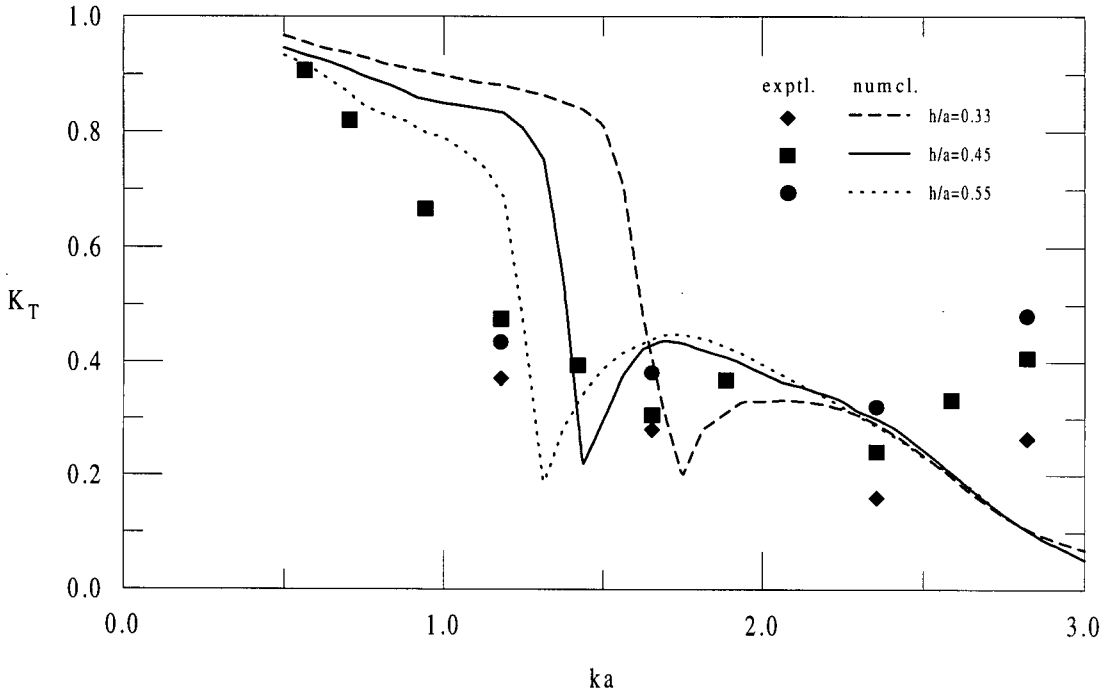

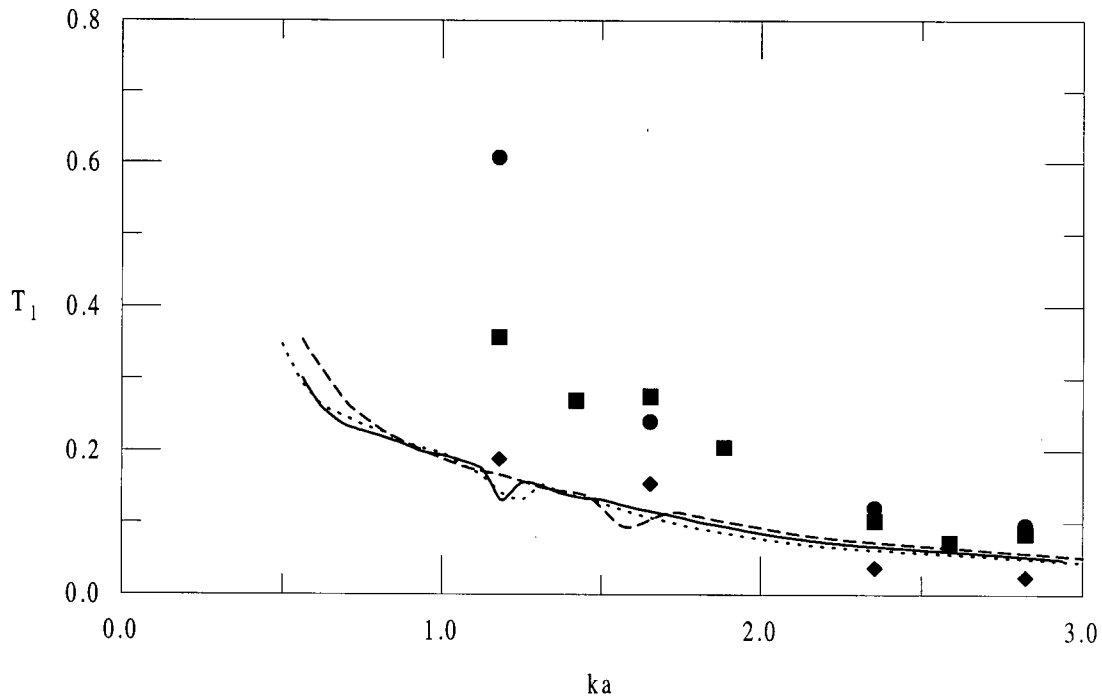

(a) influence of draft; (d/a = 1.67, b/a = 1.00, S/S_o = 1.00, β = 0°).

Fig. 4.21 Comparison of experimental values of transmission coefficient and maximum mooring line tensions at anchor with that of numerical results for a rectangular twin-pontoon breakwater with nylon mooring. (contd...)

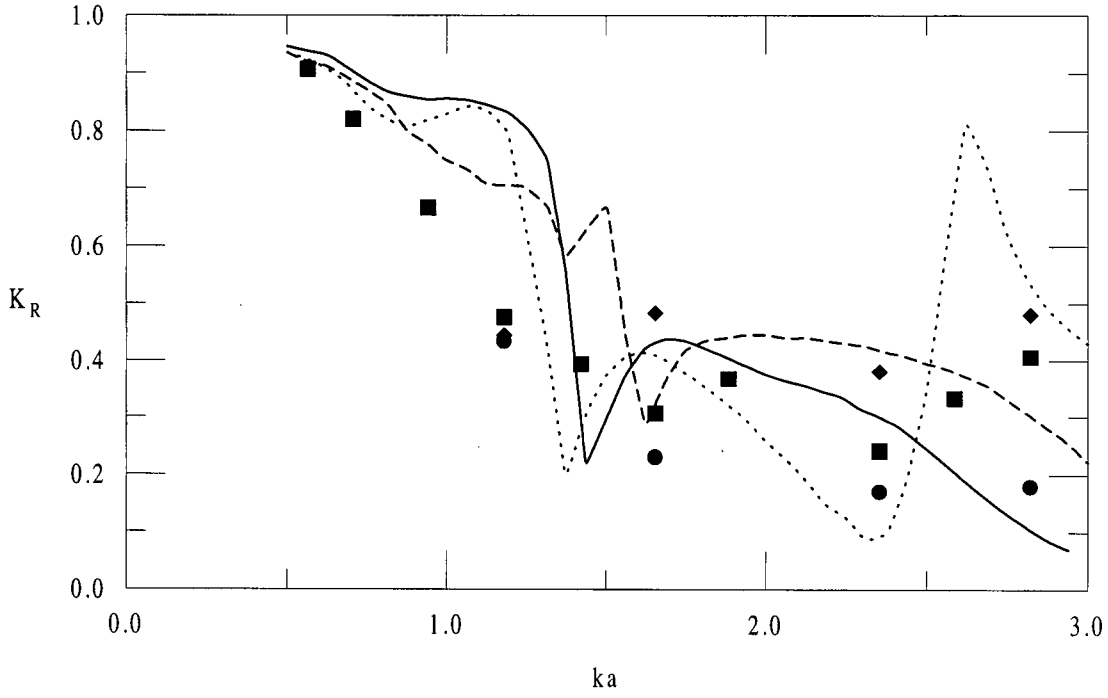

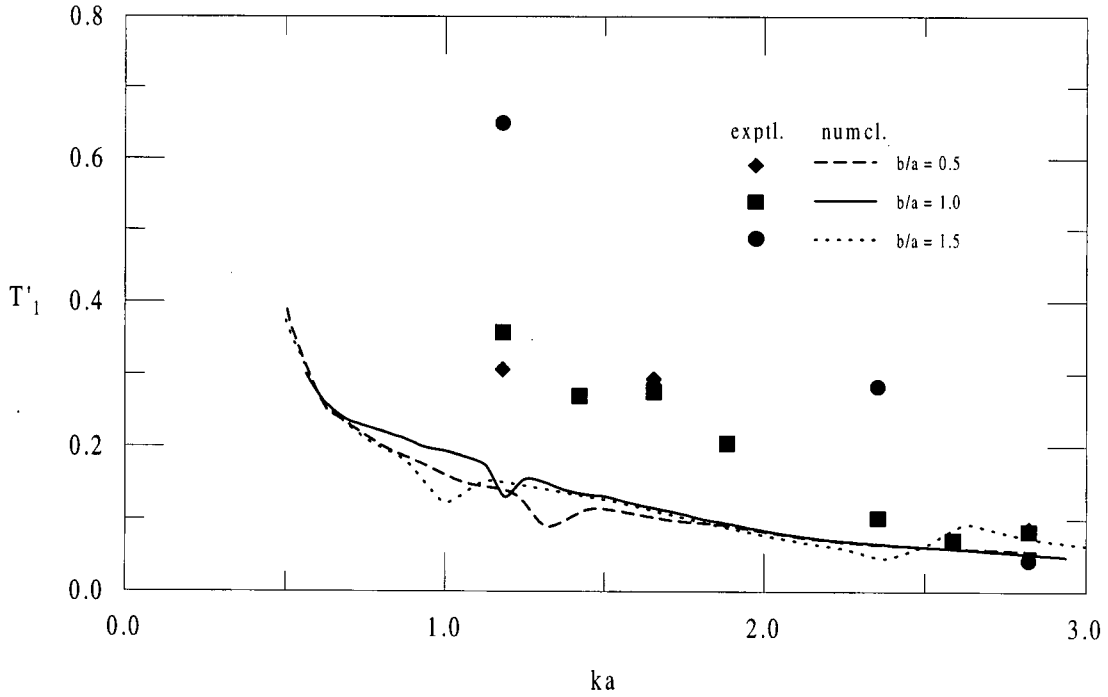

(b) influence of spacing; (d/a = 1.67, h/a = 0.50, S/S_o = 1.00, $\beta = 0°$).

Fig. 4.21.

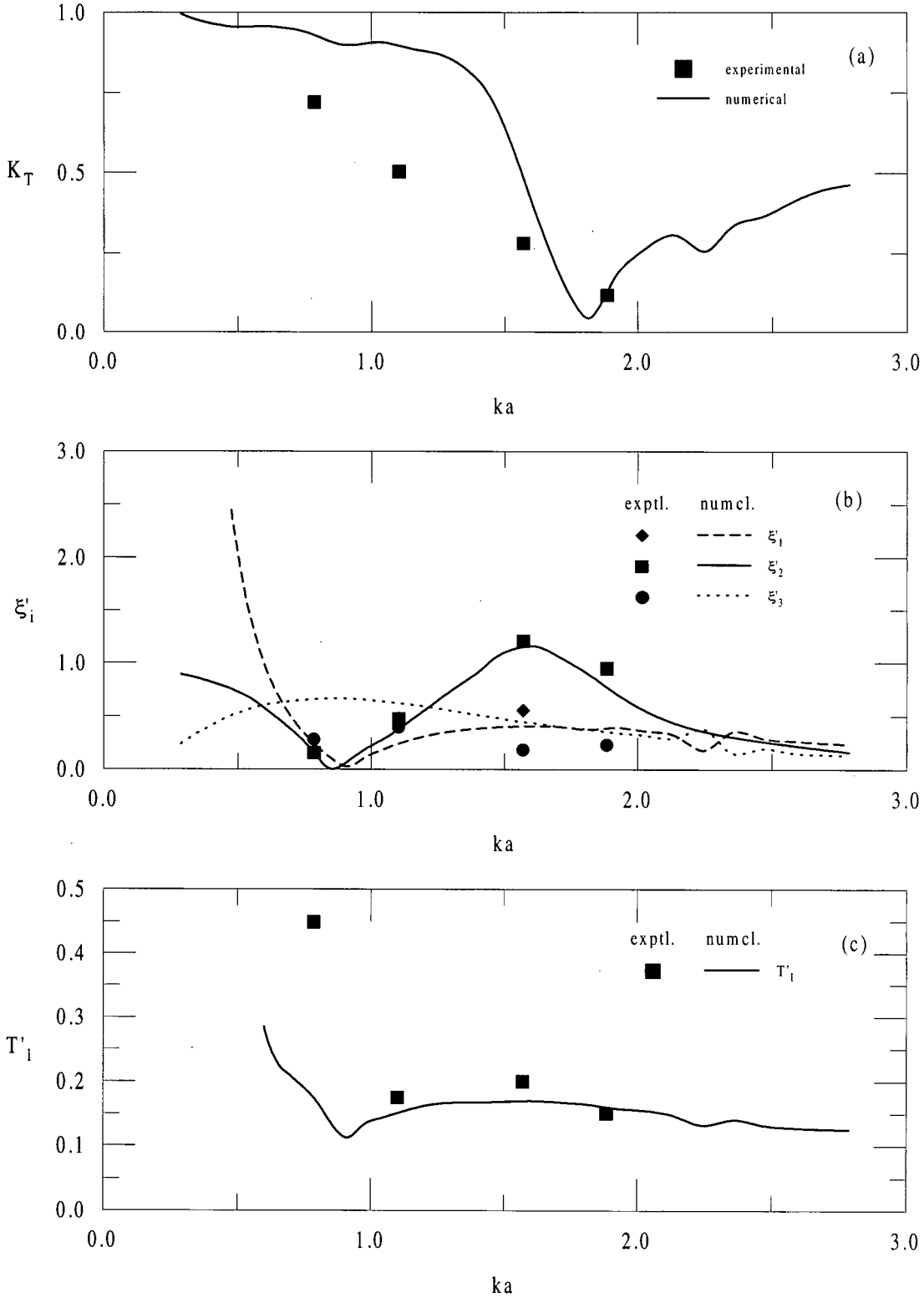

Fig. 4.22 Comparison of experimental values and numerical results for a circular section twin-pontoon breakwater with chain mooring, (d/a = 2.5, h/a = 0.5, b/a = 2.0, S/S_o = 1.08, β = 0°). (a) transmission coefficient; (b) RAO's in sway, heave and roll; (c) maximum mooring line tensions at anchor.

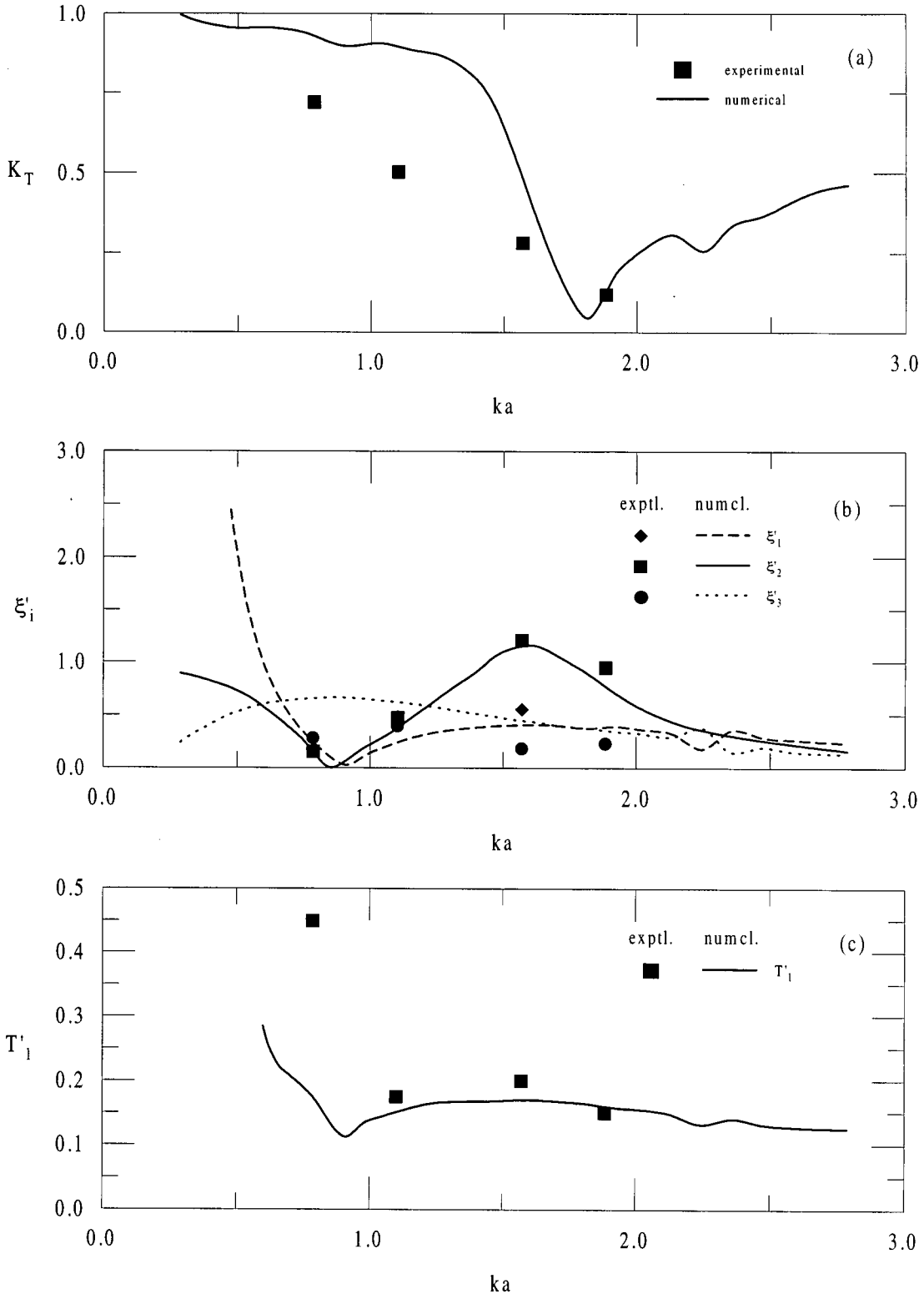

Fig. 4.23 Comparison of experimental values and numerical results for a circular section twin-pontoon breakwater with nylon mooring, (d/a = 2.5, h/a = 0.5, b/a = 2.0, $S/S_o = 1.0$, $\beta = 0°$). (a) transmission coefficient; (b) RAO's in sway, heave and roll; (c) maximum mooring line tensions at anchor.

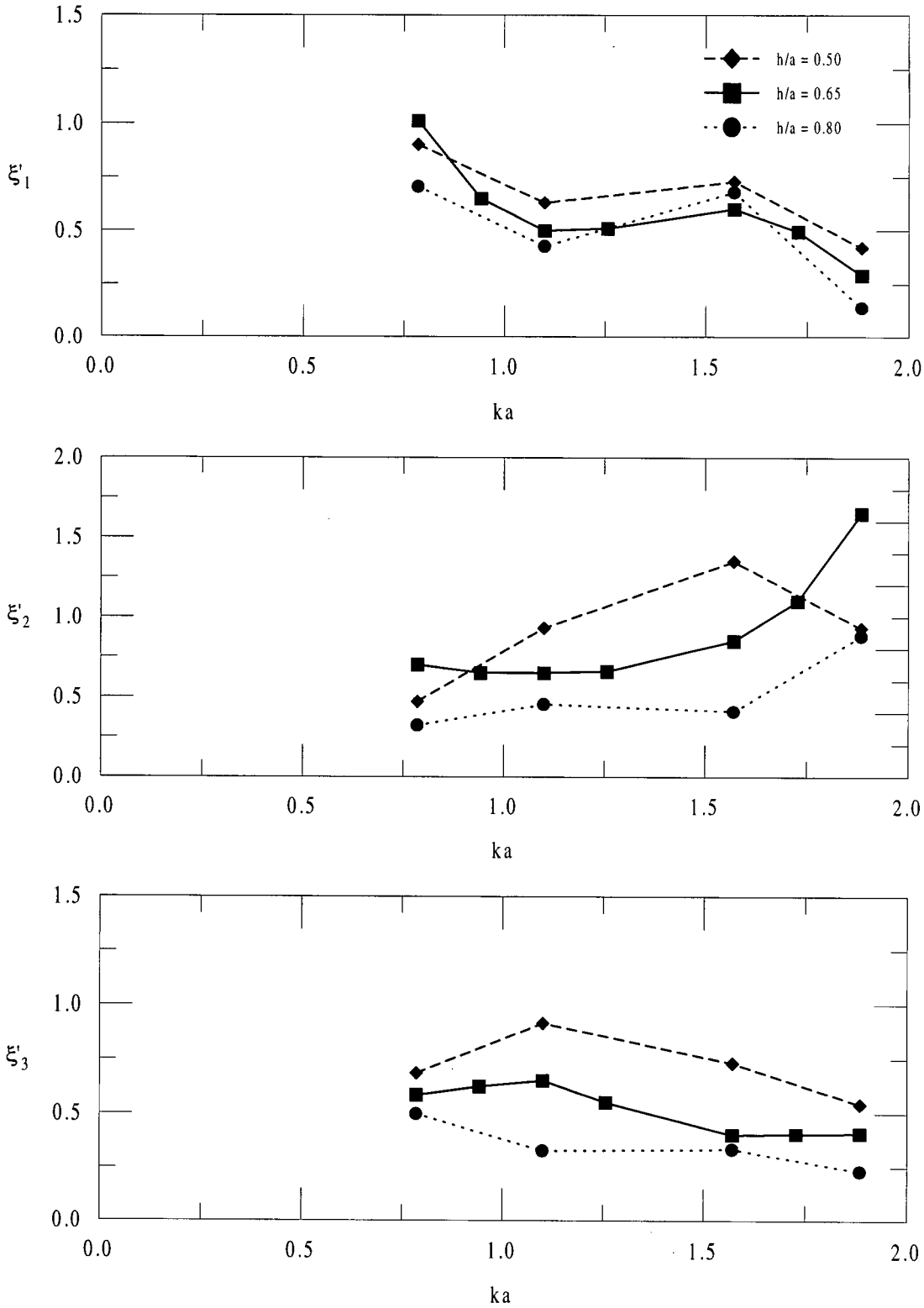

(a) RAO's in sway, heave, and roll.

Fig. 4.24 Experimental results to indicate the influence of draft for a circular twin-pontoon breakwater with chain mooring, (d/a = 2.5, b/a = 2.0, S/S_o = 1.08, $\beta = 0°$). (contd...)

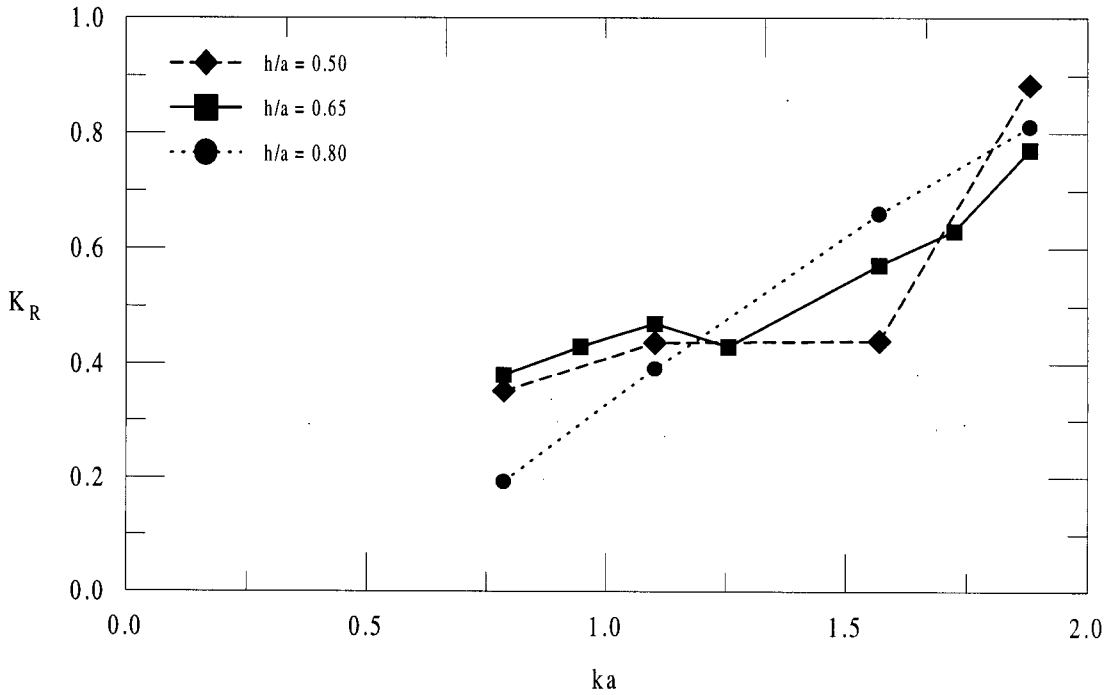

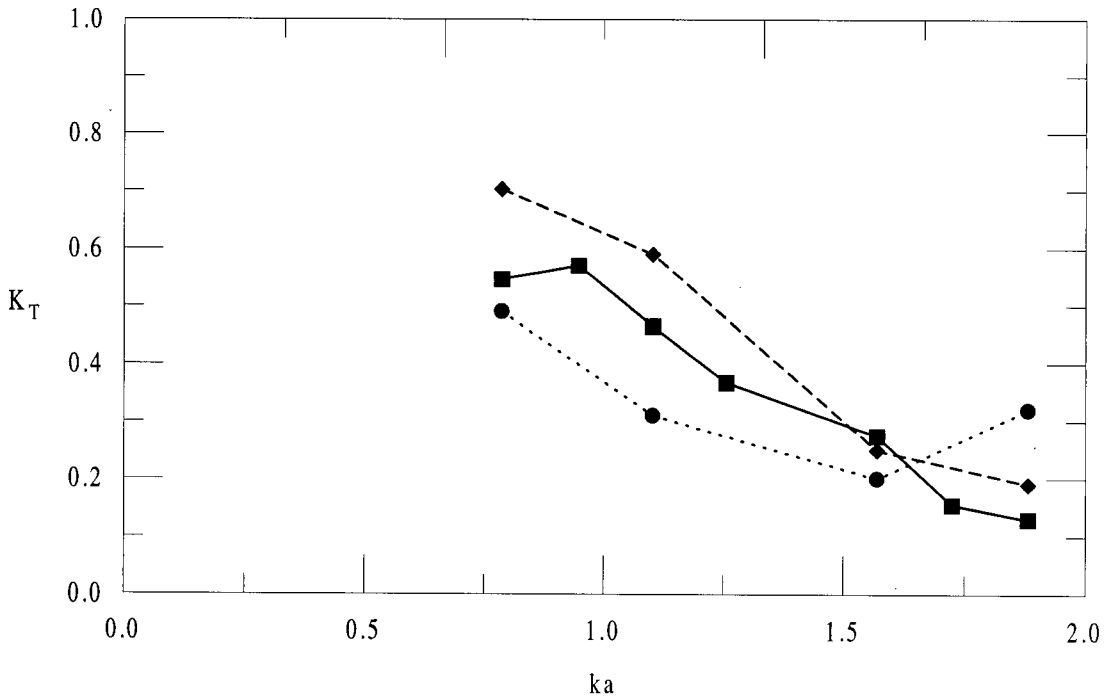

(b) reflection and transmission coefficients.

Fig. 4.24.

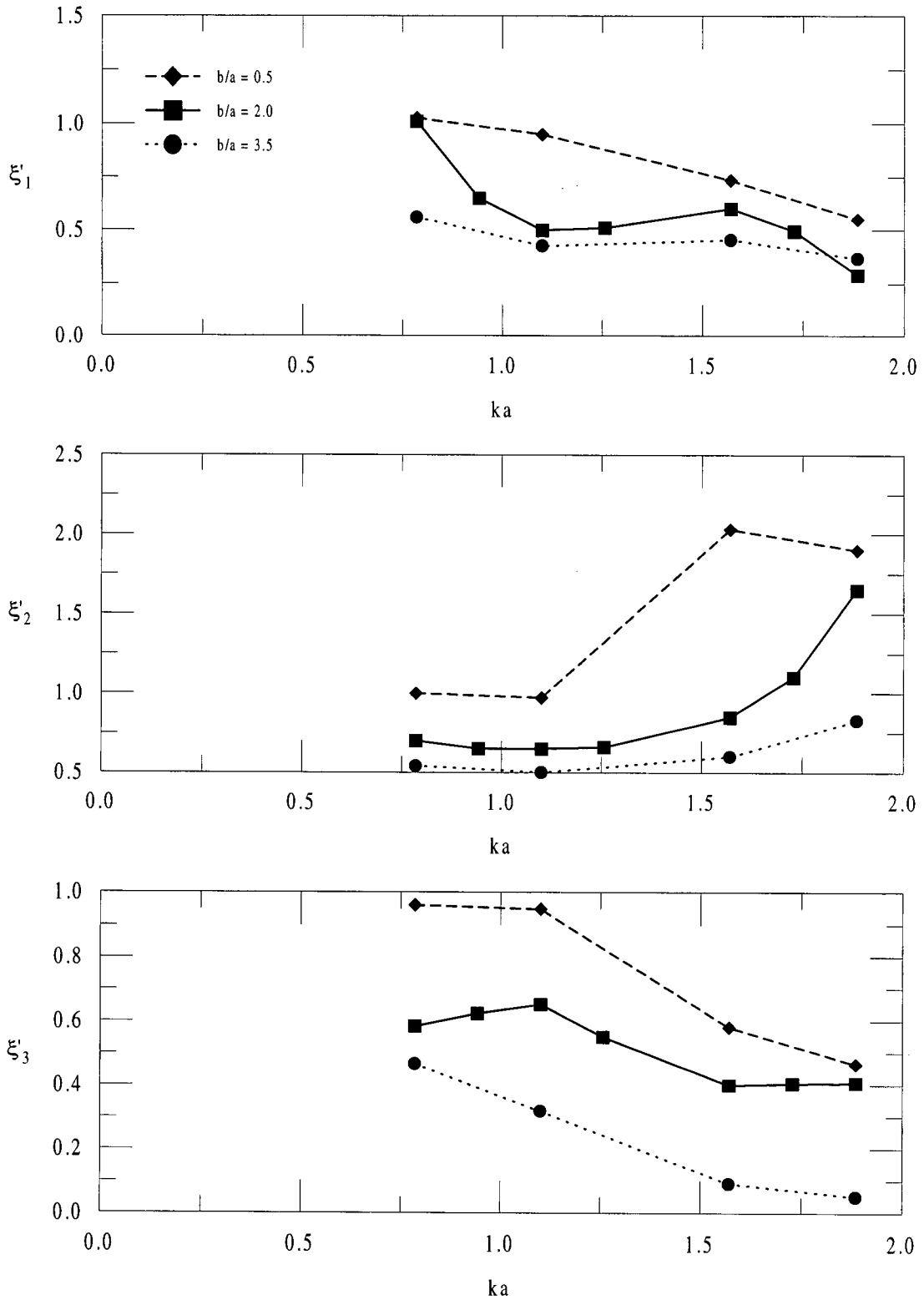

(a) RAO's in sway heave, and roll.

Fig. 4.25 Experimental results to indicate the influence of spacing for a circular twin-pontoon breakwater with chain mooring, (d/a = 2.5, h/a = 0.65, S/S_o = 1.08, $\beta = 0°$). (contd...)

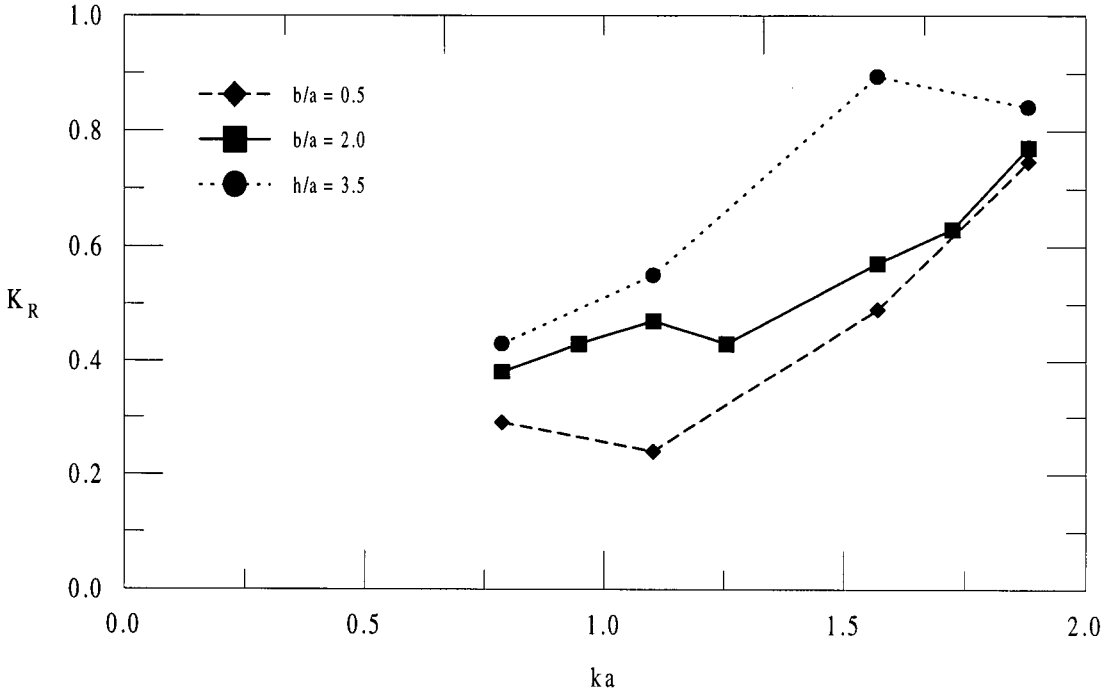

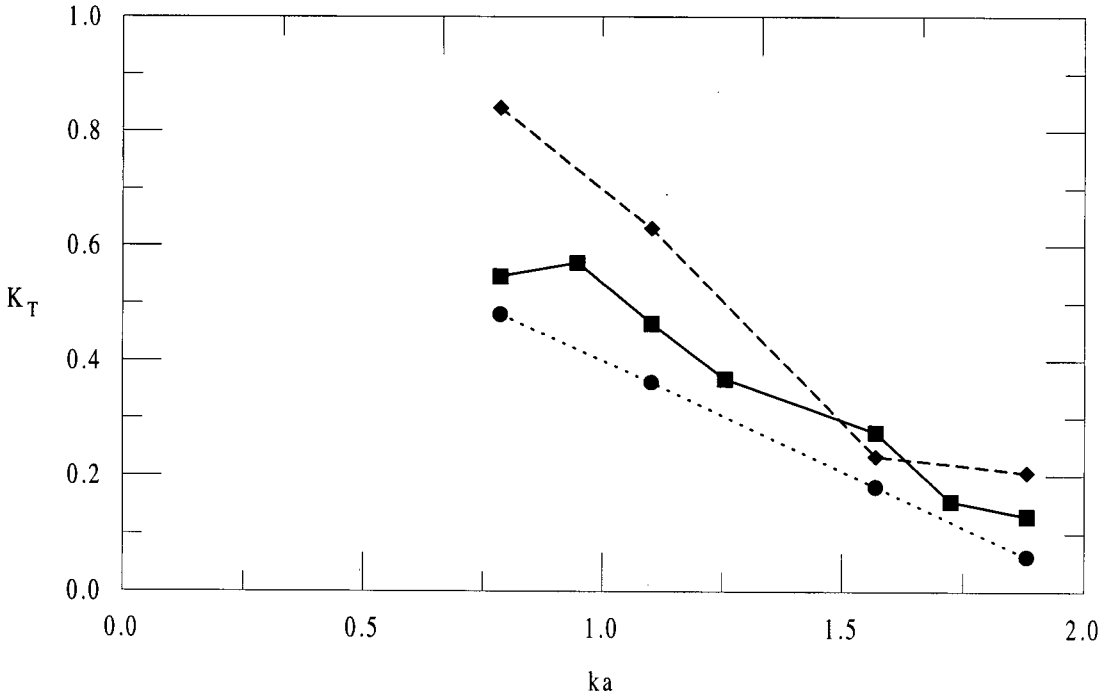

(b) reflection and transmission coefficients.

Fig. 4.25.

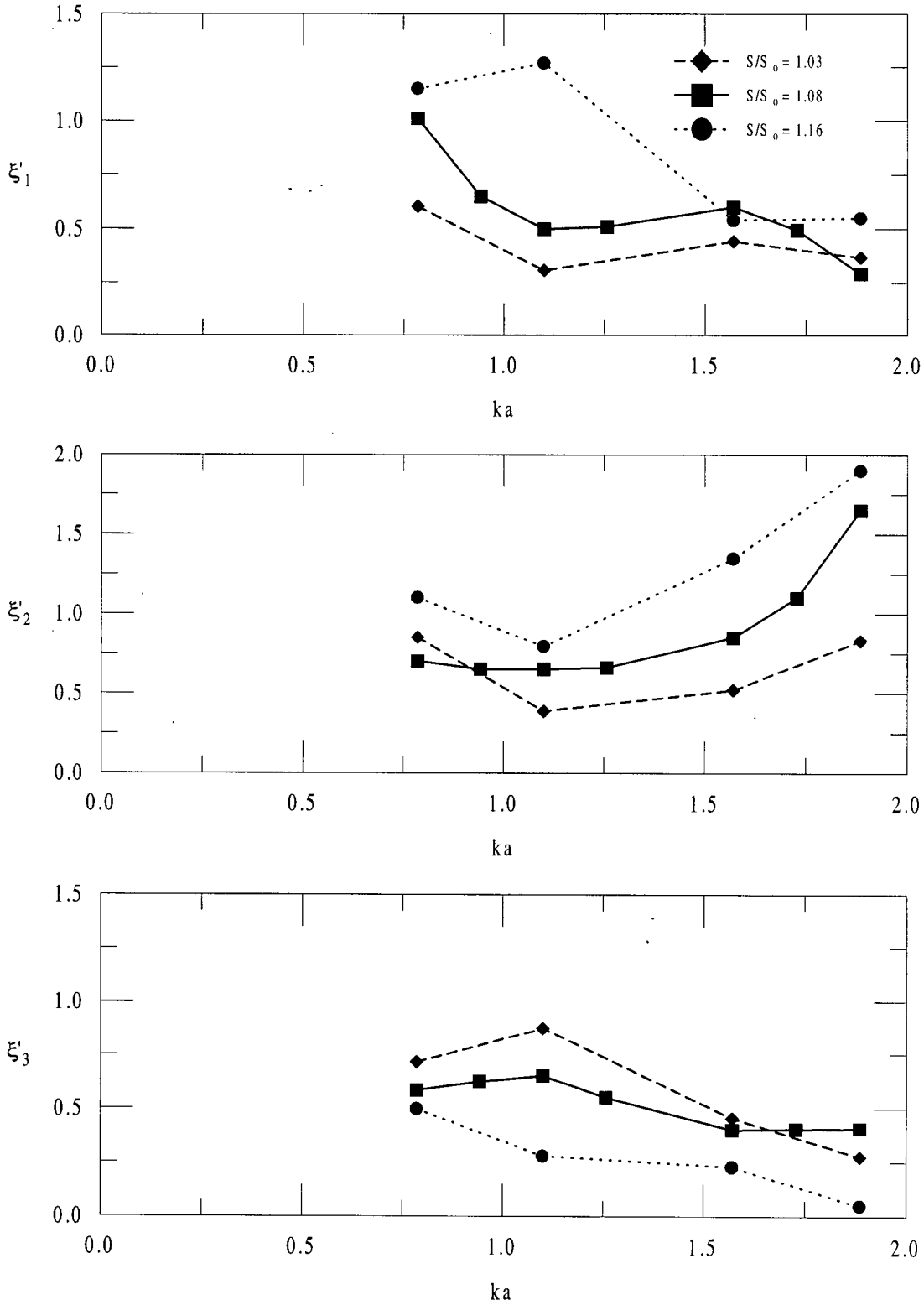

(a) RAO's in sway heave, and roll.

Fig. 4.26 Experimental results to indicate the influence of slackness for a circular twin-pontoon breakwater with chain mooring, (d/a = 2.5, b/a = 2.0, S/S_o = 1.0, $\beta = 0°$). (contd...)

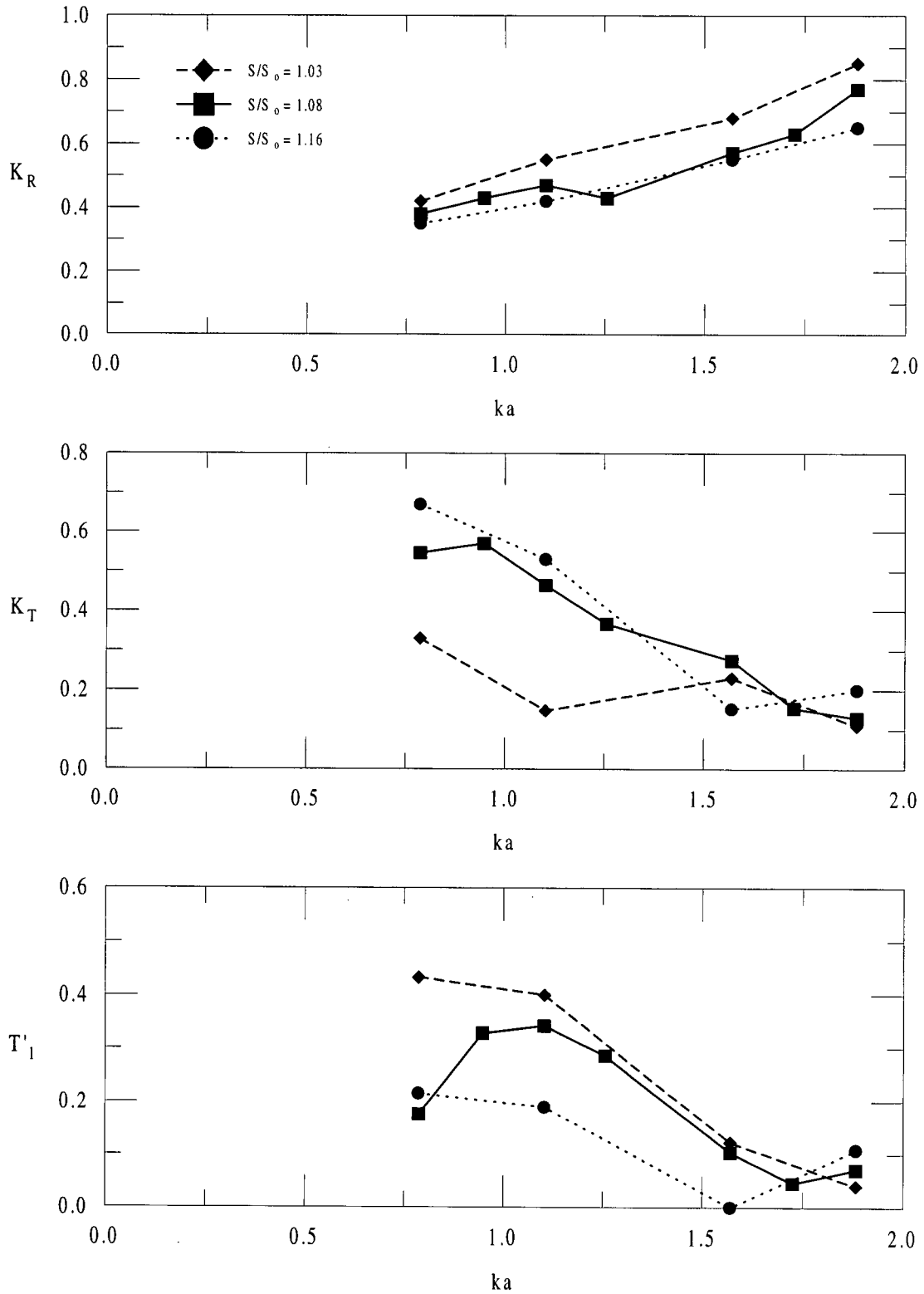

(b) reflection and transmission coefficients, and maximum mooring line tension at anchor.

Fig. 4.26.

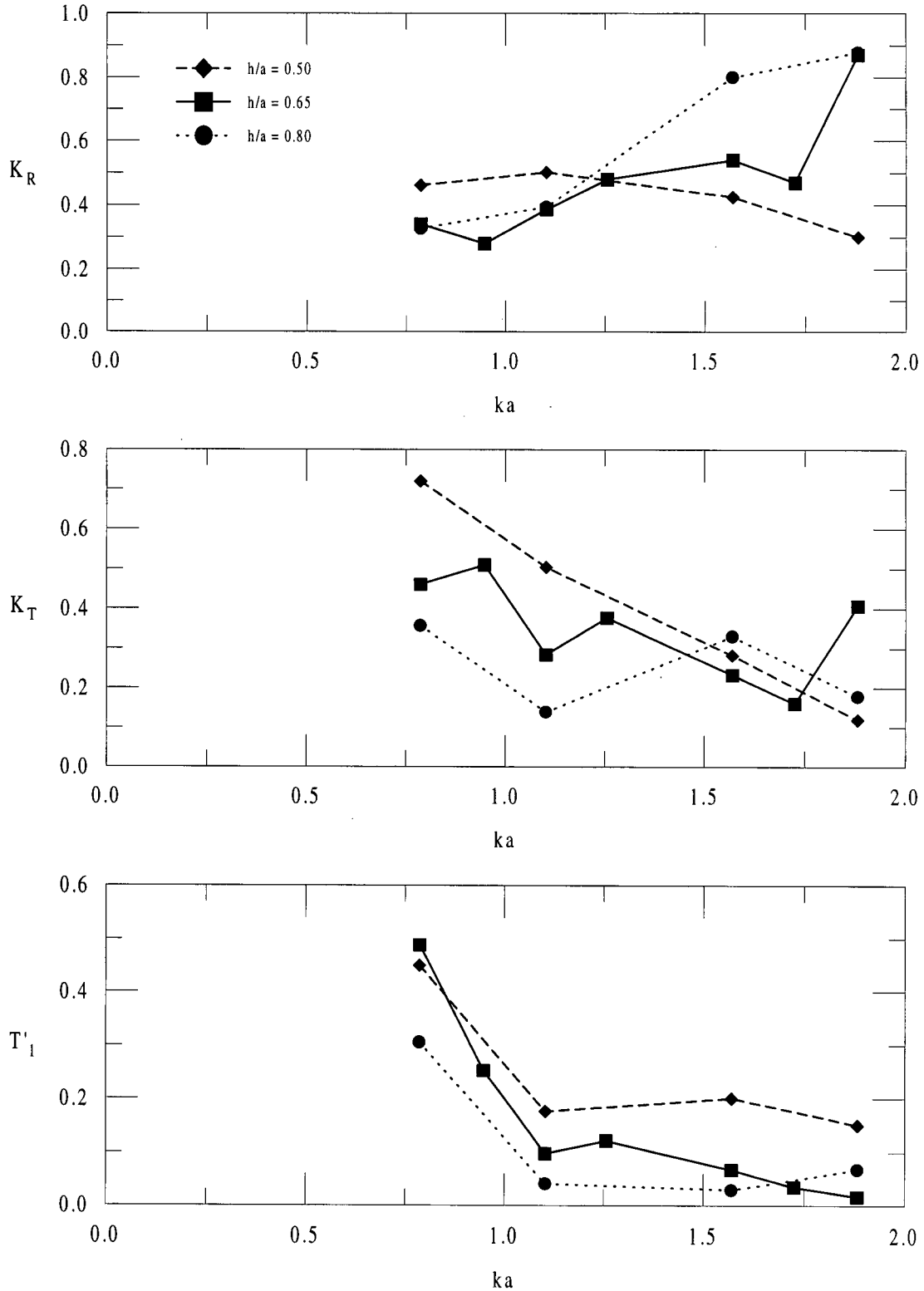

(a) influence of draft.

Fig. 4.27 Experimental results of reflection and transmission coefficients, and maximum mooring line tensions at anchor for a circular twin-pontoon breakwater with nylon mooring, (d/a = 2.5, b/a = 2.0, S/S_o = 1.0, β = 0°). (contd...)

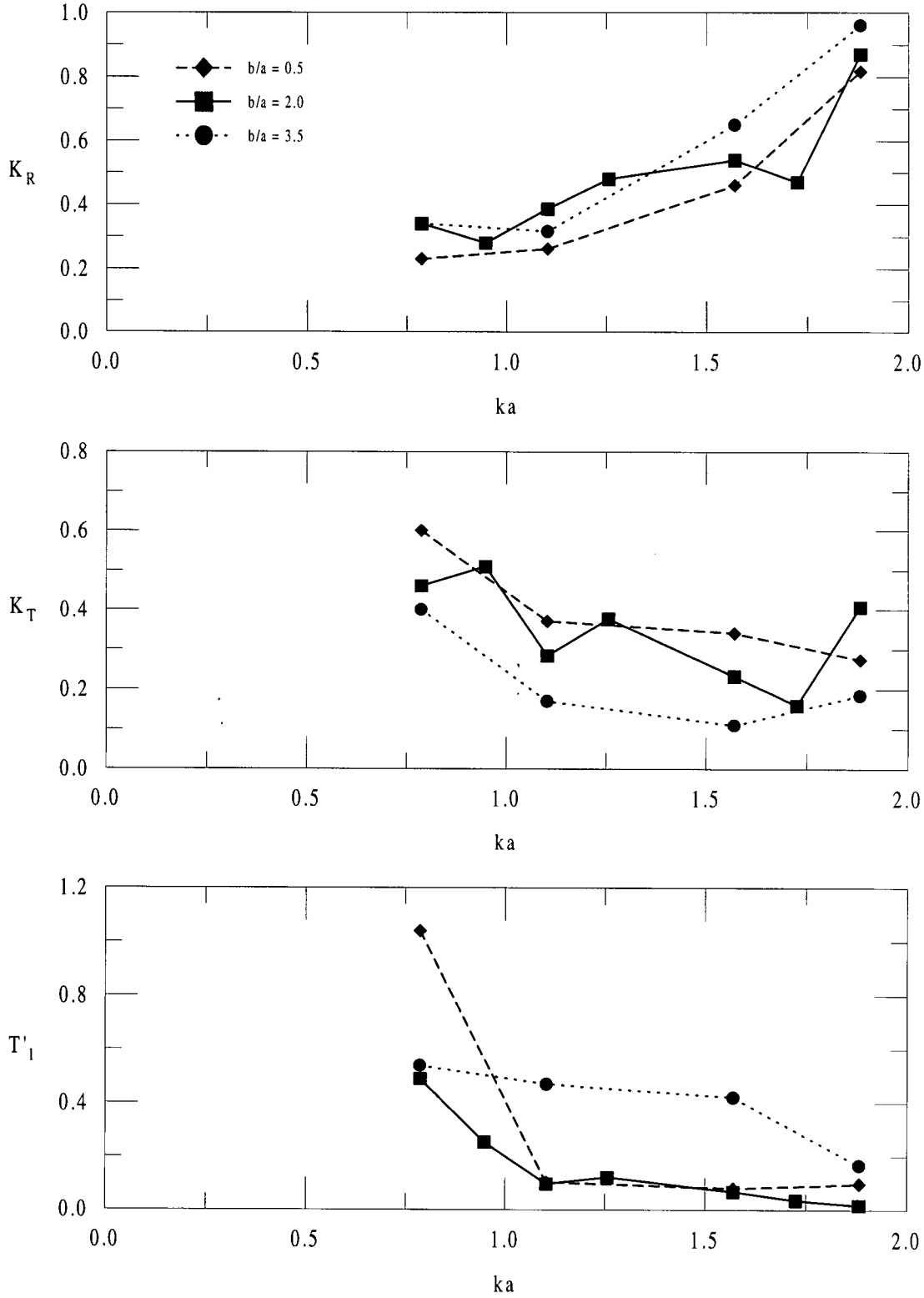

(b) influence of spacing.

Fig. 4.27.

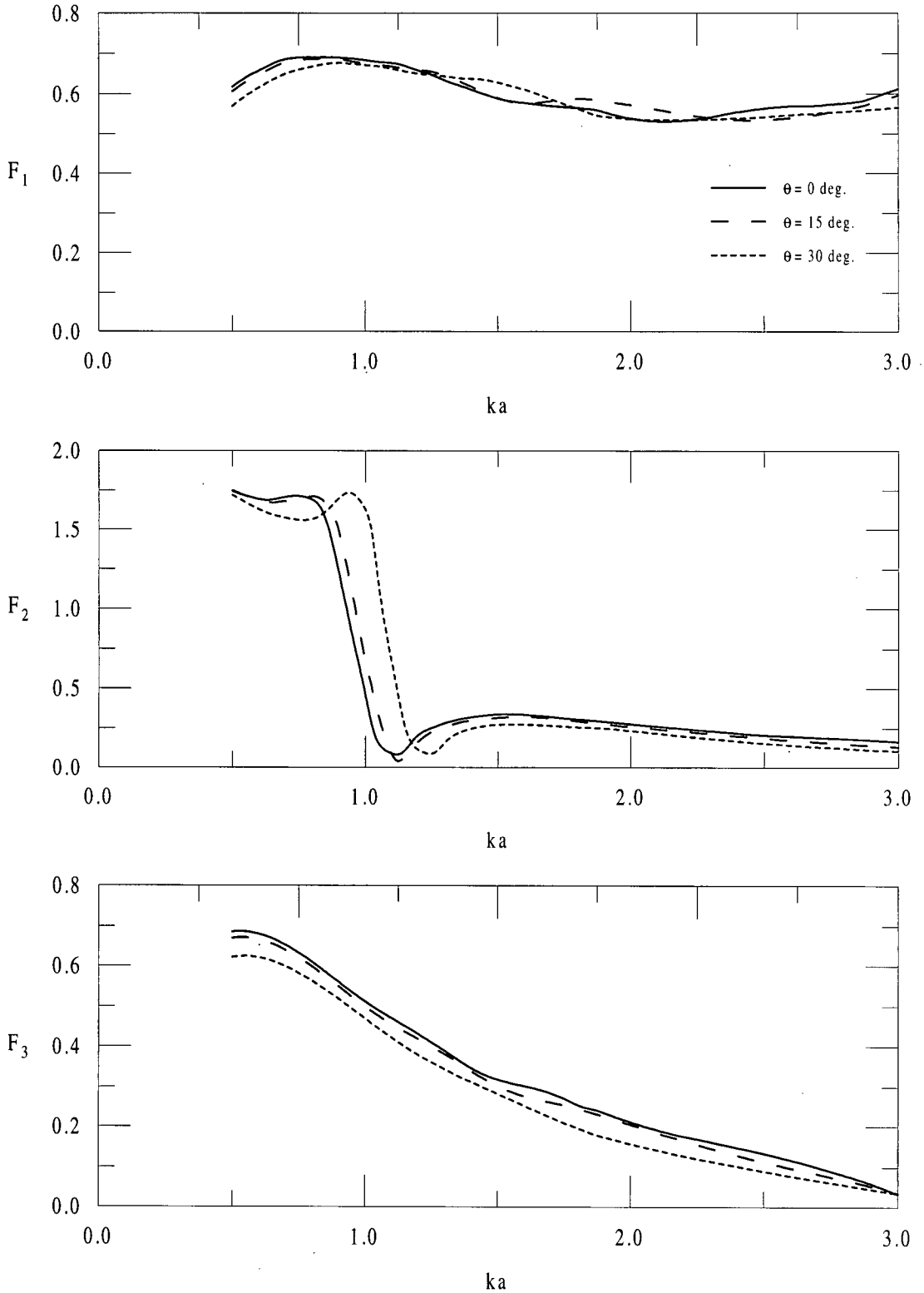

(a) exciting force coefficients.

Fig. 4.28 Numerical results indicating the influence of wave direction for a fixed rectangular twin-pontoon breakwater, (d/a = 2.5, h/a = 0.45, b/a = 1.0). (contd...)

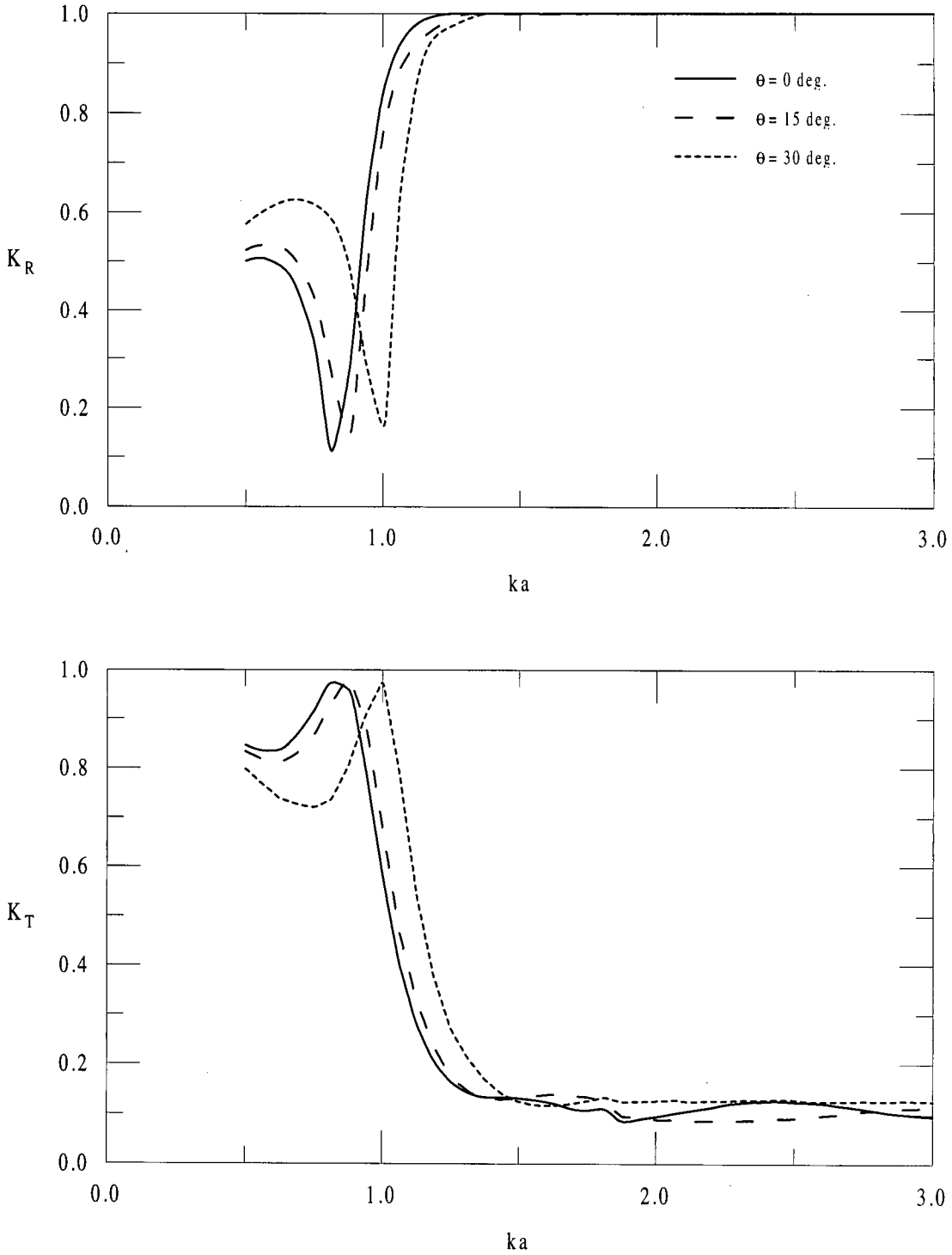

(b) reflection and transmission coefficients.
Fig. 4.28.

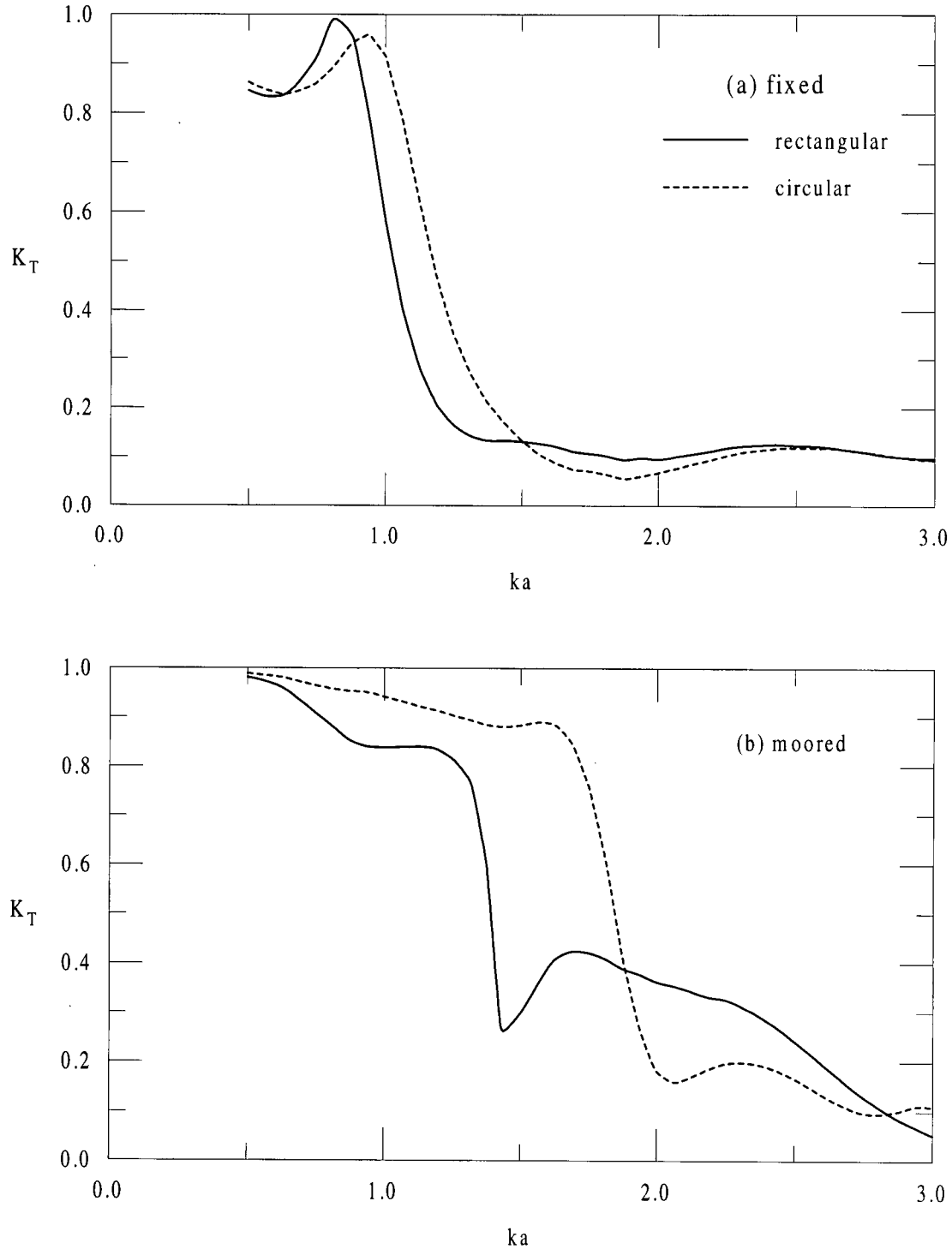

Fig. 4.29 Numerical results of transmission coefficient indicating the influence of pontoon section, (d/a = 1.67, h/a = 0.45, b/a = 1.0). (a) fixed; (b) chain mooring, $S/S_o = 1.08$.

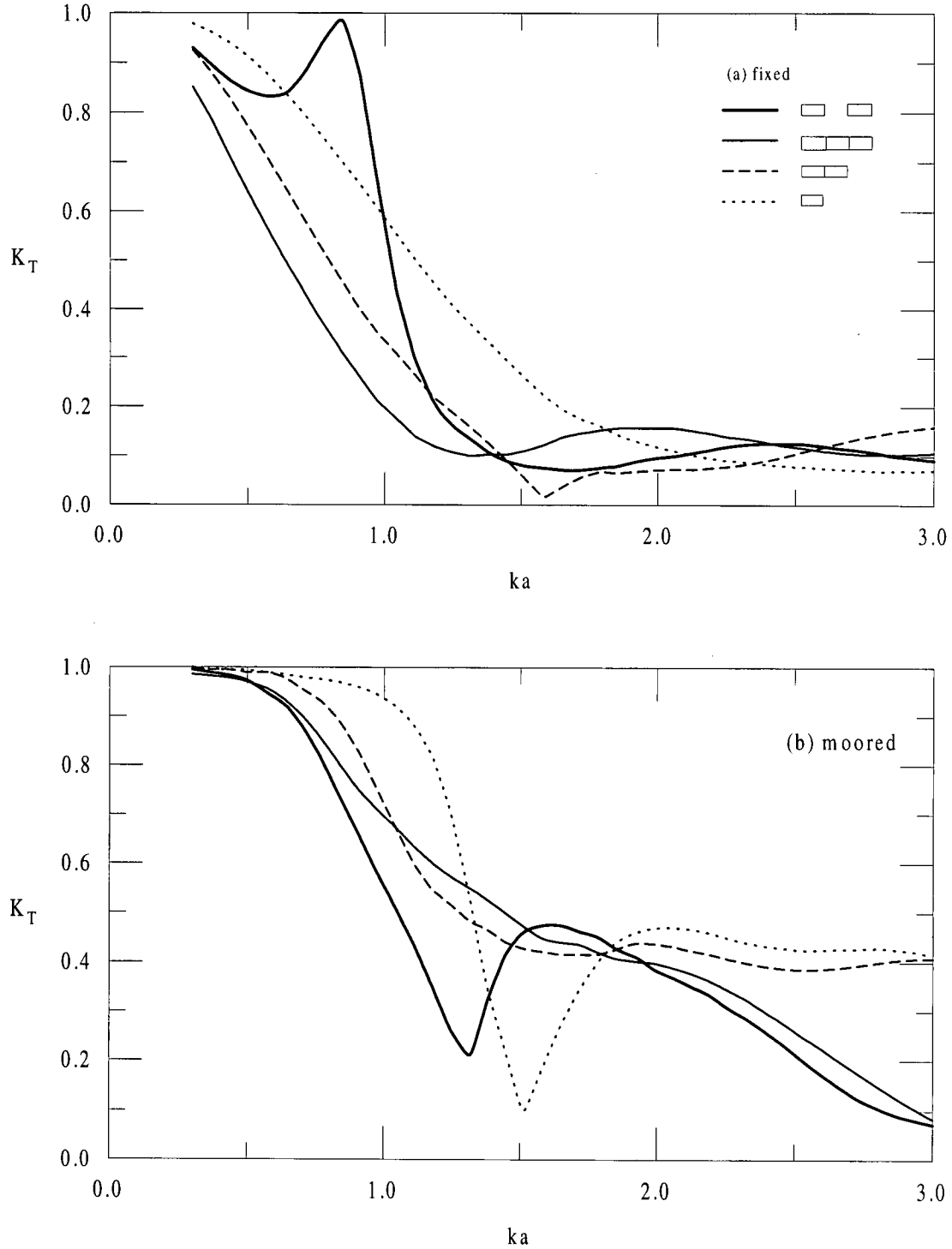

Fig. 4.30 Numerical results of transmission coefficient indicating the influence of different configurations of rectangular section breakwaters, (d/a = 2.5, h/a = 0.45). (a) fixed; (b) chain mooring, $S/S_o = 1.08$.

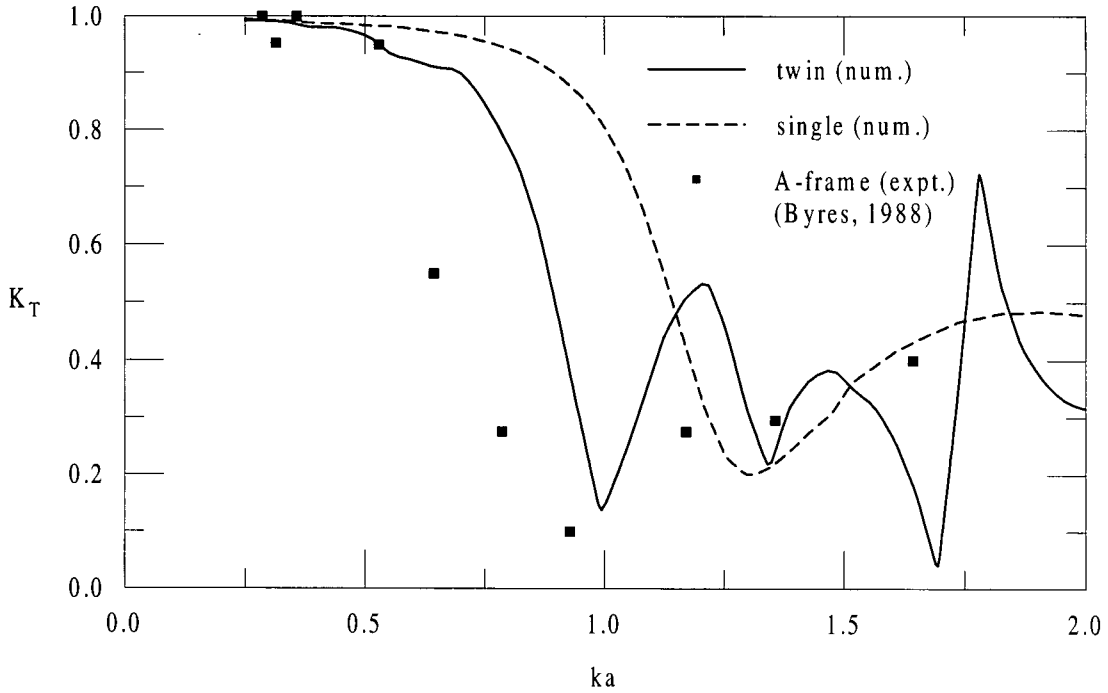

Fig. 4.31 Comparison of numerical results of transmission coefficient for the twin-pontoon and single-pontoon section breakwaters with the experimental values of an A-frame breakwater (Byres, 1988).

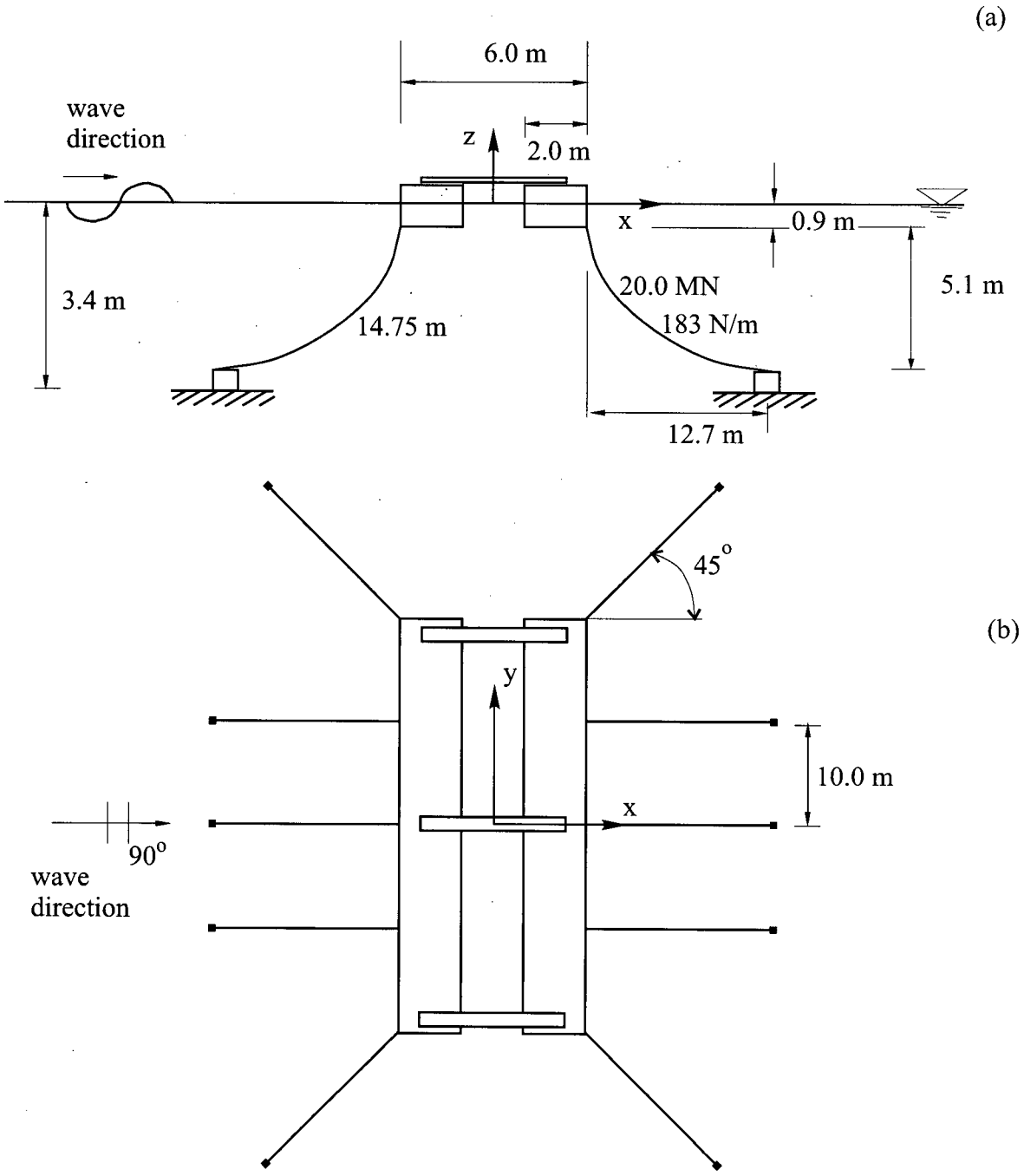

Fig. 4.32 Sketch indicating the related dimensions of a moored twin-pontoon floating breakwater. (a) elevation; (b) plan view.

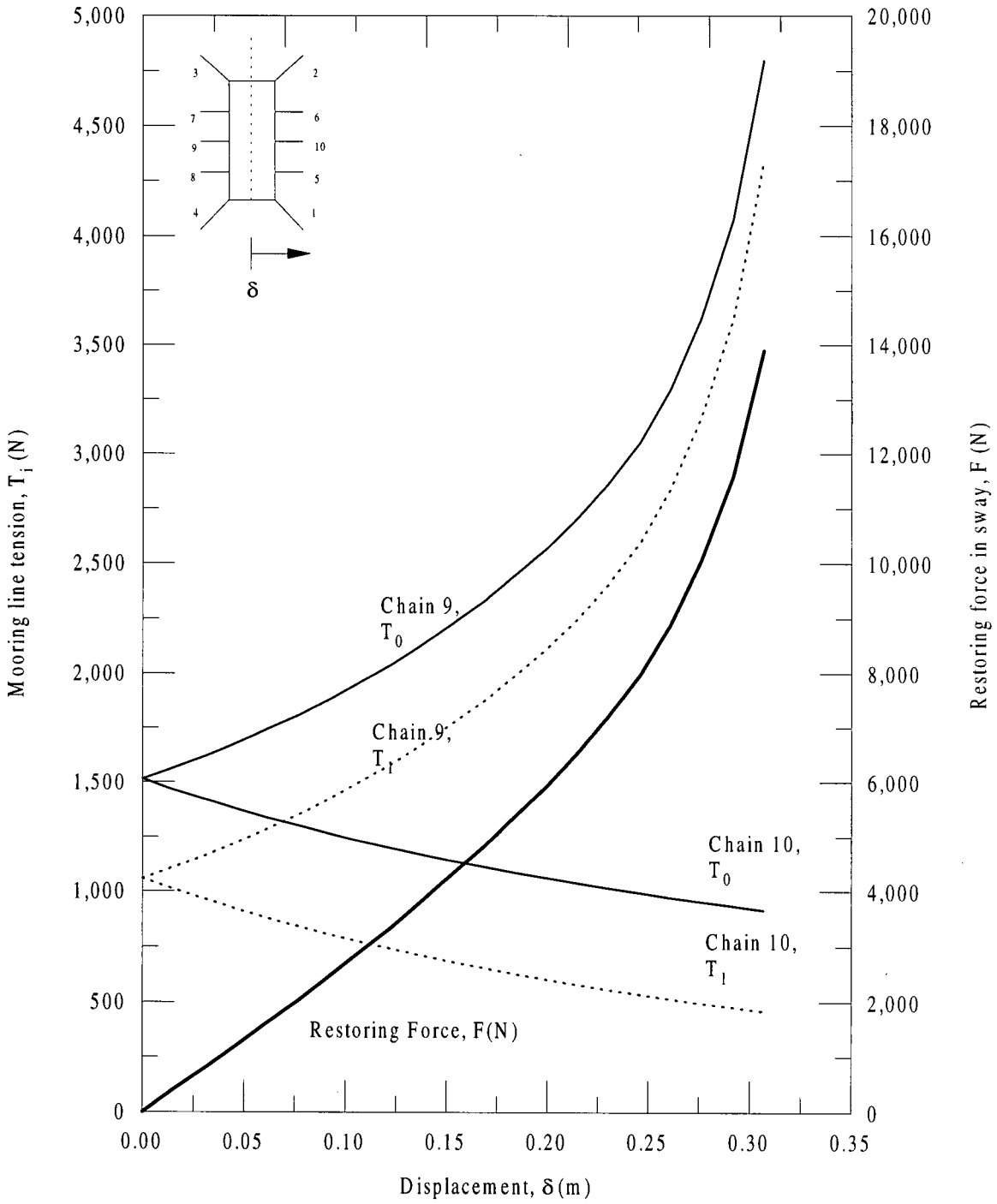

Fig. 4.33 Tension at anchor for a most heavily and the least loaded mooring line, and the associated restoring force in sway for a ten-point chain mooring system.

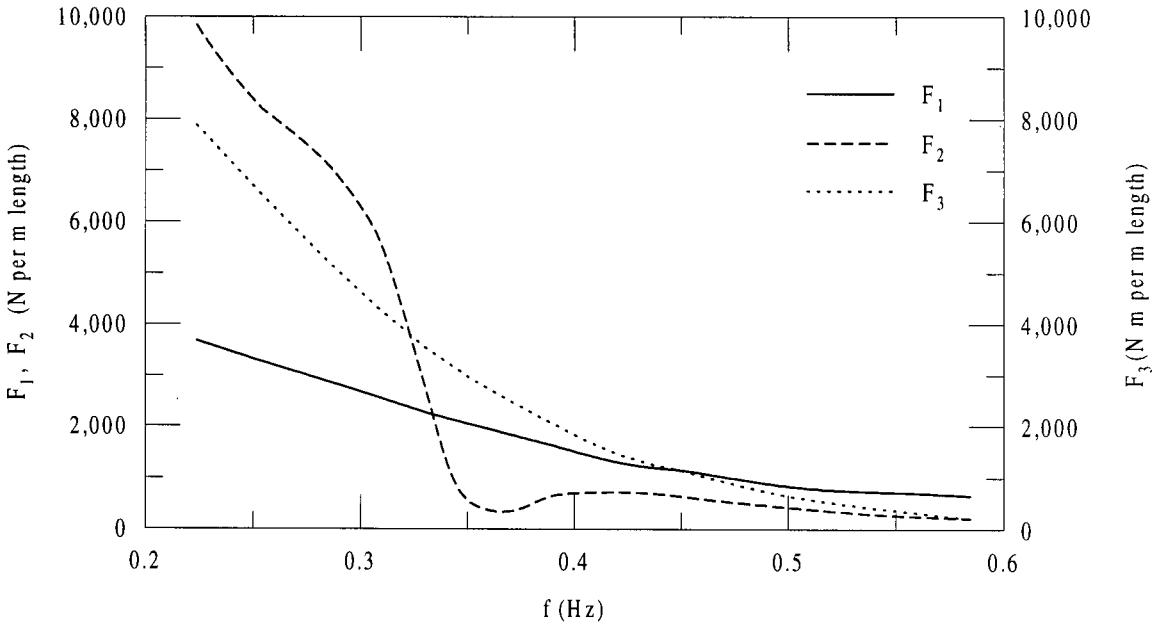

(a) exciting forces.

Fig. 4.34 Numerical results as functions of wave frequency, f, for a rectangular twin-pontoon section breakwater, (a = 2.0 m, d = 3.4 m, b = 2.0, h = 0.9 m), with chain mooring, $S/S_o = 1.08$. (contd...)

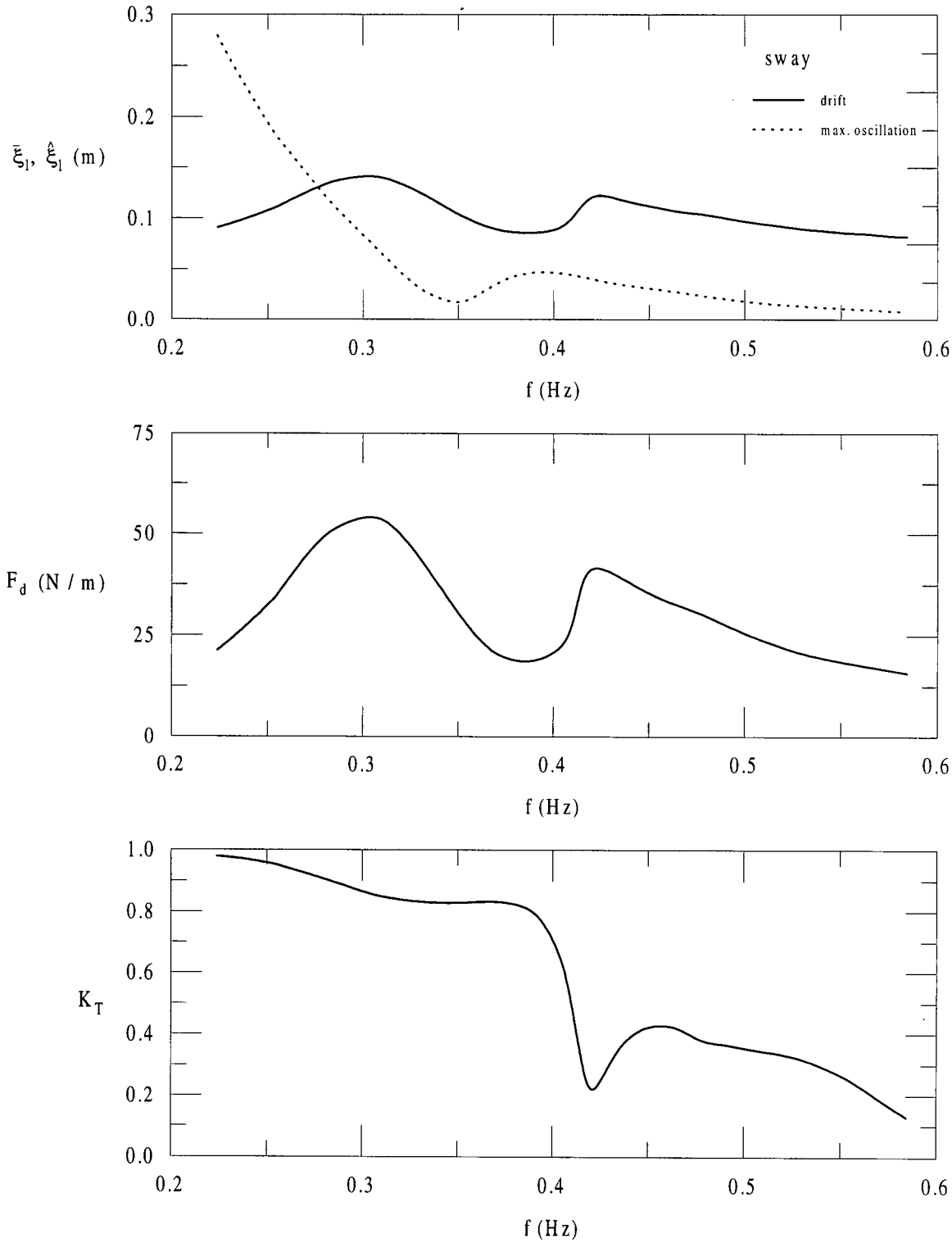

(b) drift, and sway motion, wave drift force, and transmission coefficient.

Fig. 4.32 (contd...)

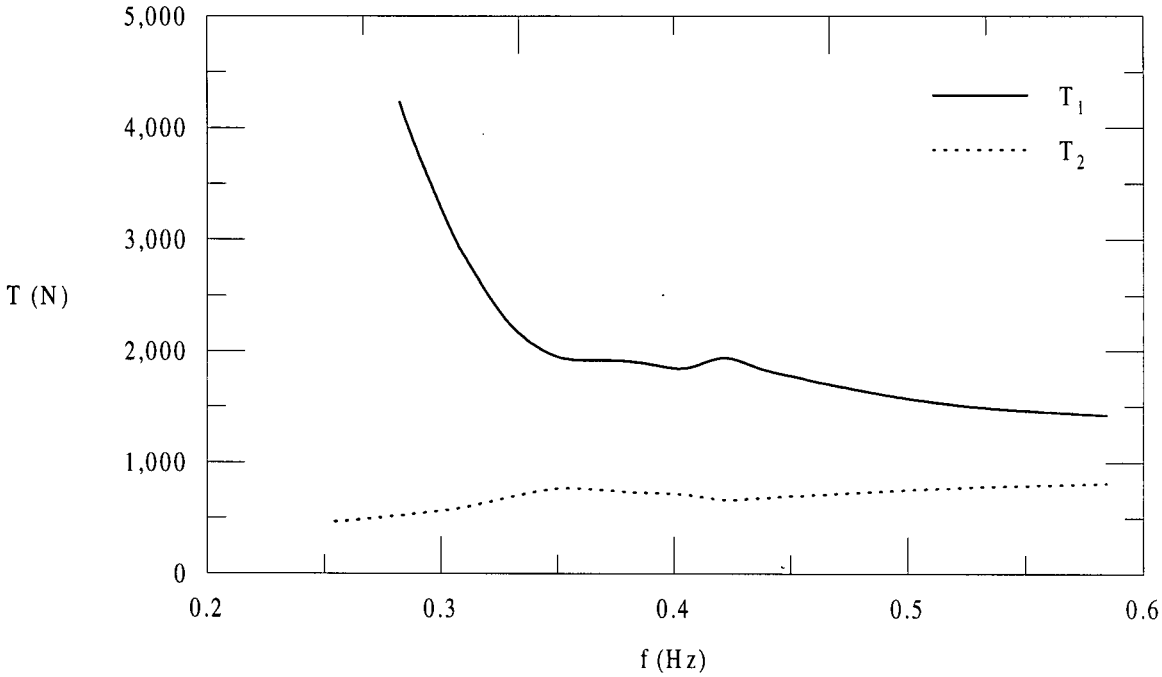

(c) maximum mooring line tension at anchor.

Fig. 4.34.

Appendix A - Reflection Analysis

In the following, a summary is given of expressions relating to three methods of predicting reflection coefficients from wave measurements at three locations (Isaacson, 1991). A definition sketch is given in Fig. A.1.

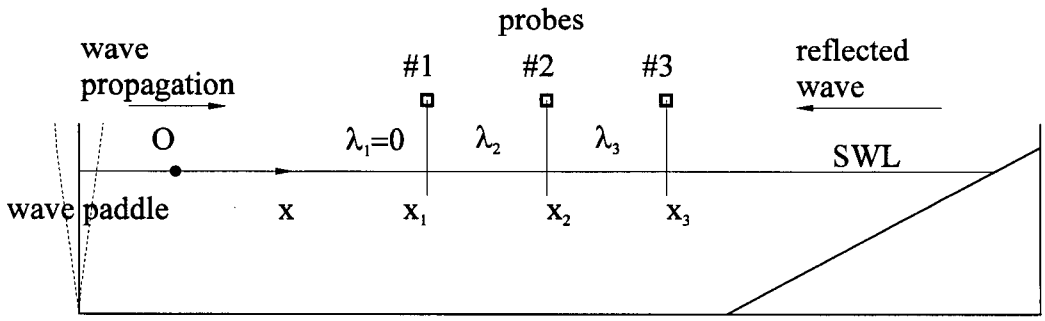

Fig. A.1 Definition sketch related to reflection analysis.

Method I

In this method, the measurements made are the two corresponding wave heights $2A_1$ and $2A_2$, and the phase difference $\delta = \delta_2$ between the two signals. Substituting these in to Eq. 3.3 and equating it to Eq. 3.4 and then simplifying gives:

$$a_i = \frac{1}{2|\sin\Delta|}\sqrt{A_1^2 + A_2^2 - 2A_1A_2\cos(\Delta+\delta)} \tag{A.1}$$

$$a_r = \frac{1}{2|\sin\Delta|}\sqrt{A_1^2 + A_2^2 - 2A_1A_2\cos(\Delta-\delta)} \tag{A.2}$$

$$\beta = 2kx_1 - \chi - 2\pi m \tag{A. 3}$$

where x_1 is the location of the probe at point 1, m equals to any integer chosen such that $0 \le \beta \le 2\pi$ and χ is given by:

$$\cos(\chi) = \frac{A_1^2 - a_i^2 - a_r^2}{2a_ia_r} \tag{A.4}$$

Method II

In this method, estimation of wave reflection is carried out by applying a least-square technique to measurements from three probes. Probe measurements provide five measured quantities, A_1, A_2, A_3, δ_1, and δ_2 from which the three unknowns H_i, K_R and β are estimated. The solution for this problem can be expressed as:

$$a_i = |X_i| \tag{A.5}$$

$$a_r = |X_r| \tag{A.6}$$

where

$$X_i = \frac{s_2 s_3 - 3s_4}{s_5} \tag{A.7}$$

$$X_r = \frac{s_1 s_3 - 3s_3}{s_5} \tag{A.8}$$

and

$$s_1 = \sum_{n=1}^{3} \exp(i2\Delta_n) \tag{A.9}$$

$$s_2 = \sum_{n=1}^{3} \exp(-i2\Delta_n) \tag{A.10}$$

$$s_3 = \sum_{n=1}^{3} A_n \exp[i(\delta_n + \Delta_n)] \tag{A.11}$$

$$s_4 = \sum_{n=1}^{3} A_n \exp[i(\delta_n - \Delta_n)] \tag{A.12}$$

$$s_5 = s_1 s_2 - 9 \tag{A.13}$$

As before, H_i and K_R are then obtained from a_i and a_r through Eq. 3.5 and 3.6, while β is obtained from χ through Eq. A.3.

Method III

For some cases, when measurements involving wave heights only are desired and phase measurements may be relatively inaccurate or may be inappropriate, this method is adopted. Solutions giving a_i and a_r are given as:

$$a_i = \frac{1}{2}\left(\sqrt{\Lambda+\Gamma}+\sqrt{\Lambda-\Gamma}\right) \tag{A.14}$$

$$a_r = \frac{1}{2}\left(\sqrt{\Lambda+\Gamma}-\sqrt{\Lambda-\Gamma}\right) \tag{A.15}$$

where

$$\Lambda = \frac{A_I^2 \sin\left[2(\Delta_3-\Delta_2)\right] - A_{21}^2 \sin(2\Delta_3) + A_{31}^2 \sin(2\Delta_2)}{\sin\left[2(\Delta_3-\Delta_2)\right] + \sin(2\Delta_2) - \sin(2\Delta_3)} \tag{A.16}$$

$$\Gamma = \frac{1}{2}\sqrt{\left[\frac{A_I^2 + A_3^2 - 2\Lambda}{\cos(\Delta_3)}\right]^2 + \left[\frac{A_I^2 - A_3^2}{\sin(\Delta_3)}\right]^2} \tag{A.17}$$

Simple substitution of measured quantities into the above expressions will yield the incident and reflected wave heights and the reflection phase angle. Hence from measurements of the amplitudes and the phases of two and three wave probes in front aligned perpendicular to the breakwater, the basic reflection parameter K_R and β can be calculated from any one the three methods.

Appendix B - Motion Analysis

Marker Position

Consider the geometry of the model as shown in Fig. B.1. Let Oxz be the reference frame with O being the origin about which the three degrees of freedom (sway, heave and roll) motions are prescribed.

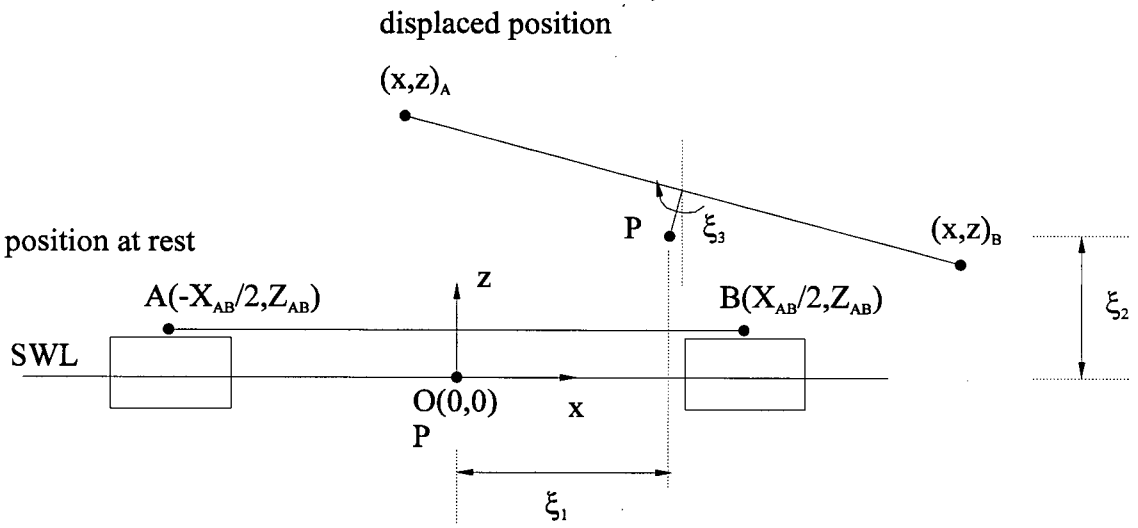

Fig. B.1 Measurement of breakwater motions.

Let P be a point fixed to the model coinciding with the origin O when the body is at rest. The displacements and rotation of point P, denoted ξ_1, ξ_2, and ξ_3, respectively are to be found in terms of the displacements of the points A and B. For the two-dimensional case, it is sufficient to know motions of only two points on the body.

Let the coordinates of points A and B be $(-X_{AB}/2, Z_{AB})$ and $(X_{AB}/2, Z_{AB})$ respectively when the body is at rest. When the body is displaced, the coordinates of A and B are denoted (x_A, z_A) and (x_B, z_B) respectively. The resulted displacements ξ_1, and ξ_2, and rotation ξ_3, may then be obtained for the following relations:

$$\xi_1 = \frac{(x_B + x_A)}{2} - Z_{AB}\sin(\xi_3) \qquad (B.1)$$

$$\xi_2 = \frac{(z_B + z_A)}{2} - Z_{AB}\cos(\xi_3) \tag{B.2}$$

$$\xi_3 = \sin^{-1}\left(\frac{z_A - z_B}{X_{AB}}\right) \tag{B.3}$$

Using these expressions, the component motions of the point P as a set of time series can be determined from the vertical and horizontal coordinates of the feature points A and B, which are themselves obtained at a series of times from every frame captured at a known rate.